Conceptual Development and Analysis of Multiple Integrated Hydrogen Production Plants with Cu-Cl Cycle

by

Maan Al-Zareer

A Thesis Submitted in Partial Fulfillment

of the Requirements for the Degree of

Masters of Applied Science

in

The Faculty of Engineering and Applied Science,

Mechanical Engineering Program

University of Ontario Institute of Technology

December 2016

Abstract

This thesis develops and analyzes four hydrogen production integrated energy systems, where hydrogen is produced via hybrid electrical and thermochemical water decomposition cycle, based on the chemical couple Cu-Cl. The first system consists of coal gasifier, membrane shift reactor, hydrogen fueled combined cycle, cryogenic air separation unit, compression system and five-step Cu-Cl cycle. The second system consists of SCWR, hydrogen fueled combined cycle, compression system and five-step Cu-Cl cycle. The third system consists of solar heliostat steam generator, Rankine cycle, compression system and five-step Cu-Cl cycle. The fourth system consists of SCWR, four-step Cu-Cl cycle, Rankine cycle and compression system. Modeling the developed systems is carried out using Aspen Plus, Aspen Hysys, and EES. The systems are assessed thermodynamically based on the energy and exergy efficiencies. The results show that the integration of nuclear reactor SCWR with the four-step copper and chlorine cycle is a promising integration in terms of energy and exergy efficiencies.

Keywords: Hydrogen production; Cu-Cl cycle; coal gasification; supercritical water-cooled nuclear reactor; solar heliostat field.

Acknowledgments

I would like to express my gratitude to my supervisor Professor Ibrahim Dincer and my co-supervisor Professor Marc Rosen, for their guidance and tolerance. They have provided me with high courage and the support to work, produce and publish. Their support and confidence in me brought out the best in me and was one of the main sources of motivation during my research and studies.

I would like to thank my father and mother for their continuous support and encouragement. They always believed and trusted me. I would also like to thank all of my brothers and sisters for their support.

Finally, I would like to thank everyone in Lab ACE 3030B in the Department of Automotive, Manufacturing and Mechanical Engineering, Faculty of Engineering and Applied Science, University of Ontario Institute of Technology.

Table of Contents

List of Tables

List of Figures

Nomenclature

COP	Coefficient of performance
d	Diameter (m)
$\dot{E}x$	Exergy rate (kW)
ex	Specific exergy (kJ/kg)
h	Specific enthalpy (kJ/kg)
h_f	Heat of formation (kJ/kg)
HHV	Higher heating value (kJ/kg)
HV	Heating value (kJ/kg)
LHV	Lower heating value (kJ/kg)
$\dot{m}$	Mass flow rate (kg/s)
P	Pressure (kPa)
$\dot{Q}$	Heat rate (kW)
$\mathcal{R}$	Universal gas constant (kJ/molK)
s	Specific entropy (kJ/kg K)
S	Sulfur content in coal (mass basis)
T	Temperature (^oC or K)
$\dot{W}$	Work rate (kW)
x	Mole fraction of constituent j in the flow (moles of j/moles of the total flow)

Greek letters

β	Coal parameter
η	Energy efficiency
ψ	Exergy efficiency
ρ	Density (kg/m^3)
ω	Moisture content in coal

Subscripts

AS#	Stream with variable # (refer to Figure 3.7)
B#	Aspen Plus block name (refer to Figure 3.7)
bs	Boundary where heat transfer takes

BrC	Brayton cycle
B#	Aspen Plus block name in Figure 3.8
C	Compressor (refer to Figure 3.9 and 3.10)
CASU	Cryogenic air separation unit
COND#	Condenser (refer to Figure 3.9 and 3.10)
Cu-Cl	Copper-chlorine cycle
coal	Coal
Comb	Combustion reactor (refer to Figure 3.7)
Compr1	Compressor (refer to Figure 3.7)
Compres2	O_2 compressor (refer to Figure 3.7)
ch	Chemical
c	Compressor
co	Compressor
Cooling	Mixer (refer to Figure 3.7)
conv	Convection
cond	Conduction
cenr	Central
Cu-Cl	Copper-chlorine cycle
d	Destruction
e	Electrical
fg	Phase change between liquid and gas
fc	Forced convection
GAST	Gas turbine (refer to Figure 3.9 and 3.10)
gen	Generation
GT	Gas turbine
GT2	Gas turbine (refer to Figure 3.7)
G	Gasifier
Gasifica	Gasification reactor (refer to Figure 3.7)
HFCC	Hydrogen fueled combined cycle
H_2	Hydrogen
HCS	Hydrogen compression system

HX	Heat exchanger (refer to Figure 3.7)
Hx-P1	Heat exchanger (see Figure 3.7)
Hwgmrp1	Reactor (see Figure 3.7)
Hwgmrp2	Separator (see Figure 3.7)
is	Isentropic
in	Input (flowing into the system boundary)
i	State point named i, inner diameter
insu	Insulation
j	Constituent name in the flow
ms	Molten salt
max	Maximum
MRP3	Pressure valve (refer to Figure 3.7)
net	Net result
ov	Overall
out	Output (flowing out of the system boundary)
o	At standard conditions, outer diameter
P#	Pump (refer to Figure 3.9 and 3.10)
Pump-W#	Water pump (see Figure 3.7)
$\dot{Q}$	Heat flow rate
QQ	Heat exchanger (refer to Figure 3.7)
QO	Heat exchanger (refer to Figure 3.7)
RC	Rankine cycle
ST	Steam turbine
STMG#	Steam generator (refer to Figure 3.7)
STMGG	Heat exchanger (refer to Figure 3.7)
SCC	Supporting combined cycle
SRC	Supporting Rankine cycle
surf	Surface
Tfcomp	Treated syngas compressor (see Figure 3.7)
W	Work
WGSMR	Water gas shift membrane reactor

Superscripts

HP	Hydrogen at high pressure of 700 bar
LP	Hydrogen at low pressure

Acronyms

BrC	Brayton cycle
CASU	Cryogenic air separation unit
Cu-Cl	Copper-chlorine cycle
ER	Electrolysis reactor
GFEMA	Gibbs free energy minimization approach
HRSG	Heat recovery steam generator
HFCC	Hydrogen fueled combined cycle
HCS	Hydrogen compression system
IGCC	Integrated gasification combined cycle
O/C	Oxygen content in the coal divided by the carbon content in the coal
RC	Rankin cycle
SCC	Supporting combined cycle
SRC	Supporting Rankin cycle
SCWR	Supercritical water-cooled nuclear reactor
WGSMR	Water gas shift membrane reactor

Aspen Plus terms (*italic* terms)

Cisolid	For homogeneous solids that have a defined molecular weight, with the option of entering the particle size distribution
Mixed	Material stream option in Aspen Plus modeling
NC	Nonconventional solid (for heterogeneous solids that have no defined molecular weight) with the option of entering the particle size distribution
Rstoic	Aspen Plus reactor model that carries out the reaction based on the stoichiometric balanced chemical reaction equation with a specified reactants conversion percentage
RGibbs	Aspen Plus reactor model that carries out the reaction based on Gibbs free energy minimization approach.

Chapter 1: Introduction

The world fossil fuels reserves have been depleted increasingly over the past several decades, forcing humanity to find alternative sources to meet the continuously rising demands for energy. Recent reports by the International Energy Agency have predicted a 50% increase in global energy demand of by 2030 [1]. The concerns about the finite nature of fossil fuels have resulted in extensive research and development on alternative sources of energy as well as on how to more efficiently use currently available fossil fuels and to look for other energy sources that are either renewable or non-carbon fuels.

1.1 Energy and Environmental Issues

Many methods are used today to increase the efficiency of energy production from fossil fuels. One of these methods is to continually run power plants at a constant rate and at full capacity; another approach is the integration of power systems. Running power plants at full capacity is not practical due to the fluctuating nature of energy demands during night and day, summer and winter. However, the successful use of energy storage systems can make that possible. Hydrogen has the advantage of being both an energy storage medium and an energy carrier (a clean energy carrier if produced from clean energy sources) [1], meaning that running power plants at full capacity and storing the excess energy in hydrogen will result in more efficient use of the available fossil fuels. Muradov and Veziroglu [2] analyzed the main methods for hydrogen production from fossil fuels as a green path for fossil-based hydrogen production. One of these methods is water electrolysis, while another promising hydrogen production process is the Cu-Cl cycle. An advantage of the thermochemical hydrogen production cycle is that it directly produces hydrogen from heat without the intermediate step of heat to electricity, which is vital for water electrolysis. Many processes can produce hydrogen from fossil fuels, such as: (a) coal gasification; (b) steam methane reforming; and (c) biomass gasification. As one of the most abundant fossil fuels, coal, plays a significant role in power production worldwide. Coal gasification is often coupled with power producing combined cycles. Currently, 18% of the hydrogen produced worldwide is from coal [3].

Due to its clean and renewable nature, solar energy has received a great deal of attention, especially in terms of research and development. Many countries plan to increase the percentage share of solar energy in the total energy supply mix, while many others consider solar energy to be one of the promising energy sources for replacing fossil fuels in the future [4–8]. There are many methods and technologies for utilizing solar energy. Solar energy can be utilized through photovoltaic for providing direct electrical power or by using solar concentrators for producing thermal energy (e.g., in the form of superheated steam). Recently, research has been undertaken on hybrid energy systems that produce thermal and electrical energy from solar energy. Despite solar energy's advantages, it has a varying and intermittent nature. Solar energy levels change during the day and vary throughout the year due to seasonal effects, often resulting in low plant capacity. One way of increasing the practicality of a solar energy systems is to integrate them with energy storage systems, to provide energy when sunlight is not available. Solar energy can be stored by using different energy storage technologies, with the main energy storage categories being thermal, electrical and chemical. An example of a chemical energy storage medium is hydrogen, which has the advantage of being both an energy storage medium and an energy carrier [1]. Hydrogen also has a very high specific energy (energy per unit mass). There are two main paths for producing hydrogen from solar energy: electrolysis or a thermochemical water decomposition cycle or a hybrid combination of both technologies.

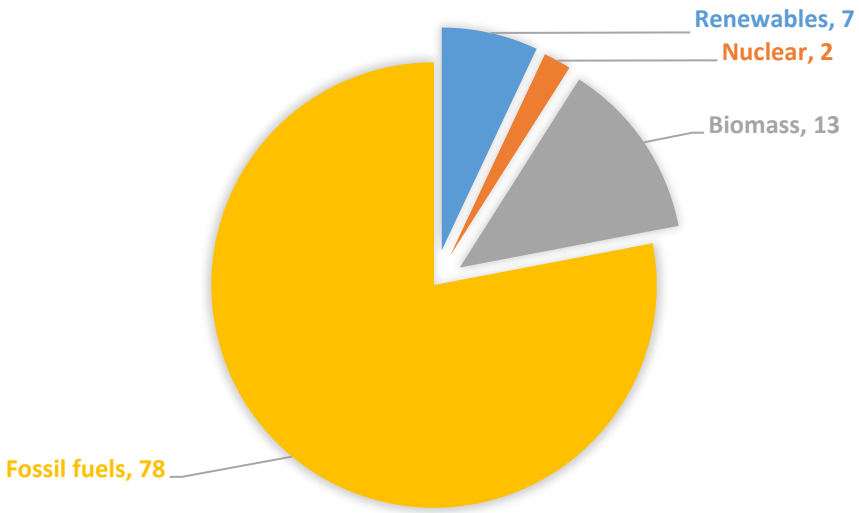

Figure 1.1 The **s**ources of energy consumption in the world in percentage (data from [1]).

For hydrogen production by electrolysis, photovoltaic (PV) solar panels can be used for the direct conversion of solar energy into electrical energy, which is used by an electrolyzer to decompose water into hydrogen and oxygen. Boggs and Botte [9] reported that water electrolysis requires 33.0 Wh per gram of hydrogen produced, for hydrogen product with conditions at atmospheric pressure. For thermochemical water-decomposition cycles, the chemicals involved are continuously recycled (ideally). Thermochemical water decomposition cycles are viewed as catalysts for water decomposition reaction. The only material outputs from the decomposition cycle are hydrogen and oxygen, which means that the cycle is a carbon-free cycle [10,11].

Regarding non-renewable and non-carbon based fuel options, nuclear energy is one of the main candidates for this category. Nuclear power production is one of the latest power production technologies. Furthermore, nuclear energy is one of the ideal solutions for power production or for hydrogen production. Hydrogen production from non-carbon based fuels avoids carbon-based emissions. A large percentage of hydrogen found on earth is in the form of water, so water decomposition to produce hydrogen using a non-carbon emitting process can be advantageous for reducing carbon emissions if the energy source is carbon-free energy source.

1.2 Motivation

The effects of global warming on the environment, greatly impact the humans, animals and plants' lives, and with continuous increase in carbon emissions, the motivation is to find an energy solution for these problems in an environmentally benign manner. Therefore, hydrogen, as a clean energy carrier (if produced from a clean energy source), has become the main theme of this research. The energy systems developed and analyzed in this research should be efficient, environmental friendly and able to meet the energy demands of today as well as the future. This research will be one step to a future where no energy losses are caused due to demand and supply mismatch. The importance of the availability of the energy sources derived this thesis research into considering wide variety of energy sources from different energy sources families.

An important point to be mentioned in the motivation section is that this work is done as a part of bigger project [12–22] aiming to develop and commercialize the water

splitting Cu-Cl cycle. This thesis will provide an early overview of the great potential of the Cu-Cl cycle.

1.3 Objectives

Most of the research in the literature about the Cu-Cl cycle do not consider the method of delivering thermal energy to Cu-Cl cycle reactors and with minor focus on integrating the Cu-Cl cycle with other systems. However, the method of delivering thermal energy to cycle reactors is of a vital importance since the heat transfer depends on the temperatures of the reactors and the heating fluid temperature. Thus, this study presents a detailed analysis of the Cu-Cl cycle and the system that will deliver thermal energy to the Cu-Cl cycle. The proposed systems are analyzed thermodynamically and simulated in Aspen Plus process simulation software.

The specific objectives of this research are listed as follows:

- To propose four different designs of hydrogen and power production integrated systems. These four conceptual designs produce high purity hydrogen for possible use in fuel cells. The main components of these four systems are: thermal energy source, a hydrogen production system, a hydrogen preparation system and required supporting systems.
- To propose different methods for delivering thermal energy to the Cu-Cl cycle reactors. One system combusts part of the hydrogen produced to produce the system's overall required power. Another system does not use any of the produced hydrogen or what is related to the Cu-Cl cycle. Another system recovers part of the Cu-Cl cycle remaining thermal energy.
- To model the four proposed conceptual designs using process simulation software, Aspen Plus and Aspen Hysys. Some systems are modeled through mathematical models that are solved using Engineering Equation Solver (EES).
- To validate the results of the developed models for the subsystems of the systems with published data. All assumptions made through the modeling of the systems are validated with what is published in the literature.

- To perform energy and exergy analyses on the proposed integrated systems through: performing a detailed energy and exergy analyses for each of the developed systems; calculating the energy and exergy efficiencies of each component in each system, plus overall results; determining the exergy destruction rates and ratios of all components in the proposed conceptual designs and the operational CO_2 emission rate.
- To present the performance assessment of the different systems in terms of energy and exergy efficiencies. The energy and exergy efficiencies of the systems is calculated for each component of the system and the overall performance measures.
- To perform a number of parametric studies on the systems, in order to check the variation of the energy and exergy efficiencies of the systems with the variation of ambient temperature and power production rates.
- The energy sources used for the developed systems consider sources from different energy groups (fossil fuels, renewable sources and advanced future groups).

In this thesis, multiple engineering simulation software are used to develop, model and simulate the proposed integrated systems namely: Aspen Plus, Aspen Hysys and Engineering Equation Solver (EES). The designs proposed in this thesis are realistic and applicable to designs available in the literature.

Hydrogen and power production plants must contain the following subsystems (see Figure 1.2): a heat or electricity generation system (based on the type of fuel used); from a heat or electricity to hydrogen production system; hydrogen preparation system; and other systems necessary to complete the plant.

The first step in developing the conceptual system for hydrogen production plant is to select the best possible combinations (based on developed criteria) of the required subsystems. After the four conceptual systems are proposed, Chapter 4 will analyze these concepts, through both energy and exergy analyses. Figure 1.2 shows the main subsystems and their interactions in hydrogen production plants. A hydrogen production plant has its principal functions of producing hydrogen and, to achieve the plant's main functions, each subsystem must achieve its duties. The subsystems making the hydrogen production plant are selected based on specific developed criteria from the literature. An important

requirement of the hydrogen produced by the hydrogen production plant is to produce high purity hydrogen that is ready to be stored, exported, filled into the H_2 fueled vehicles fuel tank, and for industrial uses.

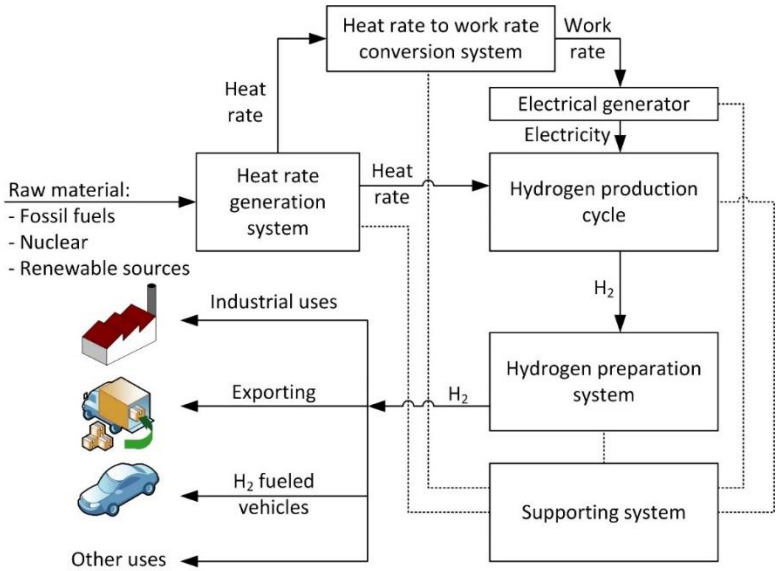

Figure 1.2 The main subsystems and their interactions in the hydrogen and power production plants.

Chapter 2: Literature Review

This chapter provides a detailed literature review on the hydrogen and power production plants while focusing on those which use water decomposition cycles. Producing hydrogen from fossil fuels can help controlling the carbon emissions locations, easing their capturing process. Having vehicles running on hydrogen produced from fossil fuels limits the equivalent carbon emission location of these vehicles to the location of the fossil fuel-based hydrogen plant. Hydrogen, can be used in fuel cells for electrical production, can be combusted to produce thermal energy and can be utilized for the production of chemicals that can be used as fuels such as ammonia. However, it is required to be in a form that will occupy less volume. There are various ways to produce hydrogen from fossil fuels, such as steam-methane reforming and coal gasification [23]. Continuous increase in global energy consumption has resulted in a faster depletion rate of the earth's fossil fuel reservoirs, and the use of fossil fuels has negatively affected the environment due to carbon emissions. Currently, 78% of total energy demand comes from fossil fuels [24]. Research and development are more directed to clean, economical, safe, stable, and abundant energy sources.

Various energy forms, such as solar, geothermal, hydropower and nuclear energy are available as candidates for reducing the dependence on fossil fuels. Many researchers and scientists predict that nuclear energy will have important share in covering the energy demands of the future [20]. Nuclear energy has been mostly used for electrical power production [20]. A proposed alternative use of the nuclear energy is for the purpose of hydrogen production. Producing hydrogen from nuclear energy has been evaluated as highly beneficial for enhancing the nuclear energy sector [25]. Regarding renewable energy sources, solar energy has been used for hydrogen production by different companies and research centers. Honda has built a solar-based hydrogen production and vehicle refueling station. In addition, Honda is presently working on an experimental home station that will produce hydrogen from natural gas while providing heat and electricity to the homes [26].

2.1 Coal Use in Hydrogen Production

Fossil fuels are depleting and current methods of using fossil fuels does not help delaying the due date of running out of fossil fuels. Some of these methods are for management purposes rather than the current technological limitations, an example on these management scenarios is the energy losses during the fluctuating energy demands on-peak and off-peak periods. One possible solution for the increasing the efficiency of the plant is to run the power plants at a constant rate and at full capacity all of its operational time. Another solution is multigenerational integrated systems that can adjust the rates of each of its multiple products based on the demand periods. One way of running the power plants at full capacity is through the successful use of energy storage systems. Hydrogen has the advantage of being both an energy storage medium and an energy carrier [1], plus if the system is an integrated system for multigeneration purposes, and two of these products are hydrogen and electrical power will provide the bridge for running the plant at full capacity through all of its operational time.

Many processes can produce hydrogen from fossil fuels, such as (a) coal gasification, (b) steam methane reforming, and (c) biomass gasification. Coal is one of the most avialable type of fossil fuels, and it plays a significant role in power production worldwide. Coal gasification is often coupled with power production combined cycles. Currently, 18% of the hydrogen produced worldwide is from coal [3]. Many systems are proposed in the literature for integrating coal gasification with other systems to increase the efficiency of the overall conversion process of coal [10,27–34]. Bicer and Dincer [35,36] proposed a multigeneration system for hydrogen production; the system integrated underground coal gasification with a solid oxide fuel cell. Researchers have proposed various integrations of the process of gasifying coal [10,27–33], biomass [34], or the combination of coal and biomass [33] with other systems such as a solar power tower [31], or with a Fischer-Tropsch unit [30]. Others have integrated the gasification system with a dual chemical looping process, namely chemical looping air separation and water gas shift with calcium looping CO_2 absorption [32]. References [27–34] performed first law analysis of their proposed integrated gasification systems, but only the references [29–34] performed second law analysis (exergy analysis). The energy and exergy efficiencies of

the proposed integrated gasification systems were assessed in references [27–34], and some exhibited an energy efficiency more than 60%, which is very promising results. Although there are many different ways of producing hydrogen, the Cu-Cl cycle is of a particular importance since it decomposes water using relatively low temperature thermal energy when compared with thermal decomposition of water.

Aghahosseini et al. [10] proposed an integrated system which combines coal gasification combined cycle (IGCC) based on Texaco gasification [10] power plant with the thermochemical copper-chlorine cycle. An integrated system in [10] is for trigeneration of hydrogen, steam, and electricity. In the integrated system in [10] the only interaction between the IGCC and the Cu-Cl cycle is in terms of heat and oxygen interactions; the copper-chlorine cycle receives heat from two sources, where one is from the IGCC which produces oxygen for the coal gasifier in the IGCC, and produces hydrogen for energy storage. In the integrated system proposed by Aghahosseini et al. [10] the copper-chlorine cycle was not simulated using Aspen Hysys software, and no clear overall energy efficiency increase in the IGCC system was demonstrated. Presented in [10] the overall efficiencies of the IGCC compared to Texaco IGCC system, which were 43% and 45% respectively. Also in [10] they proposed an integration of coal gasification combined cycle with the thermochemical copper-chlorine cycle. The copper-chlorine cycle in their proposed integrated system was not completely dependent on the heat received from the IGCC system rather it received extra heat from other sources, and no exergy analysis was performed on their proposed system. Ratlamwala and Dincer [37] proposed an integrated system of the Cu-Cl cycle with Kalina cycle and electrolyzer. The integrated system proposed in [37] is mainly for hydrogen production. After the energy and exergy analyses of the integrated system is carried out, a new copper-chlorine design layout is presented with a heat exchanger network for heat recovery within the copper-chlorine cycle to increase the overall efficiency.

2.2 Solar Hydrogen Production

The two main paths for producing hydrogen from solar energy: electrolysis or a thermochemical water decomposition cycle or hybrid system combining both technologies. For hydrogen production by electrolysis, photovoltaic (PV) solar panels can be used for

direct conversion of solar energy to electrical energy, which is done by using the electrolyzer to decompose water into hydrogen and oxygen. Boggs and Botte [9] reported that water electrolysis requires 33.0 Wh g^{-1} H_2, for hydrogen produced at atmospheric pressure. For thermochemical water-decomposition cycles, the chemicals involved are continuously recycled (idealy). Thermochemical water decomposition cycles are viewed as catalysts for the water decomposition reaction. The only material outputs are hydrogen and oxygen, so it is a carbon-free cycle [10,11]. Giaconia et al. [38] analyzed a sulfur-based thermochemical water decomposition cycle for hydrogen production. Gokon et al. [38] studied a two-step cycle for hydrogen production via thermochemical water decomposition. The cycle is based on monoclinic ZrO_2-supported $NiFe_2O_4$ and Fe_3O_4 powders and ceramic foam devices. Ozbilen et al. [21,39] developed four-step thermochemical water decomposition cycle utilizing compounds of the chemical pair of copper and chlorine. [24,25] carried out exergoeconomic and exergoenviromental analyses, as well as multi-objective optimization. Orhan et al. [40] compared various configurations of hybrid electrical and thermochemical water decomposition cycles that utilize the chemical couple copper and chlorine. Orhan et al. [20] assessed the thermochemical cycle for possible use in nuclear hydrogen production.

A brief analysis is performed for a group of different methods for water splitting technologies to determine the required energy by each technology to produce a gram of hydrogen. The analysis is carried out with the assumption that the electrical or thermal energy is produced from solar energy. A hybrid electrical and thermochemical water decomposition cycle (five-step copper-chlorine cycle [40]) requires electrical energy of 13.6 Wh per gram of hydrogen produced and thermal energy of 40.4 Wh per gram of hydrogen produced [40]. If we assume a solar thermal energy to electrical energy conversion efficiency of 9%, based on the work of [4], then the hybrid electrical and thermochemical water decomposition cycle requires electrical energy of 17.2 Wh per gram of hydrogen produced. This means that the hybrid electrical and thermochemical water decomposition cycle requires less equivalent electricicity than the electrolysis process.

Ratlamwala and Dincer [41] proposed two solar-based integrated systems for hydrogen production. The first system proposed by [28] consists of a solar heliostat field

integrated with a copper-chlorine hybrid thermochemical water-decomposition cycle. The second proposed system by [28] incorporates a solar heliostat field, a copper-chlorine cycle, a Kalina cycle, and a photocatalytic reactor. The energy and exergy efficiencies of the two systems were reported by [41]. The energy and exergy efficiencies are reported for the first system as 47.8% and 50.8% respectively, and for the second system as 56.4% and 59.6%, respectively. All energy and exergy efficiencies are determined for a solar light intensity of 1,200 W/m^2. The hydrogen production rate forSystem is 2,250 kg/day and for System 2 it is 2670 kg/day. However, the hydrogen produced by the systems is not compressed to a storage/transportation pressure; rather it is at atmospheric pressure, for which excessively large storage volumes are required. For example, the volume for storing the hydrogen produced per day is 27,300 m^3 for System 1 and 32,400 m^3 for System 2. Both volumes are impractically large. However, if the hydrogen produced is compressed to 700 bar [42] as most hydrogen fueled vehicles require, the required storage volume decreases to 57.4 m^3 for System 1 and 70.4 m^3 for System 2. That is, when hydrogen is compressed to 700 bar it requires a volume nearly 565 times less than when the hydrogen is at one bar. In the work of Ratlamwala and Dincer [41] , the hydrogen was produced at ambient pressure, which requires a storage volume of nearly 12 m^3 per kg of hydrogen produced and is not practical. Hydrogen fueled cars require hydrogen compressed to pressures of 300 to 700 bar. Little work has been reported on the integration of systems containing solar energy and hybrid thermochemical water decomposition cycles other than the work of Ratlamwala and Dincer [41,43,44].

2.3 Nuclear Energy for Hydrogen Production

Nuclear energy is clean energy in terms of carbon-based-emissions, however it has its own problems. But if the nuclear energy is used to produce hydrogen which can be stored in off-peak periods using a cycle with higher energy efficiency than the energy efficiency of a Rankine cycle integrated with an electrolyzer than more energy will be obtained from the nuclear energy.

There are many different types of nuclear reactors, some are under operations while others are at the small reactor experimental stage and others are design concepts. A simple overview of the main nuclear reactors models is presented in Figure 2.1. The relatively low

steam temperature outlet of the current nuclear reactors is one of the main reasons for reducing the efficiency of these power plants. New nuclear reactors concepts are being introduced to solve the problem of low-temperature steam. One of the promising concepts is the supercritical water-cooled nuclear reactor (SCWR). The SCWR reactors has a very high steam outlet temperature [45].

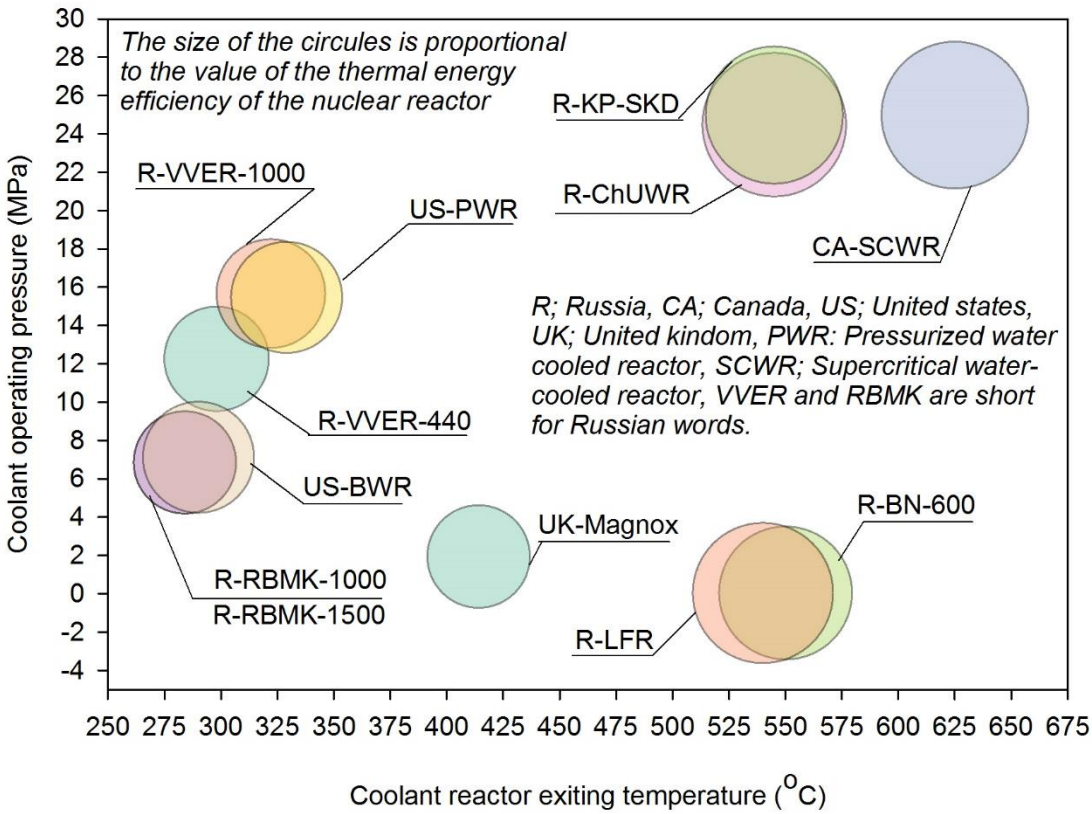

Figure 2.1 The popular nuclear reactor models based on the coolant temperature when exiting the reactor versus the coolant operating pressure, while it also present the thermal energy efficiency of the reactors (data from [45]).

One reason for coupling a Cu-Cl cycle with a SCWR rather than with a supercritical Rankine cycle where the produced energy is required in the H_2 form relates to efficiency, in that the efficiency for such a Cu-Cl cycle was reported by Orhan et al.[20,40,46] and Ratlamwala and Dincer [37] to range between 40.1% to 44.8%. However, the efficiency of a supercritical Rankine cycle with single reheat simulated by Al-Zareer et al. [47] was 36.2% and to produce hydrogen it has to be coupled with another system to convert electrical energy to hydrogen. This means that a supercritical Rankine cycle with a single reheat integrated with electrical energy to hydrogen conversion system will have an overall

energy efficiency less than 36.2%. Thus, the Cu-Cl cycle has a much higher energy efficiency of nearly 10% more when the end product that is required in the form of H_2.

2.4 Cu-Cl Hydrogen Producing Cycle

Hydrogen is abundant in nature; it accounts for 75% (mass basis) and 90% (by number of atoms) of the total matter in the universe [48]. On earth, an abundant amount of hydrogen exists connected to an oxygen atom in the form of water (H_2O) [49]. The chemical bond between a hydrogen atom and an oxygen atom in water requires 460 kJ/mol of thermal energy to break [15,50]. Hydrogen in the form of H_2 has the highest energy to mass density of any substance. But hydrogen is not readily available in nature in large amounts in the form of H_2. Hydrogen can serve as an energy storage medium and as an energy carrier. Many technologies are available for producing hydrogen from water, such as water electrolysis, thermal water decomposition, thermochemical water decomposition, and thermochemical and electrical water decomposition cycles. Water decomposition is a potentially attractive method for hydrogen production.

Hydrogen can be produced from nuclear energy either through electrolysis or thermochemical water decomposition or hybrid thermochemical water decomposition. Hybrid thermochemical and electrical water decomposition cycles have increased attention due to their lower temperature requirements compared to thermal water decomposition. Various types of hybrid thermochemical and electrical water decomposition cycles exist, and these are often differentiated based on the chemical compounds they employ and the number of steps in the cycle [14].

Investigations of hybrid thermochemical and electrical water decomposition cycles for hydrogen production have been reported, as have efforts to integrate them with other systems. One type of hybrid thermochemical and electrical water decomposition cycle uses magnesium and chlorine (the Mg-Cl cycle) [51,52]. Ozcan and Dincer [51,52] modeled and analyzed the performance of this cycle and investigated its thermal energy and electrical energy requirements. Ozcan and Dincer [52] found that the Mg-Cl cycle has energy and exergy efficiencies that allow it to compete with the other hybrid thermochemical and electrical water decomposition cycles. The Mg-Cl cycle has been integrated with a nuclear reactor, a Rankine cycle and a liquid hydrogen storage [53].

Energy and exergy analyses were performed of this integrated system and the energy and exergy efficiencies were found to be 18.6% and 31.4%, respectively [53]. An exergoeconomic analysis of the Mg-Cl cycle was also reported [54].

Another promising hybrid thermochemical and electrical water decomposition cycle is based on copper and chlorine compounds (the Cu-Cl cycle), particularly due to its relatively low-temperature requirements which permit it to be integrated with various thermal energy supply systems. Various Cu-Cl cycles exist, based on the number and type of steps comprising it [14]. Orhan, Dincer and Rosen examined the performance of several configurations of the Cu-Cl cycles with energy and exergy analyses [40,55]. The Cu-Cl cycle has also been evaluated using exergoeconomic analysis [56]. Furthermore, investigations have been reported on the integration of the Cu-Cl cycle with other hydrogen production processes [20,22,46]. The integration of the Cu-Cl cycle with nuclear plants that provide thermal energy has been examined [20,46], and the system energy and exergy efficiencies were found to be 45% and 10%, respectively [20]. In [20] integrated system a Cu-Cl cycle with five main steps is considered, while a four-step Cu-Cl cycle is examined in [57] integrated system. The various Cu-Cl cycles have been investigated extensively over the last decade, using energy, exergy, exergoeconomic, exergoenviromental, analyses, and other costing methods [10,12,13,16–22,37,39–41,43,44,46,55–65]. Nevertheless, more work is required on integrating these cycles into currently operating thermal and electrical energy producing systems to determine how well they perform after integration.

The copper-chlorine cycle has many versions which each differ in the number of steps in the cycle, and in the reactions in each step. There are in total 5 different configurations of the hybrid electrical and thermochemical water decomposition cycle [40]. The required thermal and electrical energies of the hybrid electrical and Cu-Cl cycle for water decomposition for different configurations and the required energy for electrolysis is shown in Figure 2.1. As shown in Figure 2.1 the equivalent electrical requirement of the all different configuration of the copper-chlorine cycle is nearly half of the required electrical energy from the electrolysis process. The less energy requirement with the convenience of direct water decomposition using thermal energy of the thermochemical hybrid water decomposition make it a very promising technology for a better energy future.

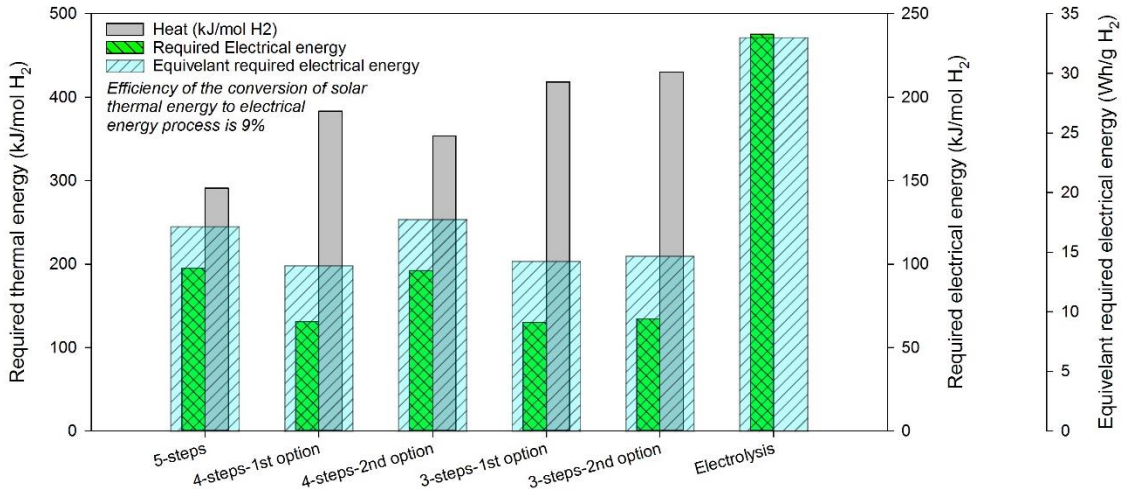

Figure 2.2 The comparison between five different Cu-Cl cycle configurations and the electrolysis process for hydrogen production based on the equivalent required electrical energy (if solar energy is used to produce the electrical power) [9,10,12-14].

Not many have studied the Cu-Cl cycle thermodynamically, and there is no clear overall presentation of the Cu-Cl cycle steam circuit. The steam circuit is the track or the flow behavior of the steam around, through and inside the reactors of the Cu-Cl cycle. Some researchers provided a heat exchanger network for transferring the required heat between the steam coming out of the nuclear reactor and the Cu-Cl cycle chemical reactors, such as [58]. However, in Ozbilen [58] work the steam mass flow rate and temperatures of the flowing steam per location for the entering and exiting flows is not clear.

Chapter 3: Systems Development

The integrated hydrogen production systems should produce electricity that at least covers the plant's internal electrical requirements, such as compressors, pumps, electrically driven reactors, control systems, lights, and emergencies. Hydrogen is not a source of energy; rather it is a clean energy carrier since it is carbon-free. Hydrogen possesses most of the advantages of fossil fuels [66]. However, large quantities of H_2 gas are not readily available in nature and must be produced.

3.1 Development of the Four Hydrogen Production Systems

The generated morphological chart shown in Figure 3.1 is used to develop the plant concepts. The morphological chart provides an easy way for generating alternative concepts by dividing the system into parts. For each part, there are different choices of subsystems; each of these choices perform a specified function and when these sub-functions operate together they fulfill a larger needed function. After formulating the morphological chart, the next step is to combine different alternatives with different integration methods, in order to try to formulate systems that are capable of performing the required overall function of the plant. The first step for developing the four hydrogen production plants that utilize the Cu-Cl cycle is to compare the different options for each subsystem.

The comparison is made based on criteria derived from the objectives and the requirements of this thesis. The first subsystem to be considered is the heat production system (the main subsystems are shown in Figure 1.2). The heat production system converts the energy from its source (coal, solar, nuclear) into a thermal form of energy. Figures 3.2-3.4 present the different options for nuclear reactors, fossil fuel based systems, and renewable energy systems, respectively, which are all options for the heat production system. Figure 3.2 shows a comparison between different types of nuclear reactors. The comparison is based on the reactor outlet temperature and the generation number of the nuclear reactor. The first and essential criterion for selecting the supercritical water-cooled nuclear reactor (SCWR) is the outlet temperature of the coolant exiting the reactor, which is 625°C, which is larger than the required maximum temperature of the thermochemical hybrid water decomposition cycle (Cu-Cl).

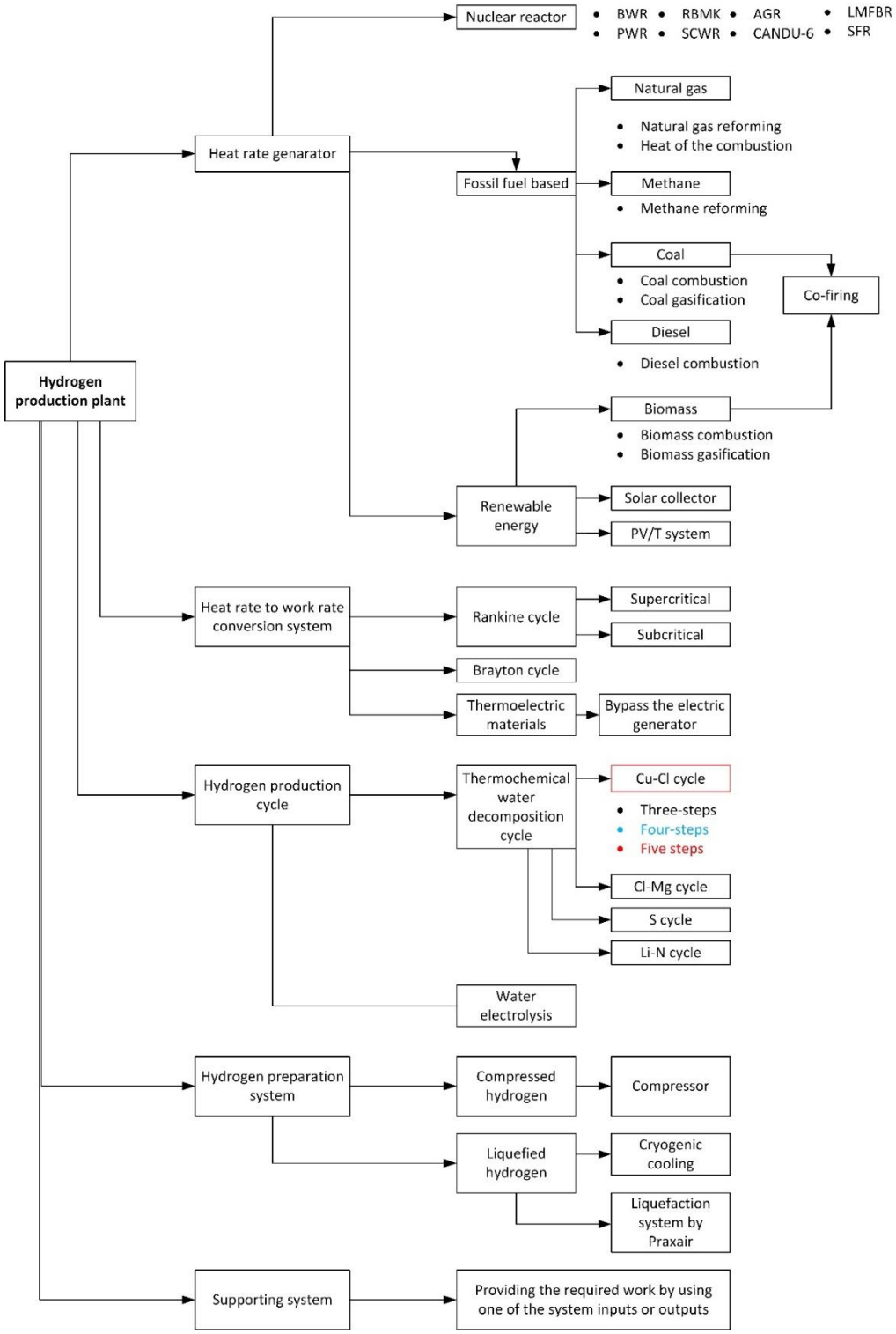

Figure 3.1 The morphological chart of a hydrogen production plant that utilizes the thermochemical hybrid water decomposition cycle which is a copper-chlorine cycle. BWR: Boiling water reactor; PWR: Pressurized water reactor; RBMK: Russian reactor; SCWR:

supercritical water-cooled nuclear reactor (Generation IV concept reactor); AGR: advanced gas cooled reactor; LMDBR: liquid-metal fast breeder reactors.

Another option is the advanced gas-cooled reactor (AGR), of which there is only one, in England. However, this type of reactor is no longer produced and is not a 4th generation reactor. Most of the considered nuclear reactors do not satisfy the minimum required temperature of 530°C for the Cu-Cl cycle. As shown in Figure 3.2, the nuclear reactor that makes a good candidate to be integrated into a hydrogen production plant for heat production is the SCWR. Advanced gas cooled reactors (AGR) have a high outlet temperature of 650°C. However, such reactors are now old and none are planned to be built in the future [32].

The second type of heat production system is the fossil fuel based system. Most (78% in 2016) of the energy consumed comes from fossil fuel based power production plants. Figure 3.2 shows a group of fossil fuels and different methods for extracting thermal energy out of them that are considered in this research. As shown in Figure 3.3, a comparison is made of the different types of fossil fuels and the heat extracting methods that are considered in this study. The comparison is based on the following considerations: whether the technology is usually used for hydrogen production; whether the technology is usually integrated with other systems in the literature; the variety of operating conditions of the technology; and the availability of the fossil fuel in nature. As also shown in Figure 3.3, coal gasification has most of the required specifications of the fossil fuel-based technology candidate to be integrated into a hydrogen production plant. Coal is the most abundant fossil fuel in the world [66]. From Figure 3.3, coal gasification is selected to be the heat generating system in the fossil fuel-based hydrogen plant. In this study, the third source of energy to be considered that will be responsible for producing heat is renewable energy. In fact, three renewable energy technologies are considered for producing the required heat in a hydrogen production plant. The comparison shown in Figure 3.4 is based on the specially selected criteria, which are: whether the technology is available in large sizes; the level of the technology life cycle carbon emissions; and the average capacity factor of the technology. Solar-based thermal energy production is selected for the renewable energy based hydrogen production plant. It is available on a large scale and has fewer life cycle carbon emissions than biomass based systems.

One of the main requirements of the hydrogen production plant is that the produced hydrogen is in a state by which it can be used in all hydrogen uses without the need to spend preparation energy. The ready to use hydrogen must be in a state such that it will not occupy large volumes since hydrogen is the gas with the lowest molecular weight.

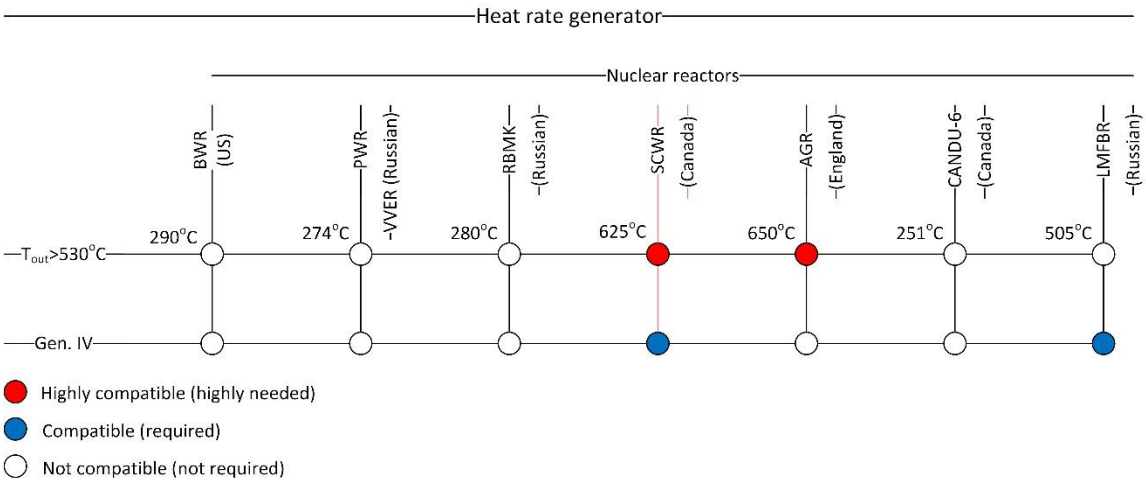

Figure 3.2 The comparison between the considered nuclear reactors. BWR: Boiling water reactor; PWR: Pressurized water reactor; RBMK: Russian reactor; SCWR: supercritical water-cooled reactor (Generation IV concept reactor); AGR: advanced gas cooled reactor; LMDBR: liquid-metal fast breeder reactors (data from [33]).

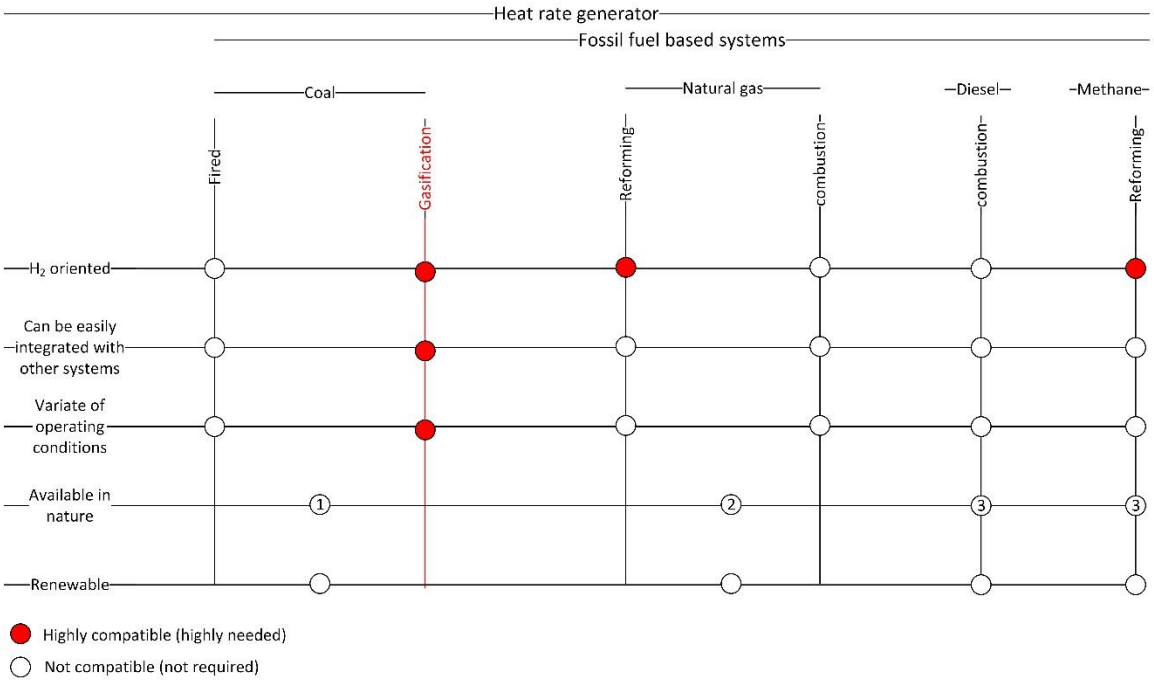

Figure 3.3 The comparison between the different fossil fuels; some of the methods used to extract from them are taken into consideration (data from [35]).

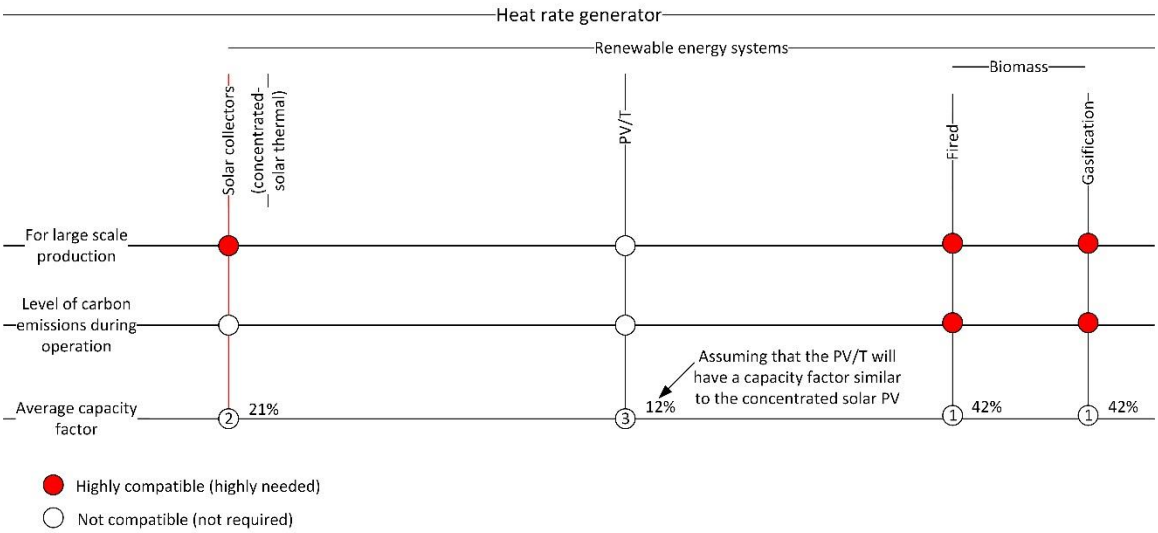

Figure 3.4 The comparison between the different renewable energy technologies to be used to produce the required heat by the hydrogen production plant (data from [69, 17]).

To increase the density, hydrogen must be compressed to very high pressures or converted into a liquid state. The technologies for increasing the density of hydrogen considered in this study are: compressing hydrogen in stages; cryogenic cooling of hydrogen; and the hydrogen liquefaction system invented by Praxair. The comparison of the three hydrogen preparation technologies is shown in Figure 3.5, where the comparison is very close between the three systems considered in this study under the selected criteria. However, the compression system scored highest, mainly because most of the hydrogen cars today use compressed hydrogen as their fuel. In addition, a compressed hydrogen storage tank will not require a very high thermal insulation; this may not be required at all in some countries. However, a very rigid tank is needed to withstand enormous pressure. Another advantage of producing compressed hydrogen is that part of the power used to compress the hydrogen in the plant can be retrieved during operation through a gas turbine if the hydrogen consuming system operates at lower pressure than that of the compressed hydrogen. Another advantage of compressed hydrogen is that since the storage tanks must be very rigid, the tank rigidity also offers protection to the hydrogen and an increase in storing and transporting safety. However, liquid hydrogen has a critical advantage over highly compressed hydrogen in that liquid hydrogen has a density nearly 1.6 times that of compressed hydrogen. The higher density of liquid hydrogen means that liquid hydrogen requires 1.6 times smaller containers to store the same mass of hydrogen.

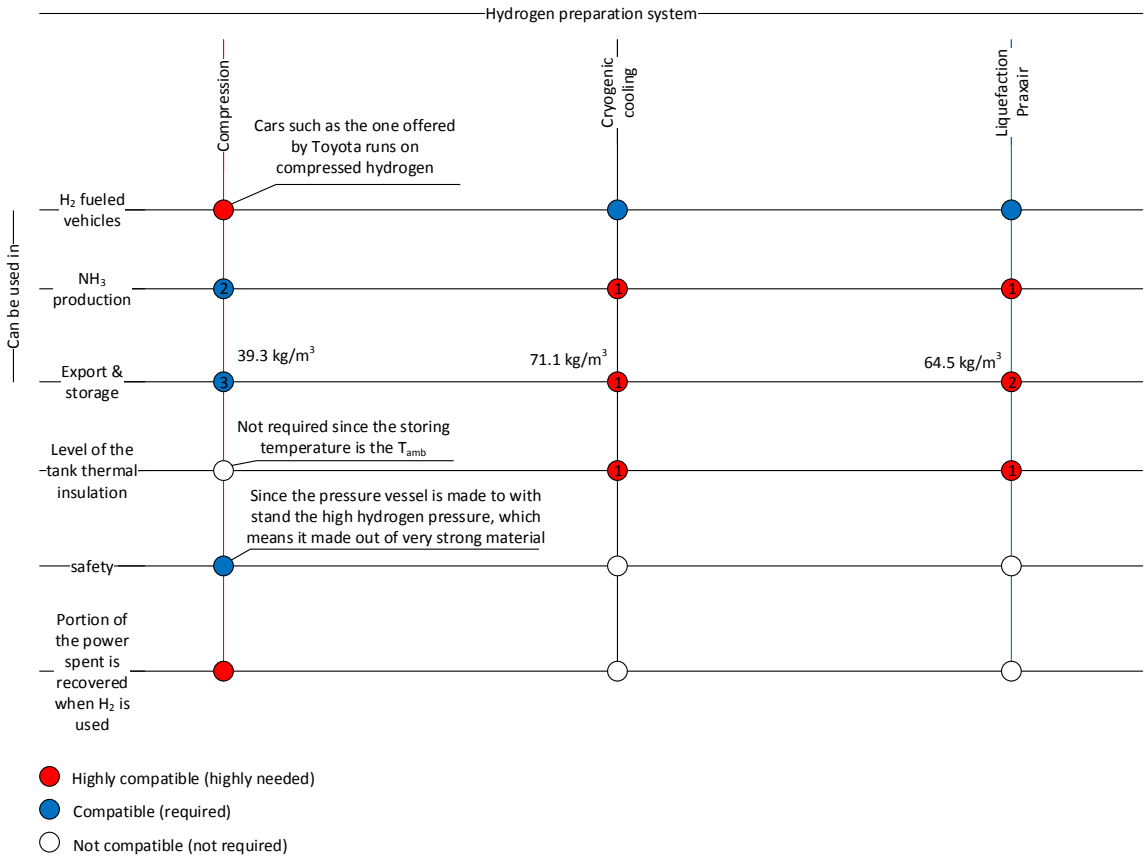

Figure 3.5 The comparison between the different hydrogen preparation technologies (data calculated based on 700 bar and 25°C for the compression system, 1 bar and saturated liquid for the results of the liquefaction systems using EES).

Finally, the supporting system can be Rankine cycle, if the heat obtained from the heat producing system is in the form of superheated steam. Alternatively, the supporting system can be a combined cycle if part of the produced hydrogen has to be combusted in order to fulfill the power needs of the hydrogen production plant.

After selecting at least one from each category of subsystems, the second step is to generate concepts for the hydrogen production plant.

3.1.1 Coal-Based Hydrogen Production Plant (System 1)

The first developed concept for a hydrogen production plant that utilizes a thermochemical hybrid water decomposition cycle and fed with a fossil fuel (coal) includes the following subsystems, which are based on the results of the comparisons previously performed:

- A heat production system, which is a coal gasification system with the following sub-systems:

a. a cryogenic air separation unit (CASU) for oxygen production.
b. a syngas turbine.
c. a water gas shift membrane reactor (WGSMR).
d. a syngas combustion chamber.
e. and a heat recovery steam generator (HRSG).

- A hybrid thermochemical and electrical water decomposition cycle.
  a. five-step copper-chlorine cycle (Cu-Cl cycle).
- A hydrogen preparation system:
  a. a four-stage hydrogen compression system consisting of multiple compression stages with intercoolers. The intercoolers generate steam for bottoming Rankine cycles, which reduce the overall power requirements of the compression system.
- A supporting system: a combined cycle, using a hydrogen fueled combustion chamber.
- A cooling tower for condensing the water.

The goal of System 1 is to produce high compressed hydrogen and generate power by integrating a coal gasifier that receives its gasification oxidant from a CASU, a WGSMR, a Brayton cycle, the thermochemical copper-chlorine cycle for thermochemical water decomposition to produce hydrogen and a hydrogen compression system. The proposed hydrogen production plant produces highly compressed hydrogen (700 bar) with only one input, which is the coal flow rate. One of the reasons behind proposing this hydrogen production plant is to provide an alternative for is currently used Rankine cycle. One alternative is the Cu-Cl cycle. The second reason for using the thermochemical water decomposition cycle is to directly produce hydrogen from heat, bypassing the electrical conversions in the middle when producing hydrogen from heat by electrolysis. The third reason is that the proposed plant can operate at a constant rate throughout the day, which produces hydrogen that is compressed and ready for storage. In addition, hydrogen is easier to store than electricity [67].

The Cu-Cl cycle is simulated in Aspen Plus software (Aspen Plus has the advantage of the ability to simulate solids, over other chemical simulation software, including Aspen

Hysys). Since the thermochemical copper-chlorine cycle contains materials in solid, liquid and gaseous states, Aspen Plus is a better tool for simulating the proposed hydrogen production plant and its main components, which are a copper-chlorine cycle and a coal gasifier. In the proposed hydrogen production plant, the copper-chlorine cycle receives the required heat from the Brayton cycle gas turbine hot exhausts. However, the required necessary electrical energy comes from the gas turbines and the generator in the cycle. The coal gasifier is based on an idealized model that is based on Gibbs free energy minimization approach. The model is validated with experimental results from Wen et al. [68]. After the gasification model is validated, and the hydrogen production plant is simulated on Aspen Plus, energy and exergy analysis is performed on the proposed hydrogen production plant.

Figure 3.6 shows an overall view of the proposed integrated system, and how the subsystems interact with each other. First, air enters the CASU where oxygen is separated from nitrogen. The CASU requires work rate for its compressors and with the help of the refrigerator unit, the CASU can separate oxygen from air in the distillation column. The refrigerator unit is crucial due to the very low condensation temperatures at which the distillation column is working. The coal gasification system consists of the pressurized entrained flow gasifier in which oxygen is the gasification oxidant, and steam is the gasification agent. The operating pressure of the gasifier is 24 atm. Type of coal fed to the gasifier is Illinois No.6 coal and its chemical analyses (including approximate and ultimate analysis), lower heating value (LHV), higher heating value (HHV) and specific exergy are provided in Table 3.1. The gasifier receives oxygen from the CASU and the steam from the steam generators located at different locations in the system that use the recovered heat to produce steam. The syngas exiting the gasifier goes to a gas turbine where its pressure is reduced to the optimum operating pressure of the WGSMR, based on the work of Augustine et al. [69], who reported that the optimum operating pressure and temperature for the WGSMR to achieve 98.2% carbon monoxide conversion, and 81.2% hydrogen recovery, are 14.4 bar and 450°C, respectively. Also, the pressure of the captured hydrogen (the retentate) is around 1 bar, with purity of 99.999% [69]. After the syngas pressure reduction in the gas turbine, the syngas is sent to a heat exchanger to cool the syngas to the optimum operating temperature of the WGSMR of 450°C [69].

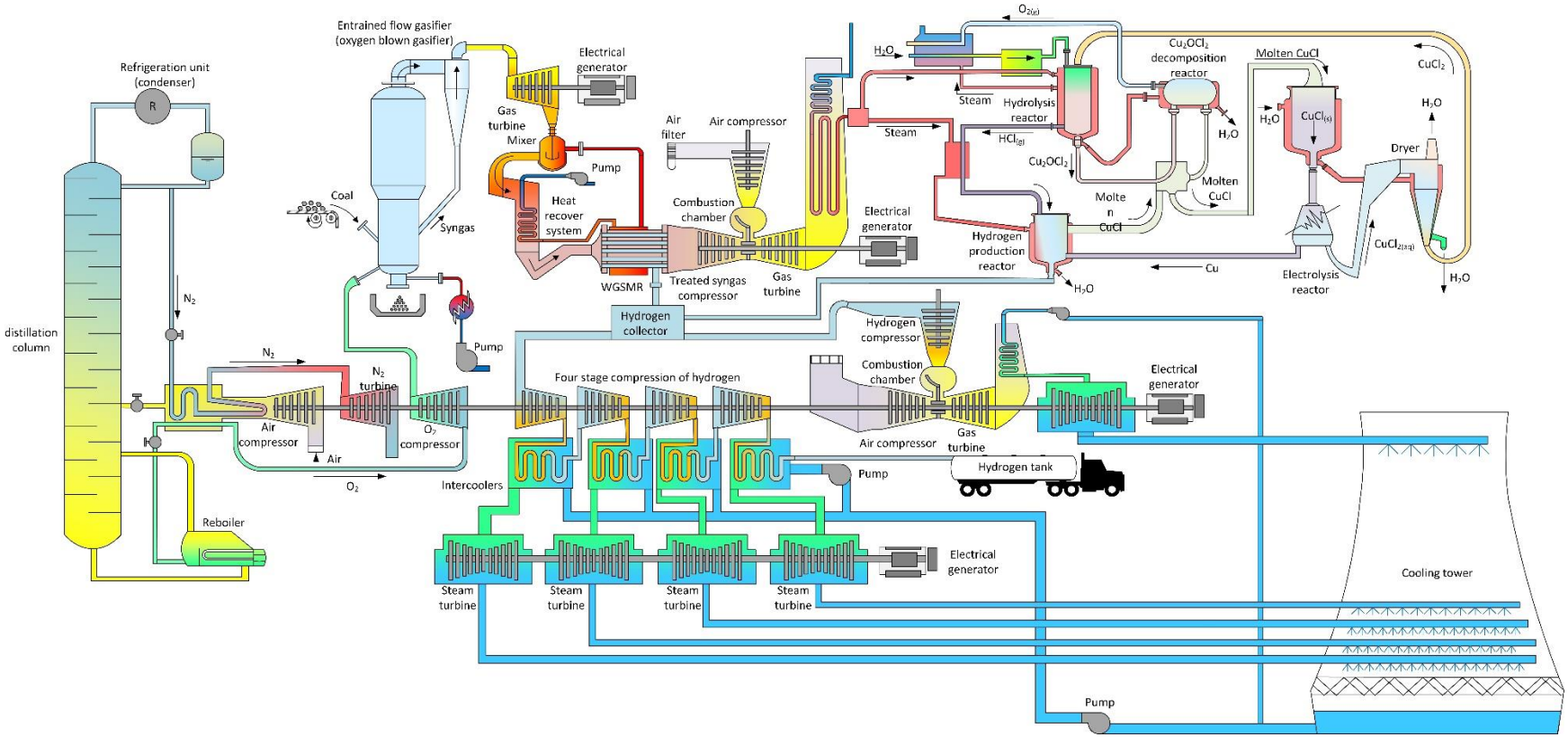

Figure 3.6 The schematic diagram of System 1 for hydrogen production that utilizes the thermochemical hybrid water decomposition cycle, which the copper-chlorine cycle. The overall system and its main components of coal gasifier, Brayton cycle, WGSMR, HRSG, CASU, and copper-chlorine five steps cycle. Material inputs are air, coal and water.

On the other side of the heat exchanger, steam is produced. The cooled syngas, mixed with saturated steam, then enters the WGSMR.

Table 3.1 The properties of Illinois No.6 coal fed to the gasifier in System 1.

		Illinois #6 [68]		
		Wet basis (wt.%)	Dry basis (wt.%)	Dry and ash free basis (wt.%)
Proximate analysis	Moisture	0.20	0.00	0.00
	Fixed carbon	58.01	58.01	68.68
	Volatile matter	26.46	26.46	31.32
	Ash	15.53	15.53	0.00
Ultimate analysis	C	73.90	74.05	87.66
	H	6.24	6.25	7.40
	N	0.71	0.71	0.84
	Cl	0.37	0.37	0.44
	S	1.77	1.77	2.10
	O	1.32	1.32	1.56
	Ash	15.53	15.53	0.00
Sulfur analysis	Pyritic	0.59	0.59	0.70
	Sulfate	0.59	0.59	0.70
	Organic	0.59	0.59	0.70
HV	HHV (MJ/kg)	25.35	29.14	33.35
	LHV (MJ/kg)	24.12	27.10	32.50
Exergy	Specific exergy (MJ/kg)		29.00	34.50

The treated syngas exiting the WGSMR enters a compressor where its pressure increases to the operating pressure of the 2300 kPa. Air is also compressed to provide the required oxygen to the combustion reaction. Both the compressed air and the compressed treated syngas enter the combustion chamber. The pressure of the combustion chamber is 2300 kPa, with the assumption that no heat losses occur in the combustion chamber. The combustion products exiting the combustion chamber are sent to a gas turbine, then to the HRSG. The produced steam is used to provide the necessary heat to the copper-chlorine cycle, which is a five step thermochemical cycle for water decomposition with a maximum temperature around 530°C [17]. The copper-chlorine cycle has a step that requires electricity which is provided to it by the gas turbines in the plant generators. Each subsystem simulation flowsheet is provided through the discussion of the model development of each of these subsystems.

The Gibbs free energy minimization approach based model (GFEMA based model) consists of two reactors when it is modeled in Aspen Plus software, as seen in Figure 3.8 (Aspen Plus flow sheet of GFEMA based mode). Before building the model, coal has to be defined to Aspen Plus as a nonconventional solid (NC), based on its chemical composition (see Table 4.1).

The GFEMA based model consists of two Aspen Plus reactors. The first reactor in the GFEMA based model is a yield reactor (the mole or mass fraction of the product should be specified). In the GFEMA based model, the yield reactor decomposes the coal to its primary elements, which are based on the coal ultimate wet chemical analysis, which is presented in Table 3.1 for Illinois No.6 (converting NC material to conventional material). The second reactor in the GFEMA based model is a Gibbs reactor (the reaction should be based on the GFEMA), where the reaction that takes place in that reactor depends on minimizing Gibbs free energy. To validate the GFEMA based model, the syngas molar fraction of its main chemical species is compared with the experimental data from the literature [68]. The syngas exiting the GFEMA based model and the experimental data for the Illinois No.6 coal are presented in Table 3.2, where the molar fraction of the main chemical species in the raw syngas, which are CO, H_2, and CO_2, are compared between the GFEMA based model results and the experimental data of the gasification process from the literature [68]. This is for Illinois No.6 coal. The difference in the carbon monoxide mole fraction in the syngas exiting the gasifier between the GFEMA based model and the experimental results [68] was 4.1%, for hydrogen 6.5%, and for carbon dioxide 5.1 %.

Table 3.2 The comparison between the results of the Gibbs-based model and the experimental data from literature. The comparison is based on the mole fraction of CO, H_2, and CO_2 species.

Components	Mole fraction (dry basis) Gibbs free energy model	Mole fraction (dry basis) Experiment [17]	Gibbs-based model % error
CO	0.552	0.576	-4.1
H_2	0.366	0.391	-6.5
CO_2	0.028	0.030	-5.1

Since the GFEMA based model exhibited a highest difference of 6.5% with experimental values, it can be used with reasonable accuracy to simulate coals for which

experimental data are lacking. From here on, the GFEMA based model is used due to its flexibility and accuracy. The main chemical reactions that occur in the gasification process are presented in the next section.

Gasification starts with coal pyrolysis. In the pyrolysis reaction, coal is broken into char and volatile matter. Volatile matter, which includes moisture and tar, is presented by C_6H_6. The pyrolysis reaction is written as follows:

$$\text{Coal} \rightarrow \text{Char} + (CO + H_2 + H_2O + CO_2 + CH_4 + H_2S + N_2 + C_6H_6) \quad (3.1)$$

After the pyrolysis reaction, the combustion of the volatile matter is performed based on the following reaction equations:

$$C_6H_6 + 7.5O_2 \rightarrow 6CO_2 + 3H_2O \quad (3.2)$$

$$H_2 + 0.5O_2 \rightarrow H_2O \quad (3.3)$$

$$CO + 0.5O_2 \rightarrow CO_2 \quad (3.4)$$

$$CH_4 + 2O_2 \rightarrow CO_2 + 2H_2O \quad (3.5)$$

However, the char is decomposed. The decomposition of char is based on the following equation:

$$\text{Char} \rightarrow C + H_2 + O_2 + N_2 + S + ASH \quad (3.6)$$

The results of the char decomposition reaction (Equation (3.6)), the results of the volatile combustion reactions, the gasification oxidant, and the gasification agent react based on the following equations:

$$C + O_2 \rightarrow CO_2 \quad (3.7)$$

$$C + 0.5O_2 \rightarrow CO \quad (3.8)$$

$$C + H_2O \rightarrow CO + H_2 \quad (3.9)$$

$$C + CO_2 \rightarrow 2CO \quad (3.10)$$

$$C + 2H_2 \rightarrow CH_4 \quad (3.11)$$

$$S + H_2 \rightarrow H_2S \quad (3.12)$$

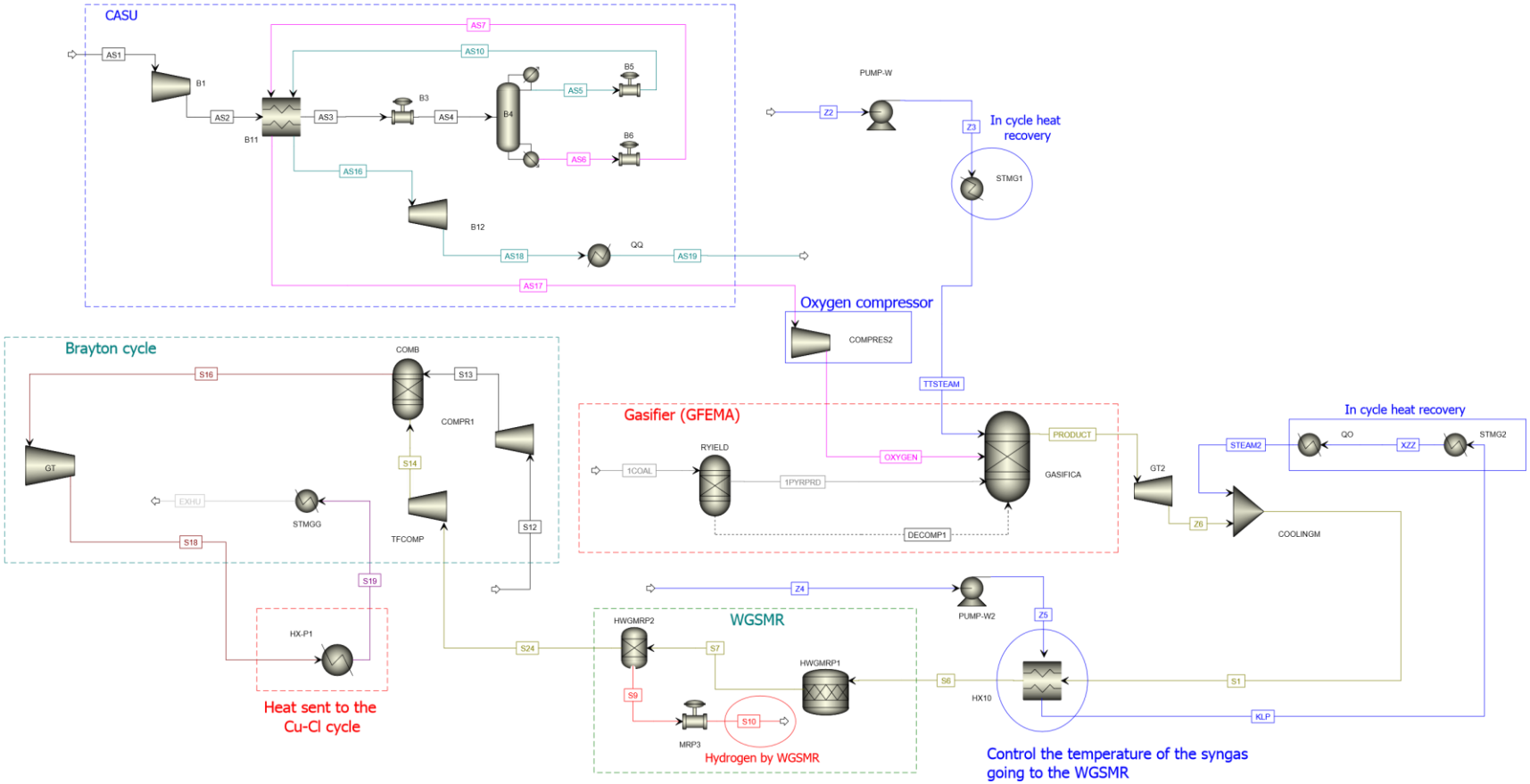

Figure 3.7 The Aspen Plus flow sheet for modeling and simulation of the gasifier (GFEMA model), CASU, Brayton cycle, WGSMR and heat exchangers plus other utilities

$$CO + H_2O \rightarrow CO_2 + H_2 \quad (3.13)$$

$$CH_4 + H_2O \rightarrow CO_2 + 3H_2 \quad (3.14)$$

The results of Equations (3.7-3.14) present the raw syngas exiting the gasifier, where the syngas is presented in the stream product in Figure 3.8.

The CASU is the system which is responsible for providing the O_2 to the gasifier. Shown in Figure 3.8 is the Aspen Plus flow sheet of the CASU, which produces O_2 with purity more than 95%. First, the air is compressed in compressor B1 (see Figure 3.8) to 8 atm, after which goes to the heat exchanger B11 where the compressed air exchanges heat with the separated O_2 and N_2 to a very low temperature of -146°C. The cooled compressed air is then throttled to a pressure of 5 atm and sent to the distillation column B4 (see Figure 3.8). The operating pressure of the distillation column is 5 atm. The gas separated at the condenser of the distillation column is N_2, and that at the boiler is O_2. Since the condenser operating temperature is -179°C, a refrigerator unit is used to keep the required cold temperature in order for condensation to take place. Both of the separated O_2 and N_2 are then sent to the heat exchanger B11 to cool the compressed air. The N_2 takes most of the heat from the compressed air and the hot compressed N_2 gas is then sent to a turbine B12. The N_2 exiting the B12 turbine is used to preheat water before going to the steam generators.

The unit responsible for both the shift reaction of the syngas exiting the gasifier, and for capturing and separating the hydrogen produced in the shift reaction, is the WGSMR. The optimum operating parameters of the WGSMR are adopted from the work of Augustine et al. [69]. The parameters of the WGSMR are presented in Table 3.3. The water gas shift reaction is represented as follows:

$$CO(g) + H_2O(g) \rightarrow CO_2(g) + H_2(g) \quad (15)$$

Since the water gas shift reaction is an exothermic reaction, continuous removal of heat is required to maintain the WGSMR operating at the optimum temperature. Water is used to absorb the WGSMR heat and maintain it at the optimum operating temperature. The water used to absorb the WGSMR heat is then heated and mixed with the syngas exiting the gasifier. The shifted syngas exiting the WGSMR is compressed and combusted

in a Gibbs free energy minimization approach reactor COMB (see Figure 3.8). The hot combustion gases leaving the combustion chamber (COMB in Figure 3.8) enter a gas turbine GT. The gas turbine GT hot exhausts go to the heat recovery steam generator that produces the steam that will be used to provide the needed heat to the copper-chlorine cycle.

The modeling and the working principle of the new copper-chlorine five step cycle configuration are next provided. The copper-chlorine thermochemical cycle decomposes water through a thermochemical process to hydrogen and oxygen by low-temperature heat relative to the required temperature of the thermal decomposition of the water. There are many copper-chlorine cycle configurations in the literature [20], but the copper-chlorine cycle configuration chosen in this research is the five step copper-chlorine cycle, the main chemical reactions of which are shown in Table 3.4.

Table 3.3 The main input parameters for the gasification system consisting of gasifier GFEMA model for the gasifier, CASU, WGSMR and Brayton cycle plus other system utilizations.

Unit	Main parameters
Gasifier	• Operating pressure is 24.0 atm • Gasification agent is steam, which is at 420ºC • Gasification oxidant is oxygen, which is at 490ºC • Steam to fuel ratio (mass basis) = 0.893 • Oxygen to fuel ratio (mass basis) = 0.241

The syngas exiting the gasifier (stream product in Figure 3.8)	• Temperature of the syngas is 1,215ºC
	• Chemical composition (mole basis):
	  ○ 0.000 for O_2
	  ○ 0.550 for CO
	  ○ 0.367 for H_2
	  ○ 0.024 for CO_2
	  ○ 0.043 for H_2O
	  ○ 0.004 for H_2S
	  ○ 0.012 for N_2
	  ○ 0.002 for CH_4

Syngas cooling unit	• Cooling water is at pressure of 14.4 bar and temperature 260ºC • Direct mixing chamber • Cooling water to syngas ratio (mass basis) is equal to 0.730
CASU	• Air at ambient condition is fed to CASU • Maximum pressure in CASU is 8.0 atm (exiting O_2 in compressed to gasifier operating pressure) • Separation method: distillation column

	• Gas turbine reduces pressure of exiting N_2 • Condenser refrigerator COP is 2.0 (to remove heat so condensing fluid can condense at a very low temperature of -179°C)
WGSMR	• Operating pressure is equal to 14.4 bar [69] • Operating temperature is equal to 450°C [69] • CO conversion percentage is equal to 98.2% [69] • H_2 capture percentage is equal to 81.2% [69] • H_2 recovered pressure is equal to 1 bar [69]
Brayton cycle	• Syngas combustion chamber operating pressure: 2300 kPa • Discharge pressure = 1.2 atm
HSC	• Compression ratio of the first three compression stages is 5 • Hydrogen final pressure is 700 bar [31] • Compressed hydrogen final temperature is 25°C, cooled down after the last compression stage
HFCC	• Compression ratio of the hydrogen and the air compressors is 36 • Combustion chamber operating pressure is 36 atm • Maximum pressure in the Rankine cycle is 200 bar
Cu-Cl	• For copper-chlorine cycle, check Table 4.4

The reactions in Table 3.4 are described in more detailed next. The equations in the Table 3.4 are the reactions of the five step copper-chlorine cycle. The methodology and the process of modeling the five step copper-chlorine cycle in Aspen Plus is then introduced.

Table 3.4 The five steps in the copper-chlorine cycle with their corresponding reactions and operating conditions.

Step	Chemical reaction	Temperature range (°C)
1	$H_2O(g) + 2CuCl_2(s) \rightarrow Cu_2OCl_2(s) + 2HCl(g)$	375-400
2	$Cu_2OCl_2(s) \rightarrow \frac{1}{2}O_2(g) + 2CuCl(l)$	500-530
3	$4CuCl(aq) \rightarrow 2Cu(s) + 2CuCl_2(aq)$	30-80
4	$CuCl_2(aq) \rightarrow CuCl_2(s)$	>100
5	$2Cu(s) + 2HCl(g) \rightarrow 2CuCl(l) + H_2(g)$	430-475

Source: [17,40]

The first reaction in the five step copper-chlorine cycle is the hydrolysis reaction, which is the first reaction in Table 3.4. In the hydrolysis reactor, superheated steam combines with cupric chloride ($CuCl_2$) to form copper oxychloride (Cu_2OCl_2) and hydrochloric acid (HCl) [17]. The hydrolysis reaction must take place at a temperature between 325-375°C [17], and since the reaction is an endothermic reaction, heat must be supplied to maintain the reactants at a temperature between 325-375°C [17]. Wang et al. [12] suggested conducting the endothermic hydrolysis reaction by providing the reactor

with superheated steam at 400°C with more steam than that required by the balanced reaction. The excess steam will drive the chemical reaction in the direction of the product due to the increase in concentration of one of the reactants. It will also supply the required reaction heat.

The second reaction in the five step copper-chlorine cycle is the thermal decomposition of copper oxychloride to oxygen gas and a molten salt of cuprous chloride (CuCl), as shown in the second step in Table 3.4. The thermal decomposition of Cu_2OCl_2 is an endothermic process, and the reaction temperature must be maintained at 530°C. A method for supplying the reaction heat to retain the temperature of the reaction at 530°C was suggested by Naterer et al. [13], who proposed that the reaction heat can be supplied by a loop of molten salt that is heated by steam in a direct contact heat exchanger and then re-introduced into the chemical reactor. In the chemical reactor, the molten salt gives the heat to the reaction, which results in producing oxygen gas and additional molten CuCl. During the decomposition, there is an intermediate step where copper oxychloride decomposes to form a crystalline structure of cupric oxide and cupric chloride ($CuO \times CuCl_2$). The decomposition of Cu_2OCl_2 into ($CuO \times CuCl_2$) occurs at 500°C and then ($CuO \times CuCl_2$) decomposes into O_2 gas and CuCl molten salt at 530°C [17].

The third step in the five step copper-chlorine cycle is the electrolysis step, where cupric chloride ($CuCl_2$) is reproduced electrochemically, as shown in Table 3.4. In the electrolysis reactor, cupric chloride and solid copper are extracted electrochemically from solid cuprous chloride (CuCl). The produced cupric chloride from the electrolysis reactor is in an aqueous form($CuCl_2 \times 2H_2O$), which is dried to reproduce the solid cupric chloride ($CuCl_2$). Zamfirescu et al. [17] reported that the electrolysis step requires nearly 63 kJ/mol H_2 of electrical power. In the drying step, all of the water in the aqueous material $CuCl_2 \times 2H_2O$ is removed, and the solid $CuCl_2$ is returned to step 1 to complete half of the cycle whereas the other half is with the solid copper and the hydrochloric acid (HCl).

The second reactor where cuprous chloride (CuCl) is produced is in the hydrogen production reactor. Here, copper from the electrolysis reactor is combined with hydrochloric acid (HCl) to produce cuprous chloride (CuCl) and hydrogen. The hydrogen production reaction is exothermic, hence there is a heat that should be extracted from the

reaction to maintain the reaction at a temperature of 450°C [17]. However, at 450°C, the hydrogen production reaction based on the Gibbs free energy minimization approach, 52.5% from the reactants are converted to products. However nearly 99% of the reactants are converted to products at the reaction temperature of 100°C. It should be noted that, for both cases, the temperature of the reactant supply for the reactor is 500°C. Even in the light of the former cases, the reaction temperature is kept at 450°C so that it can produce molten CuCl (the melting temperature of CuCl is 436°C). To have 100% conversion of the reactants at a reaction temperature of 450°C, extra heat has to be provided to the reactor.

After providing a description of the reactions of the five step copper-chlorine cycle, the next section discusses the building of the copper-chlorine cycle model on Aspen Plus. The first step in modeling the five step Cu-Cl cycle in Aspen Plus is entering the solid phase properties of the materials in the Cu-Cl cycle. The second issue that must be taken care of is the phase changes from solid phase to either liquid or gas phase, or vice versa, of the conventional solid components that are defined by the user. These phase changes must be completed manually through any reactor, but the product must be limited to the same material but in the resulting phase (the phase change reactor). However, in the case of a solid material that Aspen Plus has its data in a solid phase such as Cu, then there is no need for the phase change reactor.

In this model, a stoichiometric reactor is used to change the phase from solid to liquid or from liquid to solid. Properties and correlations of copper oxychloride (Cu_2OCl_2), cupric oxide (CuO), cupric chloride ($CuCl_2$) and cuprous chloride (CuCl) that were entered in the Aspen Plus model, are provided in Tables 3.5-3.8, respectively. Copper oxychloride properties and correlations, as presented in Table 3.5, are only for the solid phase since the Cu_2OCl_2 is present solitary throughout the copper-chlorine cycle. Shown in Figure 3.9 is the Aspen Plus model of the copper-chlorine cycle for thermochemical water decomposition for large-scale hydrogen production.

The novelty of the developed model of the copper-chlorine cycle in this thesis lies in the more practical system configuration than other copper-chlorine cycle models that were published, and in considering the latest development in the research on the copper-chlorine cycle. Based on the work of Wang et al. [12] as mentioned earlier and based on

the Gibbs free energy minimization approach, eight times more superheated steam than that required for the hydrolysis reaction balanced chemical equation is provided through stream S2 (see Figure 3.9) for the hydrolysis reactor B3, as seen in Figure 3.9. The part that goes to the copper-chlorine cycle of the steam produced by the HRSG is not directly used; rather it is used to provide only the required heat. The water in stream S2 (see Figure 3.9) enters the system at ambient conditions and is then preheated by the excess steam exiting the hydrolysis reactor S23 and the produced O_2 S11 from the Cu_2OCl_2 thermal decomposition reactor B6. The heat exchange is conducted through heat exchanger B15 in Figure 3.9.

Table 3.5 The copper oxychloride (Cu_2OCl_2, melanothallite) properties and correlations used in the developed copper-chlorine cycle Aspen Plus simulation model, for temperature range of 298-675 K and at 1 atm.

Parameter	Value or correlation*	Reference
Molecule formation	$\Delta_f H^o = -384.65 \pm 2.5 kJ/mol$; $\Delta_f S^o = 154.352 J/molK$; $\Delta_f G^o = -369.7 kJ/mol$; $\log k_f = 64.75$; $ex_{ch} = 21.08\ kJ/mol$; $c_p^o = 116.77\ kJ/kmol.K$; $T_o = 298.15\ K$ and $P_o = 1\ atm$	[17,70]
$c_p, kJ/kmolK$	$a + bT + cT^2 + dT^3$; $a = 53.7166572$; $b = 0.334033497$; $c = -5.22127940 \times 10^{-4}$; $d = 2.99950910 \times 10^{-7}$	[17]
$s, J/molK$	$a + b\ln(T) + cT + dT^2 + eT^3$; $a = 154.352$; $b = 53.7166572$: $c = 0.334033497$; $d = -0.2610639700 \times 10^{-3}$	[17]
$ex, J/mol$	$a + bT + cT^2 + dT^3 + eT^4 + f\ln(T)$; $a = 0.358948789 \times 10^5$; $b = -45.87542993$; $c = 0.2448529712$; $d = -0.2038527680 \times 10^{-3}$, $e = 1.3589 \times 10^5$, $f = -16015.62134$	[17]

* If the correlation model (i.e. $aT+bT^2$…etc, how the equation is organized) is not available in Aspen Plus, produce an Excel table of T vs "variable" and enter the data in Aspen Plus.

Table 3.6 The cupric oxide (CuO, tenorite) properties and correlations used in the developed copper-chlorine cycle Aspen Plus simulation model, for temperature range of 298-675 K and at 1 atm.

Parameter	Value or correlation*	Reference
Molecule formation	$\Delta_f H^o = -156 \pm 2.1 kJ/mol$; $\Delta_f S^o = 42.59 \pm 0.4 J/molK$; $\Delta_f G^o = -128.292 kJ/mol$; $\log k_f = 22.48$; $ex_{ch} =$	[17,71]

	$6.268\ \mathrm{kJ/mol}$; $c_p^o = 42.18\ \mathrm{kJ/kmol.K}$; $T_o = 298.15\ \mathrm{K}$ and $P_o = 1\ \mathrm{atm}$	
c_p, kJ/kmolK	$a + bT + cT^2 + dT^3 + eT^{-2}; a = 52.465081, b = -0.0145802613, c = 4.51372247 \times 10^{-5}, d = -2.91900324 \times 10^{-8};\ e = -816{,}025.22$ with $\mathrm{error}_{-0.1}^{+0.05}$kJ/kmolK	[17]
s, J/molK	$a + bT + cT^2 + dT^3 + e\ln(T) + fT^{-2}; a = -258.3259972;\ b = -0.0145802613;\ c = 2.256861235 \times 10^{-5}$: $d = -9.730010800 \times 10^{-9};\ e = 52.465081;\ f = 4.0801261 \times 10^5$	[17]
ex, J/mol	$a + bT + cT^2 + dT^3 + eT^4 + fT^{-1} + gT^{-2} + h\ln(T)\,; a = 77{,}913.62262;\ b = 56.81218591;\ c = -0.01401896242;\ d = 0.1794674429 \times 10^{-4};\ e = -7.297508100 \times 10^{-9};\ f = 8.160252200 \times 10$	[17]

* If the correlation model (i.e. $aT+bT^2$…etc, how the equation is organized) is not available in Aspen Plus, produce an Excel table of T vs "variable" and enter the data in Aspen Plus.

Table 3.7 The cuprous chloride (CuCl, nantokite) properties and correlations used in the developed copper-chlorine cycle Aspen Plus simulation model, for temperature range of 298-1000 K and at 1 atm.

Parameter	Value or correlation*						Reference
Melting point	Reported value at 436°C						[72]
Normal boiling point	Boiling starts when the temperature is 1221.85°C						[71]
Vapor pressure	The vapor pressure at the triple point is 10.19 Pa						[73,74]
	T (K)	732.15	816.15	948.15	1,187.15	1,750.15	
	P (Pa)	10	100	1,000	10,000	100,000	
Molecule formation	$\Delta_f H^o = -136.816\mathrm{kJ/mol}$; $\Delta_f S^o = 87.446\mathrm{J/molK}$; $\Delta_f G^o = -199.44\mathrm{kJ/mol}$; $\log k_f = 21.02$; $ex_{ch} = 75.0\mathrm{kJ/mol}$; $c_p^o = 53.34\mathrm{kJ/kmol.K}$; $T_o = 298.15\ \mathrm{K}$ and $P_o = 1\ \mathrm{atm}$						[17,71]
c_p, kJ/kmolK	T=298-683 K	$a + bT + cT^{-2}; a = 51.087;\ b = 17.656 \times 10^{-3};\ c = 268 \times 10^3$					[72]
s, J/molK	T=298-683 K	$a + b\ln(T) + cT + dT^{-2}; a = -210.3986829, b = 51.087;\ c = 0.017656;\ d = 1.34 \times 10^5$					[17]
ex, J/mol	T=298-683 K	$a + bT + cT^2 + dT^{-1} + eT^{-2} + f\ln(T)\,;\ a = 191{,}327.176;\ b = 45.823;\ c = 0.008828;\ d = 268{,}000; e = 3.9952 \times 10^7; f = -15{,}231.589$					[17]

* If the correlation model (i.e. $aT+bT^2$…etc, how the equation is organized) is not available in Aspen Plus, produce an Excel table of T vs "variable" and enter the data in Aspen Plus.

Stream S2 exits the heat exchanger B15 through stream S17, which is then heated to the required input temperature of 400°C by the steam from the HRSG. Steam from the HRSG is also used to heat the $CuCl_2$ from 347°C for S1 (which is the same as S37, but they are disconnected in the Aspen Plus to avoid long computational time) to 350°C for S3. Streams S3 and S4 enter the hydrolysis reactor B3, which is an isothermal reactor operating at a constant temperature of 325°C. The extra heat required by reactor B3 is provided by the steam produced from the HRSG. The results of the hydrolysis reaction exit reactor B3 in stream S5, as shown in Figure 3.9. Separator B4 separates the results of the hydrolysis reactor S5. Separator B4 separates S5 to S6 (Cu_2OCl_2) and S7 (HCl and excess H_2O). Separator B16 separates S7 to S24 (HCl) and S23 (excess H_2O at 325°C). The produced CuCl S10 heats stream S6 carrying Cu_2OCl_2 from the copper oxychloride decomposition reactor B6 in the heat exchanger B21. It should be noted that CuCl (stream S36) exits the heat exchanger B21 at 437°C, which is higher than the melting/solidification temperature 436°C of the CuCl since the heat exchanger B21 is a liquid-liquid heat exchanger.

Table 3.8 The cupric chloride ($CuCl_2$, tolbachite) properties and correlations used in the developed copper-chlorine cycle Aspen Plus simulation model, for temperature range of 298-1,000 K and at 1 atm.

Parameter	Value or correlation*		Reference
Melting point	Reported value at 498°C		[74]
Normal boiling point	Boiling starts when the temperature is 993°C		[74]
Decomposition	Melting is accompanied by decomposition in Cu_2Cl_2 at 993°C		Perry et al. [74]
Molecule formation	$\Delta_f H^o = -218.0 \text{kJ/mol}$; $\Delta_f S^o = 108.07 \text{J/molK}$; $\Delta_f G^o = -173.826 \text{kJ/mol}$; $\log k_f = 30.453$; $ex_{ch} = 82.474 \text{ kJ/mol}$; $c_p^o = 71.88 \text{ kJ/kmolK}$; $T_o = 298.15 \text{ K}$ and $P_o = 1 \text{ atm}$		[17,73]
c_p, kJ/kmolK	T=298-675 K, crystal I	$a + bT + cT^2 + dT^3 + eT^4 + fT^5$, $a = -16.3596145$; $b = 0.750699416$, $c = -2.56737967 \times 10^{-3}$; $d = 4.62107127 \times 10^{-6}$; $e = -4.34415987 \times 10^{-9}$; $f = 1.57231698 \times 10^{-12}$	[17]
	675-871 K, crystal II	82.4	
	For the liquid phase, Aspen Plus library has the required data		

$s, J/molK$	T=298-675 K, crystal I	$a + bT + cT^2 + dT^3 + eT^4 + fT^5 + g\ln(T)$; $a = 58.38957705, b = 0.750699416$; $c = -1.283689835 \times 10^{-3}$; $d = 1.54035709 \times 10^{-6}$; $e = -1.061039968 \times 10^{-9}$; $f = 3.14463396 \times 10^{-13}$; $g = -16.3596145$	[17]
	T=675-871 K, crystal II	$172.2201546 + 82.4\ln(T/675)$	
	For the liquid phase, Aspen Plus library has the required data		
$ex, J/mol$	$a + bT + cT^2 + d\ln(T)$		[17]
	T=298-675 K	$a = 1.850096 \times 10^5$; $b = 68.091341$; $c = 0.69649 \times 10^{-2}$; $d = -21{,}667.1954$	
	T=675-871 K	$a = 1.978071674$; $b = 82.4$; $c = 1.835569 \times 10^{-9}$; $d = -24{,}567.55627$	
	T=871-1,130.75 K	$a = 2.278675157$; $b = 100$; $c = -6.751777 \times 10^{-9}$; $d = -29815.02$	

* If the correlation model (i.e. $aT+bT^2$…etc, how the equation is organized) is not available in Aspen Plus, produce an Excel table of T vs "variable" and enter the data in Aspen Plus.

The stream S6 exits the heat exchanger B21 through stream S31. This is heated by the steam produced by the HRSG in the heat exchanger B5 to 530°C, which is stream S8. Cu_2OCl_2 enters the copper oxychloride decomposition reactor B6, which is an isothermal reactor kept at 530°C. The copper oxychloride decomposition reaction is an endothermic reaction, which means a continuous supply of heat to the reactor B6 is required to maintain the reactor temperature at 530°C. The products of the copper oxychloride decomposition reactor are oxygen gas and molten CuCl. The molten CuCl is separated from the oxygen gas through a liquid gas separator B7. Stream S11 exiting the B7 separator carries the oxygen gas and stream S10 carries the molten CuCl. The molten CuCl is sent to the phase change reactor B8 to conduct the phase change from liquid to solid since, as mentioned earlier, the phase change between solid and liquid must be manually performed in Aspen Plus V8.8. The solid CuCl exiting the phase change reactor B8 (stream S30) enters the heat exchanger B22 to heat up the dried $CuCl_2$ (stream S21).

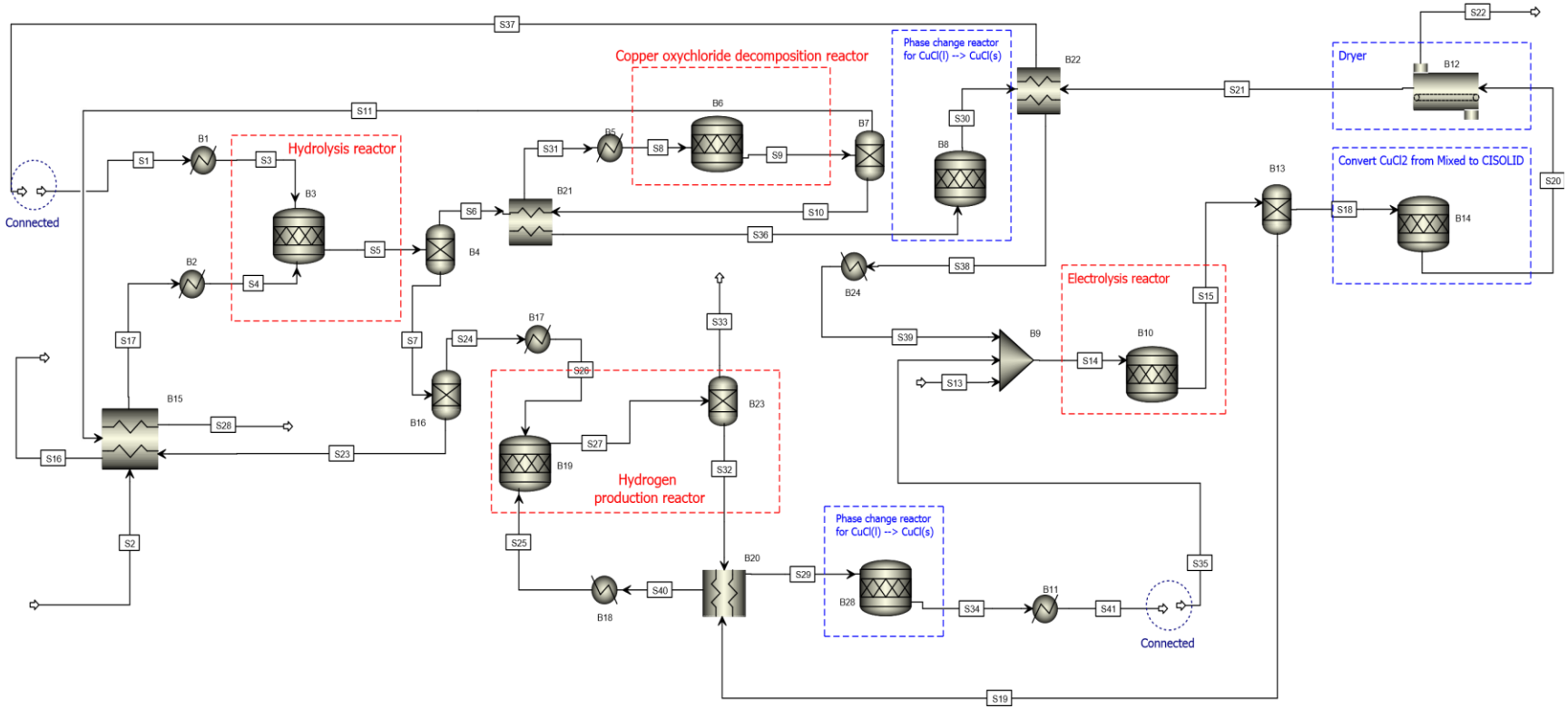

Figure 3.8 The Aspen Plus flow sheet for modeling and simulation of the copper-chlorine cycle for thermochemical decomposition of water for large-scale hydrogen production.

The solid CuCl (streams S39 and S35) is mixed with water to form an aqueous solution that is sent to the electrolysis reactor B10. The electrolysis reactor is modeled as a stoichiometric reactor (RStoic), and occurs at a constant temperature. The required heat duty reported by the model is discarded for the electrolysis reactor and the electrical power needed for the electrolysis reaction is taken from the literature. The results of the electrolysis reactor, which are Cu and $CuCl_2$ (stream S15), go to the separator B13, which separates Cu from $CuCl_2$, where Cu (stream S19) goes to the hydrogen production reactor after passing into two heat exchangers B20 and B18. In heat exchanger B20, Cu exchanges heat with molten CuCl produced by the hydrogen production reactor. However, in heat exchanger B18, Cu exchanges heat with the steam generated by the HRSG. The resulting heated Cu exiting heat exchanger B18 (stream S25) enters the hydrogen production reactor, where it reacts with HCl at an isothermal reactor operating at a constant temperature of $450^{o}C$.

As previously mentioned, heat is required to maintain the reactor at constant temperature; it is provided for the reactor from the steam generated from the HRSG. The product of the hydrogen production reactor (stream S27) is sent to the gas-liquid separator B23 to separate the hydrogen gas from the molten CuCl. The separated hydrogen exits the separator B23 in stream S33. The molten CuCl (stream S32) goes to heat exchanger B20 to a temperature slightly higher than the melting/solidification temperature, enters the phase change reactor B28 and is then cooled down by heat exchanger B11. The resulting solid CuCl (stream S35) goes to the electrolysis reactor. However, the aqueous $CuCl_2$ exiting the separator B13 (stream S18) goes to reactor B14 where the solid $CuCl_2$ is converted from Aspen stream type and mixed to stream type *cisolid* so that the drying process can take place since the dryer requires a solid in the form of cisolid. The dryer requires heat to evaporate the water from the aqueous solution ($CuCl_2(aq)$). The dried $CuCl_2$ (stream S21) goes to the heat exchanger B22 then to the hydrolysis reactor, but, as mentioned above it is first heated. The produced hydrogen from the thermochemical water decomposition copper-chlorine cycle is in stream S33, as seen in Figure 3.9.

One of the methods for storing hydrogen is by compressing it to high pressures and then storing it in gas cylinders [31]. The pressure of the storage tanks can vary between 350-700 bar, based on the size requirements of the storage tank [31].

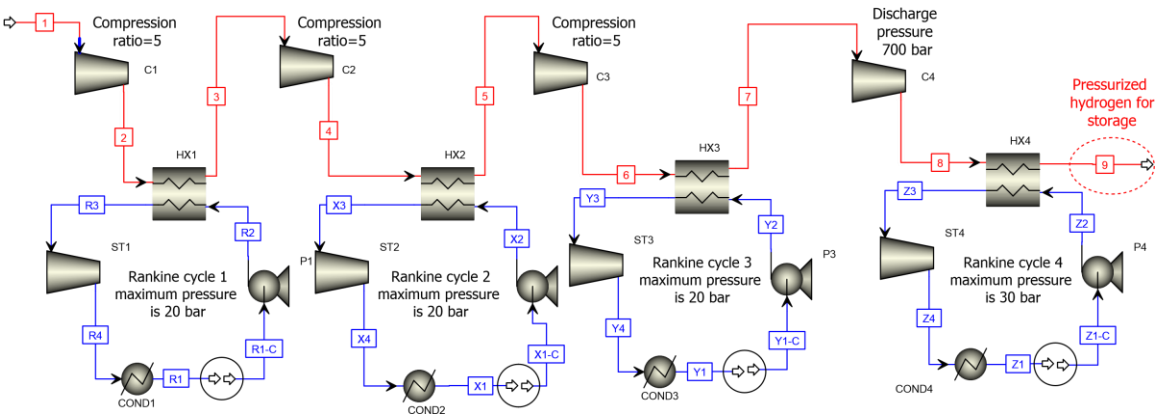

Figure 3.9 The Aspen Plus flow sheet for modeling and simulation of the hydrogen compression system, which compresses hydrogen from 1 bar to 700 bar for pressurized gas storage.

A four-stage compression system is developed and simulated on Aspen Plus, as shown in Figure 3.10. The four-stage compression system compresses hydrogen from the pressure of 1 bar to a pressure of 700 bar. Four simple Rankine cycles are integrated with the compression system to reduce the required compression power. As can be seen in Figure 3.10, hydrogen produced by the system (stream 1) enters the first compression stage, compressor C1. The first compression stage has a pressure ratio of 5. The compressed hydrogen (stream 2) exits compressor C1 and enters the heat exchanger HX1, where the high temperature compressed hydrogen exchanges heat with pressurized water at 20 bar (stream R2). Compressed hydrogen exits the heat exchanger HX1 through stream 3, while the pressurized water exits the heat exchanger HX1 through stream R3 as pressurized superheated steam. The steam turbine ST1 extracts the thermal energy of the pressurized superheated steam and produces work rate. That which exits the steam turbine ST1 then goes to the condenser, and pump P1 pumps the saturated liquid to a pressure of 20 bar. For the remaining three compression stages with intercooling, a Rankine cycle is used to benefit from the heat rejected by the compressed hydrogen at each stage in order to produce a work rate that reduces the required work rate for compressing the hydrogen.

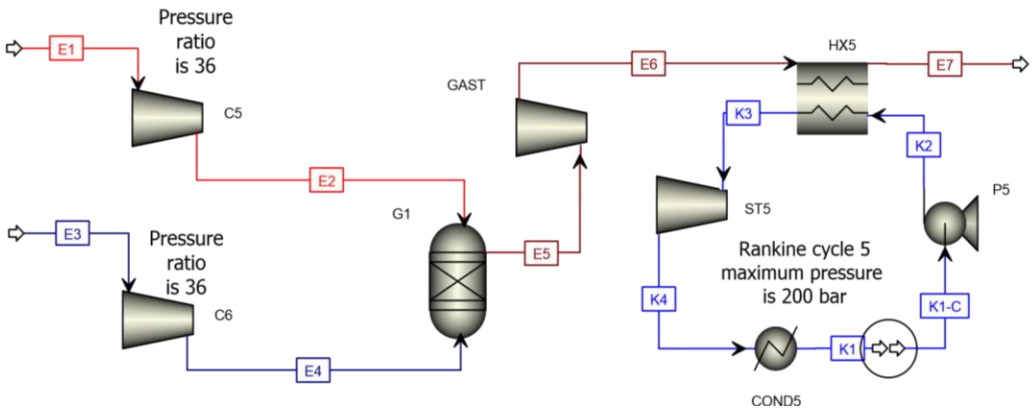

Figure 3.10 The Aspen Plus flow sheet for modeling and simulating the hydrogen combustion combined cycle, the combustion chamber of the combined cycle is operating pressure is 36 bar and a Rankine cycle with maximum pressure of 200 bar.

To provide the necessary work to compress the produced hydrogen and for other work consuming devices, a combined cycle that burns part of the hydrogen is generated by the plant to provide the needed work rate. Figure 3.11 shows the Aspen Plus model of the hydrogen fueled combined cycle (HFCC). The required amount of the produced hydrogen is compressed by compressor C5, which has a compression ratio of 36 [31]. Air is compressed by compressor C6 to provide the needed hydrogen with oxygen for complete combustion in the combustion chamber G1. G1 is a Gibbs free energy minimization reactor. Combustion gases E5 exiting the combustion chamber G1 are then expanded in the gas turbine GAST (see Figure 4.4). The exhaust gases E6 exiting the gas turbine produce steam in the heat exchanger HX5. The produced pressurized steam enters the steam turbine ST5 and goes to the condenser where P5 pumps the liquid water exiting the condenser, then sends it to the heat exchanger HX5. The produced net work rate of this cycle is used to cover the needs of the hydrogen production plant of work rate. After the hydrogen is compressed, it is stored in hydrogen pressurized tanks for commercial, industrial and transportation purposes.

3.1.2 Nuclear-Based Hydrogen Production Plant (System 2)

The developed nuclear-based System 2 for a hydrogen production plant that utilizes a thermochemical hybrid water decomposition cycle contains the following subsystems, based on the results of the comparisons previously made:

- A heat production system: a supercritical water cooled nuclear reactor (SCWR) with closed single coolant loop.
- A thermochemical hybrid water decomposition cycle: five-step Cu-Cl cycle.
- A hydrogen preparation system: a four-stage hydrogen compression system consisting of multiple compression stages with intercoolers that generate steam for bottoming Rankine cycles. The bottoming Rankine cycles reduce the overall required power by the compression system.
- A supporting system: a combined cycle with a hydrogen fueled combustion chamber.
- A condenser.

The aim of System 2 is to integrate the SCWR with the Cu-Cl cycle, using a defined steam circuit (SC) which is lacking in the literature, a hydrogen compression system (HCS) and a supporting combined cycle (SCC). The integrated system is then simulated using Aspen Plus software, and a thermodynamic analysis is performed on the proposed integrated system. The Cu-Cl cycle with a SC is compared using simulation with other cycles without a SC (based on energy requirements). The energy and exergy efficiencies and the hydrogen production flow rate are reported for each case of the Cu-Cl cycle. The SC is simulated in Aspen Hysys. Figure 3.12 shows a schematic diagram of System 2, with a description of how its subsystems interact with each other.

Table 3.9 The main parameters in the proposed integrated system, consisting of SCWR, Cu-Cl cycle, supporting the combined cycle, and a hydrogen compression system.

Main component	Parameters	Value	Unit	Ref.
SCWR	Temperature of the steam exiting the reactor	625	^{o}C	[45,75]
	Temperature of the water returning to the reactor	350	^{o}C	[45,75]
	Operating pressure of the nuclear reactor	25	MPa	[45,75]
	Thermal energy output	2,540	MW	[45,75]
	Supercritical steam mass flow rate	1,320	kg/s	[45,75]
	T_{max} cladding	850	^{o}C	[45,75]
Cu-Cl cycle	Check Table 3.4 for main cycle reactions and Tables 3.5-3.8 for thermochemical properties of the main Cu-Cl cycle materials that appear in the solid phase during the cycle			

Hydrogen compression system	Hydrogen final pressure	700	bar	[9,42]
	Number of compression stages	4	stages	
	Pressure ratio of each stage except final stage	5		
	Rankine cycle connected to the intercoolers			
	RC1 operating pressure	20	bar	
	RC2 operating pressure	20	bar	
	RC3 operating pressure	20	bar	
	RC4 operating pressure	30	bar	
	$\eta_{is,C}$ = 0.72			[76]
	$\eta_{is,ST}$ = 0.72			[76]
Supporting Combined cycle	Combustion chamber pressure	36	bar	
	Air compressor pressure ratio	36		
	hydrogen compressor pressure ratio	36		
	Rankine cycle operating pressure	200	bar	
	$\eta_{is,GT}$ = 0.72			[76]
	$\eta_{is,ST}$ = 0.72			[76]
	$\eta_{is,C}$ = 0.72			[76]

The proposed integrated system for producing compressed hydrogen is shown in Figure 3.12, which presents a new design concept for the five reactors of the Cu-Cl cycle as well as how the SC is organized. The thermal energy driving the integrated system comes from the SCWR though the steam generator, as shown in Figure 3.12. The supercritical pump is used only to restore pressure losses through the steam generator. The parameters and the outlet thermal energy of the SCWR are given in Table 3.9 [45]. Since the maximum required steam temperature by the Cu-Cl cycle is 530ºC and the SCWR can provide temperatures up to 625ºC, then the SCWR is more than perfect for integration with the Cu-Cl cycle. Since the Cu-Cl cycle requires steam at atmospheric pressure, the supercritical water of the nuclear reactor continues circulating in a closed circuit, and the steam that is sent to the Cu-Cl cycle is on a different circuit. The current design of the Cu-Cl cycle is described in detail in the following section.

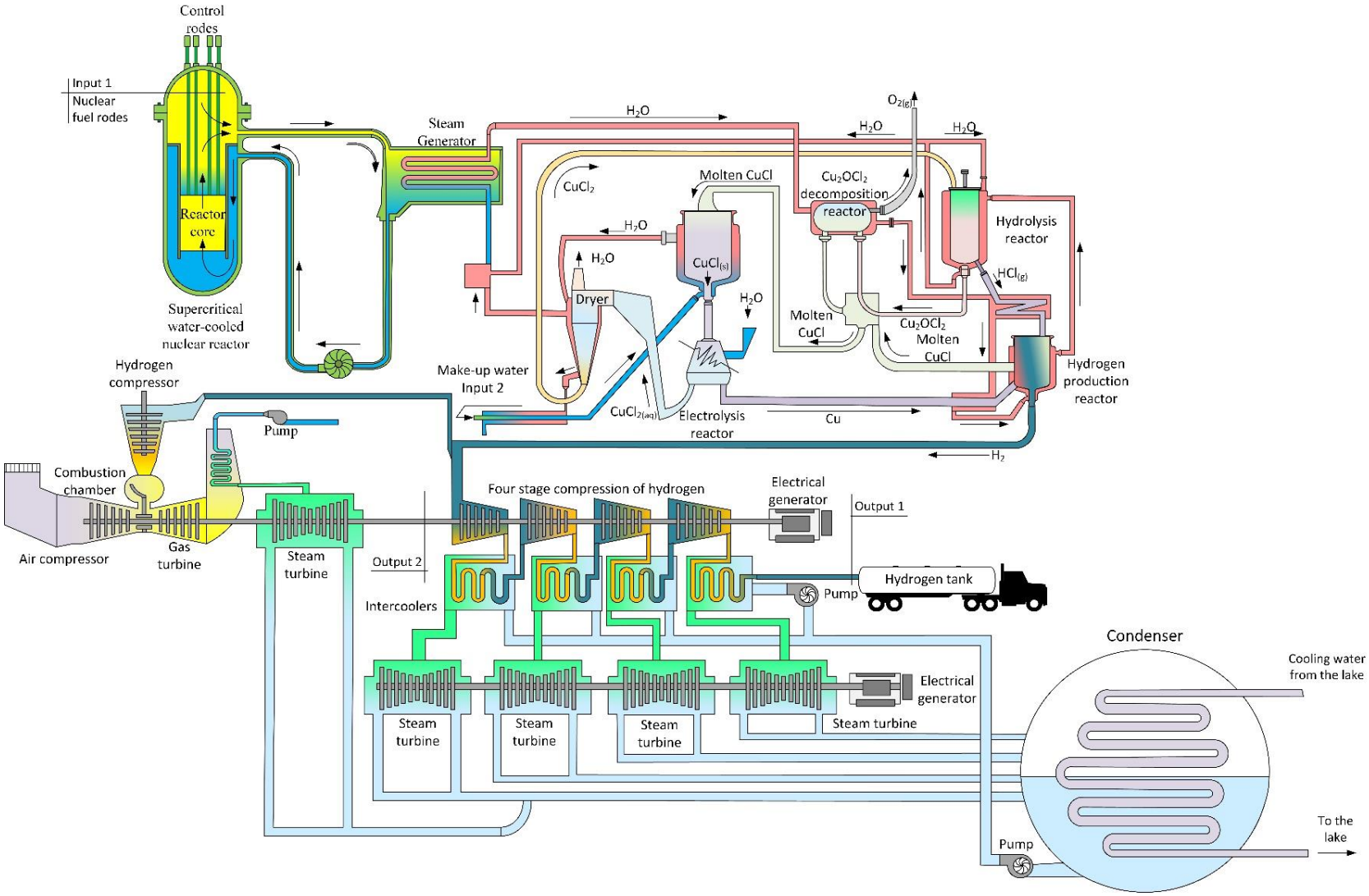

Figure 3.11 The schematic diagram System 2, which is nuclear-based integrated system for electrical power and hydrogen production. The produced hydrogen is compressed in a five-stage hydrogen compression system, and the electrical power requirements of the integrated system are fulfilled by the supporting Rankine cycle

The proposed design of the Cu-Cl cycle is shown in Figures 3.12-3.14 while the main chemical reactions that take place in the cycle are listed in Table 3.10 (which is the same as Table 3.4 but also included here for convenience).

Figure 3.14 shows the proposed steam circuit design for providing the Cu-Cl cycle with the required heat and steam and recovered part of the heat released by the Cu-Cl cycle itself. Figure 3.14 is also labeled with the names of the reactors in Figure 3.13. Water at environment conditions is first heated (in heat exchanger E-110) by the steam exiting the steam jacket of the dryer (B12). The generated steam (at 120°C in Figure 3.14) is superheated by the heat recovered from the cooling solid CuCl in the heat exchanger B11 to 140°C. Steam exiting the heat exchanger B11 enters the steam jacket (E-104) of the CuCl phase change reactors (B8 and B28) and exits at the very high temperature of 434°C.

The steam then enters the steam jacket (E-108) of the dryer and cools down to 265°C. The steam exiting the steam jacket of the dryer is split (through the splitter TEE-101) to a ratio of 1 to 60 (mole basis). A significant portion of the split steam is sent back to the heat exchanger E-101 and exits at 83.1^{o}C; before being discarded to a lake (water reservoir). The smaller portion is mixed (mixer MIX-100) with the excess steam exiting the hydrolysis reactor and with the other steam mass used to circulate in a closed cycle for heat exchange purposes.

Table 3.10 The Cu-Cl cycle reactions based on the five steps and the corresponding operating conditions.

Step	Reactor name	Chemical reaction	Temperature range (^{o}C)
1	Hydrolysis reactor	$H_2O(g) + 2CuCl_2(s) \rightarrow Cu_2OCl_2(s) + 2HCl(g)$	375-400
2	Cu_2OCl_2 decomposition reactor	$Cu_2OCl_2(s) \rightarrow \frac{1}{2}O_2(g) + 2CuCl(l)$	500-530
3	Hydrogen production reactor	$2Cu(s) + 2HCl(g) \rightarrow 2CuCl(l) + H_2(g)$	430-475
4	Electrolysis reactor (requires 63 kJ/mol of electricity) [17]	$4CuCl(aq) \rightarrow 2Cu(s) + 2CuCl_2(aq)$	30-80
5	Dryer	$CuCl_2(aq) \rightarrow CuCl_2(s)$	>100

Source: [17,40]

At this point, the mixed product enters the heat exchanger that exchanges heat with the supercritical steam exiting the nuclear reactor. The resulting superheated steam first enters the steam jacket of the Cu_2OCl_2 decomposition reactor (B6) and the preheater B5 and maintains the reactor temperature at 530°C. The steam exiting the steam jacket of B6 heats up the HCl and solid copper (in heat exchangers B17 and B18 in Figure 3.13 and E-105 in Figure 3.14) to the operating temperature of the hydrogen reactor (B19), and then enters the hydrogen reactor steam jacket (E-107). The steam exiting E-107 is sent to the hydrolysis reactor (B3) steam jacket (E-100) to provide the heat required by the hydrolysis reactor. The steam exiting E-100 is split in splitter TEE-100, part of which enters the hydrolysis reactor and part of which is consumed, whereas the rest is sent to the MIX-100 to complete the upper steam circuit cycle.

The final two reactors in the Cu-Cl cycle Aspen Plus model that are not present in the steam circuit model are the electrolysis reactor (B10) and the reactor B14. Reactors B10 and B14 are not considered in the steam circuit model because they neither require nor produce any heat. Reactor B14 is required to convert the solid form of $CuCl_2$ in its aqueous solution from *mixed* to *cisolid* solid type before feeding the aqueous solution to the dryer (B12). It should be noted that the only material defined in the steam circuit is water, and the heat rate (into or out of the water) is from the Aspen Plus model of the Cu-Cl cycle. Not all the heat released while cooling the stream S34 is transferred to the water due to temperature limitations. The HCS Aspen Plus flowsheet is shown in Figure 3.15, while the Aspen Plus flowsheet of the SCC is provided in Figure 3.16. The HCS contains four hydrogen compressors, four intercoolers, and four bottoming Rankine cycles. The first three hydrogen compressors have a compression ratio of 5, and the fourth hydrogen compressor has a discharge pressure of 700 bar. The intercooler generates steam for the bottoming Rankine cycles, whose duty is to reduce the required power for the hydrogen compression process through recovering heat from the intercoolers. The SCC takes in part of the produced hydrogen and produce work rate to fullfill the integrated system requirements of power. The SCC consist of two compressors (C5 and C6) as shown in Figure 3.16. C5 compresses hydrogen and the C6 compresses the required air for the combustion process. Both compressors have a compression ratio of 36. The molar ratio of air to hydrogen is 9.18. The combustion chamber operating pressure is 36 atm. The

combustion chamber is modeled using the *RGibbs* reactor model in Aspen Plus, which carries the reaction between the reactants based on the Gibbs free energy minimization approach. The Rankine cycle part of the combined cycle maximum operating pressure is 200 bar.

3.1.3 Solar-Based Hydrogen Production Plant (System 3)

The third developed concept for the hydrogen production plant utilizing the hybrid electrical and thermochemical water decomposition cycle. The third concept contains the following subsystems, based on the results of previous comparisons:

- A heat production system: concentrated-solar thermal, using heliostats and a collecting tower.
- A hydrogen preparation system: a hydrogen compression system consisting of multiple compression stages with intercoolers, which generate steam for bottoming Rankine cycles.
- A supporting system: a Rankine cycle that uses part of the heat generated by the solar central receiver.
- A cooling tower for condensing the water.

How the subsystems of hydrogen production plant System 3 interact with each other is illustrated in Figure 3.17. The aim of this system is to propose an integrated hydrogen production plant, which is completely dependent on solar thermal energy with highly compressed hydrogen ready for usage in almost all fields that are hydrogen based. The proposed hydrogen production plant consists of a solar heliostat farm integrated with a hybrid electrical and thermochemical water decomposition cycle, a hydrogen compression system integrated with Rankine cycles that work on the hydrogen intercoolers, and a large Rankine cycle used to fulfill the electrical power needs of the plant operated by heat from solar energy. The reason behind proposing this hydrogen production plant is to provide an alternative for the usual Rankine cycle and to analyze the functionality of the alternative, the hybrid thermochemical water decomposition cycle. The alternative is the hybrid electrical and thermochemical water decomposition cycle that uses the chemical couple copper and chlorine.

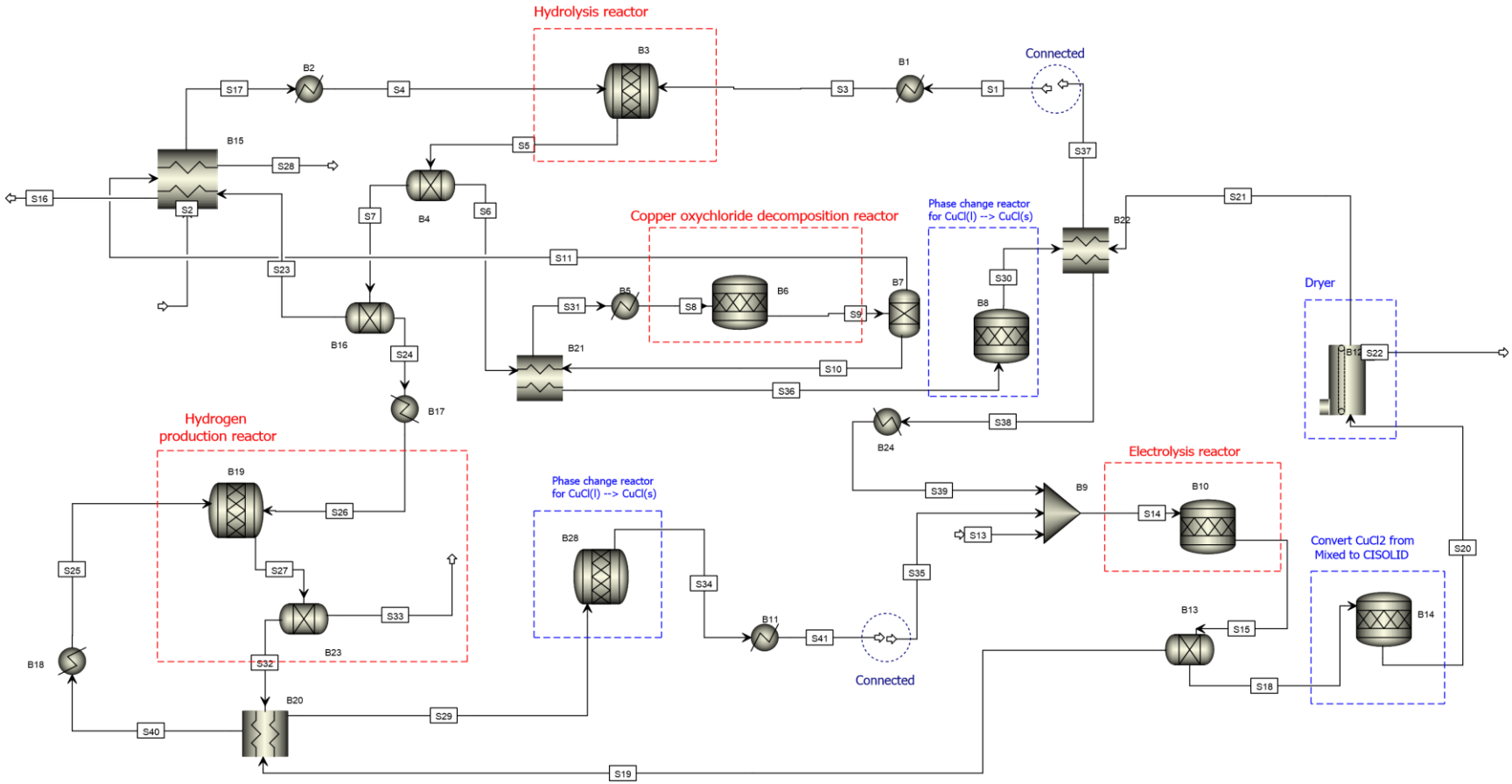

Figure 3.12 The Aspen Plus flow sheet of the Cu-Cl cycle in the proposed integrated system.

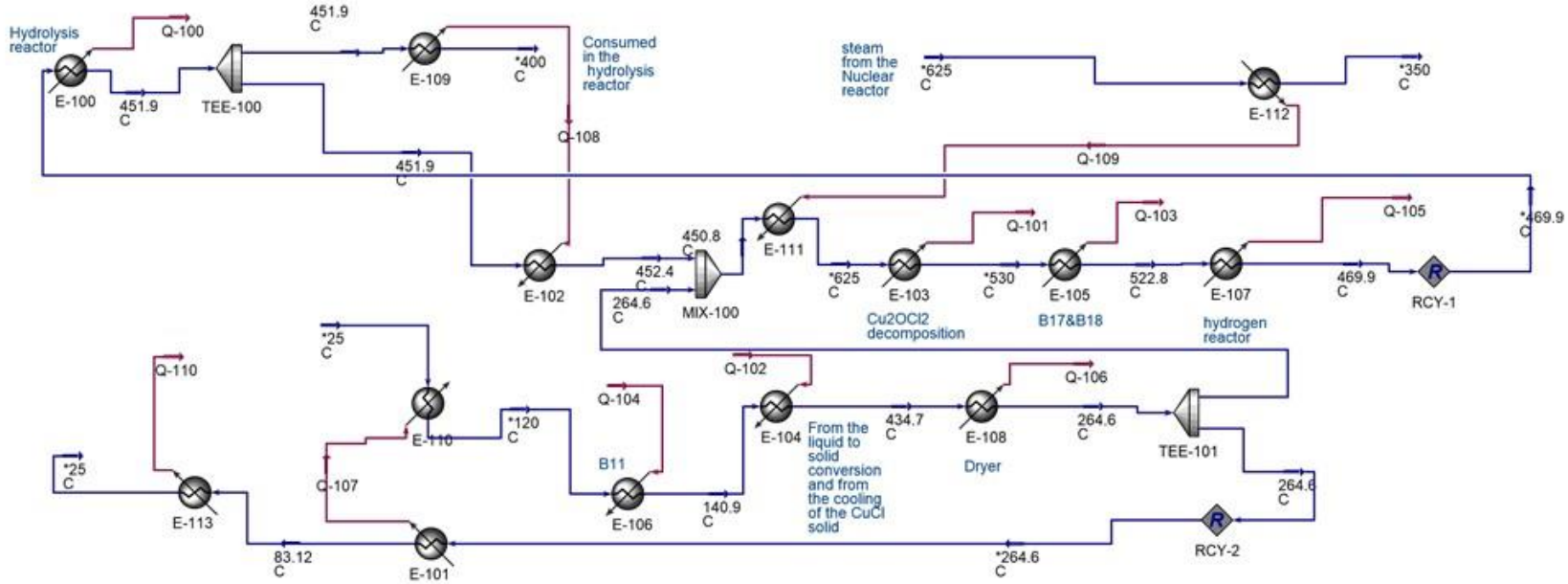

Figure 3.13 The Aspen Hysys flow sheet of the proposed steam circuit for the Cu-Cl cycle in the integrated system.

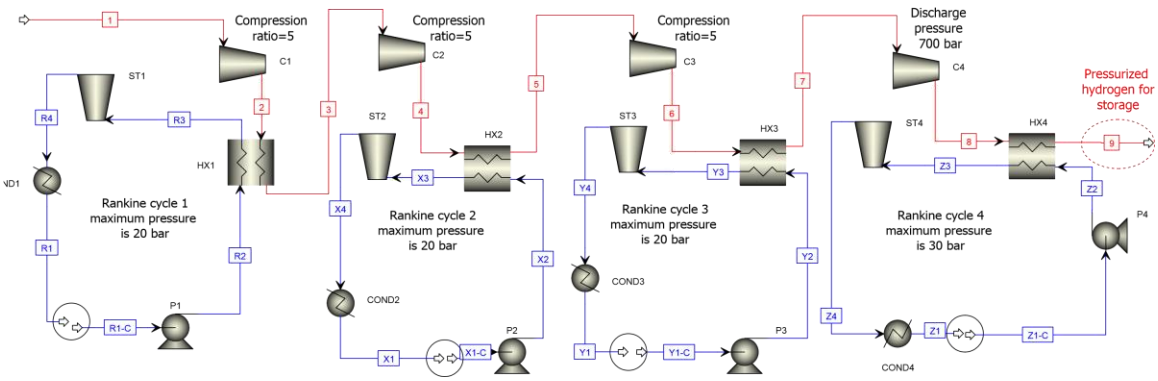

Figure 3.14 The hydrogen compression system (HCS) Aspen Plus simulation flowsheet.

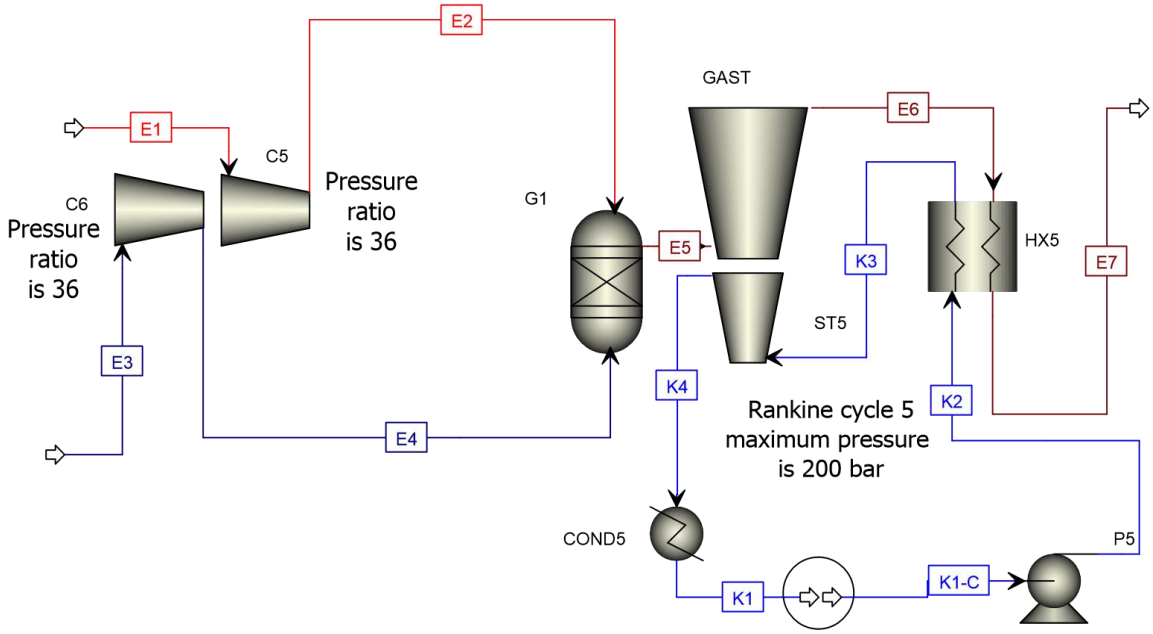

Figure 3.15 The supporting combined cycle (SCC) Aspen Plus simulation flowsheet.

The second reason for using the hybrid electrical and thermochemical water decomposition cycle with solar energy is the directly produced hydrogen from solar thermal energy, which will bypass the electrical conversions in the middle when producing hydrogen from heat by electrolysis. The third reason is that the proposed plant can store day solar thermal energy in a form that has fewer losses in quality and quantity as a function of storage time, since storing hydrogen has a higher efficiency level than electricity and a much higher level than heat.

The successful results of the proposed full hydrogen production plant will promote research and the building of an experimental scale model of the hybrid electrical and thermochemical water decomposition cycle that utilizes the copper-chlorine chemical couple for converting heat to hydrogen. The hybrid electrical and thermochemical water decomposition cycle that utilizes the copper-chlorine chemical pair is simulated in Aspen Plus software, using its advantage over other chemical simulation software, such as Aspen Hysys, with its ability to simulate solids and mixtures of solids and fluids. Since a hybrid electrical and Cu-Cl cycle contains materials in their solid, liquid and gaseous states, Aspen Plus will be the perfect tool for simulating the hydrogen production plant process and its main components, which are a copper-chlorine cycle and the hydrogen compression system. In the proposed hydrogen production plant, the hybrid copper-chlorine cycle receives the required heat from the solar heliostat field and electricity from the supporting Rankine cycle. The HCS will compress hydrogen to a very high pressure (700 bar). While HCS have multiple Rankine cycles to reduce the required power by utilizing the heat from the intercoolers and the rest from the SRC, SRC receives its required heat from the same heliostat field. The heliostat field is based on the current running 5 MW_{th} heliostat field owned by Greenway CSP in Mersin, Turkey [77]. After the hydrogen plant is simulated on Aspen Plus, energy and exergy analyses are performed. Figure 3.17 shows an overall view of the proposed solar-based hydrogen production plant that is completely dependent on the solar thermal energy coming from the heliostat farm. Table 3.11 shows the main parameters of the hydrogen production plant. The solar light coming from the sun is reflected by the heliostats to a central vacuum receiver. The central receiver heats up the molten salt, which in turn heats up the water from 239°C and 55 bar to produce superheated steam at 550°C and a pressure of 55 bar [77]. The solar generated superheat steam is used to heat up the all the water steam flowing into the plant to a temperature of 239°C. The water exiting the steam generator is sent back to the solar power to increase its temperature back again to 550°C. The pump is used to compensate any pressure losses through the steam generator. Water enters the steam generator and is heated to 550°C. The superheated steam goes to the hybrid electrical and thermochemical water decomposition cycle, which is based on the copper-chlorine chemical couple (Cu-Cl cycle). The Cu-Cl cycle decomposes water into hydrogen and oxygen. The produced hydrogen is then sent to the HCS to compress the

hydrogen from 1 bar to 700 bar. An SRC then receives heat from the steam generator and other inner preheat systems to produce the needed electrical power by the HCS and the Cu-Cl cycle.

The proposed hydrogen production plant is simulated on Aspen Plus software, with the exception of the heliostat field, which is modeled and simulated on engineering equation solver (EES) software. Each subsystem simulation flowsheet is provided through discussion of the model development of each of these subsystems.

The main heat rate provider in the hydrogen plant is the heliostat solar field. A heliostat solar farm consists of a group of flat mirrors that reflect the light from the sun to a fixed target, as shown in Figure 3.17. The heliostat solar farm produces superheated steam, the generated steam part of which goes to the thermochemical water decomposition cycle while the rest goes to the steam turbine for power generation to satisfy the requirements of the hydrogen compression system. The heliostat solar farm was modeled by using EES based on the model developed by Xu et al. [78], which was also used in the work of Ratlamwala and Dincer [41]. A description of the mathematical model of the solar heliostat farm is provided in the analysis section.

The Cu-Cl cycle decomposes water through thermochemical and electrical processes to produce hydrogen and oxygen by low-temperature heat relative to that required for the thermal decomposition of water. There are many different configurations of the Cu-Cl cycle [20]. The Cu-Cl cycle configuration integrated into the system in this research is the five-step Cu-Cl cycle, the main interactions of which are shown in Table 3.12 [17]. The reactions of the five-step Cu-Cl cycle are explained in more detail in the following section, following which the methodology and the process of modeling the five-step Cu-Cl cycle in Aspen are explained.

The first reaction in the five-step Cu-Cl cycle is the hydrolysis reaction, Reaction number 1 as seen in Table 3.12. Superheated steam reacts with cupric chloride ($CuCl_2$) in the hydrolysis reaction to form copper oxychloride (Cu_2OCl_2) and hydrochloric acid (HCl) [17]. The hydrolysis reactor must be maintained at a constant temperature between 325-375°C [17].

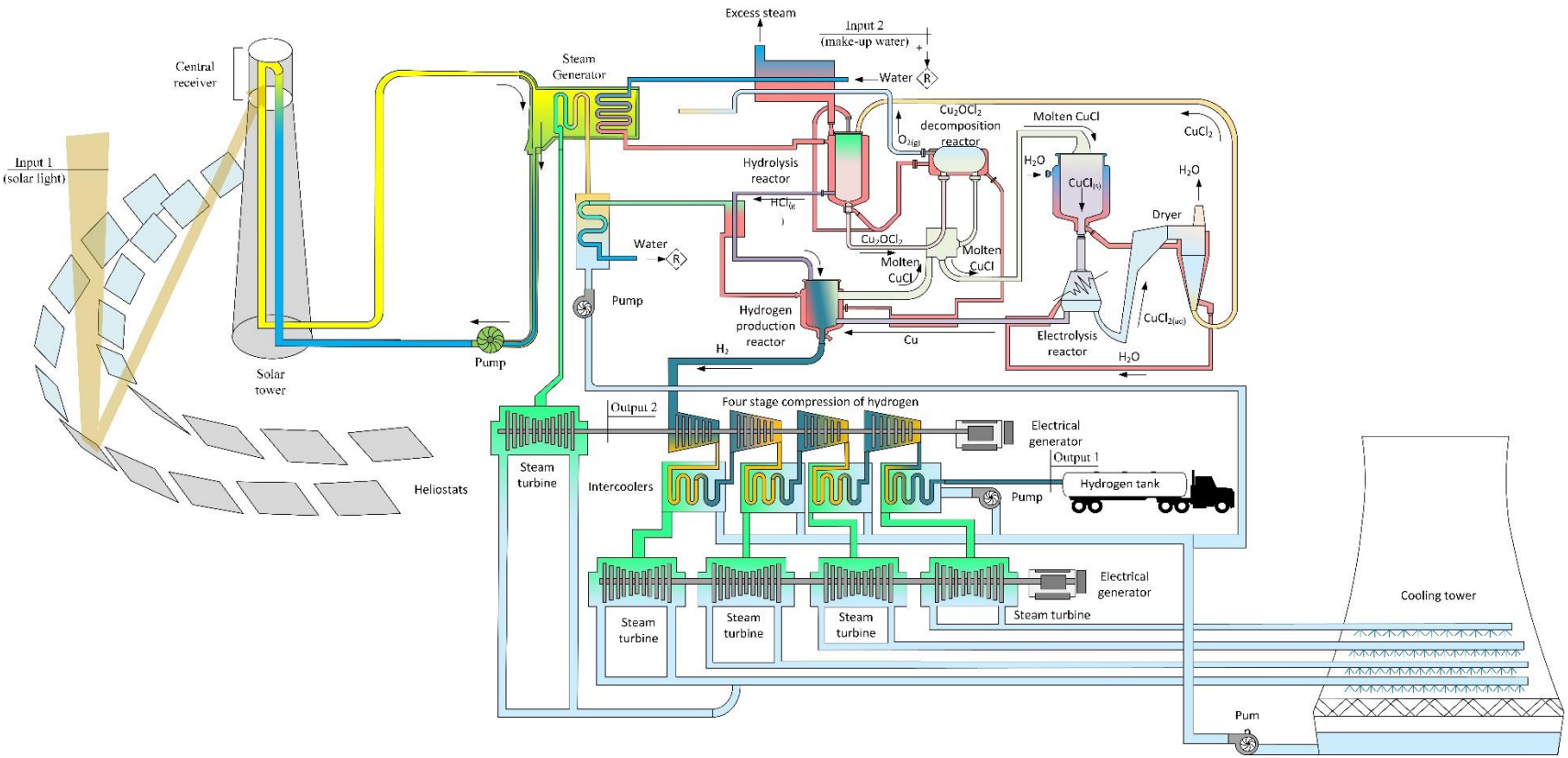

Figure 3.16 The third concept of the hydrogen production plant that utilizes the thermochemical hybrid water decomposition cycle, which the copper-chlorine cycle.

Table 3.11 The main input parameters for the gasification system consisting of gasifier GFEMA model for the gasifier, CASU, WGSMR and Brayton cycle, plus other supporting systems.

Unit	Main parameters
Heliostat field	• Radiation intensity is 800 W/m^2 • Overall field efficiency is 75% [78] • Number of heliostats is 510 [77]
Central receiver	• Aperture area is 12.5 m^2 • Inlet temperature of the molten salt is 290°C • Outlet temperature of the molten salt is 565°C • View factor equal to 0.8 [78] • Tube diameter is 0.019 m [78] • Tube thickness 0.00165 m [78] • Emissivity is 0.8 [78] • Reflectivity is 0.04 [78] • Wind velocity for forced convection heat transfer is 5.0 m/s [78]
Molten salt	• Type: Mixture of 60% of $NaNO_3$ and 40% of KNO_3 [78] • $\rho = 2{,}090 - 0.636T$ (kg/m^3) (temperature T in ^{o}C) [78] • $c_p = 1443 + 0.172T$ (J/kgK) (temperature T in ^{o}C) [78] • $k = 0.443 + 1.9 \times 10^{-4}T$ (W/mK) (temperature T in ^{o}C) [78]
HSC	• Compression ratio of the first three compression stages is 5 • Discharge pressure of the final stage is 700 bar [9] • Compressed hydrogen final temperature is 25°C
SRC	• Maximum pressure in the Rankine cycle is 12,600 kPa • Condenser operating pressure is 10 kPa
Cu-Cl	• For Cu-Cl cycle, check Table 3.12 (which is similar to Tables 3.4 and 3.10 but presented again for reader convenience).

Table 3.12 The five steps in the copper-chlorine cycle with their corresponding reactions and operating conditions.

Step	Chemical reaction	Temperature range (^{o}C)
1	$H_2O(g) + 2CuCl_2(s) \rightarrow Cu_2OCl_2(s) + 2HCl(g)$	375-400
2	$Cu_2OCl_2(s) \rightarrow 0.5O_2(g) + 2CuCl(l)$	500-530
3	$4CuCl(aq) \rightarrow 2Cu(s) + 2CuCl_2(aq)$	30-80
4	$CuCl_2(aq) \rightarrow CuCl_2(s)$	>100
5	$2Cu(s) + 2HCl(g) \rightarrow 2CuCl(l) + H_2(g)$	430-475

Source: [17,40]

Since the hydrolysis reaction is an endothermic reaction, this means that heat must be continuously supplied to the reactor to maintain it and the reactants inside it at a constant temperature between 325-375°C [17]. Wang et al. [12] suggested supplying steam superheated at 400°C with the excess amount to the hydrolysis reactor. The excess steam will force the chemical reaction equilibrium in the direction of the products since the concentration of one of the reactants is increased.

The second reaction in the five-step Cu-Cl cycle is the thermal decomposition of copper oxychloride (Cu_2OCl_2) to oxygen gas and a molten salt of cuprous chloride (CuCl), as shown in the second step in Table 3.12. The thermal decomposition of the Cu_2OCl_2 reaction is an endothermic reaction, and the reactor temperature should be maintained constant at 530°C to completely carry out the decomposition. Naterer et al. [13] provided one method of supplying the reaction heat to maintain a constant reactor temperature at 530°C. Naterer et al. [13] also mentioned that the reaction heat can be supplied by looping the molten CuCl that is heated by steam in a direct contact heat exchanger and then re-introducing it into a decomposition reactor. In the decomposition reactor, the CuCl gives the heat to the reactants, resulting in producing oxygen gas and additional molten CuCl. The suggestion of Naterer et al. [13] is not adopted in the following model since CuCl is one of the decomposition reaction products and more of it in the reactor will shift the reaction equilibrium in the reactants' direction. The process used in this Cu-Cl cycle model is steam, which is used to provide the necessary heat as well as maintain the reaction at the specified temperature, as shown in Figure 3.17. During the decomposition of the Cu_2OCl_2 process, there is an intermediate step where Cu_2OCl_2 transforms at 500°C to a crystalline structure of cupric oxide and cupric chloride ($\mathrm{CuO} \times \mathrm{CuCl_2}$). At a temperature of 530°C, $\mathrm{CuO} \times \mathrm{CuCl_2}$ then decomposes into O_2 gas and molten CuCl [17]. Since the Cu-Cl cycle is a hybrid electrical and thermochemical water decomposition cycle, there is a step where it requires an electrical energy. This is the third step in the five-step Cu-Cl cycle. The electrolysis step reproduces cupric chloride ($CuCl_2$), as shown in Table 3.12. In the electrolysis reactor, $CuCl_2$ and solid Cu are extracted electrochemically from aqueous cuprous chloride ($CuCl_{(aq)}$). The electrolysis reactor produces $CuCl_2$ in an aqueous form ($\mathrm{CuCl_2} \times 2\mathrm{H_2O}$). $\mathrm{CuCl_2} \times 2\mathrm{H_2O}$ is dried in a drying reactor to produce the solid $CuCl_2$. Based on the work of Zamfirescu et al. [17], the electrolysis step requires 63 kJ of electrical

energy per each mol of produced H_2 in the five step Cu-Cl cycle. The water in the aqueous material $CuCl_2 \times 2H_2O$ is removed during the drying process, and the solid $CuCl_2$ is recycled back to the hydrolysis reactor (step 1) to complete one-half of the cycle, while the other half is associated with the solid copper and HCl.

The hydrogen production reactor produces H_2 and molten CuCl and receives hot solid copper from the electrolysis reactor and HCl from the hydrolysis reactor. Cu and HCl react in the hydrogen production reactor to produce CuCl and H_2. The hydrogen production reaction is an exothermic reaction with a reactant conversion percentage of 99% at a reaction temperature of 100°C. However, since one of the requirements is having CuCl in a liquid state, and the melting temperature of CuCl is 436°C (see Tables 3.5, 3.6, 3.7 and 3.8) according to Zamfirescu et al. [17] the reaction must occur at a temperature of 450°C. Based on the Gibbs free energy minimization approach, 52.5% of the reactants is converted to products at a reaction temperature of 450°C. Extra heat must then be provided to the reactor to have 100% conversion of the reactants at a reaction temperature of 450°C. Following the previous description of the five-step Cu-Cl cycle reactions, the next section will discuss the process of building the Aspen Plus model for the Cu-Cl cycle.

Due to a lack of the solid properties of CuCl, $CuCl_2$, CuO, and Cu_2OCl_2 in Aspen Plus, these solid properties have to be manually entered for successful simulation of the Cu-Cl cycle. The other manual user interference in the simulation process of Cu-Cl in Aspen Plus is the phase changes between the liquid and the solid phases for defined conventional solids. A stoichiometric reactor (*Rstoic*), Gibbs free energy minimization reactor (*RGibbs*) or any other reactor should be defined for phase changes between solid and liquid phases. In this research, a stoichiometric reactor is for phase changes from solid to liquid or from liquid to solid in the Cu-Cl model. Properties and their correlations for the main Cu-Cl cycle materials Cu_2OCl_2, CuO, $CuCl_2$ and CuCl are provided in Tables 3.5-3.8. The property correlations in Table 3.12 should be entered in Aspen Plus before starting to build the process. Properties and correlations in Tables 3.5-3.8 are for the solid phase of CuCl, $CuCl_2$, CuO, and Cu_2OCl_2 since the liquid phase properties are already available in the Aspen Plus database.

The description of the Aspen Plus model of the Cu-Cl cycle and the proposed Cu-Cl configuration as explained in the light of Figures 3.17-3.19 is provided next. Figure 3.18 shows the Aspen Plus model of the Cu-Cl cycle, while Figure 3.19 shows the Aspen Hysys flowsheet of the steam circuit in the Cu-Cl cycle. Aspen Hysys is used to simulate the Cu-Cl cycle due to the ability of the Hysys to give inputs based on the outputs.

The heated Cu_2OCl_2 goes to the Cu_2OCl_2 decomposition reactor. Steam first heats the HCl exiting the hydrolysis reactor; the HCl then enters the hydrogen production reactor. The molten CuCl is first solidified in reactors B8 and B28 (see Figure 3.18) and then cools down to 25°C. During the solidification and cooling down of the CuCl, steam is produced. The cold CuCl (S39 and S35) enters the electrolysis reactor (B10 in Figure 3.18) with water (S13) at ambient conditions. Exiting the electrolysis reactor aqueous $CuCl_2$ that is sent to the dryer, the dried $CuCl_2$ is recycled back to the hydrolysis reactor. The second product of the electrolysis reactor is solid copper (S25 in Figure 3.18), which is heated before entering the hydrogen production reactor. The steam that was used to maintain the temperature of the hydrogen production reactor at 450°C is used to preheat the compressed water (K2 in Figure 3.20) exiting the SRC pump (P5 in Figure 3.20). The hydrogen produced (S33 in Figure 3.17) is cooled down to ambient operating temperature and then sent to the HCS. The oxygen (S11 in Figure 3.17) that exits the Cu_2OCl_2 decomposition reactor heats up the water that is heading to the steam generator.

For storage, hydrogen can be compressed or liquefied. The method used in this study is compressing hydrogen to high pressures and then storing it in gas cylinders [31]. The storing pressure can vary between 350-700 bar based on the required size of the storage tank which will also vary between 0.043 to 0.025 m^3 for 1 kg of hydrogen [31]. A compression system, consisting of four stages with intercoolers, is developed and simulated on Aspen Plus, as shown in Figure 3.20.

The four-stage compression system increases the pressure of the hydrogen from 1 bar to 700 bar. To reduce the required work, four simple Rankine cycles are integrated with the compression system through the intercoolers.

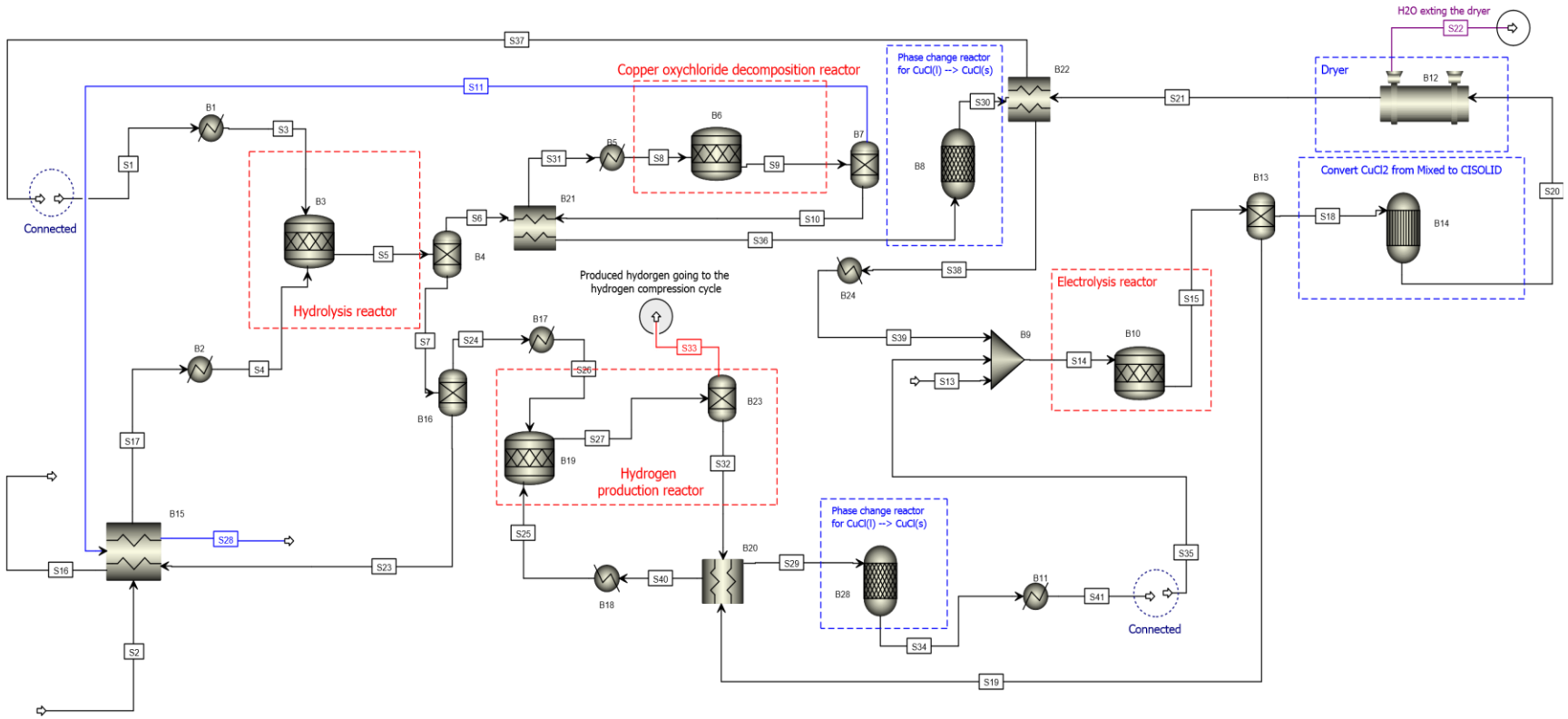

Figure 3.17 The Aspen Plus flow sheet of the Cu-Cl cycle for hybrid electrical and thermochemical decomposition of water for large-scale hydrogen production.

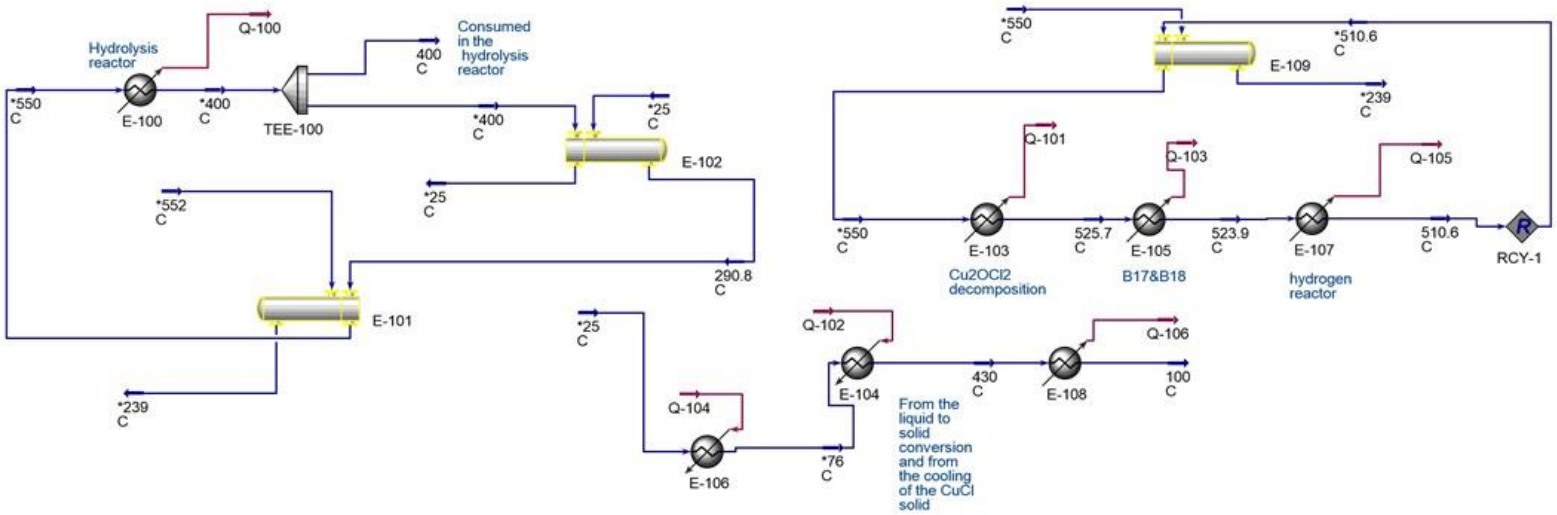

Figure 3.18 The Aspen Hysys flow sheet of the heating circuit of the Cu-Cl cycle using steam generated by the solar heliostat farm.

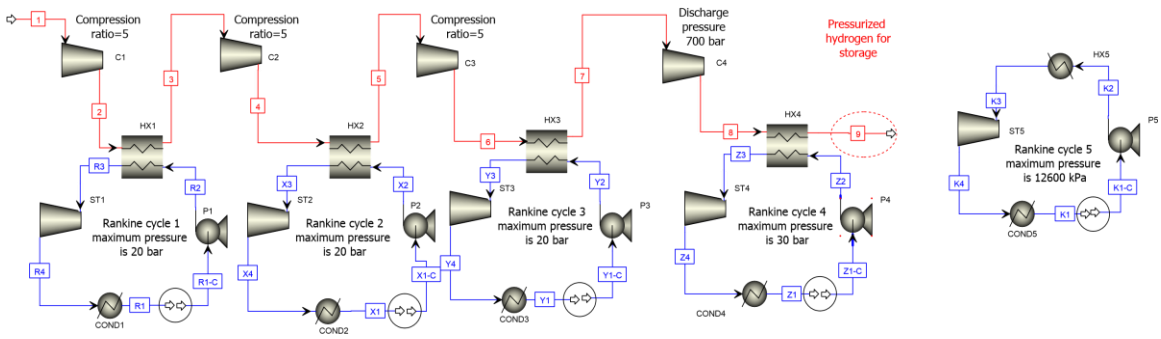

Figure 3.19 The Aspen Plus flow sheet of the hydrogen compression system, which is used to compress hydrogen from 1 bar (hydrogen exiting the Cu-Cl cycle) to 700 bar for pressurized gas storage.

As shown in Figure 3.20, hydrogen produced by the Cu-Cl cycle (stream 1 in Figure 3.20) enters compressor C1. The pressure ratio of the first compression stage is 5. The hydrogen exiting compressor C1 enters the heat exchanger HX1 (intercooler) where steam is produced at a pressure of 20 bar (stream R2) by receiving heat from the compressed hydrogen. Cooled compressed hydrogen stream 3 exits HX1 and enters the second compression stage. The pressurized water exits the heat exchanger HX1 (stream R2) as superheated steam. Steam turbine ST1 receives the superheated steam and extract the thermal energy from it and produces power. That which exits ST1 goes to the condenser, and is then pumped by pump P1 to a pressure of 20 bar. The remaining stages have the same operation as the first stage. To provide the needed power for compressing the produced hydrogen and for other power consuming devices, a simple supporting Rankine cycle (SRC) operating at a pressure of 12,600 kPa is developed. The water is pumped, preheated by steam flow rates from the Cu-Cl cycle and then superheated in the steam generator. The superheated steam is expanded in steam turbine ST5.

3.1.4 Nuclear-Based Hydrogen Production Plant (System 4)

The design of the fourth concept for a hydrogen production plant that utilizes the four-step Cu-Cl cycle contains the following subsystems, based on the results of the previously made comparisons:

- A heat production system: SCWR, which provide the integrated system with the required thermal energy in the form of superheated steam at supercritical conditions.

- A hydrogen preparation system: a hydrogen compression system consisting of a four-stage with intercoolers. The intercoolers generate steam for bottoming Rankine cycles.
- A supporting system: a Rankine cycle that uses part of the heat generated by the nuclear reactor.
- A cooling tower for condensing the water.

How the subsystems of hydrogen production plant System 4 interact with each other is shown in Figure 3.21. The aim of generating this plant concept is to propose a novel nuclear-based hydrogen and power production plant that utilizes the four-step Cu-Cl cycle, where the hydrogen produced is in a compressed state, and to promote the Cu-Cl cycle model that is being developed at the University of Ontario Institute of Technology (UOIT). The hydrogen in the proposed integrated system is produced from a four-step Cu-Cl cycle. The hydrogen is compressed in the proposed integrated system because, in a real hydrogen production plant, hydrogen must be produced in a state that allows it to be economically and physically storable. Since the Cu-Cl cycle is a hybrid thermochemical and electrical water decomposition cycle, the process of delivering thermal energy to the cycle reactors is of a critical importance, because steam at 429°C cannot provide the necessary thermal energy to one of the cycle reactors that needs to be maintained at 530°C in order for the reaction to take place. In this research, a clear and realistic steam/water circuit is proposed to deliver the heat to the four-step Cu-Cl cycle reactors. The steam/water circuit is designed to reduce the losses as much as possible. The integrated system has a Rankine cycle for power production. The Rankine cycle produced power is used to supply the Cu-Cl cycle with the required electrical power and provide the compression system with the needed power to compress the produced hydrogen. The resulting excess power will be delivered to the electrical grid. Figure 3.21 shows a nuclear-based integrated system schematic diagram, which includes the four-step Cu-Cl cycle.

Figure 3.23 shows the designed and developed Aspen Plus model for the integrated system. The integrated system consists of a supercritical water-cooled nuclear reactor (SCWR) which produces thermal energy in the form of superheated supercritical steam, a four-step Cu-Cl cycle, a supporting power production Rankine cycle, and a four-stage

hydrogen compression system. A detailed description of the Cu-Cl cycle is first presented, followed by a description of the overall system with an explanation of how the different systems interact together, accompanied by a description of the Aspen Plus model for the integrated system.

The Cu-Cl cycle has been identified by the Atomic Energy of Canada Limited corporation as a promising technology for the decomposition of water through a hybrid thermochemical and electrical process, with its thermal energy coming from the next generation supercritical water-cooled nuclear reactors. The Cu-Cl cycle has this potential due to its relatively low-temperature requirements and potentially lower cost of materials [18,31]. UOIT, Canadian Nuclear Laboratories (formerly knowns as: Atomic Energy of Canada Limited), the Argonne National Laboratory in the United States, Pennsylvania State University, and other partnered institutions are working on scaling up the Cu-Cl cycle, for use in industrial applications [31].

Many different schemes of the Cu-Cl cycle have been proposed in the literature; these different schemes differ in the number of steps that are required to complete the cycle and the type of reactions in these steps [14,46]. Although there are many different types of Cu-Cl cycle, all of them share the same overall chemical reaction, which is water decomposition to hydrogen (H_2) and oxygen (O_2). The type of Cu-Cl cycle integrated into the proposed nuclear-based integrated system is the four-step Cu-Cl cycle, which is currently being experimentally and theoretically investigated by the Clean Energy Research Laboratory at UOIT. A schematic diagram of the main interactions that occur in the four-step Cu-Cl cycle is shown in Figure 3.22, consisting of the four main chemical reactions (cycle steps) as described below:

Step 1: The hydrolysis reaction, one of the reaction requirements of which is to maintain the hydrolysis reactor at a temperature between 370°C and 400°C:

$$2CuCl_2(s) + H_2O(g) \rightarrow Cu_2OCl_2(s) + 2HCl(g) \tag{3.15}$$

Step 2: The copper oxychloride (Cu_2OCl_2) decomposition reaction where the Cu_2OCl_2 decomposition reactor is required to be maintained at a temperature between 500°C and 530°C:

$$Cu_2OCl_2(s) \rightarrow 2CuCl(l) + 0.5O_2(g) \quad (3.16)$$

Step 3: The electrolysis reaction is as follows (temperature requirement is to be less than 100°C and higher than 25°C):

$$2CuCl(aq) + HCl(g) \rightarrow H_2(g) + CuCl_2(aq) \quad (3.17)$$

Step 4: Drying the aqueous cupric chloride in the dryer at temperatures between 80°C and 100°C:

$$CuCl_2(aq) \rightarrow CuCl_2(s) + H_2O(g) \quad (3.18)$$

The energy source for the integrated system is the nuclear reactor SCWR. This thesis adopts the SCWR main operating parameters from the literature [45].

First, the supercritical gas-like water exiting the SCWR (*S43*) enters the water jacket of the Cu_2OCl_2 decomposition reactor (*B6*) providing the necessary thermal energy to the reactor, then exits the water jacket (*S44*) and heads to the hydrolysis reactor (*B1*). The supercritical fluid (*S43*) entering the water jacket of the Cu_2OCl_2 decomposition reactor (*B6*) provides the required thermal energy to carry out the decomposition of the Cu_2OCl_2 according to Equation (2). The supercritical fluid exits the hydrolysis reactor (*B6*) water jacket (*S46*) and is sent to the steam generator where it generates steam for the PSR cycle. The supercritical fluid (*S48*) then returns to the SCWR. As previously mentioned, the only interaction between the supercritical fluid of the SCWR with the Cu-Cl cycle provides the required thermal energy for the hydrolysis and the Cu_2OCl_2 decomposition reactors. The remainder of the thermal energy necessary for the remaining reactors or heat exchanger is through heat recovery from other heat producing devices in the cycle, which is the steam circuit. The first steam circuit charging phase (absorbing thermal energy) starts with water coming from ambient conditions (*S26*) that is heated by the cooling solidified CuCl (*S13*) to (*S14*) through the heat exchanger (*B17* and *B10*) to produce a saturated mixture (*S27*). S27 is then mixed (in mixer *B19*) with the steam (*S21*) exiting the dryer (*B14*) and the result is saturated steam (*S22*) that will absorb the latent heat released during the solidification of the molten CuCl (*S10*) and produce a superheated steam (S28).

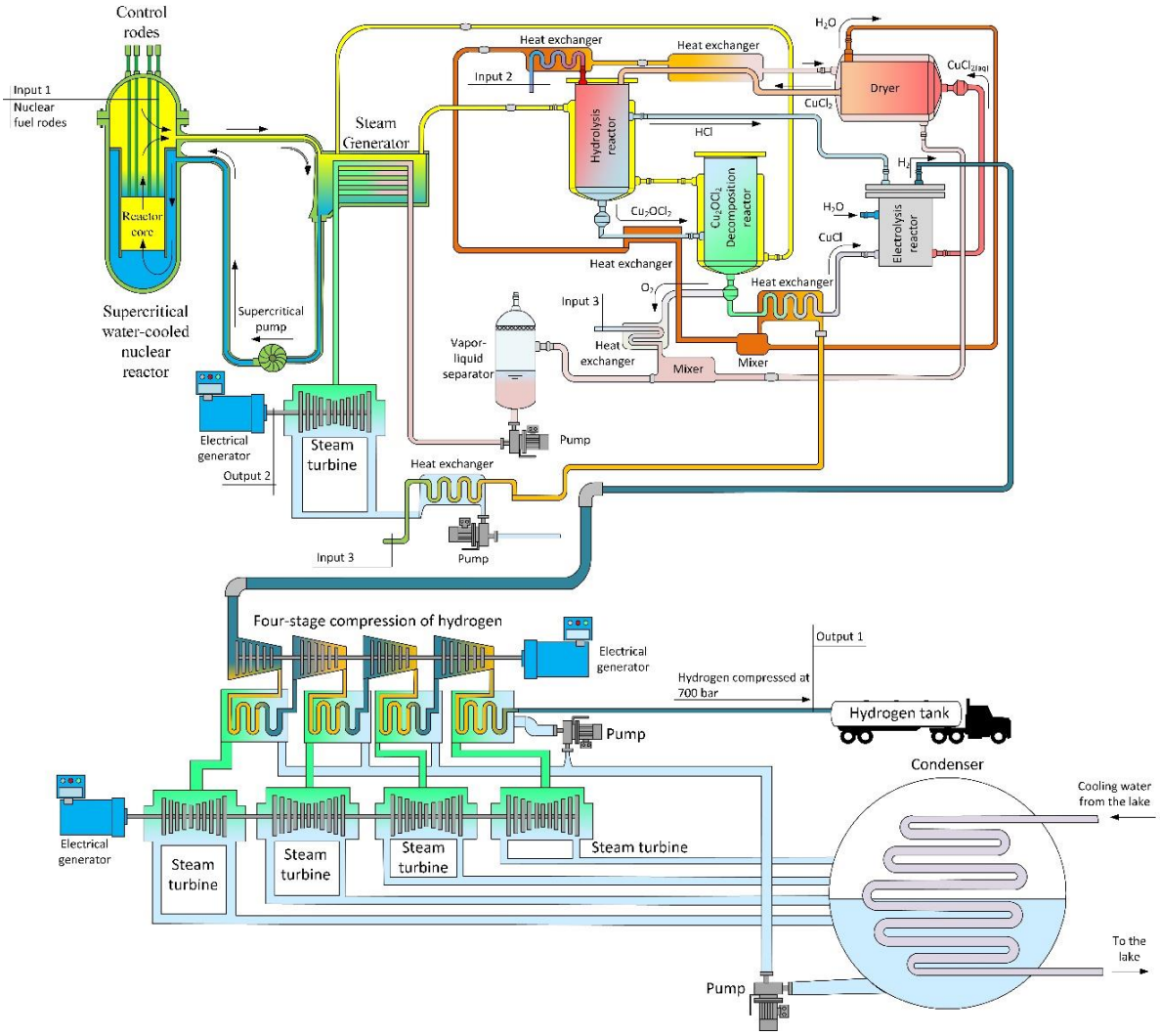

Figure 3.20 The schematic diagram of the nuclear-based integrated system for electrical power and hydrogen production. The produced hydrogen is compressed in a four-stage hydrogen compression system, and the electrical power requirements of the integrated system are fulfilled by the supporting Rankine cycle

The second phase begins when the superheated steam (*S28*) heats the Cu_2OCl_2 (*S6*) to the operating temperature of the Cu_2OCl_2 decomposition reactor (*B6*) before entering the Cu_2OCl_2 decomposition reactor. Then it heats the water before entering the hydrolysis reactor and also heats the solid $CuCl_2$ (in heat exchanger *B20* and *B3*) to the operating temperature of the hydrolysis reactor. The heating water exiting B20 provide the necessary thermal energy to the dryer (*B14*) and then mixes with heated water (*S24*) exiting the water and oxygen heat exchanger (*B8*) and the mixture (*S42*) is conveyed to the PSR cycle The

PSR cycle receives the saturated mixture water with small vapor fraction and mixes it with water that recovered heat from water exiting the turbine to produce lower quality water (*S50*). This water enters a vapor-liquid separator, recovering part of the thermal energy in the vapor exiting the vapor-liquid separator by preheating water from ambient conditions (*S4*).

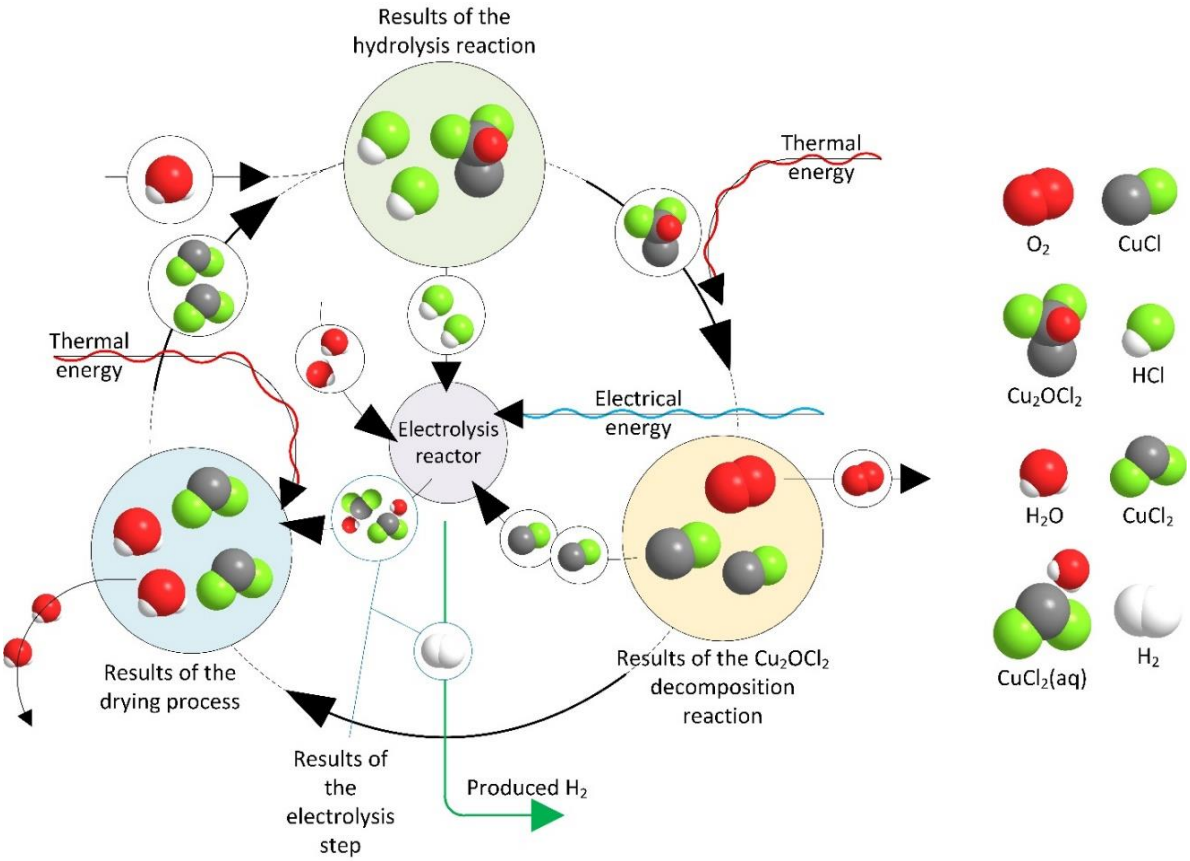

Figure 3.21 The main interactions that occur in the four-step Cu-Cl cycle for thermochemical water decomposition in the integrated system.

The liquid exiting the vapor-liquid separator (*S61*) is pumped to 200 bar and then superheated by the supercritical fluid to produce superheated steam at 621ºC (*S53*). This superheated steam expands through the steam turbine (*B32*) to produce electrical power that is used to cover the electrolysis reactor needs plus the needs for the hydrogen compression system (HCS) and other work consuming devices such as pumps. pressure of 700 bar.

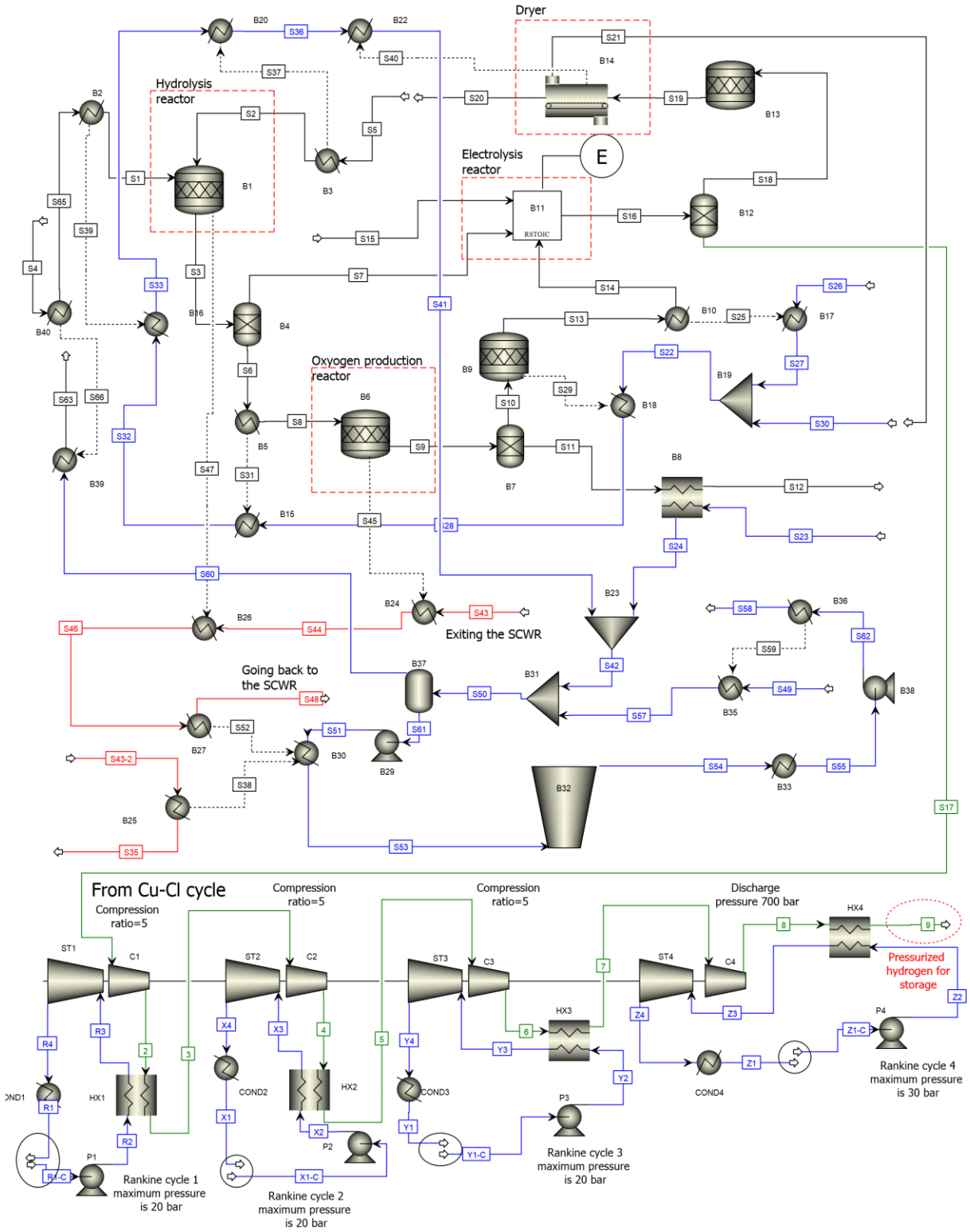

Figure 3.22 The Aspen Plus flow sheet for the simulation of the integrated nuclear-based electrical power and hydrogen production plant.

Table 3.13 The main parameters in the proposed integrated system, consisting of SCWR, Cu-Cl cycle, supporting combined cycle, and hydrogen compression system (Aspen Plus blocks or stream names are listed in parentheses and refer to the Aspen Plus model in Figure 3.23).

Component	Parameter	Value	Unit	Ref.
SCWR	Temperature of steam exiting reactor (S43)	625	ºC	[45,75]
	Temperature of water returning to reactor (S48)	350	ºC	[45,75]
	Operating pressure of nuclear reactor	25	MPa	[45,75]
	Thermal energy output	2,540	MW	[45,75]
	Supercritical steam mass flow rate	1,320	kg/s	[45,75]
	T_{max} cladding	850	ºC	[45,75]
Cu-Cl cycle	Four-step hybrid thermochemical and electrical water decomposition cycle			
	Hydrolysis reactor (B1) operating temperature	400	ºC	[57,58]
	Hydrolysis reactor (B1) operating pressure	1	bar	[57,58]
	Oxygen production reactor (Cu_2OCl_2 decomposition reactor) (B6) operating temperature	530	ºC	[57,58]
	Oxygen production reactor (Cu_2OCl_2 decomposition reactor) (B6) operating pressure	1	bar	[57,58]
	Electrolysis reactor (B11) operating temperature	25	ºC	[57,58]
	Electrolysis reactor (B11) operating pressure	1	bar	[57,58]
	Electrolysis reactor (B11) electrical unit energy requirements	55.0	kJ/mol H_2	[46,57]
	Amount of H_2O added to the electrolysis reactor.	20	mol	
	Dryer (B14) operating temperature (higher than required to superheat the evaporated water)	110	ºC	
	Dryer (B14) drying temperature	100	ºC	[57,58]
	Dryer (B14) operating pressure	1	bar	[57,58]
	Solid phase properties of the materials in the Cu-Cl cycle are reported in Table 3			
Hydrogen compression system	Hydrogen final pressure	700	bar	[9,42]
	Number of compression stages	4	stages	
	Pressure ratio of each stage except final stage	5		
	Rankine cycle connected to intercoolers			
	RC1 operating pressure	20	bar	
	RC2 operating pressure	20	bar	
	RC3 operating pressure	20	bar	

	RC4 operating pressure	30	bar	
	$\eta_{is,C}$	0.72		[76]
	$\eta_{is,ST}$	0.72		[76]
Supporting Rankine cycle	Rankine cycle operating pressure	200	bar	
	$\eta_{is,ST}$	0.72		[76]

The four-stage HCS compresses the hydrogen produced from the Cu-Cl cycle to a pressure of 700 bar. The first three stages have a compression ratio of 5 and the fourth stage has a discharge. The produced hydrogen (S17) enters the HCS first compression stage, which compresses the hydrogen from 1 bar to 5 bar; the temperature of the hydrogen rises from 25°C to 291°C across the first compression stage. The hydrogen exiting each compression stage is cooled in heat exchangers, which act as a steam generator for the bottoming Rankine cycles that are added, to recover the heat and reduce the overall electrical power required to compress the hydrogen. The remaining three compression stages use the same procedure to finally produce hydrogen at 700 bar and 25°C (*9*).

Chapter 4: Thermodynamic Analysis

In this chapter the detailed thermodynamic analysis of the four proposed system will be presented, plus the main assumptions made during the simulation and the calculations of the thermodynamic parameters.

4.1 Assumptions

In this section the assumptions made during the development and analysis of the hydrogen and power production plant are presented for each system of the four developed systems. The property methods used to find the properties of the materials in the four systems is also included in this section. The assumptions made:

For System 1:

Some assumptions are made for the analyses of the system components as follows:

- The hydrogen production plant operates at steady state conditions
- The hydrogen production plant starting up period is not considered
- The kinetic and gravitational potential energies changes are neglected throughout the plant
- All gases in the system are treated as real gases (exception for this assumption is for the gases in the chemical exergy equation, they are treated as ideal gases)
- The electrical generator thermal efficiency is $\eta_{gen} = 95\%$

The property sources used in Aspen Plus simulation are given as follows:

For H_2O:

- The 1984 NBS/NRC: Steam table correlations for thermodynamic properties are used for H_2O.
- The International Association for Properties of Steam (IAPS) correlations for transport properties for H_2O (Aspen Plus property method: STEAMNBS for the temperature range of 273.15 K to 2000 K at a maximum pressure of over 10,000 bar) are used.

For all of the remaining fluids in the hydrogen production plant, the following property methods are employed:

- The general model for real components (Aspen Plus property method: RK-SOAVE).
- As a second choice, the Redlich-Kwong-Soave (RKS) cubic equation of state with the Boston-Mathias alpha function.

For coal, the following property methods are used:

- ASTM Standard D5865-07a for measuring the gross calorific value of coal.
- The Boie correlation for calculating the heat of combustion.
- The Kirov correlation for calculating coal's heat capacity (Aspen Plus option: HCOALGEN).
- The coal density is evaluated based on equations from [79] (Aspen Plus option: DCOALIGT).
    - Input data to Aspen Plus for each type of coal are as follows:
        - Proximate analysis (wet, mass basis).
        - Ultimate analysis (dry, mass basis).
        - Sulfuric analysis (wet, mass basis).
- The solid phase properties of CuCl, $CuCl_2$, Cu_2OCl_2, and CuO, are listed in Tables 3.5, 3.6, 3.7 and 3.8 respectively.

Assumptions that are more specific for each of the subsystems of the overall systems are presented here.

Specific assumptions made for the gasifier:

- All gas and solid mixtures in the system are homogenous.
- The pressure drops are negligible in the gasifier components.
- The main syngas products can be taken to be CO, H_2, and CO_2 for the model validation.

For combustion chambers and the heat exchanger unit:

- Pressure drops are neglected.

- The combustion is based on Gibbs free energy minimization approach.
- The heat loss in the HRSG is 10% of the total exchanged heat.
- The heat loss is 10% of the total exchanged heat in the in other heat exchangers in the system (unless otherwise stated).

For gas turbines:

- The gas turbines are adiabatic (i.e., to incur no heat losses).
- The isentropic efficiency of all gas turbines are $\eta_{is,GT}$ = 0.72 [76].

For the CASU:

- The condensing fluid in the distillation column occur at a temperature of -179°C.
- In the distillation column, the condenser operating temperature is very low which requires a refrigerator system to maintain that low temperature for the fluid to condense. The refrigerator system has a COP = 2. COP = 2 was selected based on the results of the parametric study shown in Figure 4.1. Figure 4.1 indicates that the value of COP that the energy and exergy of the system stay nearly constant at 2.

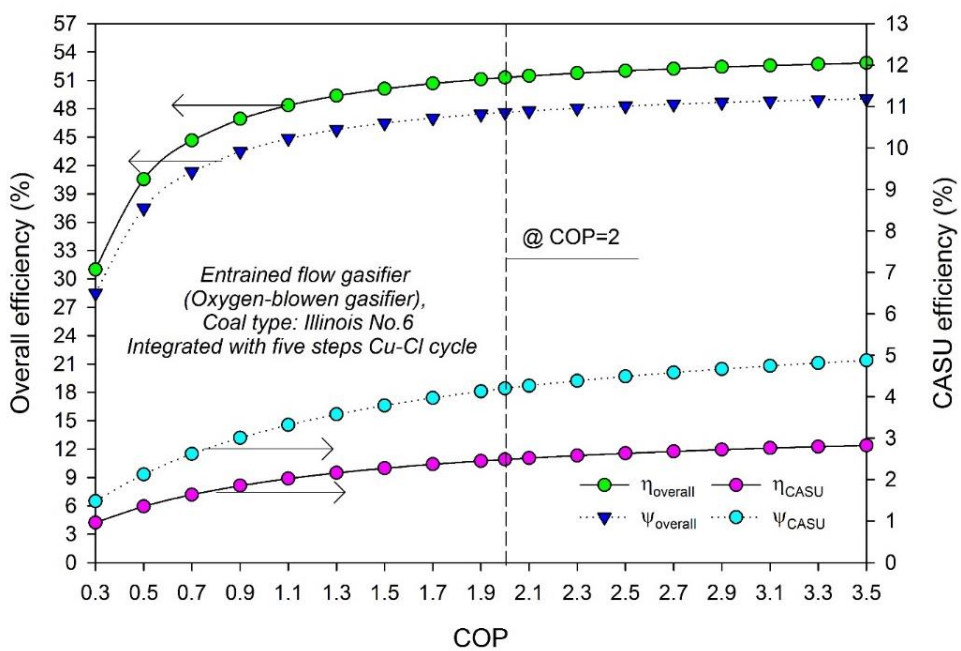

Figure 4.1 The variation of the overall energy and exergy efficiencies and the CASU energy and exergy efficiencies.

For copper-chlorine cycle:

- No heat losses occur in the copper-chlorine cycle heat exchangers
- Electrical power requirement by the electrolysis reactor is 63 kJ/mol H_2 [17]
- Electrical power generator efficiency is 95%

For hydrogen compression system:

- The isentropic efficiency of all steam turbines can be taken to be $\eta_{is,ST}$ = 0.72 [76]
- The steam turbines can be considered adiabatic (i.e., to incur no heat losses)
- The hydrogen compressors can be regarded as adiabatic (i.e., to incur no heat losses)
- The isentropic efficiency for all hydrogen compressors can be taken to be $\eta_{is,GT}$ = 0.72 [76]

For the hydrogen-fueled combined cycle:

- The isentropic efficiency of all steam turbines can be taken to be $\eta_{is,ST}$ = 0.72 [76]
- The steam turbines can be considered adiabatic (i.e., to incur no heat losses)
- The hydrogen compressors can be regarded as adiabatic (i.e., to incur no heat losses)
- The isentropic efficiency for all hydrogen compressors can be taken to be $\eta_{is,GT}$ = 0.72 [76]
- The combustion chamber oxidant is air
- The combustion is carried out based on Gibbs free energy minimization approach (Gibbs reactor)
- Hydrogen compressor has a compression ratio of 36 [31]
- Air compressor has a compression ratio of 36 [31]
- The Rankine cycle has a maximum pressure of 200 bar

For System 2:

The main assumptions made during the development process of the proposed integrated system of the SCWR, Cu-Cl cycle, HCS, and SCC and they are as follows:

- Steady state condition is applied to all components of the integrated system.
- No startup period is considered.
- The energy changes that associated with gravitational and kinetic energies are no taken into consideration.
- The electrical generator efficiency is 95%.
- Heat losses in the heat exchangers are neglected.
- Due to the high average capacity factor of the nuclear reactors, the analysis considers the reactors operates at steady state conditions [45,80].
- Reference temperature and pressure for exergy calculations are 25°C and 1 atm.
- Pressure losses are neglected in all heat exchangers.
- Compressors and turbines operate under adiabatic conditions.

An important step in building the Aspen Plus model and successfully running the simulation is selecting the appropriate property method. The properties chosen for the construction of the models are as follows:

Aspen Plus selected property methods:

- For H_2O: *Steamnbs* for the temperature range of 273 K to 2000 K at a maximum pressure of over 10,000 bar.
- For the remaining materials: Rk-Soave.

Aspen Hysys selected property methods:

- For H_2O: NBS steam.

For System 3:

A group of assumptions are made during the modeling and simulation of the proposed hydrogen production plant:

- The hydrogen production plant is operating through steady state conditions, at the instance were the solar heliostat system is producing 5MW_{th} power.
- Starting up period is not considered.

- Energy changes associated with elevation and kinetic energy are neglected throughout the plant.
- Gasses are treated as real gasses (exception for is the calculations of the chemical exergy, they are treated as ideal gasses).
- Efficiency of the conversion process from work rate to electrical power is $\eta_{gen} = 95\%$.

Property sources selected from Aspen Plus data based in order to carry out the simulation are as follows:

- Steam tables used are: the 1984 NBS/NRC steam tables.
- Aspen Plus property method: *Steamnbs* for H_2O and for a temperature range of 273K to 2,000 K. The maximum pressure is over 10,000 bar.
- Aspen Plus property method: *Rk-soave*.
- The solid phase properties of CuCl, $CuCl_2$, Cu_2OCl_2, and CuO, are listed in Tables 4.5, 4.6, 4.7 and 4.8.

Assumptions that are more specific for each of the subsystems of the overall systems are presented here.

- The pressure losses are neglected through the heat exchangers
- The heat loss is 10% of the total exchanged heat in the in other heat exchangers in the system (unless otherwise stated)
- No heat losses associated with the Cu-Cl cycle heat exchangers
- Electrolysis reactor requires 63 kJ per each mol of H_2 is produced [17]
- Steam turbines have $\eta_{is,ST} = 0.72$ [76]
- Steam turbines are assumed adiabatic
- Hydrogen compressors are assumed adiabatic
- Hydrogen compressors have $\eta_{is,co} = 0.72$ [76]
- Mechanical efficiency of compressors is 95% [81]

The following assumptions are made during the design, development and analysis of the integrated hydrogen and electrical power production system consisting of a SCWR, a four-step Cu-Cl cycle, a HCS, and a PSR:

- All components operate at steady-state conditions
- The startup period is not considered
- Changes in gravitational and kinetic energies are neglected
- The electrical generator energy efficiency (η_{gen}) is 95%
- Heat losses are neglected in heat exchangers
- Pressure drops are neglected in heat exchangers
- Heat losses are neglected in turbines and compressors

The reference environment conditions are taken to be 25°C and 1 atm. A successful simulation of the integrated system requires the proper selection of property methods for the different categories of materials involved. The following property methods are used for the integrated system:

- *Steamnbs* is selected because it can accommodate supercritical water (for a temperature range of 273 K to 2000 K and a maximum pressure of over 10,000 bar)
- Properties for solid phase materials in the Cu-Cl cycle from other sources are listed in Table 3 and are entered into Aspen Plus
- *Solid* is used for other materials
- Peng-Robinson (*Peng-Rob*) is used for gases

4.2 Thermodynamic Analysis of System 1

For the gasification system consisting of gasifier GFEMA model for the gasifier, CASU, WGSMR and Brayton cycle plus another system utilizes main input parameters are presented in Table 4.3.

General steady-state thermodynamic rate balance equations for mass and energy, for open systems and with kinetic and gravitational potential energies neglected follow:

$$\sum \dot{m}_{in} = \sum \dot{m}_{out} \tag{4.1}$$

$$\dot{Q}_{in} - \dot{Q}_{out} + \dot{W}_{in} - \dot{W}_{out} = \sum_{out} \dot{m}\left(h_{P\&T} - h_{T_o\&P_o} + h_f\right) - \sum_{in} \dot{m}\left(h_{P\&T} - h_{T_o\&P_o} + h_f\right) \tag{4.2}$$

where $\dot{m}$ is the mass flow rate, $\dot{Q}$ is the heat rate, $\dot{W}$ is the work rate, h is the specific enthalpy, and the subscripts in and out denote input and output. The energy and exergy balance equations for each component in the system are presented in Tables 4.1-4.3 for each of the components in Figures 3.7-3.10 respectively.

Table 4.1 The energy and exergy balance equations for the components of the system shown in Figure 3.7, the subscripts refer to the component name, and stream names in Figure 3.7.

Component	Energy balance equation	Exergy balance equation
B1 (compressor)	$\dot{m}_{AS1}h_{AS1} + \dot{W}_{in} = \dot{m}_{AS2}h_{AS2}$	$\dot{m}_{AS1}ex_{AS1} + \dot{W}_{in} = \dot{m}_{AS2}ex_{AS2} + \dot{E}x_d$
B11 (heat exchanger)	$\dot{m}_{AS3}h_{AS3} - \dot{m}_{AS3}h_{AS3} = (\dot{m}_{AS10}h_{AS10} - \dot{m}_{AS16}h_{AS16}) + (\dot{m}_{AS7}h_{AS7} - \dot{m}_{AS17}h_{AS17})$	$\dot{m}_{AS3}ex_{AS3} - \dot{m}_{AS3}ex_{AS3} = (\dot{m}_{AS10}ex_{AS10} - \dot{m}_{AS16}ex_{AS16}) + (\dot{m}_{AS7}ex_{AS7} - \dot{m}_{AS17}ex_{AS17}) + \dot{E}x_d$
B3 (pressure valve)	$\dot{m}_{AS3}h_{AS3} = \dot{m}_{AS4}h_{AS4}$	$\dot{m}_{AS3}ex_{AS3} = \dot{m}_{AS4}ex_{AS4} + \dot{E}x_d$
B4 (distillation column)	$\dot{m}_{AS4}h_{AS4} + \dot{Q}_{RB} = \dot{m}_{AS5}h_{AS5} + \dot{m}_{AS6}h_{AS6} + \dot{Q}_{RC}$	$\dot{m}_{AS4}ex_{AS4} + \dot{E}x_{\dot{Q}_{RB}} = \dot{m}_{AS5}ex_{AS5} + \dot{m}_{AS6}ex_{AS6} + \dot{E}x_d + \dot{E}x_{\dot{Q}_{RC}}$
RC[1]	$\dot{Q}_{Rc} + \dot{W}_{RC} = \dot{Q}_{out}$	$\dot{E}x_{\dot{Q}_{Rc}} + \dot{W}_{RC} = \dot{E}x_{\dot{Q}_{out}} + \dot{E}x_d$
B5 (pressure valve)	$\dot{m}_{AS5}h_{AS5} = \dot{m}_{AS10}h_{AS10}$	$\dot{m}_{AS5}ex_{AS5} = \dot{m}_{AS10}ex_{AS10} + \dot{E}x_d$
B6 (pressure valve)	$\dot{m}_{AS6}h_{As6} = \dot{m}_{AS7}h_{AS7}$	$\dot{m}_{AS6}ex_{As6} = \dot{m}_{AS7}ex_{AS7} + \dot{E}x_d$
B12 (N_2 turbine)	$\dot{m}_{AS16}h_{AS16} - \dot{m}_{AS18}h_{AS18} = \dot{W}_{B12}$	$\dot{m}_{AS16}ex_{AS16} - \dot{m}_{AS18}ex_{AS18} = \dot{W}_{B12} + \dot{E}x_d$
QQ (heat exchanger)	$\dot{m}_{AS18}h_{AS18} - \dot{m}_{AS18}h_{AS18} = \dot{Q}_{QQ}$	$\dot{m}_{AS18}ex_{AS18} - \dot{m}_{AS18}ex_{AS18} = \dot{E}x_{\dot{Q}_{QQ}} + \dot{E}x_d$
Pump-W	$\dot{m}_{Z2}h_{Z2} + \dot{W}_{in} = \dot{m}_{z3}h_{Z3}$	$\dot{m}_{Z2}ex_{Z2} + \dot{W}_{in} = \dot{m}_{z3}ex_{Z3} + \dot{E}x_d$
STMG1 (heat exchanger)	$\dot{m}_{Z3}h_{Z3} + \dot{Q}_{in} = \dot{m}_{ttsteam}h_{ttsteam}$	$\dot{m}_{Z3}ex_{Z3} + \dot{E}x_{\dot{Q}_{in}} = \dot{m}_{ttsteam}ex_{ttsteam} + \dot{E}x_d$
Compres2 (O_2 compressor)	$\dot{m}_{AS17}h_{AS17} + \dot{W}_{in} = \dot{m}_{oxygen}h_{oxygen}$	$\dot{m}_{AS17}ex_{AS17} + \dot{W}_{in} = \dot{m}_{oxygen}ex_{oxygen} + \dot{E}x_d$
Ryield (Yield reactor)	$\dot{m}_{coal}LHV_{coal} + \dot{Q}_{DECOMP1} = \dot{m}_{pyrprd}LHV_{pyrprd}$	$\dot{m}_{coal}ex_{coal} = \dot{E}x_{\dot{Q}_{DECOMP1}} + \dot{m}_{pyrprd}ex_{pyrprd} + \dot{E}x_d$

Gasifica (Gibbs free energy minimization reactor)	$\dot{m}_{ttsteam}h_{ttsteam} + \dot{m}_{oxygen}h_{oxygen} + \dot{m}_{pyrprd}LHV_{pyrprd} - \dot{Q}_{DECOMP1} = \dot{m}_{product}h_{product}$	$\dot{m}_{ttsteam}ex_{ttsteam} + \dot{m}_{oxygen}ex_{oxygen} + \dot{m}_{pyrprd}ex_{pyrprd} - \dot{E}x_{\dot{Q}_{DECOMP1}} = \dot{m}_{product}ex_{product} + \dot{E}x_d$
GT2 (gas turbine)	$\dot{m}_{product}h_{product} = \dot{m}_{Z6}h_{Z6} + \dot{W}_{out}$	$\dot{m}_{product}ex_{product} = \dot{m}_{Z6}ex_{Z6} + \dot{W}_{out} + \dot{E}x_d$
Cooling (mixer)	$\dot{m}_{steam2}h_{steam2} + \dot{m}_{Z6}h_{Z6} = \dot{m}_{S1}h_{S1}$	$\dot{m}_{steam2}ex_{steam2} + \dot{m}_{Z6}ex_{Z6} = \dot{m}_{S1}ex_{S1} + \dot{E}x_d$
QO and STMG2 (heat exchanger)	$\dot{m}_{klp}h_{klp} = \dot{Q}_{out} + \dot{m}_{steam2}h_{steam2}$	$\dot{m}_{klp}ex_{klp} = \dot{E}x_{\dot{Q}_{out}} + \dot{m}_{steam2}ex_{steam2} + \dot{E}x_d$
HX10 (heat exchanger)	$\dot{m}_{s1}h_{s1} - \dot{m}_{s6}h_{s6} = \dot{m}_{klp}h_{klp} - \dot{m}_{z5}h_{z5}$	$\dot{m}_{s1}ex_{s1} - \dot{m}_{s6}ex_{s6} = \dot{m}_{klp}ex_{klp} - \dot{m}_{z5}ex_{z5} + \dot{E}x_d$
Pump-W2	$\dot{m}_{z4}h_{z4} + \dot{W}_{in} = \dot{m}_{z5}h_{z5}$	$\dot{m}_{z4}ex_{z4} + \dot{W}_{in} = \dot{m}_{z5}ex_{z5} + \dot{E}x_d$
Hwgmrp1 (stoichiometric reactor[2])	$\dot{m}_{s6}h_{s6} = \dot{Q}_{out} + \dot{m}_{s7}h_{s7}$	$\dot{m}_{s6}ex_{s6} = \dot{E}x_{\dot{Q}_{out}} + \dot{m}_{s7}ex_{s7} + \dot{E}x_d$
Hwgmrp2 (separator)	$\dot{m}_{s7}h_{s7} = \dot{m}_{s24}h_{s24} + \dot{m}_{s9}h_{s9}$	$\dot{m}_{s7}ex_{s7} = \dot{m}_{s24}ex_{s24} + \dot{m}_{s9}ex_{s9} + \dot{E}x_d$
MRP3 (pressure valve)	$\dot{m}_{s9}h_{s9} = \dot{m}_{s10}h_{s10}$	$\dot{m}_{s9}ex_{s9} = \dot{m}_{s10}ex_{s10} + \dot{E}x_d$
Compr1 (air compressor)	$\dot{m}_{s12}h_{s12} + \dot{W}_{in} = \dot{m}_{s13}h_{s13}$	$\dot{m}_{s12}ex_{s12} + \dot{W}_{in} = \dot{m}_{s13}ex_{s13} + \dot{E}x_d$
Tfcomp (treated syngas compressor)	$\dot{m}_{s24}h_{s24} + \dot{W}_{in} = \dot{m}_{s14}h_{s14}$	$\dot{m}_{s24}ex_{s24} + \dot{W}_{in} = \dot{m}_{s14}ex_{s14} + \dot{E}x_d$
Comb (Gibbs free energy minimization reactor)	$\dot{m}_{s13}h_{s13} + \dot{m}_{s14}h_{s14} = \dot{m}_{s16}h_{s16} + \dot{Q}_{out}$	$\dot{m}_{s13}ex_{s13} + \dot{m}_{s14}ex_{s14} = \dot{m}_{s16}ex_{s16} + \dot{E}x_{\dot{Q}_{out}} + \dot{E}x_d$
GT (gas turbine)	$\dot{m}_{s16}h_{s16} = \dot{m}_{s18}h_{s18} + \dot{W}_{out}$	$\dot{m}_{s16}ex_{s16} = \dot{m}_{s18}ex_{s18} + \dot{W}_{out} + \dot{E}x_d$
Hx-P1 (heat exchanger)	$\dot{m}_{s18}h_{s18} = \dot{m}_{s19}h_{s19} + \dot{Q}_{out}$	$\dot{m}_{s18}ex_{s18} = \dot{m}_{s19}ex_{s19} + \dot{E}x_{\dot{Q}_{out}} + \dot{E}x_d$
STMGG (heat exchanger)	$\dot{m}_{s19}h_{s19} = \dot{m}_{exhu}h_{exhu} + \dot{Q}_{out}$	$\dot{m}_{s19}ex_{s19} = \dot{m}_{exhu}ex_{exhu} + \dot{E}x_{\dot{Q}_{out}} + \dot{E}x_d$

1 The refrigerator system used to remove the heat from the condensing fluid in the distillation column in the condenser is not simulated in the Aspen Plus model, however it is considered in the energy analysis

2 Stoichiometric reactor is a reactor that carries the reaction based on the conversion percentage of one of the reactants set by the user, with mass and energy balance

Table 4.2 The energy and exergy balance equations for the components of the system shown in Figure 3.8, the subscripts refer to the component name, and stream names in Figure 3.8.

Component	Energy balance equation	Exergy balance equation
B1(heat exchanger)	$\dot{m}_{s1}h_{s1} = \dot{m}_{s3}h_{s3} + \dot{Q}_{out}$	$\dot{m}_{s1}ex_{s1} = \dot{m}_{s3}ex_{s3} + \dot{E}x_{\dot{Q}_{out}} + \dot{E}x_d$
B2(heat exchanger)	$\dot{m}_{s17}h_{s17} = \dot{m}_{s4}h_{s4} + \dot{Q}_{out}$	$\dot{m}_{s17}ex_{s17} = \dot{m}_{s4}ex_{s4} + \dot{E}x_{\dot{Q}_{out}} + \dot{E}x_d$
B3(stoichiometric reactor[1])	$\dot{m}_{s3}h_{s3} + \dot{m}_{s4}h_{s4} + \dot{Q}_{in} = \dot{m}_{s5}h_{s5}$	$\dot{m}_{s3}ex_{s3} + \dot{m}_{s4}ex_{s4} + \dot{E}x_d + \dot{E}x_{\dot{Q}_{in}} = \dot{m}_{s5}ex_{s5}$
B4(separator)	$\dot{m}_{s5}h_{s5} = \dot{m}_{s6}h_{s6} + \dot{m}_{s7}h_{s7}$	$\dot{m}_{s5}ex_{s5} = \dot{m}_{s6}ex_{s6} + \dot{E}x_d + \dot{m}_{s7}ex_{s7}$
B5(heat exchanger)	$\dot{m}_{s31}h_{s31} + \dot{Q}_{in} = \dot{m}_{s8}h_{s8}$	$\dot{m}_{s31}ex_{s31} + \dot{E}x_{\dot{Q}_{in}} = \dot{m}_{s8}ex_{s8} + \dot{E}x_d$
B6(stoichiometric reactor[1])	$\dot{m}_{s8}h_{s8} + \dot{Q}_{in} = \dot{m}_{s9}h_{s9}$	$\dot{m}_{s8}ex_{s8} + \dot{E}x_{\dot{Q}_{in}} = \dot{m}_{s9}ex_{s9} + \dot{E}x_d$
B7(separator)	$\dot{m}_{s9}h_{s9} = \dot{m}_{s11}h_{s11} + \dot{m}_{s10}h_{s10}$	$\dot{m}_{s9}ex_{s9} = \dot{m}_{s11}ex_{s11} + \dot{m}_{s10}ex_{s10} + \dot{E}x_d$
B8(stoichiometric reactor[1], used for phase change)	$\dot{m}_{s36}h_{s36} = \dot{Q}_{out} + \dot{m}_{s30}h_{s30}$	$\dot{m}_{s36}ex_{s36} = \dot{E}x_{\dot{Q}_{out}} + \dot{m}_{s30}ex_{s30} + \dot{E}x_d$
B9(mixer)	$\dot{m}_{s39}h_{s39} + \dot{m}_{s35}h_{s35} + \dot{m}_{s13}h_{s13} = \dot{m}_{s14}h_{s14}$	$\dot{m}_{s39}ex_{s39} + \dot{m}_{s35}ex_{s35} + \dot{m}_{s13}ex_{s13} = \dot{m}_{s14}ex_{s14} + \dot{E}x_d$
B10(stoichiometric reactor[1])	$\dot{m}_{s14}h_{s14} + \dot{W}_e = \dot{m}_{s15}h_{s15}$	$\dot{m}_{s14}ex_{s14} + \dot{W}_e = \dot{m}_{s15}ex_{s15} + \dot{E}x_d$
B11(heat exchanger)	$\dot{m}_{s34}h_{s34} = \dot{m}_{s41}h_{s41} + \dot{Q}_{out}$	$\dot{m}_{s34}ex_{s34} = \dot{m}_{s41}ex_{s41} + \dot{E}x_{\dot{Q}_{out}} + \dot{E}x_d$
B12(Dryer)	$\dot{m}_{s20}h_{s20} + \dot{Q}_{in} = \dot{m}_{s22}h_{s22} + \dot{m}_{s21}h_{s21}$	$\dot{m}_{s20}ex_{s20} + \dot{E}x_{\dot{Q}_{in}} = \dot{m}_{s22}ex_{s22} + \dot{m}_{s21}ex_{s21} + \dot{E}x_d$
B13(separator)	$\dot{m}_{s15}h_{s15} = \dot{m}_{s18}h_{s18} + \dot{m}_{s19}h_{s19}$	$\dot{m}_{s15}ex_{s15} = \dot{m}_{s18}ex_{s18} + \dot{m}_{s19}ex_{s19} + \dot{E}x_d$
B14(stoichiometric reactor[1])	$\dot{m}_{s18}h_{s18} = \dot{m}_{s20}h_{s20}$	$\dot{m}_{s18}ex_{s18} = \dot{m}_{s20}ex_{s20} + \dot{E}x_d$
B15(heat exchanger)	$\dot{m}_{s2}h_{s2} - \dot{m}_{s17}h_{s17} = (\dot{m}_{s23}h_{s23} - \dot{m}_{s16}h_{s16}) + (\dot{m}_{s11}h_{s11} - \dot{m}_{s28}h_{s28})$	$\dot{m}_{s2}ex_{s2} - \dot{m}_{s17}ex_{s17} = (\dot{m}_{s23}ex_{s23} - \dot{m}_{s16}ex_{s16}) + (\dot{m}_{s11}ex_{s11} - \dot{m}_{s28}ex_{s28}) + \dot{E}x_d$
B16(separator)	$\dot{m}_{s7}h_{s7} = \dot{m}_{s24}h_{s24} + \dot{m}_{s23}h_{s23}$	$\dot{m}_{s7}ex_{s7} = \dot{m}_{s24}ex_{s24} + \dot{m}_{s23}ex_{s23} + \dot{E}x_d$

B17(heat exchanger)	$\dot{m}_{s24}h_{s24} + \dot{Q}_{in} = \dot{m}_{s26}h_{s26}$	$\dot{m}_{s24}ex_{s24} + \dot{E}x_{\dot{Q}_{in}} = \dot{m}_{s26}ex_{s26} + \dot{E}x_d$
B18(heat exchanger)	$\dot{m}_{s40}h_{s40} + \dot{Q}_{in} = \dot{m}_{s25}h_{s25}$	$\dot{m}_{s40}ex_{s40} + \dot{E}x_{\dot{Q}_{in}} = \dot{m}_{s25}ex_{s25} + \dot{E}x_d$
B19(stoichiometric reactor[1])	$\dot{m}_{s25}h_{s25} + \dot{m}_{s26}h_{s26} + \dot{Q}_{in} = \dot{m}_{s27}h_{s27}$	$\dot{m}_{s25}ex_{s25} + \dot{m}_{s26}ex_{s26} + \dot{E}x_{\dot{Q}_{in}} = \dot{m}_{s27}ex_{s27} + \dot{E}x_d$
B20(heat exchanger)	$\dot{m}_{s32}h_{s32} - \dot{m}_{s29}h_{s29} = \dot{m}_{s40}h_{s40} - \dot{m}_{s19}h_{s19}$	$\dot{m}_{s32}ex_{s32} - \dot{m}_{s29}ex_{s29} = \dot{m}_{s40}ex_{s40} - \dot{m}_{s19}ex_{s19} + \dot{E}x_d$
B21(heat exchanger)	$\dot{m}_{s10}h_{s10} - \dot{m}_{s36}h_{s36} = \dot{m}_{s31}h_{s31} - \dot{m}_{s6}h_{s6}$	$\dot{m}_{s10}ex_{s10} - \dot{m}_{s36}ex_{s36} = \dot{m}_{s31}ex_{s31} - \dot{m}_{s6}ex_{s6} + \dot{E}x_d$
B22(heat exchanger)	$\dot{m}_{s30}h_{s30} - \dot{m}_{s38}h_{s38} = \dot{m}_{s37}h_{s37} - \dot{m}_{s21}h_{s21}$	$\dot{m}_{s30}ex_{s30} - \dot{m}_{s38}ex_{s38} = \dot{m}_{s37}ex_{s37} - \dot{m}_{s21}ex_{s21} + \dot{E}x_d$
B23(separator)	$\dot{m}_{s27}h_{s27} = \dot{m}_{s32}h_{s32} + \dot{m}_{s33}h_{s33}$	$\dot{m}_{s27}ex_{s27} = \dot{m}_{s32}ex_{s32} + \dot{m}_{s33}ex_{s33} + \dot{E}x_d$
B24(heat exchanger)	$\dot{m}_{s38}h_{s38} = \dot{m}_{s39}h_{s39} + \dot{Q}_{out}$	$\dot{m}_{s38}ex_{s38} = \dot{m}_{s39}ex_{s39} + \dot{E}x_{\dot{Q}_{out}} + \dot{E}x_d$
B28(stoichiometric reactor[1], used for phase change)	$\dot{m}_{s29}h_{s29} = \dot{Q}_{out} + \dot{m}_{s34}h_{s34}$	$\dot{m}_{s29}ex_{s29} = \dot{E}x_{\dot{Q}_{out}} + \dot{m}_{s34}ex_{s34} + \dot{E}x_d$

1 Stoichiometric reactor is a reactor that carries the reaction based on the conversion percentage of one of the reactants set by the user, with mass and energy balance

Table 4.3 The energy and exergy balance equation for the components of the system shown in Figure 3.9 and 3.10, the subscripts refer to the component name, and stream names in Figures 3.9 and 3.10.

Component	Energy balance equation	Exergy balance equation
C1(compressor)	$\dot{m}_1h_1 + \dot{W}_{in} = \dot{m}_2h_2$	$\dot{m}_1ex_1 + \dot{W}_{in} = \dot{m}_2ex_2 + \dot{E}x_d$
C2(compressor)	$\dot{m}_3h_3 + \dot{W}_{in} = \dot{m}_4h_4$	$\dot{m}_3ex_3 + \dot{W}_{in} = \dot{m}_4ex_4 + \dot{E}x_d$
C3(compressor)	$\dot{m}_5h_5 + \dot{W}_{in} = \dot{m}_6h_6$	$\dot{m}_5ex_5 + \dot{W}_{in} = \dot{m}_6ex_6 + \dot{E}x_d$
C4(compressor)	$\dot{m}_7h_7 + \dot{W}_{in} = \dot{m}_8h_8$	$\dot{m}_7ex_7 + \dot{W}_{in} = \dot{m}_8ex_8 + \dot{E}x_d$
C5(compressor)	$\dot{m}_{E1}h_{E1} + \dot{W}_{in} = \dot{m}_{E2}h_{E2}$	$\dot{m}_{E1}ex_{E1} + \dot{W}_{in} = \dot{m}_{E2}ex_{E2} + \dot{E}x_d$
C6(compressor)	$\dot{m}_{E3}h_{E3} + \dot{W}_{in} = \dot{m}_{E4}h_{E4}$	$\dot{m}_{E3}ex_{E3} + \dot{W}_{in} = \dot{m}_{E4}ex_{E4} + \dot{E}x_d$
HX1(heat exchanger)	$\dot{m}_2h_2 - \dot{m}_3h_3 = \dot{m}_{R3}h_{R3} - \dot{m}_{R2}h_{R2}$	$\dot{m}_2ex_2 - \dot{m}_3ex_3 = \dot{m}_{R3}ex_{R3} - \dot{m}_{R2}ex_{R2} + \dot{E}x_d$
HX2(heat exchanger)	$\dot{m}_4h_4 - \dot{m}_5h_5 = \dot{m}_{x3}h_{x3} - \dot{m}_{x2}h_{x2}$	$\dot{m}_4ex_4 - \dot{m}_5ex_5 = \dot{m}_{x3}ex_{x3} - \dot{m}_{x2}ex_{x2} + \dot{E}x_d$

HX3(heat exchanger)	$\dot{m}_6 h_6 - \dot{m}_7 h_7 = \dot{m}_{Y3} h_{Y3} - \dot{m}_{Y2} h_{Y2}$	$\dot{m}_6 ex_6 - \dot{m}_7 ex_7 = \dot{m}_{Y3} ex_{Y3} - \dot{m}_{Y2} ex_{Y2} + \dot{E}x_d$
HX4(heat exchanger)	$\dot{m}_8 h_8 - \dot{m}_9 h_9 = \dot{m}_{z3} h_{z3} - \dot{m}_{z2} h_{z2}$	$\dot{m}_8 ex_8 - \dot{m}_9 ex_9 = \dot{m}_{z3} ex_{z3} - \dot{m}_{z2} ex_{z2} + \dot{E}x_d$
HX5(heat exchanger)	$\dot{m}_{E6} h_{E6} - \dot{m}_{E7} h_{E7} = \dot{m}_{k3} h_{k3} - \dot{m}_{k2} h_{k2}$	$\dot{m}_{E6} ex_{E6} - \dot{m}_{E7} ex_{E7} = \dot{m}_{k3} ex_{k3} - \dot{m}_{k2} ex_{k2} + \dot{E}x_d$
ST1(steam turbine)	$\dot{m}_{R3} h_{R3} = \dot{W}_{out} + \dot{m}_{R4} h_{R4}$	$\dot{m}_{R3} ex_{R3} = \dot{W}_{out} + \dot{m}_{R4} ex_{R4} + \dot{E}x_d$
ST2(steam turbine)	$\dot{m}_{x3} h_{x3} = \dot{W}_{out} + \dot{m}_{x4} h_{x4}$	$\dot{m}_{x3} ex_{x3} = \dot{W}_{out} + \dot{m}_{x4} ex_{x4} + \dot{E}x_d$
ST3(steam turbine)	$\dot{m}_{Y3} h_{Y3} = \dot{W}_{out} + \dot{m}_{Y4} h_{Y4}$	$\dot{m}_{Y3} ex_{Y3} = \dot{W}_{out} + \dot{m}_{Y4} ex_{Y4} + \dot{E}x_d$
ST4(steam turbine)	$\dot{m}_{z3} h_{z3} = \dot{W}_{out} + \dot{m}_{z4} h_{z4}$	$\dot{m}_{z3} ex_{z3} = \dot{W}_{out} + \dot{m}_{z4} ex_{z4} + \dot{E}x_d$
ST5(steam turbine)	$\dot{m}_{k3} h_{k3} = \dot{W}_{out} + \dot{m}_{k4} h_{k4}$	$\dot{m}_{k3} ex_{k3} = \dot{W}_{out} + \dot{m}_{k4} ex_{k4} + \dot{E}x_d$
COND1(condenser and a heat exchanger)	$\dot{m}_{R4} h_{R4} = \dot{Q}_{out} + \dot{m}_{R1} h_{R1}$	$\dot{m}_{R4} ex_{R4} = \dot{E}x_{\dot{Q}_{out}} + \dot{m}_{R1} ex_{R1} + \dot{E}x_d$
COND2(condenser and a heat exchanger)	$\dot{m}_{X4} h_{X4} = \dot{Q}_{out} + \dot{m}_{X1} h_{X1}$	$\dot{m}_{X4} ex_{X4} = \dot{E}x_{\dot{Q}_{out}} + \dot{m}_{X1} ex_{X1} + \dot{E}x_d$
COND3(condenser and a heat exchanger)	$\dot{m}_{Y4} h_{Y4} = \dot{Q}_{out} + \dot{m}_{Y1} h_{Y1}$	$\dot{m}_{Y4} ex_{Y4} = \dot{E}x_{\dot{Q}_{out}} + \dot{m}_{Y1} ex_{Y1} + \dot{E}x_d$
COND4(condenser and a heat exchanger)	$\dot{m}_{Z4} h_{Z4} = \dot{Q}_{out} + \dot{m}_{Z1} h_{Z1}$	$\dot{m}_{Z4} ex_{Z4} = \dot{E}x_{\dot{Q}_{out}} + \dot{m}_{Z1} ex_{Z1} + \dot{E}x_d$
COND5(condenser and a heat exchanger)	$\dot{m}_{K4} h_{K4} = \dot{Q}_{out} + \dot{m}_{K1} h_{K1}$	$\dot{m}_{K4} ex_{K4} = \dot{E}x_{\dot{Q}_{out}} + \dot{m}_{K1} ex_{K1} + \dot{E}x_d$
P1(pump)	$\dot{m}_{R1-C} h_{R1-C} + \dot{W}_{in} = \dot{m}_{R2} h_{R2}$	$\dot{m}_{R1-C} ex_{R1-C} + \dot{W}_{in} = \dot{m}_{R2} ex_{R2}$
P2(pump)	$\dot{m}_{X1-C} h_{X1-C} + \dot{W}_{in} = \dot{m}_{X2} h_{X2}$	$\dot{m}_{X1-C} ex_{X1-C} + \dot{W}_{in} = \dot{m}_{X2} ex_{X2} + \dot{E}x_d$
P3(pump)	$\dot{m}_{Y1-C} h_{Y1-C} + \dot{W}_{in} = \dot{m}_{Y2} h_{Y2}$	$\dot{m}_{Y1-C} ex_{Y1-C} + \dot{W}_{in} = \dot{m}_{Y2} ex_{Y2} + \dot{E}x_d$
P4(pump)	$\dot{m}_{Z1-C} h_{Z1-C} + \dot{W}_{in} = \dot{m}_{Z2} h_{Z2}$	$\dot{m}_{Z1-C} ex_{Z1-C} + \dot{W}_{in} = \dot{m}_{Z2} ex_{Z2} + \dot{E}x_d$
P5(pump)	$\dot{m}_{K1-C} h_{K1-C} + \dot{W}_{in} = \dot{m}_{K2} h_{K2}$	$\dot{m}_{K1-C} ex_{K1-C} + \dot{W}_{in} = \dot{m}_{K2} ex_{K2} + \dot{E}x_d$
G1(Gibbs free energy	$\dot{m}_{E2} h_{E2} + \dot{m}_{E4} h_{E4} = \dot{m}_{E5} h_{E5}$	$\dot{m}_{E2} ex_{E2} + \dot{m}_{E4} ex_{E4} = \dot{m}_{E5} ex_{E5} + \dot{E}x_d$

minimization reactor)		
GAST(gas turbine)	$\dot{m}_{E5}h_{E5} = \dot{W}_{out} + \dot{m}_{E6}h_{E6}$	$\dot{m}_{E5}ex_{E5} = \dot{W}_{out} + \dot{m}_{E6}ex_{E6} + \dot{E}x_d$

The energy efficiencies of the subsystems in the hydrogen production plant that produce hydrogen from coal by utilizing the thermochemical water decomposition cycle, and the WGSMR.

The energy efficiency of the gasification system is as follows:

$$\eta_G = \frac{\dot{m}_{syngas}LHV_{syngas}}{\dot{m}_{coal}LHV_{coal}+\dot{W}_{pump-w}+\dot{W}_{pump-W2}+\dot{W}_{compres2}+\dot{Q}_{STMG1}+\dot{Q}_{STGM2}+\dot{Q}_{QO}} \quad (4.3)$$

where the syngas in the numerator of the gasifier energy equation (Equation (4.3)), referring to stream S1 in Figure 3.7. Note that the subscripts are referring to components names in Figure 3.8 except for syngas (stream S1) and coal (stream 1coal in Figure 3.7). The gasification system refers to the gasifier (GFEMA model), oxygen compressor, the two in-cycle heat recovery systems and the two water pumps. The coal LHV used in Equation (4.6) is on a dry basis (see Table 3.1).

The Brayton cycle energy efficiency is as follows:

$$\eta_{BrC} = \frac{\dot{W}_{GT}-\dot{W}_{COMPR1}-\dot{W}_{TFCOMP}}{\dot{m}_{S24}LHV_{S24}} \quad (4.4)$$

Here, the subscripts refer to the component name or the stream name shown in Figure 3.7.

The CASU energy efficiency is as follows:

$$\eta_{CASU} = \frac{\dot{m}_{AS17}h_{As17}}{\dot{W}_{B1}+\dot{m}_{AS1}h_{AS1}+\dot{Q}_{RB(B4)}+\dot{W}_{RC}} \quad (4.5)$$

where the subscripts refer to the component name or the stream name shown in Figure 3.7 except for RC, which denotes to the refrigerator removing the heat from the distillation column condenser.

The WGSMR energy efficiency is as follows:

$$\eta_{WGSMR} = \frac{\dot{m}_{S10}LHV_{H2}+\dot{m}_{S24}LHV_{S24}}{\dot{m}_{S6}LHV_{S6}} \quad (4.6)$$

Here, the subscripts refer to the stream name shown in Figure 3.7.

The copper-chlorine thermochemical water decomposition cycle is as follows:

$$\eta_{Cu-Cl} = \frac{\dot{m}_{H_2} LHV_{H_2}}{\dot{Q}_{in} + \dot{W}_e} = \frac{\dot{m}_{S33} LHV_{S33}}{(\dot{m}_{S2} - \dot{m}_{s23}) h_{S2} + \dot{Q}_{in} + \dot{W}_e} \tag{4.7}$$

$$\dot{Q}_{in} = \dot{Q}_{B2} + \dot{Q}_{B3} + \dot{Q}_{B1} + \dot{Q}_{B3} + \dot{Q}_{B17} + \dot{Q}_{B19} + \dot{Q}_{B18} + \dot{Q}_{B5} + \dot{Q}_{B6} + \dot{Q}_{B8} + \dot{Q}_{B24} + \dot{Q}_{B26} + \dot{Q}_{B11} + \dot{Q}_{B10} + \dot{Q}_{B14} + \dot{Q}_{B12} \tag{4.8}$$

Here, the subscripts refer to the component name or the stream name shown in Figure 3.8. The sign convention for the heat transfer rate is, positive for heat flowing into the system and negative for heat flowing out of the system.

The HCS energy efficiency is as follows:

$$\eta_{HCS} = \frac{\dot{m}_9 h_9}{\dot{W}_{C1} + \dot{W}_{C2} + \dot{W}_{C3} + \dot{W}_{C4} - \dot{W}_{ST1} - \dot{W}_{ST2} - \dot{W}_{ST3} - \dot{W}_{ST4} + \dot{W}_{P1} + \dot{W}_{P2} + \dot{W}_{P3} + \dot{W}_{P4}} \tag{4.9}$$

Here, the subscripts refer to the component name or the stream name shown in Figure 3.9. The sign convention for the work transfer rate is positive for all work interactions.

$$\eta_{CC} = \frac{\dot{W}_{GAST} + \dot{W}_{ST5} - \dot{W}_{C5} - \dot{W}_{C6} - \dot{W}_{P5}}{\dot{m}_{E1} LHV_{H_2} + \dot{m}_{E3} h_{E3}} \tag{4.10}$$

Here, the subscripts refer to the component name or the stream name shown in Figure 3.10.

The hydrogen production plant overall energy efficiency is as follows:

$$\eta_{ov} = \frac{\dot{m}_{H_2} LHV_{H_2} + \dot{W}_{net}}{\dot{m}_{coal} LHV_{coal}} \tag{4.11}$$

For $\dot{W}_{net}$, $\dot{W}_{HCS}$, $\dot{W}_{CASU}$, and $\dot{W}_e$:

$$\dot{W}_{net} = \dot{W}_{COMPRES2} + \dot{W}_{COMPR1} + \dot{W}_{TFCOMP} + \dot{W}_{PUMP-W2} + \dot{W}_{PUMP-W} - \dot{W}_{GT} - \dot{W}_{GT2} + \dot{W}_{HCS} + \dot{W}_e \tag{4.12}$$

$$\dot{W}_{HCS} = \dot{W}_{C1} + \dot{W}_{C2} + \dot{W}_{C3} + \dot{W}_{C4} - \dot{W}_{ST1} - \dot{W}_{ST2} - \dot{W}_{ST3} - \dot{W}_{ST4} + \dot{W}_{P1} + \dot{W}_{P2} + \dot{W}_{P3} + \dot{W}_{P4} \tag{4.13}$$

$$\dot{W}_e = \dot{W}_{Cu-Cl} / \eta_{gen} \tag{4.14}$$

$$\dot{W}_{CASU} = \dot{W}_{B1} + \dot{W}_{RC} \tag{4.15}$$

Here, subscripts refer to system component in Figures 3.7-3.10.

$$\dot{m}_{H_2} = \dot{m}_{S10}(\text{see Figure 3.7}) + \dot{m}_{S33}(\text{see Figure 3.8}) - \dot{m}_{E1}(\text{see Figure 3.9}) = \dot{m}_1(\text{see Figure 3.10}) \tag{4.16}$$

Here, subscripts refer to the stream number in Figures 3.7-3.10.

General steady-state thermodynamic rate balance equations for exergy, for open systems and with kinetic and gravitational potential energies neglected, is given in the following equation:

$$\dot{E}x_{\dot{Q}_{net\,in}} + \sum_{in} \dot{m}_{in} ex_{in} = \dot{E}x_{\dot{w}_{net\,out}} + \sum_{out} \dot{m}_{out} ex_{out} + \dot{E}x_d \tag{4.18}$$

where $\dot{m}$ is the mass flow rate, $\dot{Q}$ is the heat rate, $\dot{W}$ is the work rate, ex is the specific exergy and the subscripts in and out denote input and output . The exergy rate balance in Equation (4.18) is used to determine the exergy destruction rate $\dot{E}x_d$, i.e., the irreversibility rate, for the system and each of its components, as well as overall and component exergy efficiencies.

The exergy rate due to heat transfer $\dot{E}x_{\dot{Q}}$ in Equation (4.18), for T_s is the temperature of the boundary where heat transfer takes place, and a dead state temperature T_o, is as follows:

$$\dot{E}x_{\dot{Q}} = \dot{Q}\left(1 - \frac{T_0}{T_s}\right) \tag{4.19}$$

where $\dot{Q}$ is the heat transfer rate.

The exergy rate of work (mechanical shaft work or electrical work) $\dot{E}x_w$ is the same as the work rate:

$$\dot{E}x_{\dot{w}} = \dot{W} \tag{4.20}$$

Here, the specific exergy ex of a flowing fluid can be expressed for state i in the system as follows:

$$ex_i = (h_i - h_0) - T_0(s_i - s_0) + ex_{ch} \tag{4.21}$$

where h_i and s_i are the specific enthalpy and specific entropy of the flow respectively at the state i, and h_0 and s_0 are the specific enthalpy and specific entropy of the flow respectively at the dead state. Also, ex_{ch} denotes the specific chemical exergy of the flow and can be expressed as follows:

$$ex_{ch} = \sum x_j ex_{ch}^0 + RT_0 \sum x_j \ln(x_j) \tag{4.22}$$

where x_j denotes the mole fraction of constituent j in the flow, ex_{ch}^0 is the standard specific chemical exergy of the constituent j in kJ/mol, and R is the universal gas constant in kJ/molK. The specific chemical exergy of coal is calculated as follows:

$$ex_{ch}^{coal} = \left[\left(LHV + \omega h_{fg}\right) \times \beta + 9.417S\right] \tag{4.23}$$

which is used to calculate the specific exergy of any type of coal. Here, LHV is the lower heating value of the coal, h_{fg} is the latent heat of water at T_0, ω is the moisture content in the coal and S is the mass fraction of sulfur in the coal. In Equation (4.23), LHV is based on dry and ash free coal and finally β is expressed based on the dry analysis of the coal used as the following [11].

$$\beta = 0.1882\frac{H}{C} + 0.061\frac{O}{C} + 0.0404\frac{N}{C} + 1.0437 \tag{4.24}$$

Here, H, O, C, and N denote respectively the mass fractions of hydrogen, oxygen, carbon, and nitrogen in the coal used on a dry basis. Equation (4.24) can is valid only when the parameter O/C is less than 0.667, which is the case for the coals considered in this research.

The exergy efficiencies of the subsystems in the hydrogen production plant from coal by utilizing the thermochemical water decomposition cycle, via the copper-chlorine cycle.

The exergy efficiency of the gasification system is as follows:

$$\psi_G = \frac{\dot{m}_{syngas} ex_{syngas}}{\dot{m}_{coal} ex_{ch}^{coal} + \dot{W}_{pump-w} + \dot{W}_{pump-W2} + \dot{W}_{compres2} + \dot{E}x_{\dot{Q}_{STMG1}} + \dot{E}x_{\dot{Q}_{STGM2}} + \dot{E}x_{\dot{Q}_{QO}}} \tag{4.25}$$

Where the syngas in the numerator refers to stream S1 in Figure 3.8. Note that the subscripts are referring to components names in Figure 3.7 except for syngas (stream S1) and coal (stream 1coal in Figure 3.7). The coal exergy is on dry basis (see Table 3.8).

The Brayton cycle exergy efficiency is as follows:

$$\psi_{BrC} = \frac{\dot{W}_{GT} - \dot{W}_{COMPR1} - \dot{W}_{TFCOMP}}{\dot{m}_{S24} ex_{S24}} \tag{4.26}$$

Here, the subscripts refer to the component name or the stream name shown in Figure 3.7.

The CASU exergy efficiency is as follows:

$$\psi_{CASU} = \frac{\dot{m}_{AS17} ex_{As17}}{\dot{W}_{B1} + \dot{m}_{AS1} ex_{AS1} + \dot{E}x_{\dot{Q}_{RB(B4)}} + \dot{W}_{RC}} \tag{4.27}$$

Here, the subscripts refer to the component name or the stream name shown in Figure 3.7 except for RC, which denotes to the refrigerator removing the heat from the distillation column condenser.

The WGSMR exergy efficiency is as follows:

$$\psi_{WGSMR} = \frac{\dot{m}_{S10} ex_{H_2} + \dot{m}_{S24} ex_{S24}}{\dot{m}_{S6} ex_{S6}} \tag{4.28}$$

where the subscripts refer to the stream name shown in Figure 3.7.

The copper-chlorine thermochemical water decomposition cycle is as follows:

$$\psi_{Cu-Cl} = \frac{\dot{m}_{S33} ex_{S33}}{(\dot{m}_{S2} - \dot{m}_{S23}) ex_{S2} + \dot{E}x_{\dot{Q}_{in}} + \dot{W}_e} \tag{4.29}$$

The $\dot{E}x_{\dot{Q}_{in}}$ is calculated by the following equation:

$$\dot{E}x_{\dot{Q}_{in}} = \dot{E}x_{\dot{Q}_{B2}} + \dot{E}x_{\dot{Q}_{B3}} + \dot{E}x_{\dot{Q}_{B1}} + \dot{E}x_{\dot{Q}_{B3}} + \dot{E}x_{\dot{Q}_{B17}} + \dot{E}x_{\dot{Q}_{B19}} + \dot{E}x_{\dot{Q}_{B18}} + \dot{E}x_{\dot{Q}_{B5}} + \dot{E}x_{\dot{Q}_{B6}} + \dot{E}x_{\dot{Q}_{B8}} + \dot{E}x_{\dot{Q}_{B24}} + \dot{E}x_{\dot{Q}_{B26}} + \dot{E}x_{\dot{Q}_{B11}} + \dot{E}x_{\dot{Q}_{B10}} + \dot{E}x_{\dot{Q}_{B14}} + \dot{E}x_{\dot{Q}_{B12}} \tag{4.30}$$

Here, the subscripts refer to the component name or the stream name shown in Figure 3.8.

The HCS exergy efficiency is as follows:

$$\psi_{HCS} = \frac{\dot{m}_9 ex_9}{\dot{W}_{C1} + \dot{W}_{C2} + \dot{W}_{C3} + \dot{W}_{C4} - \dot{W}_{ST1} - \dot{W}_{ST2} - \dot{W}_{ST3} - \dot{W}_{ST4} + \dot{W}_{P1} + \dot{W}_{P2} + \dot{W}_{P3} + \dot{W}_{P4}} \tag{4.31}$$

where the subscripts refer to the component name or the stream name shown in Figure 4.3. In Equation (45), the sign convention for the work transfer rate is positive for all work interactions.

$$\psi_{CC} = \frac{\dot{W}_{GAST}+\dot{W}_{ST5}-\dot{W}_{C5}-\dot{W}_{C6}-\dot{W}_{P5}}{\dot{m}_{E1}ex_{H_2}+\dot{m}_{E3}ex_{E3}} \quad (4.32)$$

Here, the subscripts refer to the component name or the stream name shown in Figure 4.4. In Equation (46), the sign convention for the work transfer rate is positive for all work interactions

The hydrogen production plant overall exergy efficiency is givem as follows:

$$\psi_{ov} = \frac{\dot{m}_{H_2}ex_{H_2}+\dot{W}_{net}}{\dot{m}_{coal}ex_{ch}^{coal}} \quad (4.33)$$

4.3 Thermodynamic Analysis of System 2

The balance equations can be applied to the integrated system as a whole, to subsystems, and to each component of the system. The energy and exergy efficiencies for the integrated system as a whole, or for a subsystem, or for each component of the system are calculated using the following equations respectively:

$$\eta = \frac{En_{products}}{En_{inputs}} \quad (4.34)$$

$$\psi = \frac{Ex_{product}}{Ex_{inputs}} \quad (4.35)$$

where η is the energy efficiency and ψ is the exergy efficiency. Next the energy and exergy efficiencies of the integrated system's subsystems are provided, plus the overall integrated system energy and exergy efficiencies are provided. The integrated system is divided into subsystems; these subsystems include the following; SCWR, Cu-Cl cycle, HCS, and SCC. Regarding the SCWR efficiencies they will not be calculated since the nuclear reaction was not modeled, rather its outputs were adopted from the work of Bushby et al. [75], and these adopted values were presented in Table 4.9. While measuring the energy and exergy efficiencies and the hydrogen mass flow rate produced two cases are taken into consideration. The two cases study the effect of the design of the steam circuit on the performance of the Cu-Cl cycle and the integrated system as a whole.

The energy and exergy efficiencies of the Cu-Cl cycle, HCS, and SCC are presented next.

$$\eta_{Cu-Cl} = \frac{\dot{m}_{H_2}(LHV_{H_2})}{\dot{Q}_{net,in}+\dot{W}_e} \tag{4.36}$$

$$\psi_{Cu-Cl} = \frac{\dot{m}_{H_2} ex_{H_2}}{\dot{E}x_{\dot{Q}_{net,in}}+\dot{W}_e} \tag{4.37}$$

where $\dot{Q}_{net,in}$ is for the first case (without considering a steam circuit design) the summation of all heat rate interactions in the Cu-Cl cycle, for the second case (considering a novel steam circuit design) is the heat rate that the cycle absorbs from the supercritical steam from SCWR. $\dot{E}x_{\dot{Q}_{net,in}}$ is the exergy rate of $\dot{Q}_{net,in}$ mentioned earlier.

$$\eta_{HCS} = \frac{\left(\dot{m}_{H_2}^{HP} h_{H_2}^{HP} - \dot{m}_{H_2}^{LP} h_{H_2}^{LP}\right)}{\dot{W}_C - \dot{W}_{ST} + \dot{W}_p} \tag{4.38}$$

$$\psi_{HCS} = \frac{\left(\dot{m}_{H_2}^{HP} ex_{H_2}^{HP} - \dot{m}_{H_2}^{LP} ex_{H_2}^{LP}\right)}{\dot{W}_C - \dot{W}_{ST} + \dot{W}_p} \tag{4.39}$$

Here the superscripts HP and LP denotes high-pressure hydrogen and low-pressure hydrogen. The subscripts C, ST, and P refers to compressors, steam turbines, and pumps respectively.

$$\eta_{SCC} = \frac{\dot{W}_{net,out}}{\dot{m}_{H_2} LHV_{H_2}} \tag{4.40}$$

$$\psi_{SCC} = \frac{\dot{W}_{net,out}}{\dot{m}_{H_2} ex_{H_2}} \tag{4.41}$$

The overall energy and exergy efficiencies of the integrated system is calculated using the following equation:

$$\eta_{ov} = \frac{\dot{m}_{H_2}^{HP}\left(LHV_{H_2} + \left(h_{T\&P} - h_{T_o\&P_o}\right)\right)}{\dot{Q}_{SCWR}} \tag{4.42}$$

$$\psi_{ov} = \frac{\dot{m}_{H_2}^{HP}(ex_{H_2})}{\dot{E}x_{\dot{Q}_{SCWR}}} \tag{4.43}$$

4.4 Thermodynamic Analysis of System 3

In this section the energy efficiencies of the subsystems in the hydrogen production plant are defined that are completely dependent on the solar thermal energy by utilizing the

thermochemical water decomposition cycle, and compressed hydrogen product. The main subsystems of the hydrogen production plant are:

- Solar heliostat farm
- Cu-Cl cycle
- HCS
- SRC

The heat rate of the solar light reflected by the heliostats to the central receiver which is a molten salt cavity receiver type is calculated by the following equation:

$$\dot{Q}_{su} = I \times A_{farm} \tag{4.44}$$

where I is the solar light intensity, and A_{farm} is the heliostat farm area, and subscript s refers to solar. However, not all the heat rate is received by the central receiver, and based on the efficiency of the solar system the heat rate received by the central collector is calculated by the following equation:

$$\dot{Q}_{cenr} = \eta_H \dot{Q}_{su} \tag{4.45}$$

where η_H is the heliostat efficiency, $\dot{Q}_{cenr}$ is the heat rate received by the central receiver, subscripts cenr, and H refers to the central receiver and heliostat respectively. The heat received by the central collector not all of it is transferred to the molten salt, the losses that were considered in the model are the following;

The first source of heat losses is due to the emissivity in the central receiver are calculated by the following equation:

$$\dot{Q}_{cenr,em} = \frac{\varepsilon_{avg}\sigma\left(T_{cenr,surf}^4 - T_o^4\right)A_{farm}}{C} \tag{4.46}$$

where the subscripts em refers to emissivity, sur for surface, o for standard room conditions.

The second source of losses in the heat transfer process are due to reflections in the central receiver, and the rate of the heat loss due to reflections is calculated by the following equation:

$$\dot{Q}_{cenr,ref} = \frac{\dot{Q}_{cenr}\rho F_r}{A_{farm}} \tag{4.47}$$

where F_r refers to view factor and subscript ref refers to reflective.

Another source of heat losses in during the heat transfer process from the heat received by the central receiver to the circulating heat transfer fluid, is the losses due to convection, which is calculated by the following equation:

$$\dot{Q}_{cenr,conv} = \frac{\left(\left(h_{air,fc,insu}\left(T_{cenr,surf}-T_o\right)\right)+\left(h_{air,nc,insu}\left(T_{cenr,surf}-T_o\right)\right)\right)A_{farm}}{F_r \times C} \tag{4.48}$$

where h is the heat transfer coefficient based on the conditions stated in the subscripts, fc refers to forced convection, nc refers to natural convection and insu for insulation. For losses due to conduction heat transfer, or the resistance due to heat transferring through conduction is calculated by the following equation:

$$\dot{Q}_{cenr,cond} = \frac{\left(T_{cenr,surf}-T_o\right)A_{farm}}{\left(\frac{\partial_{insu}}{\lambda_{insu}}+\frac{1}{h_{air,o}}\right)C \times F_r} \tag{4.49}$$

where ∂_{insu} is the thickness of the insulation, and λ_{insu} the thermal conductivity of the insulation. The rest of the heat is transferred to the heat transfer fluid (molten salt), which is presented by the following equation:

$$\dot{Q}_{cenr,ms} = \dot{m}_{ms} c_p \left(T_{ms,out} - T_{ms,in}\right) \tag{4.50}$$

where $\dot{m}_{ms}$ is the mass flow rate of the molten salt, c_p is the heat capacity of the molten salt. Subscripts ms refers to molten salt, in for inlet, and out for outlet. Summing the heat rates in Equations 4.46-4.50 will equal all of the heat transferred to the central collector as shown in the following equation:

$$\dot{Q}_{cenr} = \dot{Q}_{cenr,ms} + \dot{Q}_{cenr,cond} + \dot{Q}_{cenr,conv} + \dot{Q}_{cenr,ref} + \dot{Q}_{cenr,em} \tag{4.51}$$

In order to calculate the surface temperature of the absorber can be calculated using the following equation:

$$\frac{\dot{Q}_{cenr}}{A_{farm}/F_r/C} = \frac{\left(T_{cenr,surf}-T_{ms}\right)}{d_o/d_i/h_{ms}+d_o \ln(d_o/d_i)/2/\lambda_{tube}} \tag{4.52}$$

where d_o is the outer diameter, di is the inner diameter, and λ_{tube} is the thermal conductivity of the tube. When $\dot{Q}_{cenr}$ is known then using an iterative process the surface temperature of the central receiver, the different type of heat losses, and the receiver thermal efficiency can be found as what was done in the work of Li et al. [82]. For more details of the process please check Li et al. [82] work for avoiding repetition of the work.

The heliostat farm thermal energy efficiency is as follows:

$$\eta_{SHF} = \frac{\dot{Q}_{cenr,ms}}{\dot{Q}_{su}} \tag{4.53}$$

where the subscript SHF denotes for solar heliostat farm.

The energy efficiency of the Cu-Cl cycle for hybrid electrical and thermochemical water decomposition cycle is as follows:

$$\eta_{Cu-Cl} = \frac{\dot{m}_{H_2} LHV_{H_2}}{\dot{Q}_{in}+\dot{W}_e} = \frac{\dot{m}_{S33} LHV_{S33}}{\dot{Q}_{in}+\dot{W}_e} \tag{4.54}$$

Here $\dot{Q}_{in}$ is the total heat transferred to the cycle, $\dot{W}_e$ is the electrical power required by the cycle, the subscripts refer to the component name or the stream name shown in Figure 3.19.

The HCS energy efficiency is as follows:

$$\eta_{HCS} = \frac{\dot{m}_9 h_9}{\dot{W}_{C1}+\dot{W}_{C2}+\dot{W}_{C3}+\dot{W}_{C4}-\dot{W}_{ST1}-\dot{W}_{ST2}-\dot{W}_{ST3}-\dot{W}_{ST4}+\dot{W}_{P1}+\dot{W}_{P2}+\dot{W}_{P3}+\dot{W}_{P4}} \tag{4.55}$$

where the subscripts of the work rate refer to the compressor or turbine name, the mas flow rate or property subscript refers to the stream name shown in Figure 4.11. The sign convention for the work transfer rate is positive for all work interactions (since the equation takes care of the work rate in and out)

The energy efficiency of the supporting RC is calculated using the following equation:

$$\eta_{SRC} = \frac{\dot{W}_{ST5}-\dot{W}_{C5}-\dot{W}_{P5}}{\dot{Q}_{HX5}} \tag{4.56}$$

Here, the subscripts refer to the component name or in Figure 4.11.

The hydrogen production plant that is completely dependent on the solar thermal energy overall energy efficiency is as follows:

$$\eta_{ov} = \frac{\dot{m}_{H_2} LHV_{H_2} + \dot{W}_{net} + \dot{m}_{H_2} h_{H_2}}{\dot{Q}_{su}} \tag{4.57}$$

For $\dot{W}_{net}$, $\dot{W}_{HCS}$, and $\dot{W}_e$:

$$\dot{W}_e = \dot{W}_{Cu-Cl}/\eta_{gen} \tag{4.58}$$

$$\dot{W}_{SRC} = \dot{W}_{ST5} - \dot{W}_{P5} \tag{4.59}$$

where subscripts refers to a system component in Figures 4.10 and 4.11.

The exergy efficiencies are next; the heliostat farm thermal energy efficiency is as follows:

$$\psi_{SHF} = \frac{\dot{E}x_{\dot{Q}cenr,ms}}{\dot{E}x_{\dot{Q}su}} \tag{4.60}$$

The Cu-Cl thermochemical water decomposition cycle is as follows:

$$\psi_{Cu-Cl} = \frac{\dot{m}_{H_2} ex_{H_2}}{\dot{E}x_{\dot{Q}_{in}} + \dot{W}_e} = \frac{\dot{m}_{S33} LHV_{S33}}{\dot{E}x_{\dot{Q}_{in}} + \dot{W}_e} \tag{4.61}$$

The $\dot{E}x_{\dot{Q}_{in}}$ which present the summation of all exergy rates associated with heat transfer rate in the process of the Cu-Cl cycle. for subscripts see Figure 4.9. The HCS exergy efficiency is as follows:

$$\psi_{HCS} = \frac{\dot{m}_9 ex_9}{\dot{W}_{C1} + \dot{W}_{C2} + \dot{W}_{C3} + \dot{W}_{C4} - \dot{W}_{ST1} - \dot{W}_{ST2} - \dot{W}_{ST3} - \dot{W}_{ST4} + \dot{W}_{P1} + \dot{W}_{P2} + \dot{W}_{P3} + \dot{W}_{P4}} \tag{4.62}$$

here the subscripts for the work rate terms refer to the component name, and those for the properties and mass flow rates are for stream names as shown in Figure 4.11.

The exergy efficiency of the supporting RC is as follows:

$$\eta_{SRC} = \frac{\dot{W}_{ST5} - \dot{W}_{C5} - \dot{W}_{P5}}{\dot{Q}_{HX5}} \tag{4.63}$$

See Figure 4.11 for subscripts. The hydrogen production plant overall exergy efficiency is as follows:

$$\psi_{ov} = \frac{\dot{m}_{H_2} ex_{H_2} + \dot{W}_{net}}{\dot{E}x_{\dot{Q}_{su}}} \tag{4.64}$$

4.5 Thermodynamic Analysis of System 4

By applying the balance equations to the integrated system and its components, energy and exergy efficiencies terms are generated for the overall integrated system and its components. The energy and exergy efficiencies of the integrated system and its main subsystems are presented next, whereas for the Cu-Cl reactors, work producing and consuming devices and all heat exchangers in the integrated system their exergy efficiency and exergy destruction rate equations are presented next.

The first subsystem considered is the four-step Cu-Cl cycle, for which energy and exergy efficiencies respectively can be expressed as follows:

$$\eta_{Cu-Cl} = \frac{\dot{m}_{H_2} LHV_{H_2}}{\dot{Q}_{net,in} + \dot{W}_e} = \frac{\dot{m}_{S17} LHV_{H_2}}{(\dot{m}_{S43} h_{S43} - \dot{m}_{S46} h_{S46}) + \dot{W}_e} \tag{4.65}$$

$$\psi_{Cu-Cl} = \frac{\dot{m}_{H_2} ex_{H_2}}{\dot{E}x_{\dot{Q}_{net,in}} + \dot{W}_e} = \frac{\dot{m}_{S17} ex_{H_2}}{(\dot{m}_{S43} ex_{S43} - \dot{m}_{S46} ex_{S46}) + \dot{W}_e} \tag{4.66}$$

where $\dot{Q}_{net,in}$ is the amount of heat provided to the four-step Cu-Cl cycle by the superheated gas-like supercritical fluid, calculated as the thermal power delivered by the supercritical fluid (based on enthalpy). The exergy content of that thermal power is calculated as the difference in exergy flow rates provided by the supercritical fluid to the hydrolysis reactor and the Cu_2OCl_2 decomposition reactor. Note that the subscripts refer to the streams or blocks names in the Aspen Plus flow sheet for the integrated system in Figure 3.22.

The second main subsystem is the PSR cycle, which receives some of its heat from the supercritical fluid and the remainder through recovering heat from other streams. Its energy and exergy efficiencies can be expressed respectively as:

$$\eta_{PSR} = \frac{(\dot{W}_{B32} - \dot{W}_{B29} - \dot{W}_{B38})}{(\dot{m}_{S50} h_{S50} + \dot{m}_{S58} h_{S58} + \dot{Q}_{B27})} \tag{4.67}$$

$$\psi_{PSR} = \frac{(\dot{W}_{B32} - \dot{W}_{B29} - \dot{W}_{B38})}{\left(\dot{m}_{S50} ex_{S50} + \dot{m}_{S58} ex_{S58} + \dot{E}x_{\dot{Q}_{B27}}\right)} \tag{4.68}$$

The third main subsystem is the HCS, for which energy and exergy efficiencies respectively are as follows:

$$\eta_{HCS} = \frac{\left(\dot{m}_{H_2}^{HP} h_{H_2}^{HP} - \dot{m}_{H_2}^{LP} h_{H_2}^{LP}\right)}{\dot{W}_C - \dot{W}_{ST} + \dot{W}_p} = \frac{\dot{m}_9 h_9}{\dot{W}_{C1} + \dot{W}_{C2} + \dot{W}_{C3} + \dot{W}_{C4} - \dot{W}_{ST1} - \dot{W}_{ST2} - \dot{W}_{ST3} - \dot{W}_{ST4} + \dot{W}_{P1} + \dot{W}_{P2} + \dot{W}_{P3} + \dot{W}_{P4} + \dot{m}_{S17} h_{S17}} \quad (4.69)$$

$$\psi_{HCS} = \frac{\left(\dot{m}_{H_2}^{HP} ex_{H_2}^{HP} - \dot{m}_{H_2}^{LP} ex_{H_2}^{LP}\right)}{\dot{W}_C - \dot{W}_{ST} + \dot{W}_p} = \frac{\dot{m}_9 ex_9}{\dot{W}_{C1} + \dot{W}_{C2} + \dot{W}_{C3} + \dot{W}_{C4} - \dot{W}_{ST1} - \dot{W}_{ST2} - \dot{W}_{ST3} - \dot{W}_{ST4} + \dot{W}_{P1} + \dot{W}_{P2} + \dot{W}_{P3} + \dot{W}_{P4} + \dot{m}_{S17} ex_{S17}} \quad (4.70)$$

Here, superscripts HP and LP refer to high-pressure hydrogen and low-pressure hydrogen, respectively, while the subscripts C, ST, and P denote compressor, steam turbine, and pump, respectively.

For the assessment of the overall integrated system, based on the proposed design and the selected operating parameters, the energy and exergy efficiencies are as follows:

$$\eta_{ov} = \frac{\dot{m}_{H_2}^{HP}(LHV_{H_2}) + \dot{W}_{net,out}}{\dot{Q}_{SCWR}} = \frac{\dot{m}_{S17} LHV_{H_2} + \dot{W}_{PSR} - \dot{W}_{HCS} - \dot{W}_e}{(\dot{m}_{S43} h_{S43} - \dot{m}_{S48} h_{S48})} \quad (4.71)$$

$$\psi_{ov} = \frac{\dot{m}_{H_2}^{HP}(ex_{H_2}) + \dot{W}_{net,out}}{\dot{E}x_{\dot{Q}_{SCWR}}} = \frac{\dot{m}_{S17} ex_{S17} + \dot{W}_{PSR} - \dot{W}_{HCS} - \dot{W}_e}{(\dot{m}_{S43} ex_{S43} - \dot{m}_{S48} ex_{S48})} \quad (4.72)$$

For the Cu-Cl cycle reactors, the work producing and consuming devices and all heat exchangers in the integrated system, expressions for exergy efficiency and exergy destruction rate are reported in Tables 4.4-4.6. The energy efficiency is not reported because they are straighforward and simplified. For instance, since it was assumed that no heat losses occur in heat exchangers, they have 100% energy efficiencies.

Table 4.4 The exergy efficiencies and exergy destruction rates for the four-step Cu-Cl cycle reactors, water jackets and heat exchangers.

Group	Device	Exergy efficiency	Exergy destruction rate
Reactors	B1 (hydrolysis reactor)	$\psi_{B1} = \frac{\dot{m}_{S3}ex_{S3}}{\dot{m}_{S1}ex_{S1}+\dot{m}_{S2}ex_{S2}+\dot{E}x_{\dot{Q}_{S47}}}$	$\dot{E}x_{d,B1} = (\dot{m}_{S1}ex_{S1} + \dot{m}_{S2}ex_{S2} + \dot{E}x_{\dot{Q}_{S47}}) - \dot{m}_{S3}ex_{S3}$
	B6 (Cu_2OCl_2 decomposition reactor)	$\psi_{B6} = \frac{\dot{m}_{S9}ex_{S9}}{\dot{m}_{S8}ex_{S8}+\dot{E}x_{\dot{Q}_{S45}}}$	$\dot{E}x_{d,B6} = \dot{m}_{S8}ex_{S8} + \dot{E}x_{\dot{Q}_{S45}} - \dot{m}_{S9}ex_{S9}$
	B11 (electrolysis reactor)	$\psi_{B11} = \frac{\dot{m}_{S16}ex_{S16}}{\dot{W}_e+\dot{m}_{S15}ex_{S15}+\dot{m}_{S7}ex_{S7}+\dot{m}_{S14}ex_{S14}}$	$\dot{E}x_{d,B11} = \dot{W}_e + \dot{m}_{S15}ex_{S15} + \dot{m}_{S7}ex_{S7} + \dot{m}_{S14}ex_{S14} - \dot{m}_{S16}ex_{S16}$
	B14 (dryer)	$\psi_{B14} = \frac{\dot{m}_{S21}ex_{S21}+\dot{m}_{S20}ex_{S20}}{\dot{E}x_{\dot{Q}_{S40}}+\dot{m}_{S19}ex_{S19}}$	$\dot{E}x_{d,B14} = \dot{E}x_{\dot{Q}_{S40}} + \dot{m}_{S19}ex_{S19} - \dot{m}_{S21}ex_{S21} - \dot{m}_{S20}ex_{S20}$
Water jackets for heating and cooling the reactors and phase change chambers	B22 (water jacket for the dryer B14)	$\psi_{B22} = \frac{\dot{E}x_{\dot{Q}_{S40}}}{\dot{m}_{S36}ex_{S36}-\dot{m}_{S41}ex_{S41}}$	$\dot{E}x_{d,B22} = (\dot{m}_{S36}ex_{36} - \dot{m}_{41}ex_{S41}) - \dot{E}x_{\dot{Q}_{S40}}$
	B26 (water jacket for the hydrolysis reactor)	$\psi_{B26} = \frac{\dot{E}x_{\dot{Q}_{S47}}}{\dot{m}_{S44}ex_{S44}-\dot{m}_{S46}ex_{S46}}$	$\dot{E}x_{d,B26} = (\dot{m}_{S44}ex_{S44} - \dot{m}_{46}ex_{S46}) - \dot{E}x_{\dot{Q}_{S47}}$
	B24 (water jacket for the Cu_2OCl_2 decomposition reactor)	$\psi_{B24} = \frac{\dot{E}x_{\dot{Q}_{S45}}}{\dot{m}_{S43}ex_{S43}-\dot{m}_{S44}ex_{S44}}$	$\dot{E}x_{d,B24} = (\dot{m}_{S43}ex_{S43} - \dot{m}_{44}ex_{S44}) - \dot{E}x_{\dot{Q}_{S45}}$
	B18 (water jacket for the CuCl solidifier)	$\psi_{B19} = \frac{\dot{E}x_{\dot{Q}_{S29}}}{\dot{m}_{S28}ex_{S28}-\dot{m}_{S22}ex_{S22}}$	$\dot{E}x_{d,B19} = (\dot{m}_{S28}ex_{S28} - \dot{m}_{S22}ex_{S22}) - \dot{E}x_{\dot{Q}_{S29}}$
Heat exchangers	B15B5	$\psi_{B15B5} = \frac{\dot{m}_{S8}ex_{S8}-\dot{m}_{S6}ex_{S6}}{\dot{m}_{S28}ex_{S28}-\dot{m}_{S32}ex_{S32}}$	$\dot{E}x_{d,B15B5} = (\dot{m}_{S28}ex_{S28} - \dot{m}_{S32}ex_{32}) - (\dot{m}_{S8}ex_{S8} - \dot{m}_{S6}ex_{S6})$
	B16B2	$\psi_{B16B2} = \frac{\dot{m}_{S1}ex_{S1}-\dot{m}_{S65}ex_{S65}}{\dot{m}_{S32}ex_{S32}-\dot{m}_{S33}ex_{S33}}$	$\dot{E}x_{d,B16B2} = (\dot{m}_{S32}ex_{S32} - \dot{m}_{S33}ex_{33}) - (\dot{m}_{S1}ex_{S1} - \dot{m}_{S65}ex_{S65})$

	B39B40	$\psi_{B39B40} = \frac{\dot{m}_{S65}ex_{S65} - \dot{m}_{S4}ex_{S4}}{\dot{m}_{S60}ex_{S60} - \dot{m}_{S63}ex_{S63}}$	$\dot{E}x_{d,B16B2} = (\dot{m}_{S60}ex_{S60} - \dot{m}_{S63}ex_{63}) - (\dot{m}_{S65}ex_{S65} - \dot{m}_{S4}ex_{S4})$
	B20B3	$\psi_{B20B3} = \frac{\dot{m}_{S2}ex_{S2} - \dot{m}_{S5}ex_{S5}}{\dot{m}_{S33}ex_{S33} - \dot{m}_{S36}ex_{S36}}$	$\dot{E}x_{d,B20B3} = (\dot{m}_{S33}ex_{S33} - \dot{m}_{S36}ex_{36}) - (\dot{m}_{S2}ex_{S2} - \dot{m}_{S5}ex_{S5})$
	B17B10	$\psi_{B17B10} = \frac{\dot{m}_{S27}ex_{S27} - \dot{m}_{S26}ex_{S26}}{\dot{m}_{S13}ex_{S13} - \dot{m}_{S14}ex_{S14}}$	$\dot{E}x_{d,B17B10} = (\dot{m}_{S13}ex_{S13} - \dot{m}_{S14}ex_{S14}) - (\dot{m}_{S27}ex_{S27} - \dot{m}_{S26}ex_{S26})$

Table 4.5 The exergy efficiencies and exergy destruction rates for devices in the power supporting Rankine cycle.

Group	Device	Exergy efficiency	Exergy destruction rate
Power supporting Rankine cycle	B29 (pump)	$\psi_{B29} = \frac{\dot{m}_{S51}ex_{S51}}{\dot{m}_{S61}ex_{S61} + \dot{W}_{B29}}$	$\dot{E}x_{d,B29} = \dot{m}_{S61}ex_{S61} + \dot{W}_{B29} - \dot{m}_{S51}ex_{S51}$
	B32 (steam turbine)	$\psi_{B32} = \frac{\dot{m}_{S54}ex_{S54} + \dot{W}_{B32}}{\dot{m}_{S53}ex_{S53}}$	$\dot{E}x_{d,B32} = \dot{m}_{S53}ex_{S53} - \dot{m}_{S54}ex_{S54} - \dot{W}_{B32}$
	B38 (pump)	$\psi_{B38} = \frac{\dot{m}_{S62}ex_{S62}}{\dot{m}_{S55}ex_{S55} + \dot{W}_{B38}}$	$\dot{E}x_{d,B38} = \dot{m}_{S55}ex_{S55} + \dot{W}_{B38} - \dot{m}_{S62}ex_{S62}$
	B27B30 (heat exchanger)	$\psi_{B27B30} = \frac{\dot{m}_{S53}ex_{S53} - \dot{m}_{S51}ex_{S51}}{\dot{m}_{S46}ex_{S46} - \dot{m}_{S48}ex_{S48}}$	$\dot{E}x_{d,B27B30} = (\dot{m}_{S46}ex_{S46} - \dot{m}_{S48}ex_{S48}) - (\dot{m}_{S53}ex_{S53} - \dot{m}_{S51}ex_{S51})$
	B33 (condenser)	$\psi_{B33} = \frac{\dot{m}_{S54}ex_{S54} - \dot{m}_{S55}ex_{S55}}{\dot{E}x_{\dot{Q}_{B33}}}$	$\dot{E}x_{d,B33} = \dot{E}x_{\dot{Q}_{B33}} - (\dot{m}_{S54}ex_{S54} - \dot{m}_{S55}ex_{S55})$

	B35B36 (heat exchanger)	$\psi_{B35B36} = \frac{\dot{m}_{S57}ex_{S57} - \dot{m}_{S49}ex_{S49}}{\dot{m}_{S62}ex_{S62} - \dot{m}_{S58}ex_{S58}}$	$\dot{E}x_{d,B35B36} = (\dot{m}_{S62}ex_{S62} - \dot{m}_{S58}ex_{S58}) - (\dot{m}_{S57}ex_{S57} - \dot{m}_{S49}ex_{S49})$
	B31 (mixer)	$\psi_{B31} = \frac{\dot{m}_{S50}ex_{S50}}{\dot{m}_{S57}ex_{S57} - \dot{m}_{S42}ex_{S42}}$	$\dot{E}x_{d,B31} = (\dot{m}_{S57}ex_{S57} - \dot{m}_{S42}ex_{S42}) - \dot{m}_{S50}ex_{S50}$
	B23 (mixer)	$\psi_{B23} = \frac{\dot{m}_{S42}ex_{S42}}{\dot{m}_{S24}ex_{S24} - \dot{m}_{S41}ex_{S41}}$	$\dot{E}x_{d,B23} = (\dot{m}_{S24}ex_{S24} - \dot{m}_{S41}ex_{S41}) - \dot{m}_{S42}ex_{S42}$
	B37 (separator)	$\psi_{B23} = (\dot{m}_{S61}ex_{S61}) / (\dot{m}_{S50}ex_{S50})$	$\dot{E}x_{d,B37} = (\dot{m}_{S50}ex_{S50} - \dot{m}_{S61}ex_{S61}) + \dot{m}_{S60}ex_{S60}$

Table 4.6 the exergy efficiencies and exergy destruction rates for the devices in the hydrogen compression system.

Group	Device	Exergy efficiency	Exergy destruction rate
Compressors	C1	$\psi_{C1} = \frac{\dot{m}_2 ex_2}{\dot{m}_{S17}ex_{S17} + \dot{W}_{C1}}$	$\dot{E}x_{d,C1} = \dot{m}_{S17}ex_{S17} + \dot{W}_{C1} - \dot{m}_2 ex_2$
	C2	$\psi_{C2} = \frac{\dot{m}_4 ex_4}{\dot{m}_3 ex_3 + \dot{W}_{C2}}$	$\dot{E}x_{d,C2} = \dot{m}_{S3}ex_{S3} + \dot{W}_{C2} - \dot{m}_4 ex_4$
	C3	$\psi_{C3} = \frac{\dot{m}_6 ex_6}{\dot{m}_5 ex_5 + \dot{W}_{C3}}$	$\dot{E}x_{d,C3} = \dot{m}_{S5}ex_{S5} + \dot{W}_{C3} - \dot{m}_6 ex_6$
	C4	$\psi_{C4} = \frac{\dot{m}_8 ex_8}{\dot{m}_7 ex_7 + \dot{W}_{C4}}$	$\dot{E}x_{d,C4} = \dot{m}_7 ex_7 + \dot{W}_{C4} - \dot{m}_8 ex_8$
Steam turbines	ST1	$\psi_{ST1} = \frac{\dot{W}_{ST1} + \dot{m}_{R4}ex_{R4}}{\dot{m}_{R3}ex_{R3}}$	$\dot{E}x_{d,ST1} = \dot{m}_{R3}ex_{R3} - (\dot{W}_{ST1} + \dot{m}_{R4}ex_{R4})$
	ST2	$\psi_{ST2} = \frac{\dot{W}_{ST2} + \dot{m}_{X4}ex_{X4}}{\dot{m}_{X3}ex_{X3}}$	$\dot{E}x_{d,ST2} = \dot{m}_{X3}ex_{X3} - (\dot{W}_{ST2} + \dot{m}_{X4}ex_{X4})$
	ST3	$\psi_{ST3} = \frac{\dot{W}_{ST3} + \dot{m}_{Y4}ex_{Y4}}{\dot{m}_{Y3}ex_{Y3}}$	$\dot{E}x_{d,ST3} = \dot{m}_{Y3}ex_{Y3} - (\dot{W}_{ST3} + \dot{m}_{Y4}ex_{Y4})$
	ST4	$\psi_{ST4} = \frac{\dot{W}_{ST4} + \dot{m}_{Z4}ex_{Z4}}{\dot{m}_{Z3}ex_{Z3}}$	$\dot{E}x_{d,ST4} = \dot{m}_{Z3}ex_{Z3} - (\dot{W}_{ST4} + \dot{m}_{Z4}ex_{Z4})$
Pumps	P1	$\psi_{P1} = \frac{\dot{m}_{R2}ex_{R2}}{\dot{W}_{P1} + \dot{m}_{R1-C}ex_{R1-C}}$	$\dot{E}x_{d,P1} = \dot{W}_{P1} + \dot{m}_{R1-C}ex_{R1-C} - \dot{m}_{R2}ex_{R2}$
	P2	$\psi_{P2} = \frac{\dot{m}_{X2}ex_{X2}}{\dot{W}_{P2} + \dot{m}_{X1-C}ex_{X1-C}}$	$\dot{E}x_{d,P2} = \dot{W}_{P2} + \dot{m}_{X1-C}ex_{X1-C} - \dot{m}_{X2}ex_{X2}$
	P3	$\psi_{P3} = \frac{\dot{m}_{Y2}ex_{Y2}}{\dot{W}_{P3} + \dot{m}_{Y1-C}ex_{Y1-C}}$	$\dot{E}x_{d,P3} = \dot{W}_{P3} + \dot{m}_{Y1-C}ex_{Y1-C} - \dot{m}_{Y2}ex_{Y2}$

	P4	$\psi_{P4} = \frac{\dot{m}_{Z2}ex_{Z2}}{\dot{W}_{P4}+\dot{m}_{Z1-C}ex_{Z1-C}}$	$\dot{E}x_{d,P4} = \dot{W}_{P4} + \dot{m}_{Z1-C}ex_{Z1-C} - \dot{m}_{Z2}ex_{Z2}$
Heat exchangers	HX1	$\psi_{HX1} = \frac{\dot{m}_{R3}ex_{R3}-\dot{m}_{R2}ex_{R2}}{\dot{m}_{2}ex_{2}-\dot{m}_{3}ex_{3}}$	$\dot{E}x_{d,HX1} = (\dot{m}_{2}ex_{2} - \dot{m}_{3}ex_{3}) - (\dot{m}_{R3}ex_{R3} - \dot{m}_{R2}ex_{R2})$
	HX2	$\psi_{HX2} = \frac{\dot{m}_{X3}ex_{X3}-\dot{m}_{X2}ex_{X2}}{\dot{m}_{4}ex_{4}-\dot{m}_{5}ex_{5}}$	$\dot{E}x_{d,HX2} = (\dot{m}_{4}ex_{4} - \dot{m}_{5}ex_{5}) - (\dot{m}_{X3}ex_{X3} - \dot{m}_{X2}ex_{X2})$
	HX3	$\psi_{HX3} = \frac{\dot{m}_{Y3}ex_{Y3}-\dot{m}_{Y2}ex_{Y2}}{\dot{m}_{6}ex_{6}-\dot{m}_{7}ex_{7}}$	$\dot{E}x_{d,HX3} = (\dot{m}_{6}ex_{6} - \dot{m}_{7}ex_{7}) - (\dot{m}_{Y3}ex_{Y3} - \dot{m}_{Y2}ex_{Y2})$
	HX4	$\psi_{HX4} = \frac{\dot{m}_{Z3}ex_{Z3}-\dot{m}_{Z2}ex_{Z2}}{\dot{m}_{8}ex_{8}-\dot{m}_{9}ex_{9}}$	$\dot{E}x_{d,HX4} = (\dot{m}_{8}ex_{8} - \dot{m}_{9}ex_{9}) - (\dot{m}_{Z3}ex_{Z3} - \dot{m}_{Z2}ex_{Z2})$
Condensers	Cond1	$\psi_{Cond1} = \frac{\dot{E}x_{\dot{Q}_{cond1}}+\dot{m}_{R1}ex_{R1}}{\dot{m}_{R4}ex_{R4}}$	$\dot{E}x_{d,Cond1} = \dot{m}_{R4}ex_{R4} - (\dot{E}x_{\dot{Q}_{cond1}} + \dot{m}_{R1}ex_{R1})$
	Cond2	$\psi_{Cond2} = \frac{\dot{E}x_{\dot{Q}_{cond2}}+\dot{m}_{X1}ex_{X1}}{\dot{m}_{X4}ex_{X4}}$	$\dot{E}x_{d,Cond2} = \dot{m}_{X4}ex_{X4} - (\dot{E}x_{\dot{Q}_{cond2}} + \dot{m}_{X1}ex_{X1})$
	Cond3	$\psi_{Cond3} = \frac{\dot{E}x_{\dot{Q}_{cond3}}+\dot{m}_{Y1}ex_{Y1}}{\dot{m}_{Y4}ex_{Y4}}$	$\dot{E}x_{d,Cond3} = \dot{m}_{Y4}ex_{Y4} - (\dot{E}x_{\dot{Q}_{cond3}} + \dot{m}_{Y1}ex_{Y1})$
	Cond4	$\psi_{Cond4} = \frac{\dot{E}x_{\dot{Q}_{cond4}}+\dot{m}_{Z1}ex_{Z1}}{\dot{m}_{Z4}ex_{Z4}}$	$\dot{E}x_{d,Cond4} = \dot{m}_{Z4}ex_{Z4} - (\dot{E}x_{\dot{Q}_{cond4}} + \dot{m}_{Z1}ex_{Z1})$

Chapter 5: Results and Discussion

In this chapter, the results of the simulation and the thermodynamic analysis of the four proposed hydrogen production plants are presented. Each hydrogen production plant has a separate section in this chapter which includes the specific results.

5.1 Results of System 1

The proposed hydrogen production plant is analyzed energetically and exergetically and the results of the simulation and the thermodynamic analysis are presented in this chapter. All stream properties are calculated using Aspen Plus software, while chemical exergies, efficiencies, and exergy destruction rates are calculated using a programed Excel sheet. The reference environment temperature and pressure are 25°C and 1 atm respectively.

The overall results of the performance of the hydrogen production plant are discussed in this section. The results contain energy efficiency, exergy efficiency and exergy destruction rate and the plant operational requirements for large-scale hydrogen production. The plant operational requirements for large-scale hydrogen production plus the overall energy and exergy efficiencies are reported in Table 5.1. As given in Table 5.1 for the proposed hydrogen production plant for every 8.95 kg/s of Illinois No.6 coal is fed to the plant, 1 kg/s of compressed hydrogen is produced. For hydrogen production plant where the required production capacity of the plant to be 500 kg/day of stored hydrogen ready to be transported, combusted or to be used in electrolysis.

Table 5.1 The overall results of the hydrogen production plant from coal (System 1).

Hydrogen production plant parameters	**Value**	**Unit**
Energy efficiency	51.3	%
Exergy efficiency	47.6	%
Coal feed rate for hydrogen production of 1 kg/s (coal type: Illinois No.6)	8.95	kg/s
Contribution of Cu-Cl cycle in the total hydrogen production	7.43	%
Work rate extra produced by the system for each 1 kg/s of hydrogen produced by the hydrogen production system	4.64	MW
Pressure of the produced hydrogen	700	bar
Temperature of the produced hydrogen	25	^{o}C
Exergy destruction rate	187.5	MW

A production of 500 kg/day for a plant that is operating 24 hours per day will require a flow rate of 186 kg/hr of coal to be fed to the gasifier and it will produce 20.8 kg of H_2/hr (500 kg of H_2/day) and to produce 3.06 kJ/s. The produced hydrogen from the hydrogen production plant is compressed to 700 bar by the HCS. The overall energy efficiency of the proposed hydrogen production plant is 51.3%. The overall exergy efficiency of the proposed hydrogen production plant is 47.6%.

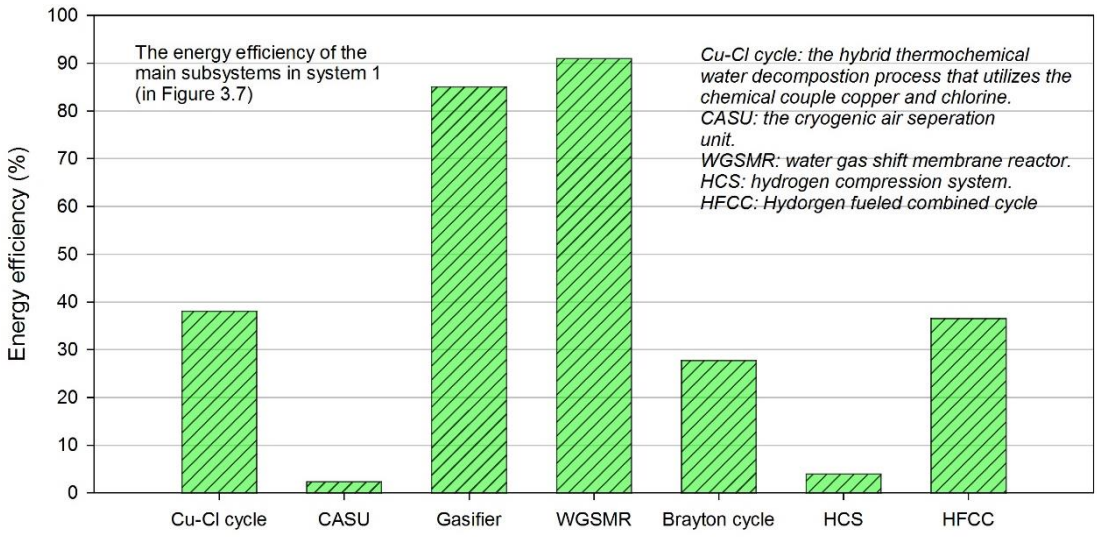

Figure 5.1 The energy efficiency of System 1 main subsystems.

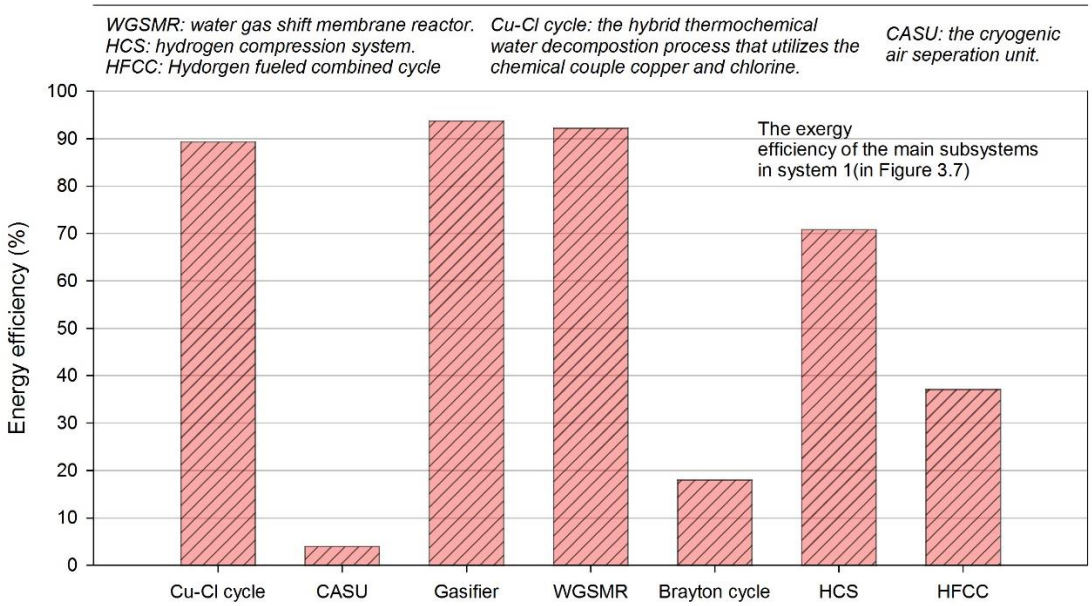

Figure 5.2 The exergy efficiency of System 1 main subsystems.

The performance of the hydrogen production plant subsystems is discussed here. These subsystems include gasifier, CASU, WGSMR, Brayton cycle, copper-chlorine cycle, HCS and HFCC. The energy and exergy efficiencies of the hydrogen production plant subsystems is shown in Figures 5.1 and 5.2. The exergy destruction ratio of the main subsystems of the hydrogen production plant is shown in Figure 5.3. As shown in Figure 5.3 the copper-chlorine cycle (Cu-Cl cycle) has the lowest exergy destruction ratio of 1% of the total exergy destruction in the hydrogen production plant. The energy and exergy efficiencies of the copper-chlorine cycle are 38.2% and 89.4%, which are very close to those reported by Orhan et al. [40] for the five steps copper-chlorine cycle. The energy and exergy efficiencies of the five steps copper-chlorine cycle reported by Orhan et al. [40] are 44.8% and 73.0%. The difference between the energy and exergy efficiencies found in this research and those that were reported by Orhan et al. [40] is because of the different cycle design.

In the proposed copper-chlorine cycle design (see Figure 3.8) the differences were the following:

- In the proposed design of the copper-chlorine cycle the produced hydrogen was not sent back to heat up the coming water, unlike what Orhan et al. [40] did, which they recovered heat from the produced hydrogen. The reason behind not recovering the hydrogen heat before storing it is for safety reasons. This point results in reduction in the energy efficiency.
- In the proposed design of the copper-chlorine cycle the water is first preheated by the extra steam that was sent to the hydrolysis reactor and then the steam is superheated by heat coming from the gasification cycle. However in Orhan et al. [40] it was not considered the extra steam to shift the reaction to products side, so they directly heat the water from ambient conditions to superheated steam at 400°C. This point results in higher exergy efficiency for the proposed design of the copper-chlorine cycle.
- In the proposed design of the copper-chlorine cycle special reactors that recovered high quality heat during the phase changes of the materials in the cycle resulting in higher exergy efficiency.

- In the proposed design of the copper-chlorine cycle, the turbines in the plant provide the needed electricity through an electrical generator.

The heat interactions in the five step copper-chlorine cycle design proposed here is shown in Figures 5.4 and 5.5. The reactor with the highest heat energy interaction is the Cu_2OCl_2 decomposition reactor B6 (see Figure 3.8).

Where also the Cu_2OCl_2 decomposition reactor B6 also possesses the highest exergy interaction, since it requires heat at high temperature of 530°C. Reactors B8 and B28, which are both responsible for phase change of CuCl from liquid state, releases the highest amount of heat and exergy recovered in the cycle. The high exergy is due to the high and constant temperature at which the heat release takes place. Regarding the exergy destruction contribution of the copper-chlorine cycle in that of the hydrogen production plant. Copper-chlorine cycle has the least contribution as shown in Figure 5.4. The low exergy destruction ratio (1%) of the copper-chlorine cycle is due to its high exergy efficiency, which was increased by the differences made to the cycle structure compared to that proposed in the literature. The second reason for the low exergy destruction ratio of the copper-chlorine cycle is the small hydrogen production contribution percentage in the proposed hydrogen production plant, which is 7.43%. Regarding an experimental validation of the generated model, the copper-chlorine cycle is still in the proof-of-principle and bench-scale apparatus stage. Thus, there are a very limited number of studies on the simulation and thermodynamic analysis of the Cu-Cl cycle to compare with. Most work done on the copper-chlorine cycle regarding full cycle simulation and integration was done by Orhan et al. [20,40,46,56] and Ozbilen et al. [21,39]. The CASU has the second highest exergy destruction of the subsystems in the hydrogen production plant after combined cycle (see Figure 5.4). It has the lowest exergy efficiency in all of the subsystems in the hydrogen production plant. The low exergy efficiency and the high exergy destruction rate for the CASU is because the system consumes large amount of work for separation process. The results of the separation process is O_2 and at a low pressure of 152 kPa, which is not a combustible gas. Having high quality and high amount of energy input to the CASU plus low energy in both quality and quantity in the output of the CASU, resulting in low exergy

efficiency. This also explains the reason for having the lowest energy efficiency among all of the subsystems.

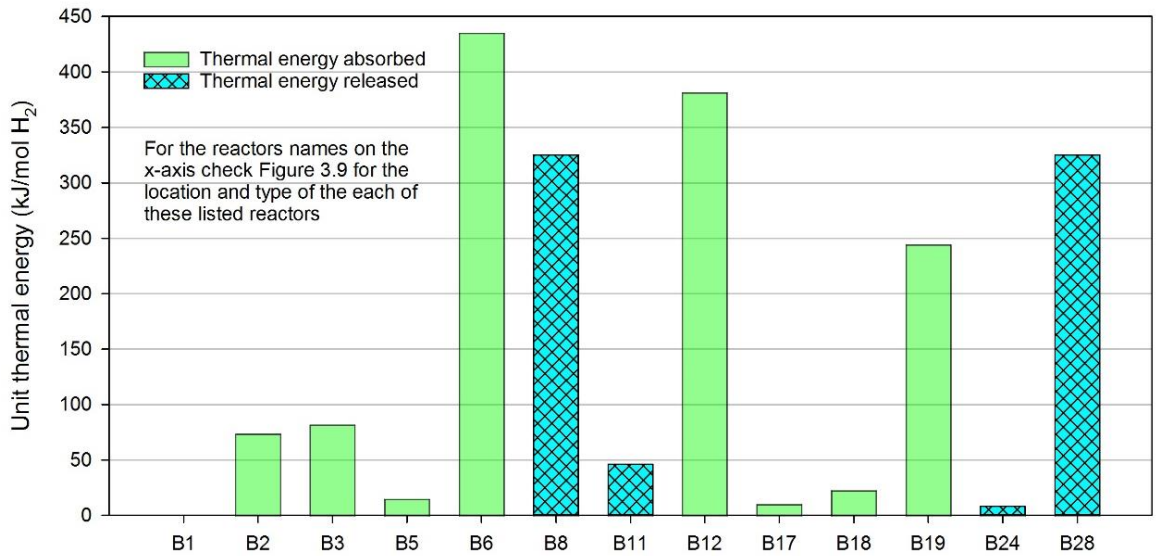

Figure 5.3 The unit thermal energy interactions in the proposed design of the copper-chlorine cycle in System 1 (see Figure 3.9 for the location of the reactions in the x-axis of the graph).

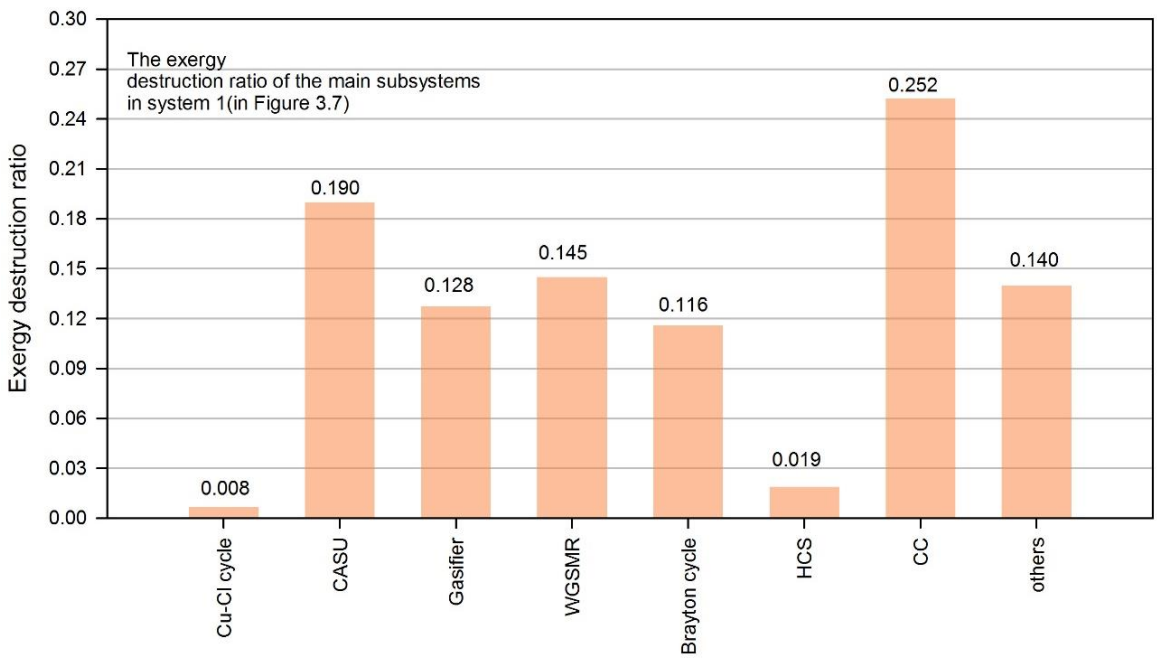

Figure 5.4 The exergy destruction ratios of the main subsystems of System 1.

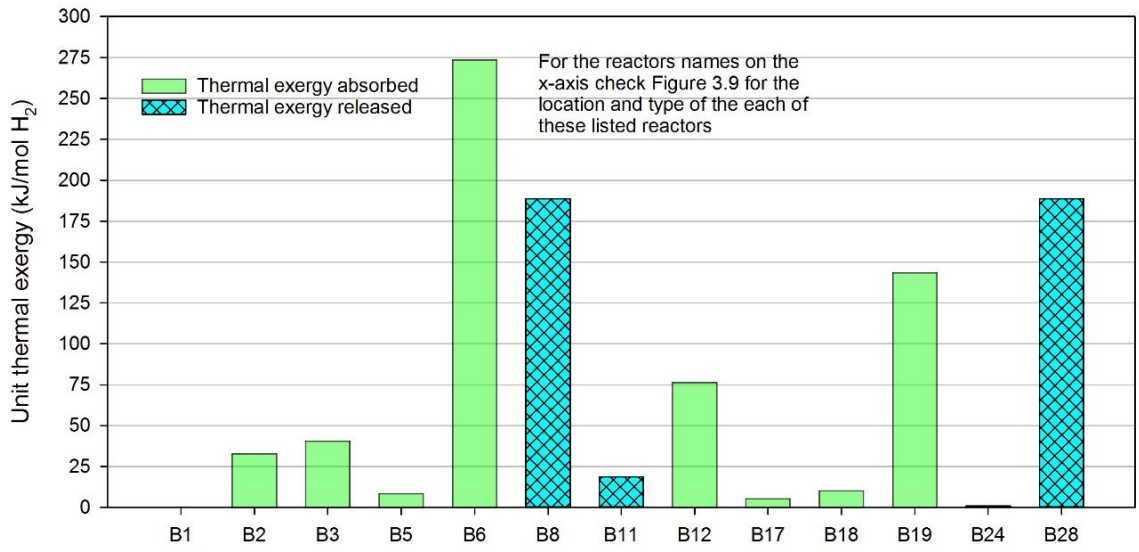

Figure 5.5 The unit thermal exergy interactions in the proposed design of the copper-chlorine cycle in System 1 (see Figure 3.9 for the location of the reactions in the x-axis of the graph).

Regarding the contribution of the CASU in the total exergy destruction rate of the system, it has the second highest contribution ratio of 19% after the combine cycle as shown in Figure 5.3. The gasifier and the WGSMR have the highest energy and exergy efficiencies of all the subsystems of the hydrogen production plant. However, the WGSMR and the gasifier have the third and the fourth place in the most contributors in the total exergy destruction of the plant. The exergy destruction ratio of the WGSMR and the gasifier are 15% and 13%, respectively. The syngas compositions and the gasifier operating conditions are given in Table 4.3.

The subsystem with the highest exergy destruction rate is the HFCC as shown in Figure 6.1. Having the highest exergy destruction rate in all the proposed hydrogen production plant subsystems results in making the HFCC the main contributor in the overall plant exergy destruction ratio of 25% as shown in Figure 5.3.

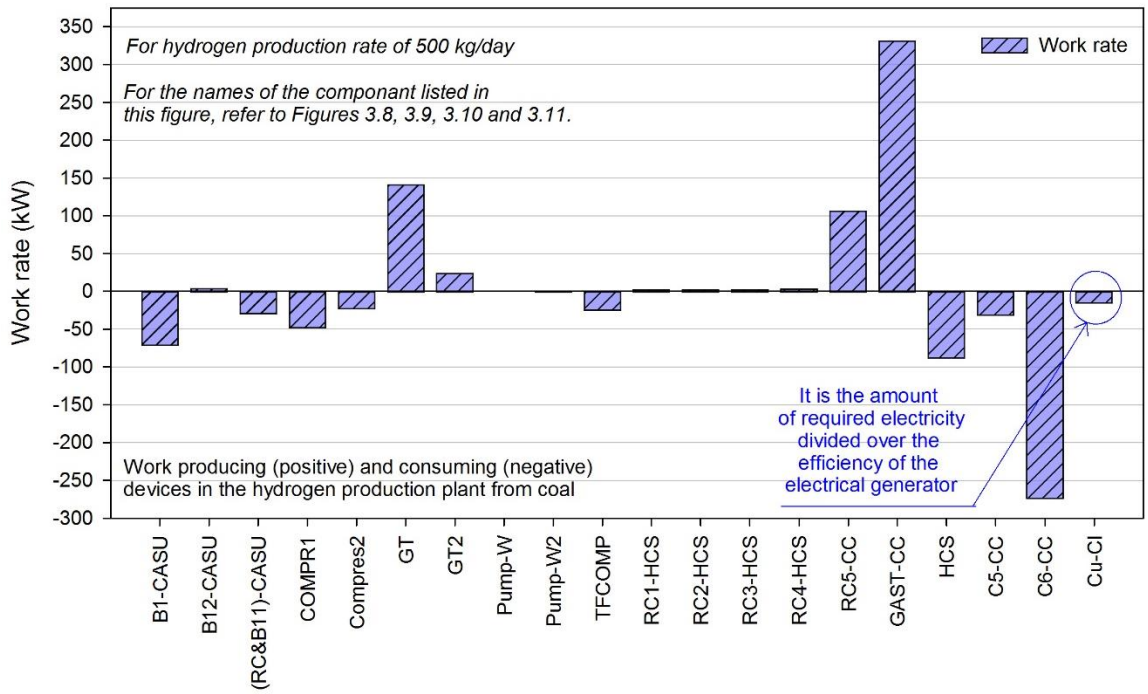

Figure 5.6 The work rates of the work producing and consuming devices in System 1.

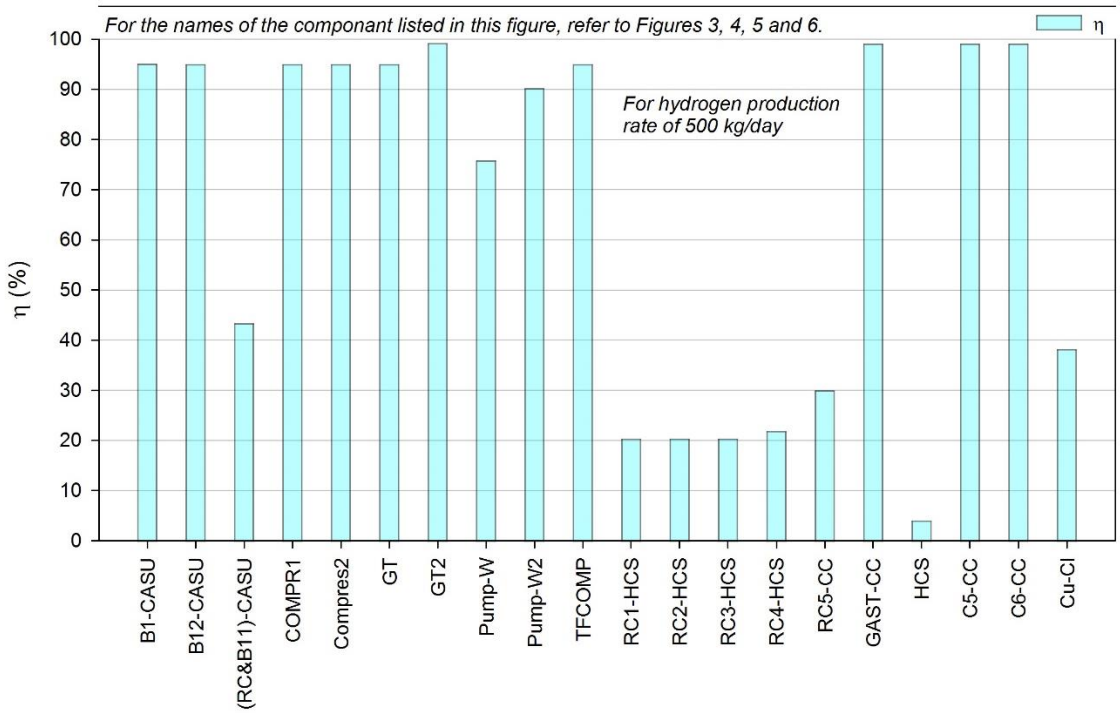

Figure 5.7 The energy efficiency of the work consuming and producing devices in System 1.

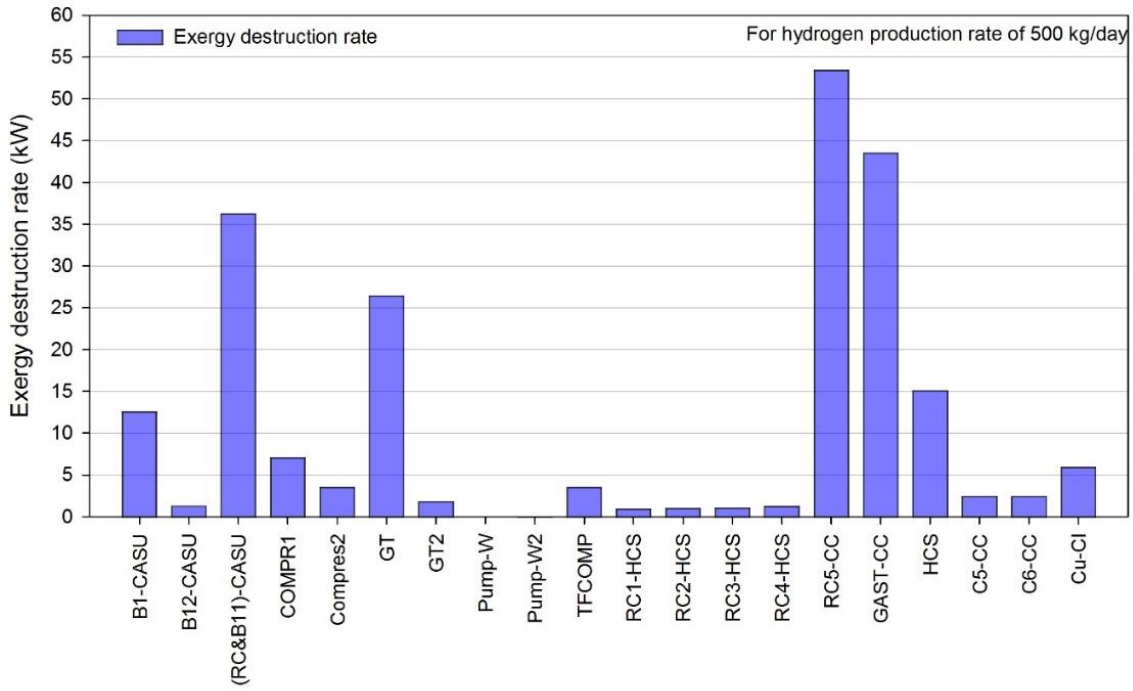

Figure 5.8 The exergy destruction rates of the work producing and consuming devices in System 1.

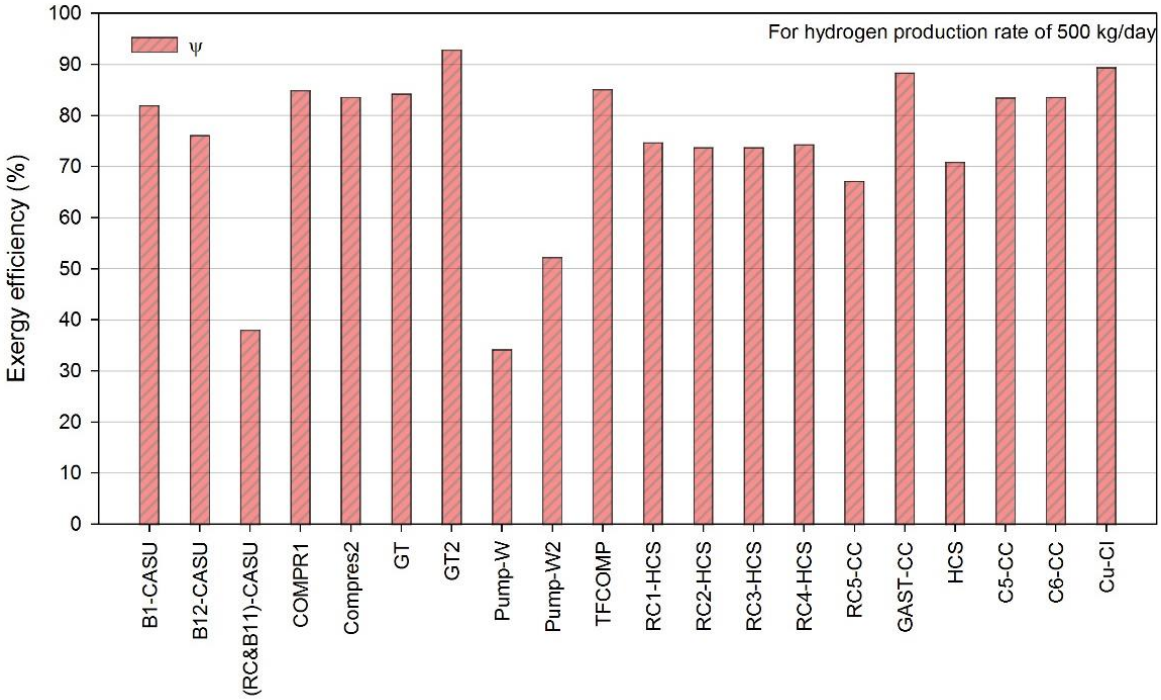

Figure 5.9 The exergy efficiency of the work producing and consuming devices in System 1.

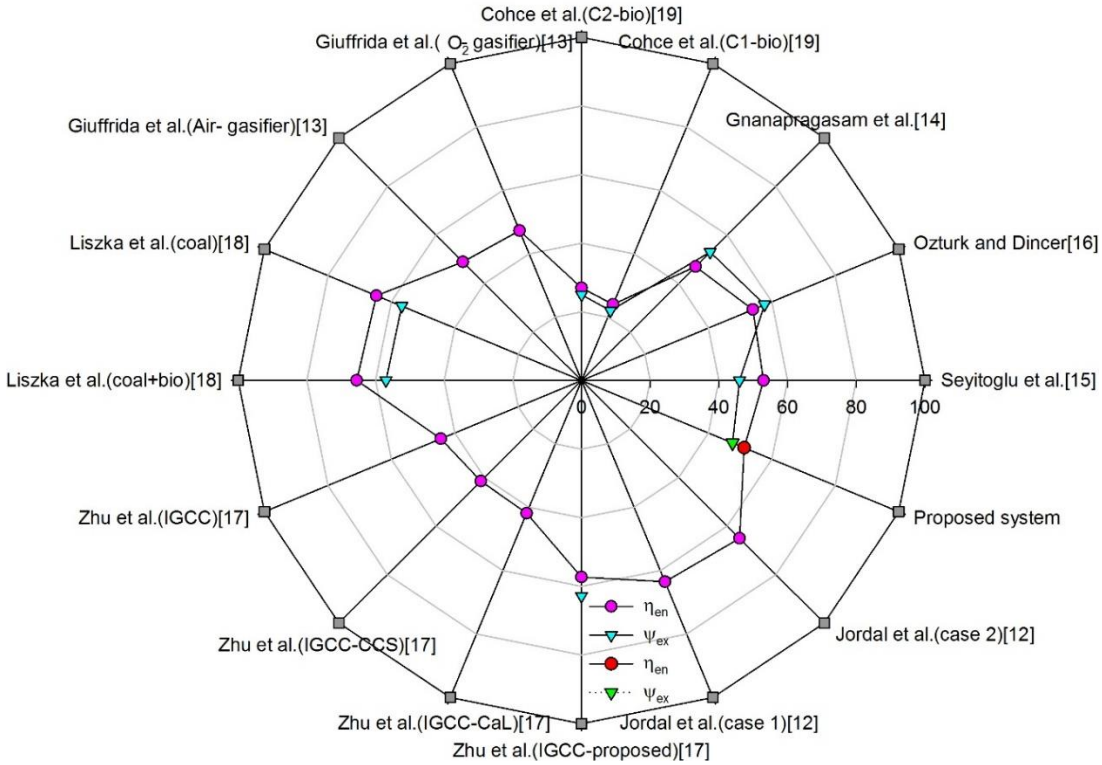

Figure 5.10 The energy and exergy efficiencies comparisons of the integrated gasification systems proposed in [27–34] with the results of the proposed hydrogen production plant in this research.

The main and the largest work consuming and producing devices in the proposed hydrogen production plant is the Brayton cycle, HCS, HFCC and CASU. All of the work consuming and producing devices in the proposed hydrogen production plant results are shown in Figures 5.6-5.9. Shown in Figure 5.6 the work rate produced or consumed by these devices for the case of hydrogen production rate of 500 kg/day. Shown in Figure 5.7 the energy efficiency of each of the work consuming and producing devices in the proposed hydrogen production plant. The highest work rate producing device is the gas turbine in the HFCC cycle (GAST see Figure 3.10) as shown in Figure 5.6. The highest work rate consuming device is the air compressor in the HFCC cycle (C5 see Figure 3.10) as shown in Figure 5.6. Shown in Figures 5.8 and 5.9 the exergy destruction rate and the exergy efficiency of each of the work producing or consuming devices. The work producing or consuming cycle or the device that has the highest exergy destruction rate is the Rankine cycle part of the HFCC (RC5 see Figure 3.10). However, the work producing or consuming cycle or the device with the lowest exergy destruction rate is the heat recovery from the

hydrogen compression intercooler Rankine cycles RC1, RC2, RC3 and RC4 (see Figure 3.9). The Rankine cycle part of the HFCC has the highest exergy destruction rate is because it receives heat at high temperature but since the steam turbines has a maximum steam inlet temperature of 650°C [83], resulting in losing a huge amount of exergy when limiting the temperature of the steam exiting the heat exchanger HX5 see Figure 3.10. The lowest exergy destruction rate of the Rankine cycles RC1, RC2, RC3 and RC4 (see Figure 3.9) is because the temperature of the compressed hydrogen exiting each stage in the HCS is below the steam turbines maximum steam inlet temperature of 650°C [83], which results in less amount of exergy lost. Since the inlet temperature of the compressed hydrogen entering heat exchanger is very close to the steam temperature exiting the heat exchanger. It is recommended to use another cycle to produce the needed work rate of the hydrogen production plant in the place of the HFCC system, due to its large exergy destruction rate.

Finally, the proposed system energy and exergy efficiencies are compared to that available in the literature regarding hydrogen production through coal gasification. Note that none of the systems that were proposed in the literature and are mentioned here in the comparison try to compress the hydrogen produced. The comparison is presented in Figure 5.10 which present the comparison in an easy way to comprehend the results.

5.2 Results of System 2

The results of the simulation and thermodynamic analysis of the proposed integrated system are reported in Table 5.2, which lists the energy and exergy efficiencies of the proposed integrated system plus the hydrogen production rate for the two cases considered. The heat interactions and the associated exergy for each reactor in the Cu-Cl cycle (see Figure 3.12 for reactor names) are shown in Figure 5.11. The Cu-Cl cycle reactor that requires most of the cycle heat per mole of hydrogen produced is the Cu_2OCl_2 decomposition reactor (B6 in Figure 3.12). The Cu_2OCl_2 decomposition reactor also has the highest exergy consumption in the Cu-Cl cycle. The reactor that produces the most of the heat per mole of hydrogen produced within the cycle is the CuCl solidification reactor (B8 and B28 in Figure 3.12).

The work rates per kilogram of hydrogen produced for work rate consuming and producing devices in the integrated system are shown in Figure 3.12 and their energy and

exergy efficiencies are shown in Figure 3.13. The component with the highest work rate production is the gas turbine (GAST) in the SCC system. Since the SCC system provide the required power by the compression system and by the Cu-Cl cycle electrolysis reactor. The component with the highest work rate per hydrogen produced consumption is the hydrogen compressor (C6) in the SCC system. The work producing or consuming device with the highest exergy destruction rate per kg of hydrogen produced is the SCC gas turbine (GAST). The SCC system gas turbine have the highest exergy destruction rate makes sense since it is responsible for the production of high work rates per each kg of hydrogen produced.

The energy and exergy efficiencies of the Cu-Cl cycle without considering the steam circuit are close to those reported in the literature. Without considering the steam circuit means without considering the method of delivering the heat to the cycle, and instead considering the heat required by the reaction and other heating or cooling processes. The energy and exergy efficiencies for non-steam circuit Cu-Cl cycle are found here to be 38.2% and 69.2% respectively. These values are very close to the corresponding efficiencies of 44.8% and 73.0% respectively reported by Orhan et al. [20,40,46].

Table 5.2 The results of the simulation of the proposed (nuclear-based) integrated system for hydrogen production for the two cases (System 2).

Parameters	Case 1	Case 2
Case description	Including the steam circuit design that was proposed	Without including the steam circuit in the design
SCC energy efficiency (η_{SCC})	39.7%	39.7%
SCC energy efficiency (ψ_{SCC})	40.4%	40.4%
HCS energy efficiency (η_{HCS})	14.7%	14.7%
HCS exergy efficiency (ψ_{HCS})	36.1%	36.1%
Integrated system energy efficiency (η_{ov})	16.8%	24.8%
Integrated system exergy efficiency (ψ_{ov})	27.8%	40.9%
Hydrogen production rate	6.28 kg/s	9.12 kg/s
Hydrogen consumed for SCC	2.72 kg/s	3.88 kg/s
Net hydrogen produced at high pressure (700 bar)	3.56 kg/s	5.24 kg/s

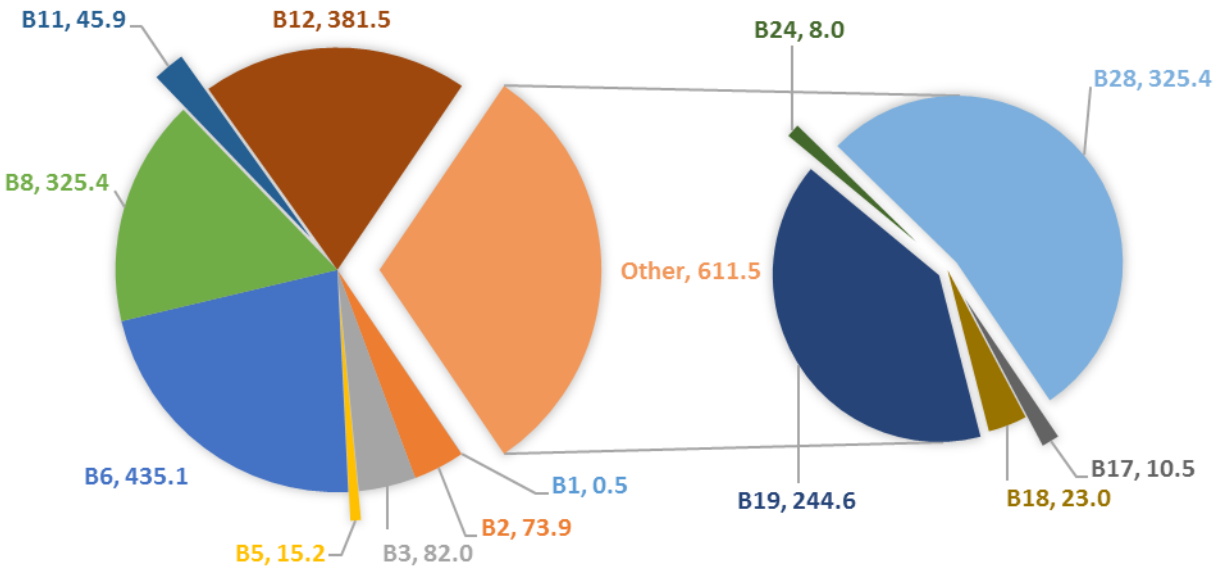

Figure 5.11 The unit thermal energy interaction in the Cu-Cl cycle reactors per each mole of hydrogen the cycle produces in System 2 (kJ/mol H_2).

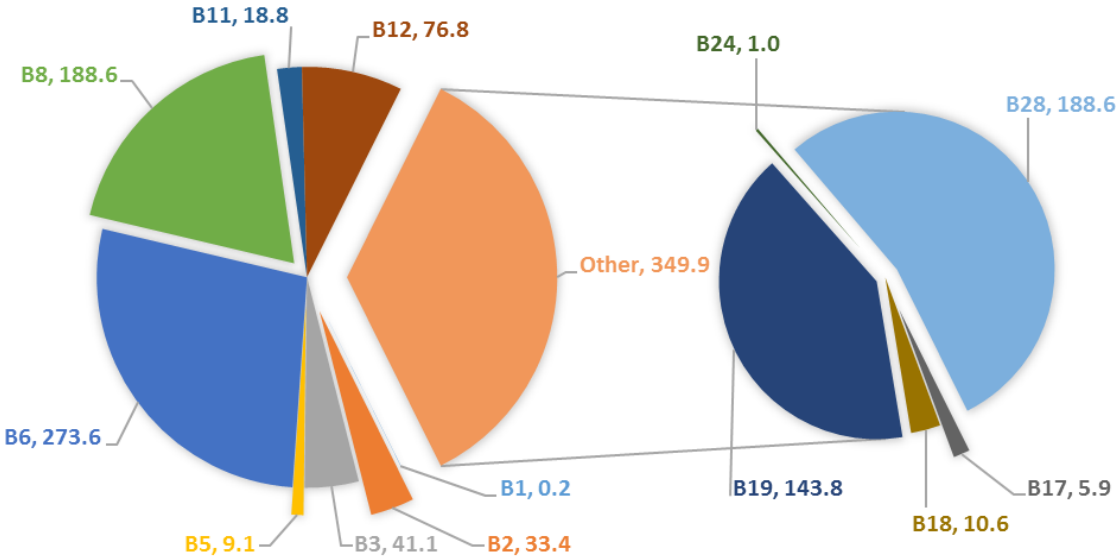

Figure 5.12 The unit thermal exergy content interaction in the Cu-Cl cycle reactors per each mole of hydrogen the cycle produces in System 2 (kJ/mol H_2).

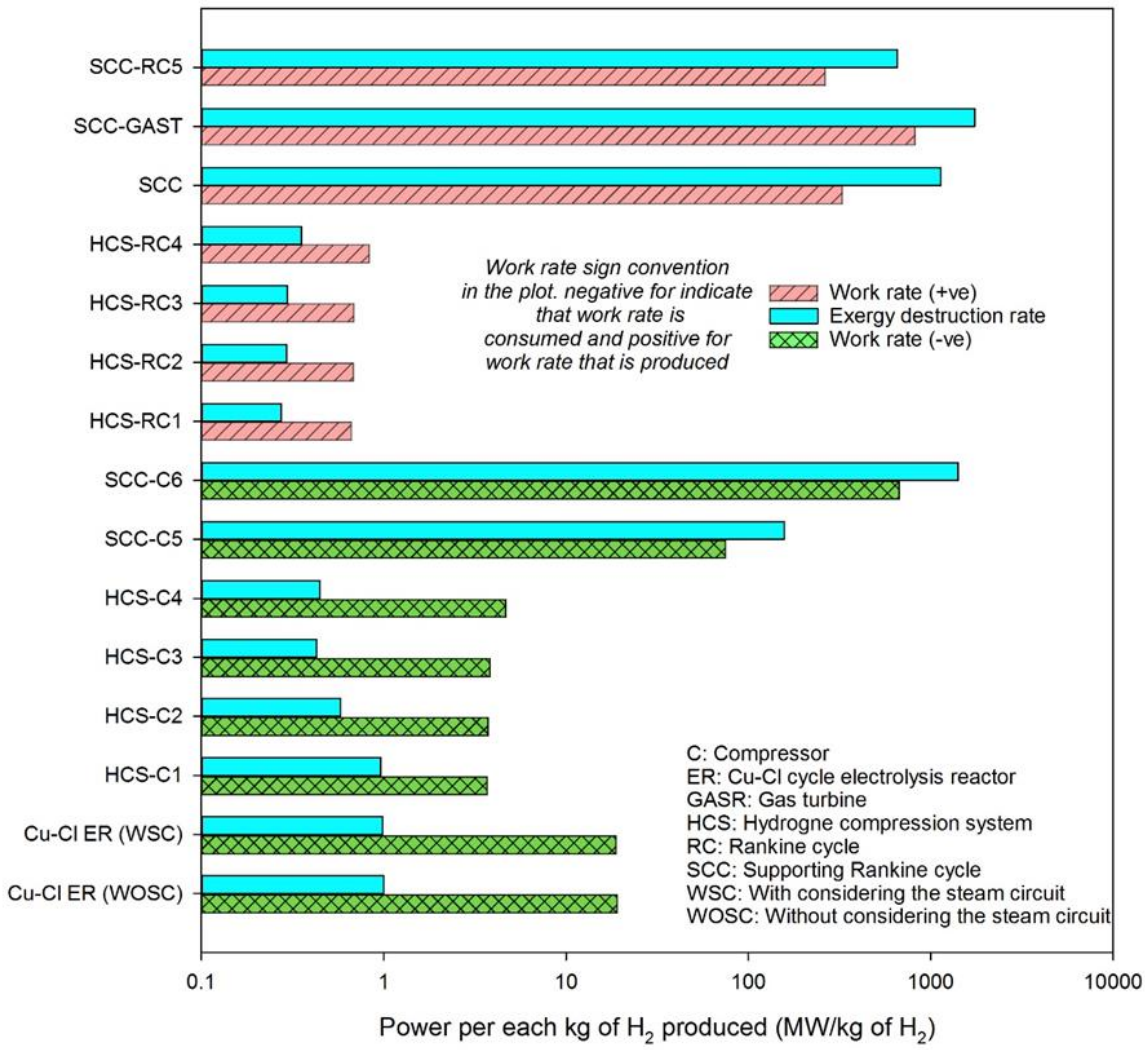

Figure 5.13 The work rate and exergy destruction rate per kg of hydrogen produced by the integrated system of all work rate producing or consuming devices in System 2.

There are several reasons for the differences. First, in the current design the hydrogen produced is allowed to cool without recovering the heat for safety purposes. The extra steam provided to the hydrolysis reactor to obtain 100% conversion of the reactants is considered in this model, but not by Orhan et al.[20,40,46]. Since the Cu-Cl cycle is integrated with a nuclear reactor producing heat in the form of supercritical superheated steam, the steam circuit which provides and recovers heat for the cycle needs to be considered.

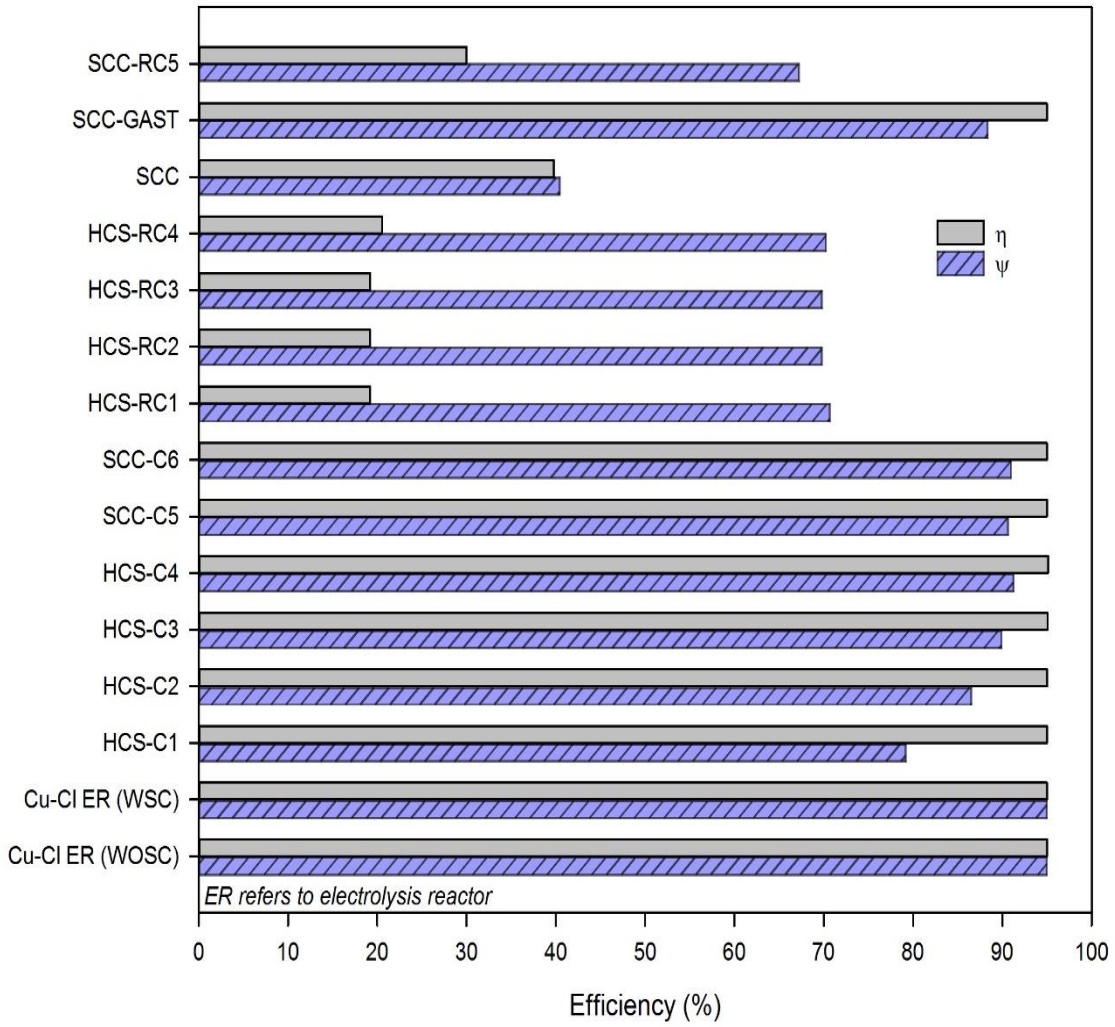

Figure 5.14 The energy and exergy efficiencies and the work rates of the producing or consuming devices in the nuclear-based integrated system (System 2).

The HCS bottoming Rankine cycles are found to reduce the required compression power by 18%. The remaining 82% is covered by the SCC. Most (90%) of the power produced by the SCC cycle is used for the electrolysis reactor in the Cu-Cl cycle and the remaining 10% drives the HCS compressors. As shown in Figure 5.15 the energy efficiency of the HCS is 14.7%. This low value is due to the high work rate that is provided to the system to increase the pressure of the hydrogen while maintaining a final temperature of the compressed hydrogen as low as possible. The exergy efficiency of the HCS is 36.1%, which is higher than its energy efficiency because in the exergy analysis the high pressure compressed gas has a high exergy content. Also shown in Figure 5.15 and 5.16 is are the energy and exergy efficiencies of the SCC, which are 39.7% and 40.4% respectively.

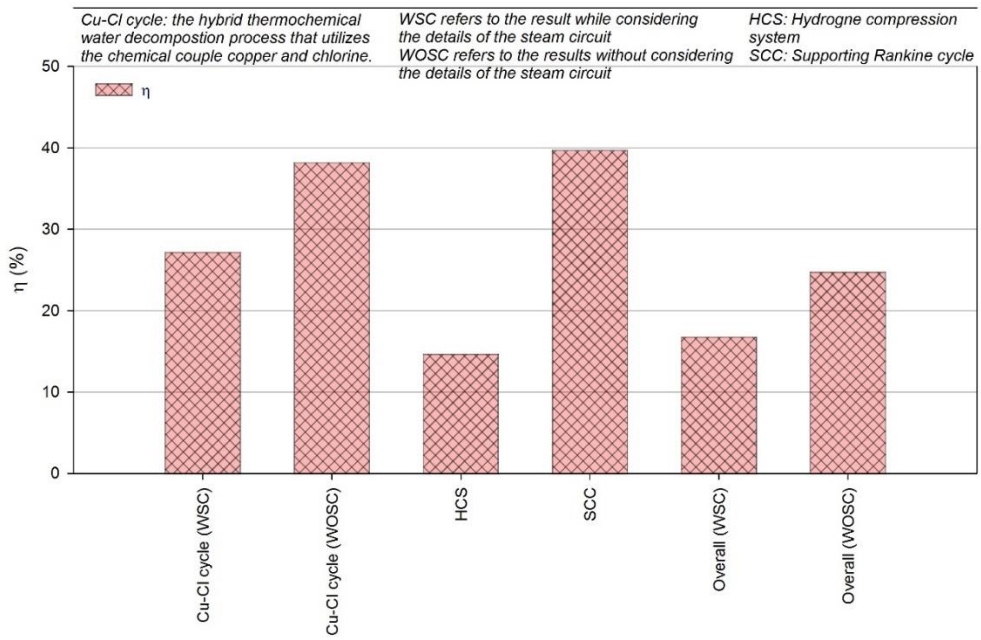

Figure 5.15 The energy efficiency of the main subsystems of the integrated system (System 2) while considering the two cases taken into consideration.

In the first case, a specific steam circuit design was proposed which is presented in Figures 3.11 and 3.13. The proposed steam circuit design consumed heat from the nuclear reactor per each kg of hydrogen produced more than what the Cu-Cl cycle actually needs. The extra heat absorbed from the nuclear reactor was to accommodate the heat losses in the circuit. Due to that, the energy efficiency of the Cu-Cl cycle was lower than what the cycle can offer. The second case was considering only the heat that is required by the Cu-Cl cycle to produce the hydrogen. The energy and exergy efficiencies of the main components of the integrated system for the first and the second cases are shown in Figures 5.15 and 5.16. The exergy destruction ratio of the main components of the integrated system for the two cases considered are shown in Figure 5.17. The energy and exergy efficiencies of the Cu-Cl cycle (see Table 5.2) decreases from 38.2% and 69.2% to 27.2% and 50.7% when the proposed steam circuit design is considered. The drop in the efficiencies of the Cu-Cl cycle indicates the importance of considering the steam circuit in the analysis of the Cu-Cl cycle when the heat provided to the cycle is from steam. Considering the steam circuit is also important due to its effect on the overall efficiencies and the mass flow rate of the hydrogen produced.

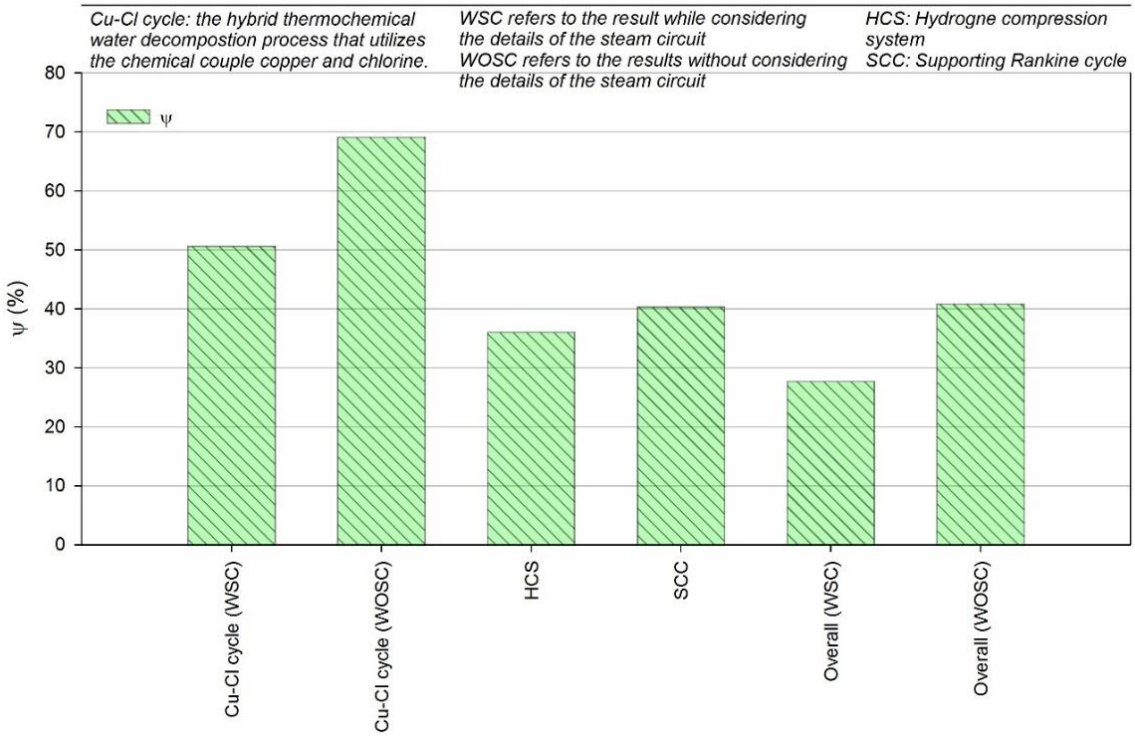

Figure 5.16 The exergy efficiency of the main subsystems of integrated System 2 while considering the two cases taken into consideration.

The overall energy and exergy efficiencies and the mass flow rate of net hydrogen produced from the plant drops from 24.8%, 40.9%, and 5.24 kg/s to 16.8%, 27.8%, and 3.56 kg/s (see Table 5.2). Note that the hydrogen produced is at high pressure of 700 bar. Regarding the exergy destruction contribution, the contribution percentage of the main components is shown in Figure 5.17. The contribution of the Cu-Cl cycle to the overall exergy destruction rate of the integrated system increases when the steam circuit is considered. One of the reasons for that is the increase in the mass flow rate of the hydrogen sent to the SCC. The mass ratio of the hydrogen sent to the SCC increase from 42.5% to 43.3% when the steam circuit is considered in the analysis. Figure 5.18 compares between published results of nuclear-based integrated systems and the two cases proposed in this thesis for the nuclear-based System 2.

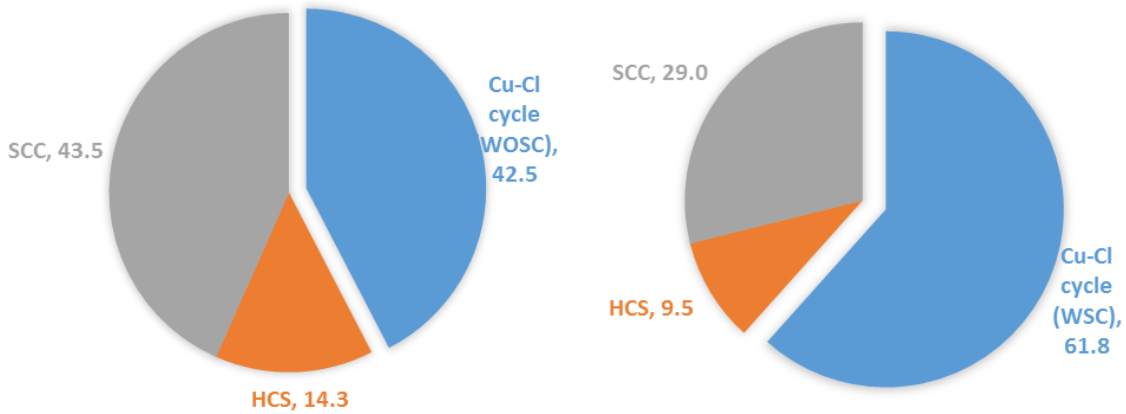

Figure 5.17 The exergy destruction contribution percentage (%) for the two cases, on the right the case where the steam circuit is considered in the analysis, and on the left the case where the steam circuit is not considered.

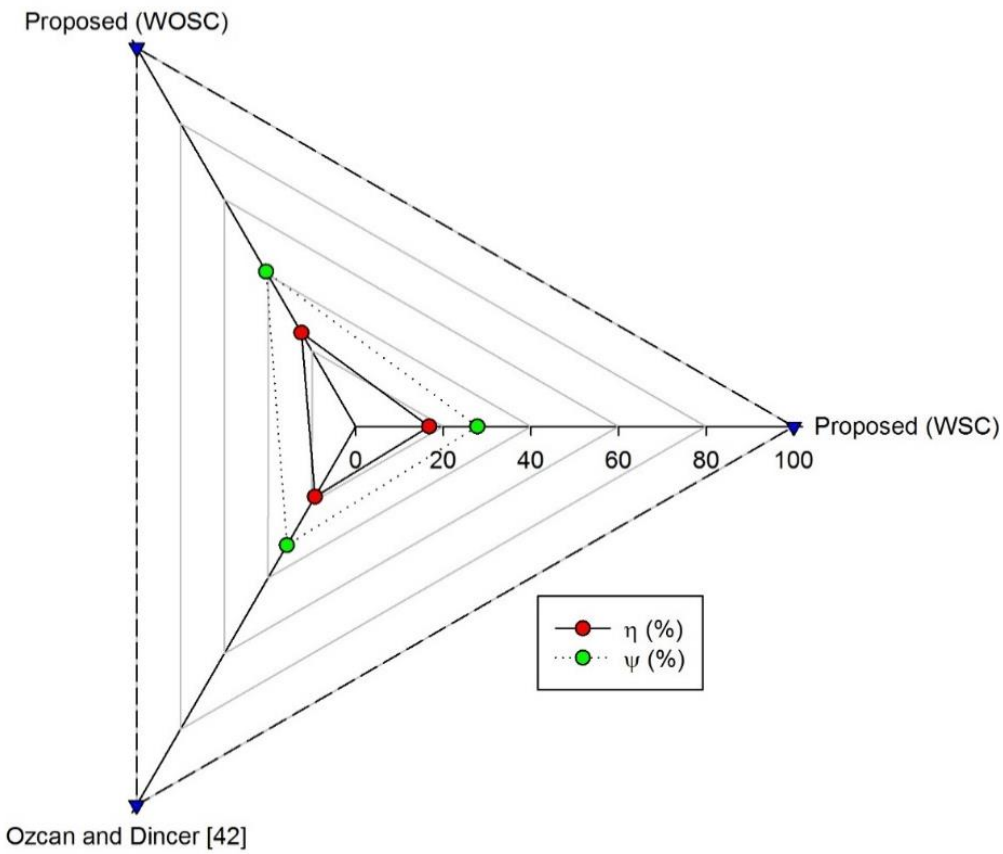

Figure 5.18 The energy and exergy efficiencies comparisons of the integrated nuclear-based systems proposed in this thesis and in the work of Ozcan and Dincer [42].

5.3 Results of System 3

The simulation results and the results of the energy and the exergy analyses are reported next for the hydrogen production plant and its components. All results are calculated using Aspen Plus software and Aspen Hysys. However chemical exergies, efficiencies, and exergy destruction rates are calculated using a programmed Excel sheet, and the heliostat solar farm is simulated using EES in the light of the currently running 5 MW_{th} heliostat field own by Greenway CSP in Mersin, Turkey [77]. The reference environment temperature and pressure are 25°C and 1 atm respectively. The overall performance of the hydrogen production plant that is completely dependent on clean solar thermal energy is reported next. The overall performance of the plant is summarized in Table 5.3. Reported in Table 5.3, the overall energy and exergy efficiencies of the proposed hydrogen production plant are 13.6% and 22.3%. The hydrogen production plant has the ability to produce 4.97 g of hydrogen per second as long as the solar intensity is 800 W/m^2. The properties of the produced hydrogen are at a pressure and temperature of 700 bar and 25°C.

The plant also produces 78.0 kW of electricity for a factor of safety and for any component electrical requirement or losses that were not considered. The performance results of the hydrogen production plant subsystems is provided next. These subsystems include solar heliostat farm, Cu-Cl cycle, HCS, and SRC. The energy and exergy efficiencies are shown in Figures 5.19 and 5.20 and the exergy destruction rate is shown in Figure 5.21 of the hydrogen production plant main components. As shown in Figure 5.21 the Cu-Cl cycle has the lowest exergy destruction rate due to its high exergy efficiency and the high-quality product it produces.

Table 5.3 The overall results of the hydrogen production plant which is completely dependent on the solar thermal energy (System 3).

Parameter	Value	Unit
Energy efficiency	12.6	%
Exergy efficiency	20.7	%
Hydrogen production rate*	6.97	g/s
Electricity generation rate by the system*	322	kW
Pressure of produced hydrogen	700	bar
Temperature of produced hydrogen	25	^{o}C
Exergy destruction rate*	3.54	MW

* at the specified solar intensity in Table 4.3.

The solar heliostat farm model and the parameters selected were able to produce 5 MW_{th} in the form of superheated steam at 550°C and 55 bar. The energy and exergy efficiencies of the Cu-Cl cycle are 38.2% and 89.4% respectively, similar to the results reached by Orhan et al. [40] for the five-step Cu-Cl cycle. The heat rate and the associated exergy with that heat for the Cu-Cl cycle is shown in Figure 5.22. The energy and exergy efficiencies of the five-step Cu-Cl cycle reported by Orhan et al. [40] were 44.8% and 73.0%. The energy efficiency and the work rate interaction of the main work rate producing devices is shown in Figures 5.23 and 5.24. The exergy efficiency and the exergy destruction rate of the work rate producing device is shown in Figures 5.25 and 5.26. The differences between this research Cu-Cl cycle design results and those by Orhan et al. [40] are due to mainly the different configuration of the components in the system and the way they interact with each other's. The main differences between the Cu-Cl cycle design in this research and Orhan et al. [40] designs are next. In the proposed design of the Cu-Cl cycle the produced hydrogen is not recovered, unlike what Orhan et al. [40] proposed, which is recovering the hydrogen heat. Not recovering the hydrogen heat before storing it rather it was allowed to cool down to ambient temperature is for safety reasons. This design difference reduces the energy efficiency. In the proposed design of the Cu-Cl cycle the water is first preheated by the extra steam and by the separated oxygen after that, the steam is superheated by the solar thermal energy.

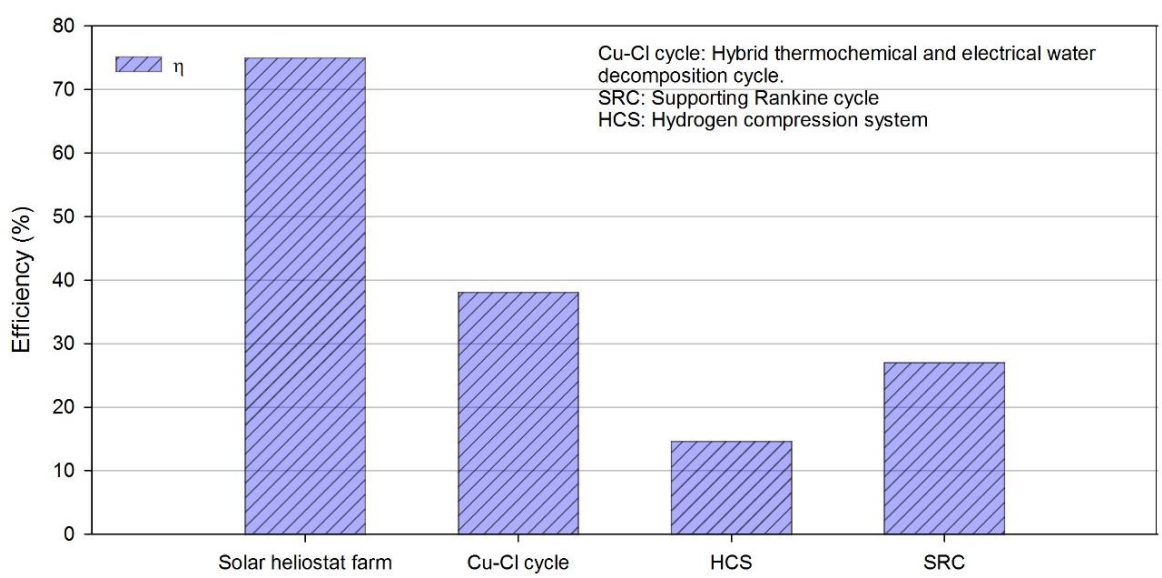

Figure 5.19 The energy efficiency of the main components of System 3 subsystems.

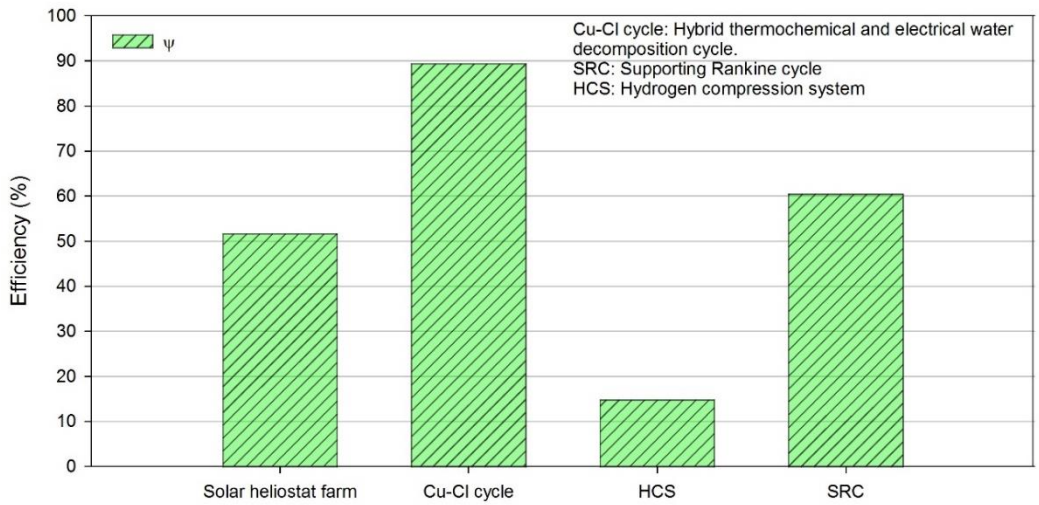

Figure 5.20 The exergy efficiency of the main components of System 3 subsystems.

In contrast, Orhan et al. [40] did not consider the extra steam suggestion by Wang et al. [12] to provide the needed reaction heat and shift the equilibrium direction. Results in increasing the exergy efficiency while adding more realistic approach to the cycle. In the proposed design of the Cu-Cl cycle recovering the solidification latent heat of CuCl was done in a way to produce steam at high temperatures to maintain high exergy content of that heat. In the proposed design of the Cu-Cl cycle, the electricity requirement of the Cu-Cl cycle is provided by the SRC and the electrical generators.

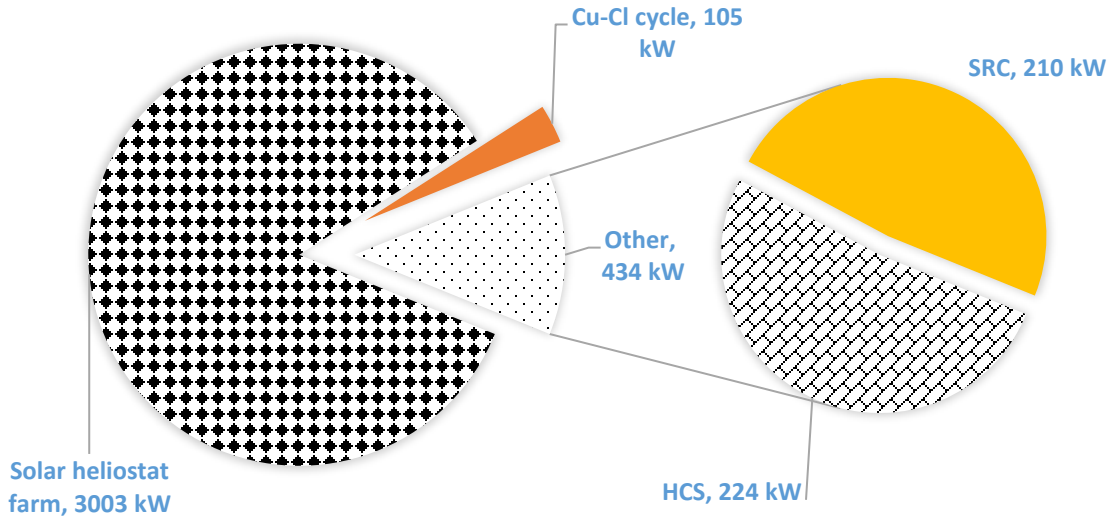

Figure 5.21 The exergy destruction rate for the main components of the hydrogen production plant subsystems.

The heat interactions and their exergy content in the proposed design of the five-step Cu-Cl cycle are shown in Figure 5.22. The Cu_2OCl_2 decomposition reactor B6 has the second highest heat energy interaction and the second highest exergy interaction since it requires heat at the highest temperature in the cycle of 530°C. The highest energy and exergy interactions are for the solidification of the CuCl. The high exergy content of the solidification of the CuCl is due to the high and constant temperature of the heat release. Regarding the Cu-Cl cycle exergy destruction role in the plant. The Cu-Cl cycle has the least contribution as shown in Figure 5.21. The low exergy destruction contribution of the Cu-Cl cycle is due to its high exergy efficiency. The Cu-Cl cycle exergy efficiency was increased by the proposed design of cycle structure and its differences with the designs that were proposed in the literature.

The Cu-Cl cycle model was not experimentally validated since the Cu-Cl cycle is still in the proof-of-principle and still, there is no experimental full Cu-Cl cycle. The number of studies on the simulation and thermodynamic analysis of the Cu-Cl cycle is also limited. A huge percentage of the work done on the Cu-Cl cycle regarding its simulation and integrating it to another system was done by Orhan et al. [20,40,46,56] and Ozbilen et al. [21,39].

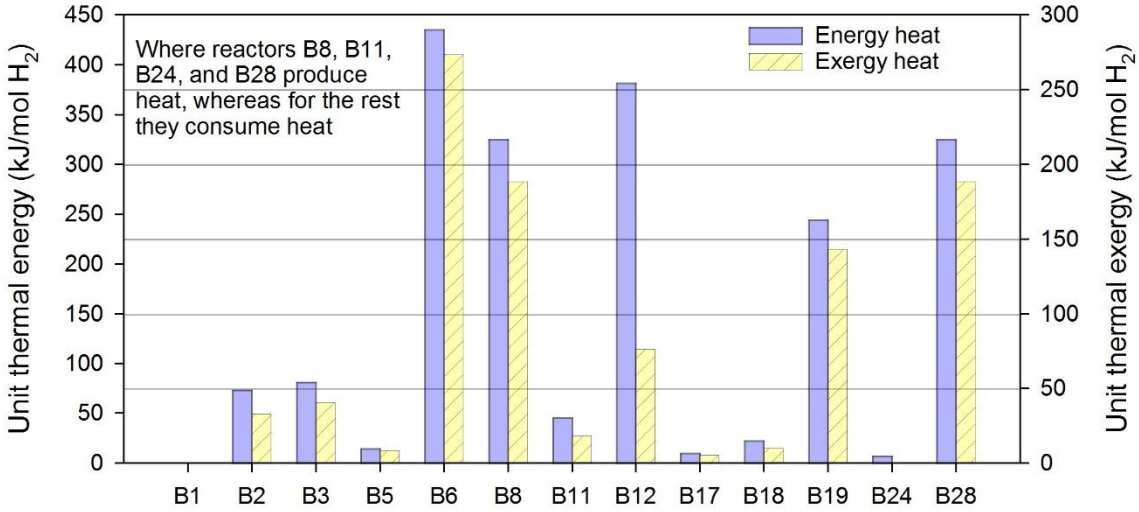

Figure 5.22 The thermal energy and thermal exergy interactions in the proposed design of the copper-chlorine cycle in System 3.

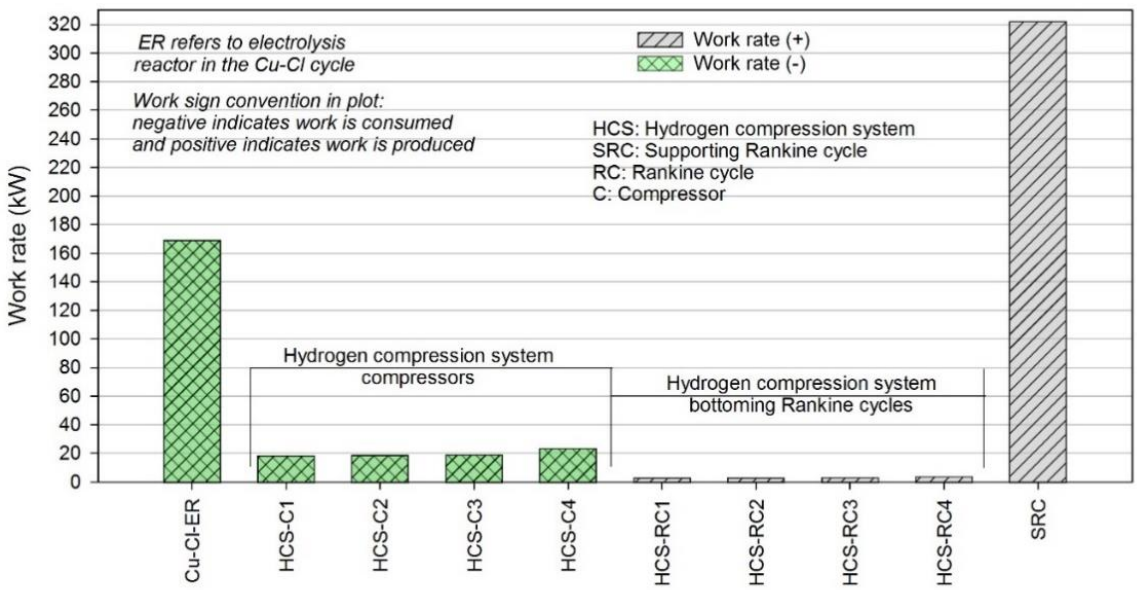

Figure 5.23 The work rates interactions of the work producing and consuming devices in System 3.

The largest exergy destruction rate in the proposed hydrogen production plant is the HCS. Since a large amount of high-quality energy (work rate) is consumed and the result increases in the pressure of hydrogen. Where hydrogen energy content as a fuel is much larger than that of the energy associated with high pressure. The second highest exergy destruction rate belongs to the SRC. It is recommended to use new technologies for compressing the hydrogen such as electrochemical compression systems.

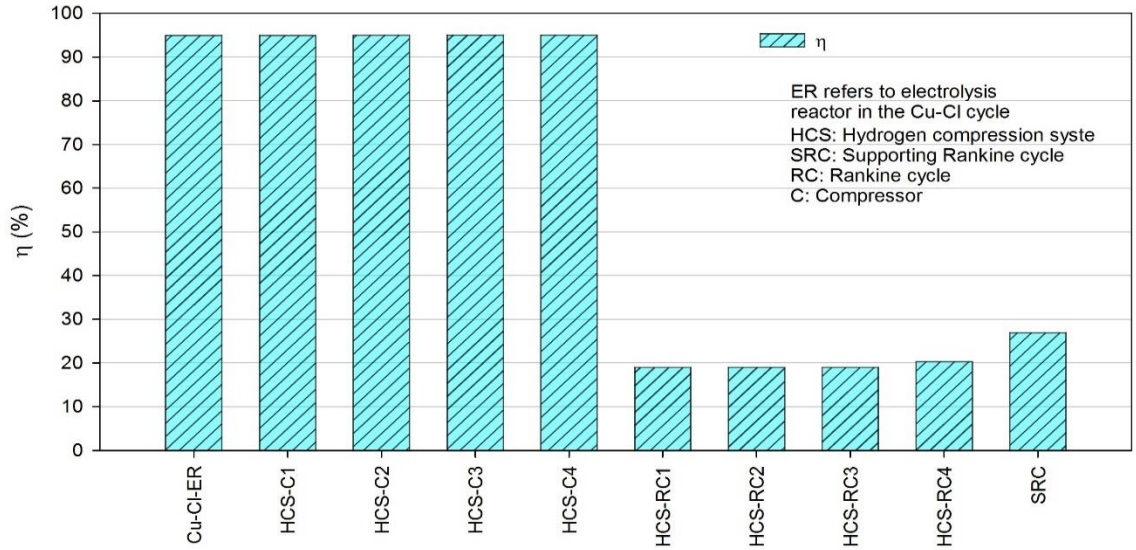

Figure 5.24 The energy efficiency of the work producing and consuming devices in System 3.

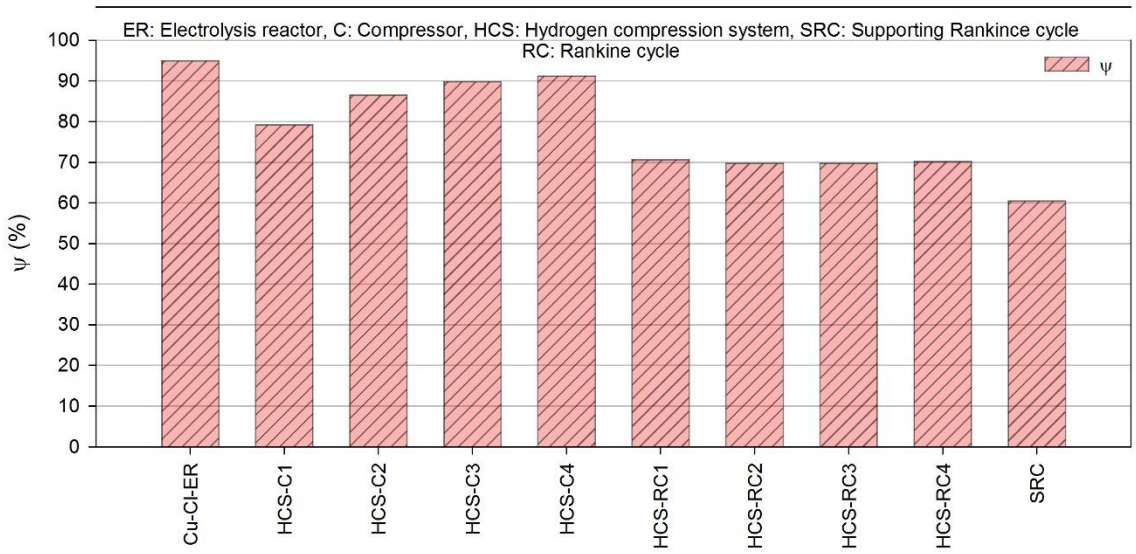

Figure 5.25 The exergy efficiency of the work producing and consuming devices in System 3.

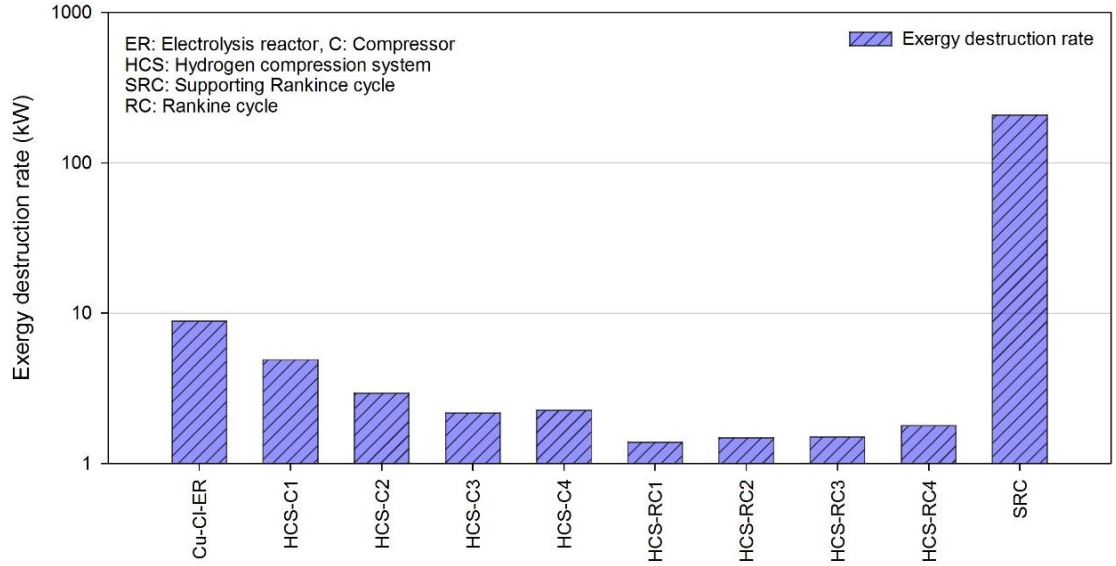

Figure 5.26 The exergy destruction of the work producing and consuming devices in System 3.

The results for the nuclear-based hydrogen and power production integrated system are reported in Table 5.4, including the hydrogen production rate, pressure and temperature, the overall net power output, the overall energy and exergy efficiencies, and the energy and exergy efficiencies of the subsystems of the integrated system. It is seen that the system is able to produce 2.02 kg/s of compressed hydrogen at a pressure of 700

bar and at a low temperature of 25°C, and with a net electrical power output of 553 MW. The energy and exergy efficiencies of the HCS are 35.8% and 64.8%, respectively.

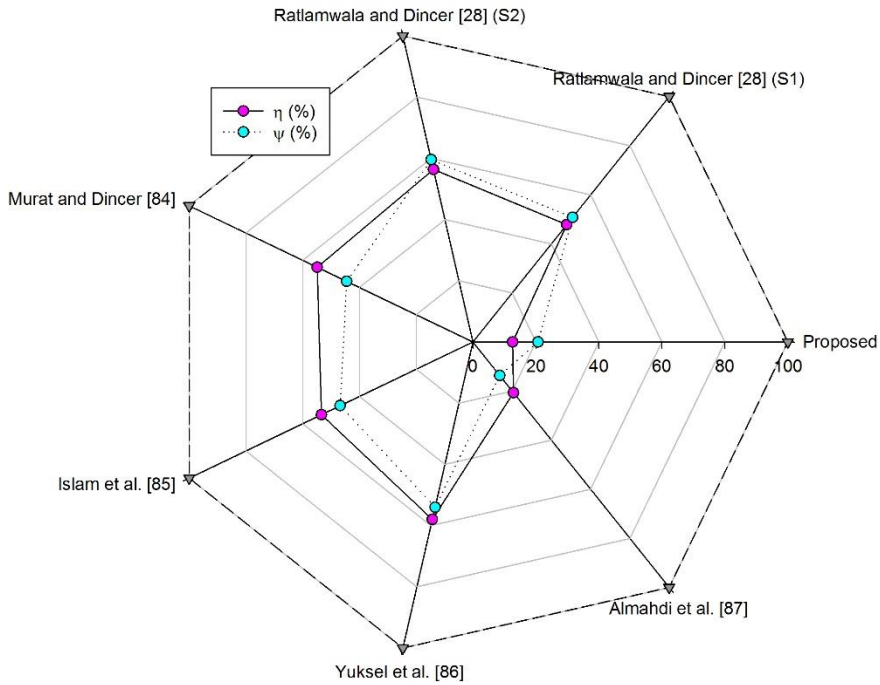

Figure 5.27 The energy and exergy efficiencies comparisons of the integrated solar-based systems proposed in [28, 84-87] and the proposed System 3 in this thesis.

Figure 5.27 compare the results of energy and exergy efficiencies of the proposed solar-based hydrogen and power production system and published solar-based hydrogen and production systems.

5.4 Results of System 4

The energy and exergy efficiencies of the Cu-Cl cycle, as shown in Table 5.4, are 40.1% and 60.2%, respectively, which are similar to the 40.1% energy efficiency and 70% exergy efficiency found by Orhan [46] for the four-step cycle. The reason for the lower exergy efficiency in this article is that here the method of delivering the required heat is considered and the energy and exergy inputs to the cycle are based on the supercritical fluid energy and exergy. The unit thermal energy associated with the Cu-Cl cycle reactors and the heat exchangers are presented in Figure 5.28. The unit thermal exergy linked to each of Cu-Cl cycle reactors and heat exchangers are shown in Figure 5.29. The component in the four-step Cu-Cl cycle associated with the highest unit thermal energy is the dryer (*B14*), which is a reason for the exergy efficiency being lower that reported in the literature.

Table 5.4 The overall hydrogen production rate, pressure and temperature, the overall net power output, the overall system energy and exergy efficiencies, and the energy and exergy efficiencies of the subsystems of the integrated system.

Parameter		value	unit
Overall hydrogen production rate		2.02	kg/s
Temperature of the produced hydrogen		25.0	^{o}C
Pressure of the produced hydrogen		700	bar
Overall net produced power		553	MW
Integrated system overall energy efficiency		31.6	%
Integrated system overall exergy efficiency		56.2	%
Integrated system overall exergy destruction rate		630	MW
Subsystems energy and exergy efficiencies	Four-step Cu-Cl cycle energy efficiency	40.1	%
	Four-step Cu-Cl cycle exergy efficiency	60.2	%
	Power supporting Rankine cycle energy efficiency	36.1	%
	Power supporting Rankine cycle exergy efficiency	70.8	%
	Hydrogen compression system energy efficiency	35.8	%
	Hydrogen compression system exergy efficiency	64.8	%

The dryer is required to convert the aqueous $CuCl_2$ to solid $CuCl_2$ by evaporating the water, and is the third step in the four-step Cu-Cl cycle. The amount of water in the aqueous solution determines the amount of thermal energy required to carry out the drying process. The amount of water should be at least the minimum amount required to dissolve the $CuCl_2$ that is produced, and is found to be 20 moles of H_2O for each 2 moles of $CuCl_2$. The second highest thermal energy supply is to the Cu_2OCl_2 decomposition reactor (*B6*). However, the component in the four-step Cu-Cl cycle that is associated with the highest unit thermal exergy is the Cu_2OCl_2 decomposition reactor, since it has to be maintained at a temperature of 530°C and is the second highest unit thermal energy consumer. The second highest thermal exergy supply is to the dryer. Although it is maintained at relatively low temperature, the dryer requires more than twice the thermal energy than the Cu_2OCl_2 decomposition reactor. As shown in Figures 5.28 and 5.29 the electrolysis reaction requires zero thermal energy and exergy since it is operated at environment conditions and any heat generated is allowed to transfer to the surrounding environment to maintain the reactor at 25°C. However, as reported elsewhere [46], the four-step Cu-Cl cycle requires nearly 55.0 kJ/mol H_2 of electrical power. The exergy efficiencies and the unit exergy destruction rates associated with the components of the four-step Cu-Cl cycle are presented in Figures 5.30 and 5.31. The Cu_2OCl_2 decomposition reactor is seen there to be the component with the

highest unit exergy destruction rate, at 85.2 kJ/mol H_2. This is expected since that device has the highest unit thermal exergy interaction in the Cu-Cl cycle. The second highest unit exergy destruction is attributable to the water jacket of the CuCl solidification reactor (*B18*), at 54.8 kJ/mol H_2. Since the solidification of CuCl first starts from molten CuCl at 530°C and then the latent heat released at a relatively high temperature of 436°C, compared to the 100°C temperature of the thermal energy absorbing fluid (water), which means high-quality heat is used for a process requiring lower quality thermal energy. The lowest unit exergy destruction rate is associated with the exchangers B5 and B40, since the unit thermal exergy associated with each of these reactors is low compared to the cycle reactors.

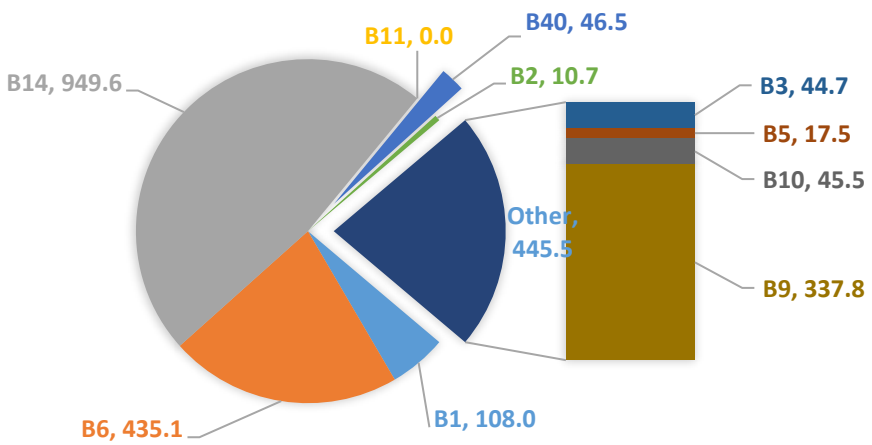

Figure 5.28 The breakdown of unit thermal energy $(\dot{Q})$ (represented by second value for each item and in kJ/mol H_2) associated with each of Cu-Cl cycle reactors and heat exchangers (identified by first alphanumeric indicator for each item) in System 4.

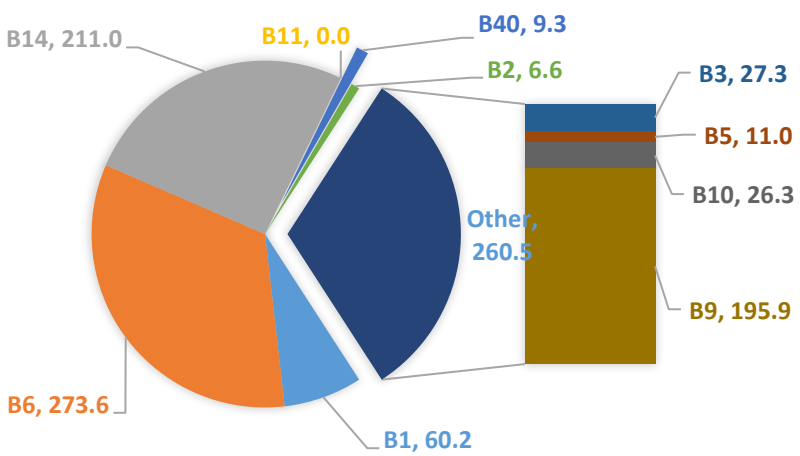

Figure 5.29 The Breakdown of unit thermal exergy $(\dot{E}x_{\dot{Q}})$ (represented by second value for each item and in kJ/mol H_2) associated with each of Cu-Cl cycle reactors and heat exchangers (identified by first alphanumeric indicator for each item) in System 4.

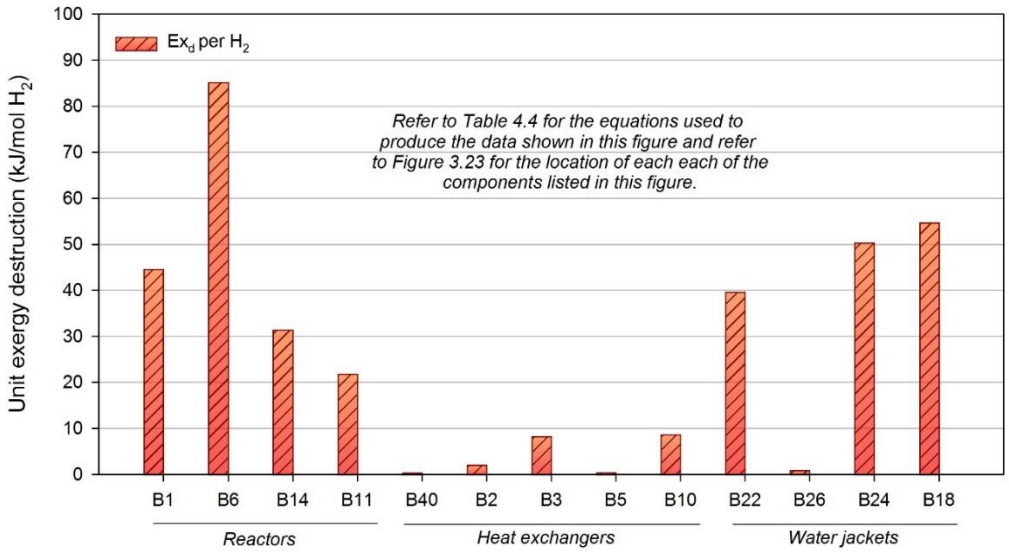

Figure 5.30 The unit exergy destruction associated with each of the components of the four-step Cu-Cl cycle in System 4.

The PSR has an energy efficiency of 36.1% and an exergy efficiency of 70.8%, as shown in Table 5.4. The PSR is able to produce the electrical power required by the Cu-Cl cycle and the HCS, and also to export 553 MW of electrical power to the grid. The main components of the PSR are shown in Figures 3.24, while the component exergy efficiencies and unit exergy destruction rates are shown in Figures 5.32 and 5.33.

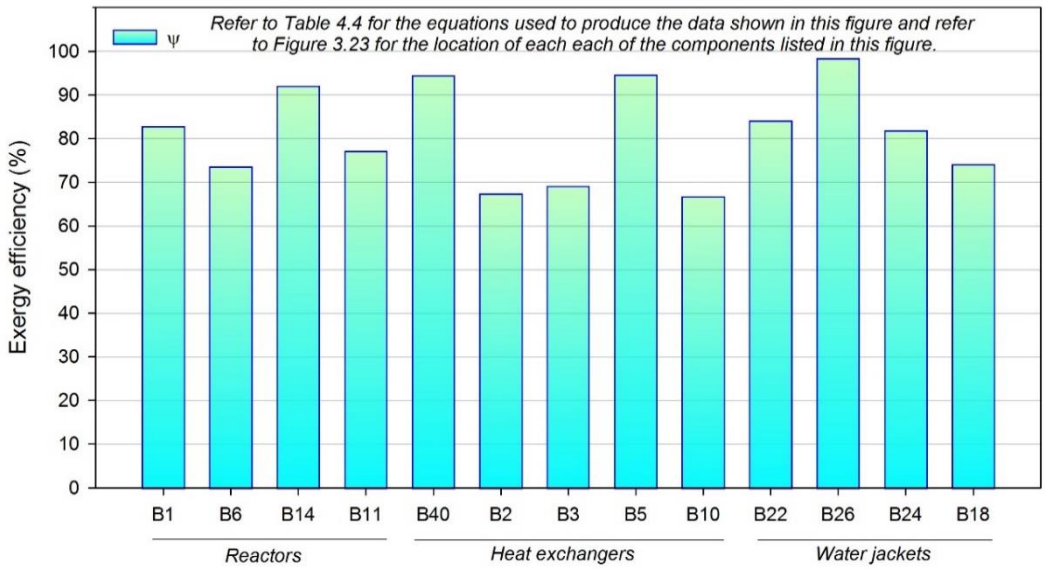

Figure 5.31 The exergy efficiency associated with each of the components of the four-step Cu-Cl cycle in System 4.

The unit with the highest unit exergy destruction rate is the steam turbine (*B32*), at 304 kJ/mol H_2, which is expected since it has the highest energy interaction between the components of the SPR system. The unit with the second highest unit exergy destruction rate is the boiler (*B27B30*), in which thermal energy with high quality (minimum temperature of 350ºC) is used to raise the temperature of water from 100ºC. The lowest unit exergy destruction rate is the condenser, since the thermal energy is rejected at low constant temperature and the fluid experiences only phase change, for which the exergy efficiency is high.

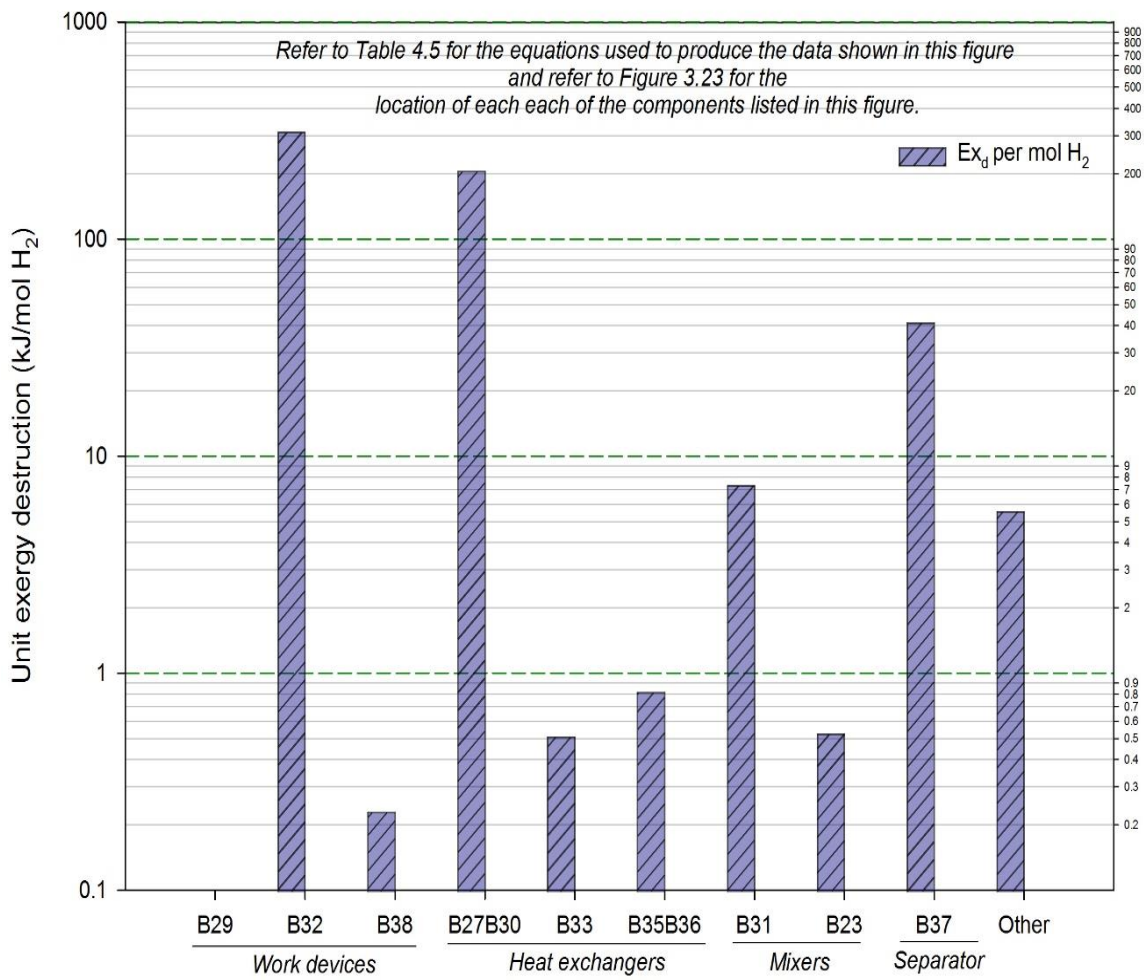

Figure 5.32 The unit exergy destruction of the components of the PSR in System 4.

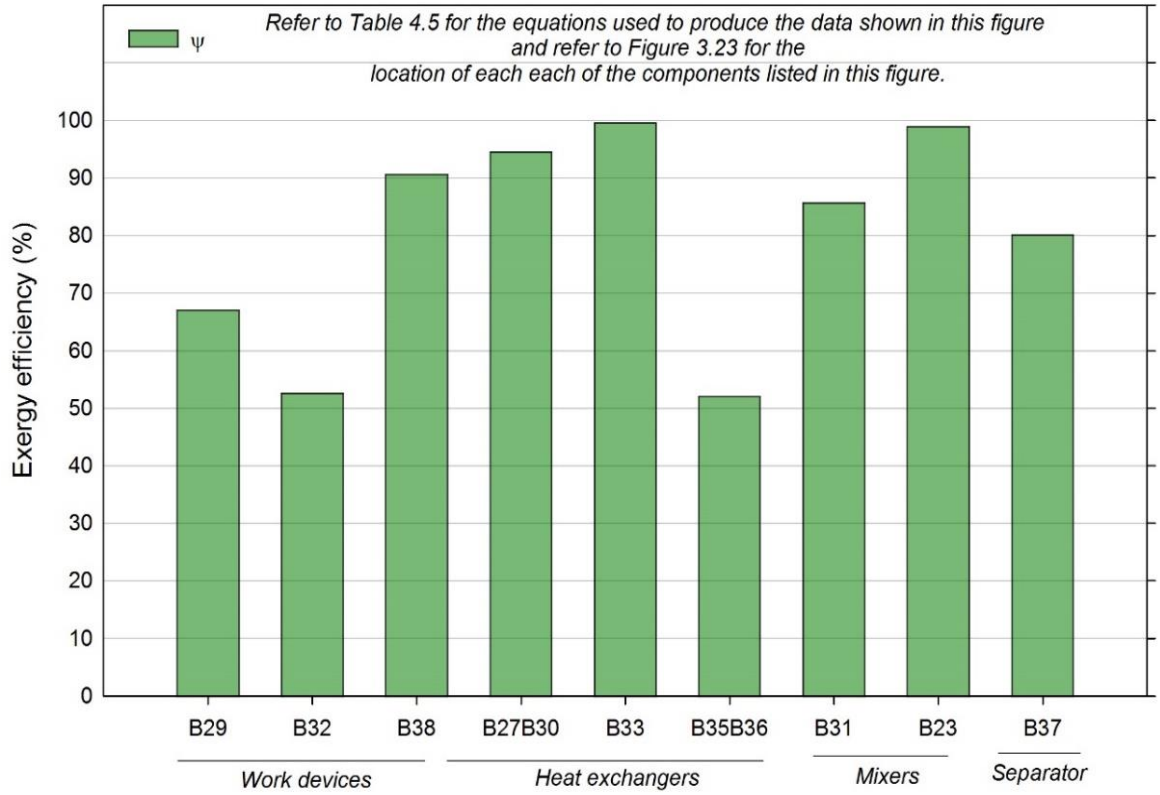

Figure 5.33 The exergy efficiency of the components of the PSR in System 4.

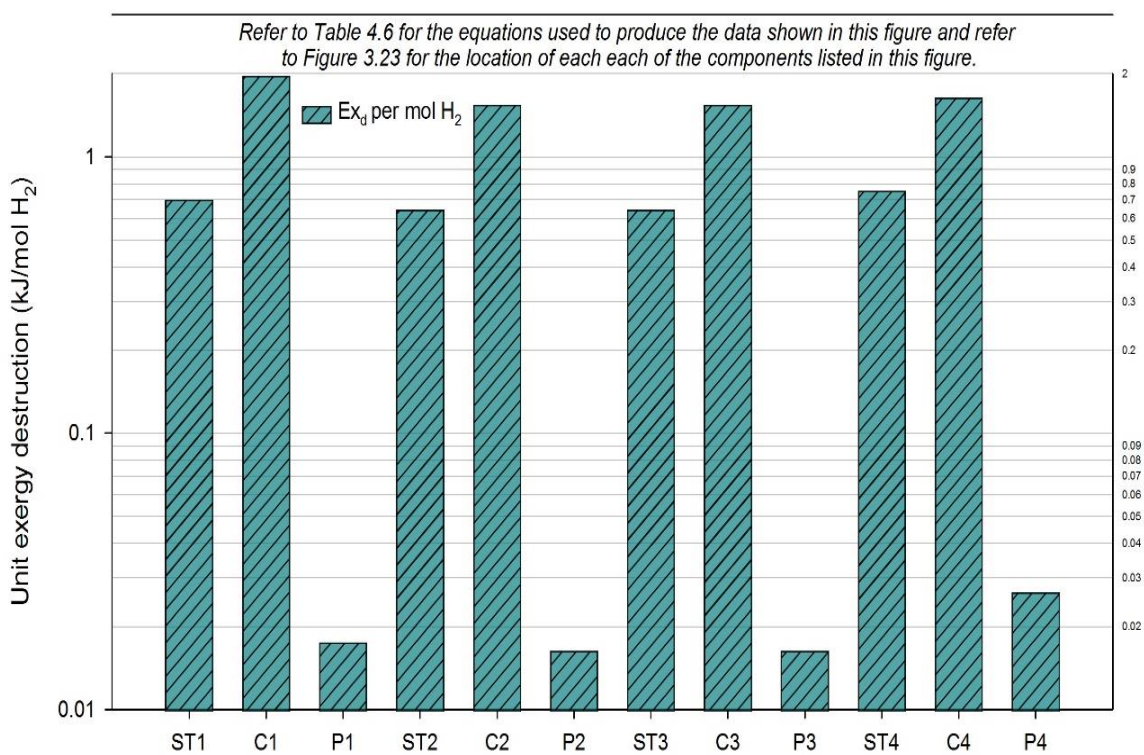

Figure 5.34 The unit exergy destruction of the work producing and consuming components in the HCS in System 4.

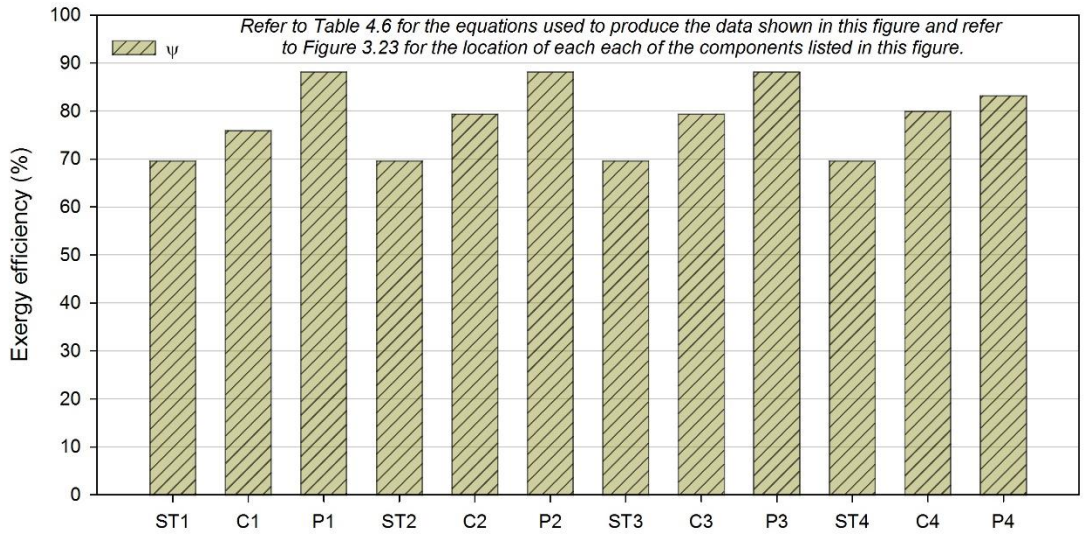

Figure 5.35 The exergy efficiency of the work producing and consuming components in the HCS in System 4.

The exergy efficiency and the unit exergy destruction rate of the work producing and consuming components in the HCS are shown in Figures 5.34 and 5.35. This is because it starts compressing the hydrogen from the dead state conditions, which means that the total exergy input to the compressor is just the work rather than having two exergy inputs, since the physical exergy of hydrogen at the dead state conditions is equal to zero.

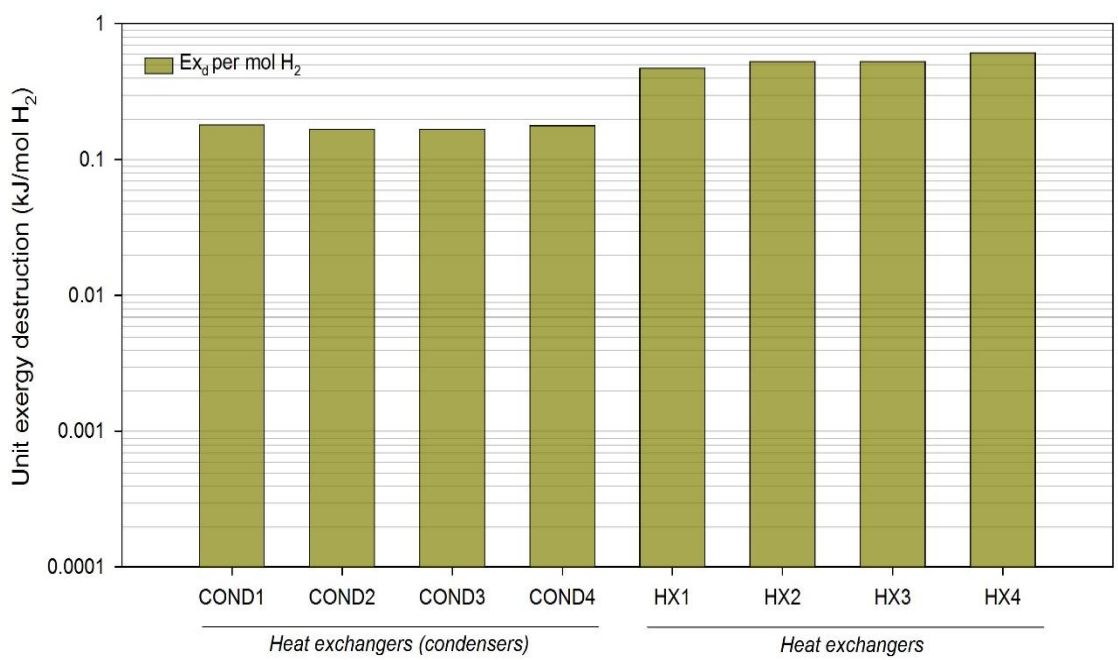

Figure 5.36 The unit exergy destruction of the condensers and heat exchangers in the HCS in System 4.

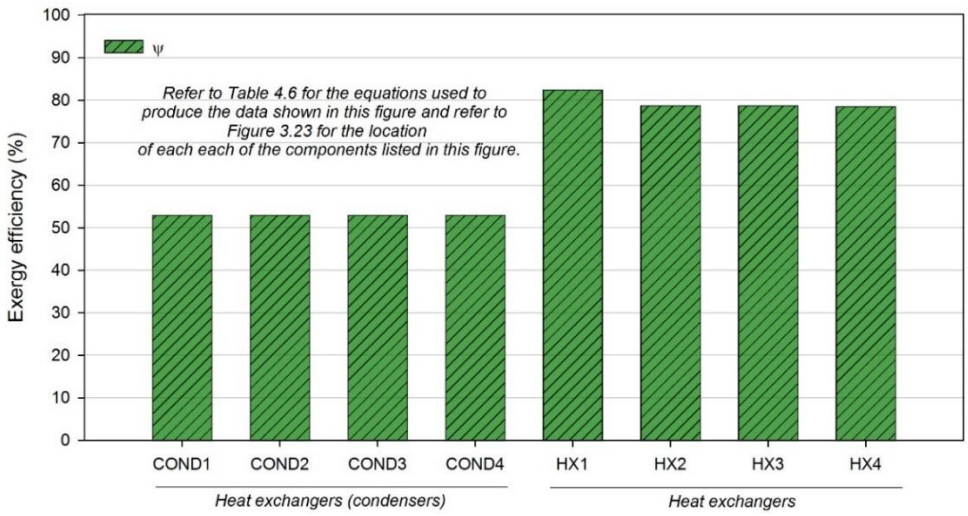

Figure 5.37 The exergy efficiency of the condensers and heat exchangers in the HCS in System 4.

The exergy efficiencies and the unit exergy destruction of the heat exchangers and the condensers in the HCS system are shown in Figures 5.36 and 5.37. The unit exergy destruction of the main three subsystems are shown in Figure 5.38, where the subsystem with the greatest unit exergy destruction rate in the integrated system is seen to be the PSR. Figure 5.39 shows the comparison of the resulting energy and exergy efficiencies of the proposed System 4, the two cases of the proposed System 2 and Ozcan and Dincer [42] proposed nuclear-based integrated system.

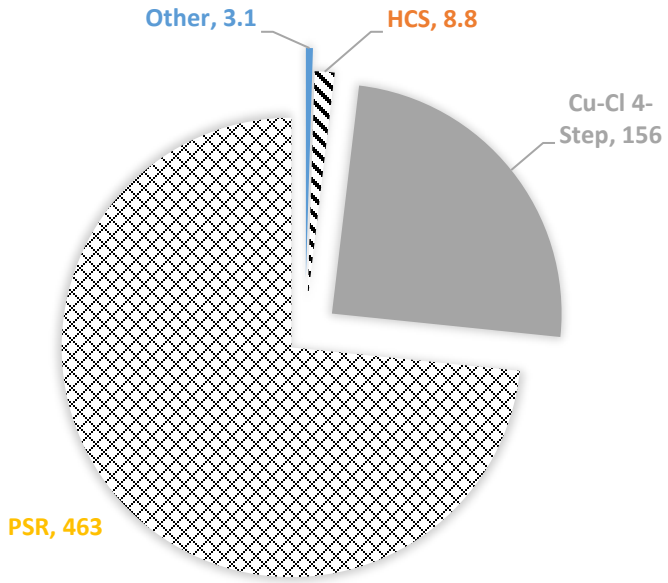

Figure 5.38 The unit exergy destruction of the main subsystems in the nuclear-based integrated system (kW/mol H_2).

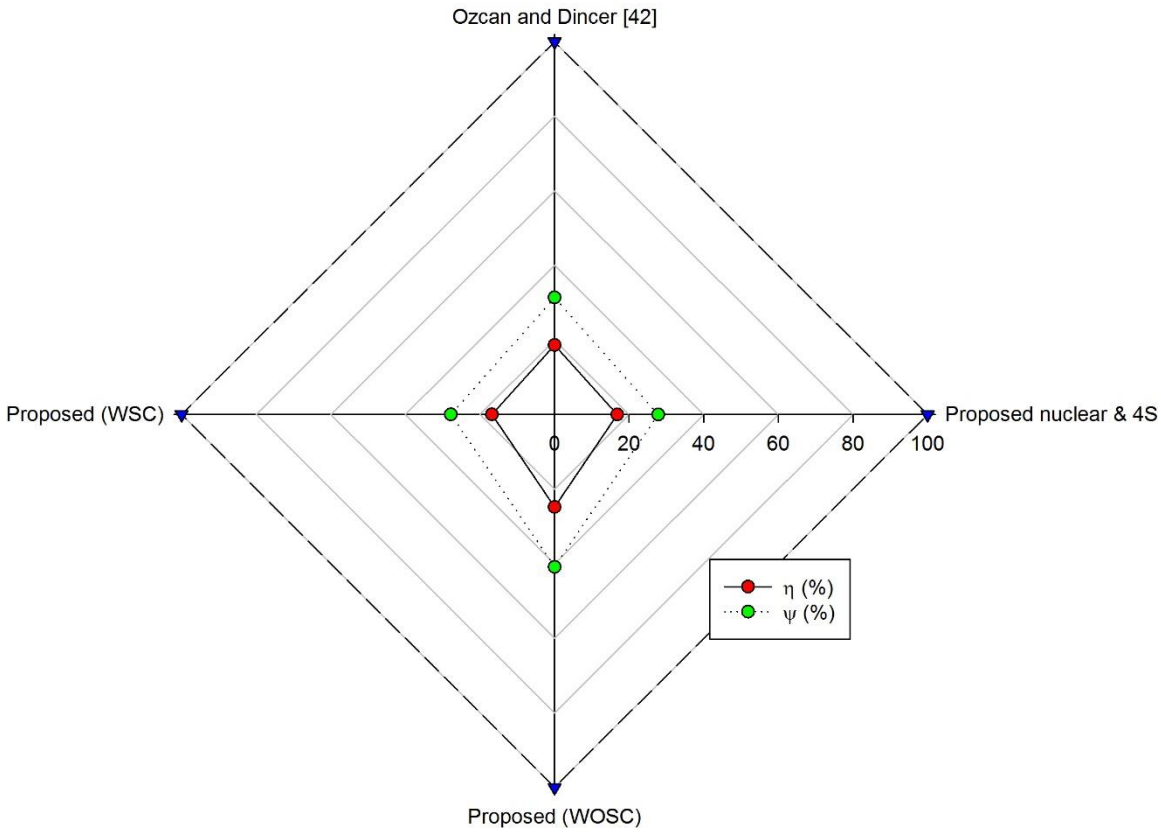

Figure 5.39 The energy and exergy efficiencies of the proposed nuclear-based System 4 with literature nuclear-based system and the two cases of the nuclear-based System 2.

5.5 Systems Comparison

After proposing four different hydrogen and power production plants that utilize the hybrid thermochemical and electrical water decomposition cycle that uses the copper and chlorine compounds. They will be compared based on the energy and exergy efficiencies. Figure 5.40 shows the energy efficiency for each of the four concepts for hydrogen and power production plants. The concept with the highest energy efficiency is the coal-based concept, which is because large portion of the produced hydrogen is from the gasification of coal (removing hydrogen from the coal) and the gasification system already have high energy efficiency. Figure 5.41 shows the exergy efficiency of the four hydrogen and power production systems plant concepts. The highest exergy efficiency goes to the nuclear-based concept with the four-step Cu-Cl cycle. The steam circuit design used in the fourth concept has a proven to better than the design used in concept 2. Concept 4 produces power from the supporting Rankine cycle that is also integrated in the steam circuit unlike what is

happening in concept 2 where the power produced from hydrogen fueled combined cycle. Concept 3 uses a supporting Rankine cycle but it is standalone not integrated in the steam circuit. The system with the lowest exergy destruction per each kg of hydrogen produced is System 1 (coal-based system), due to its high exergy efficiency. Although System 4 had a higher exergy efficiency than System 1, but the exergy input to System 4 is higher than the exergy content of coal which explains why System 4 has higher exergy destruction per each kg of hydrogen produced as shown in Figure 5.42.

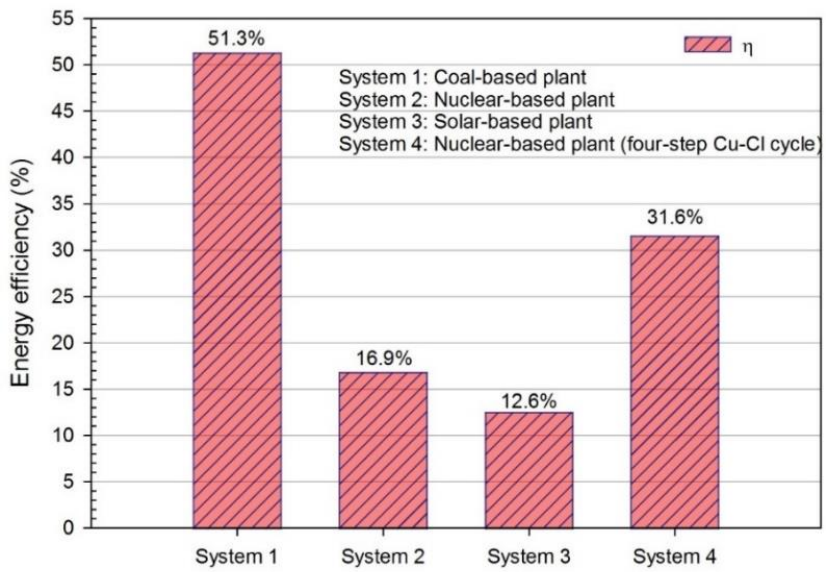

Figure 5.40 The energy efficiency of the four hydrogen and power production systems.

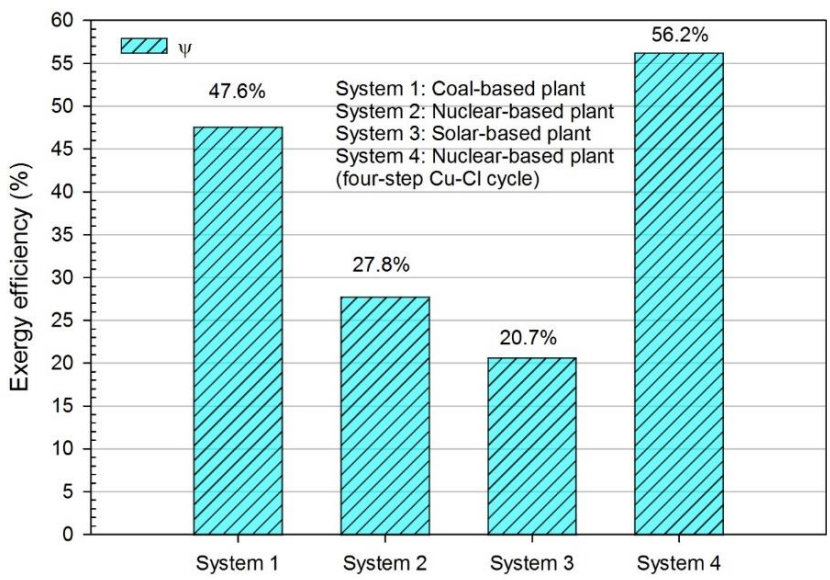

Figure 5.41 The exergy efficiency of the four proposed hydrogen and power production systems.

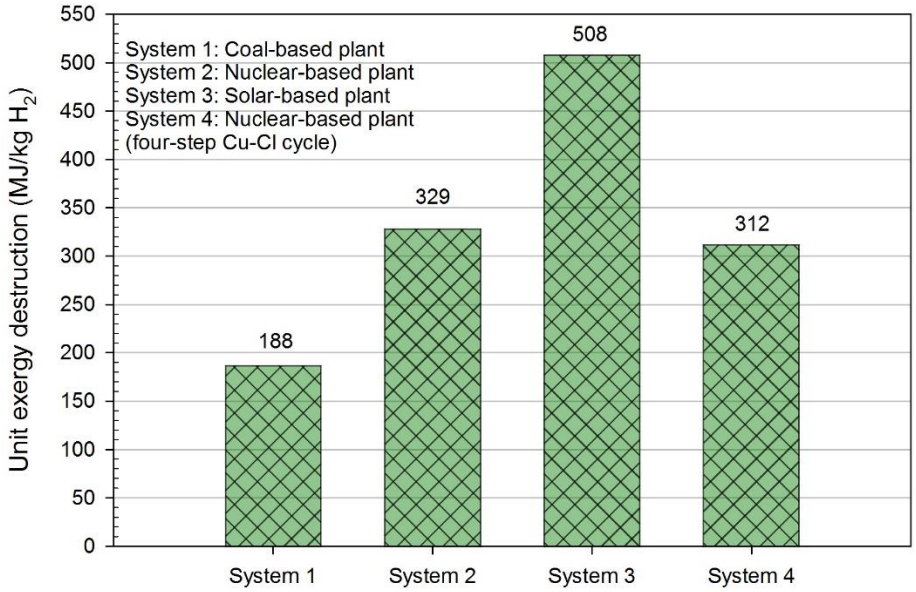

Figure 5.42 The associated exergy destruction per each kg of hydrogen produced for each of the four proposed hydrogen and power production plants.

Shown in Figure 5.43 a comparison between the two nuclear-based proposed systems, System 2 and 4. System 2 produce electrical power only to fulfil the system power requirements. However, System 4 produces large amount of power of 552 MW.

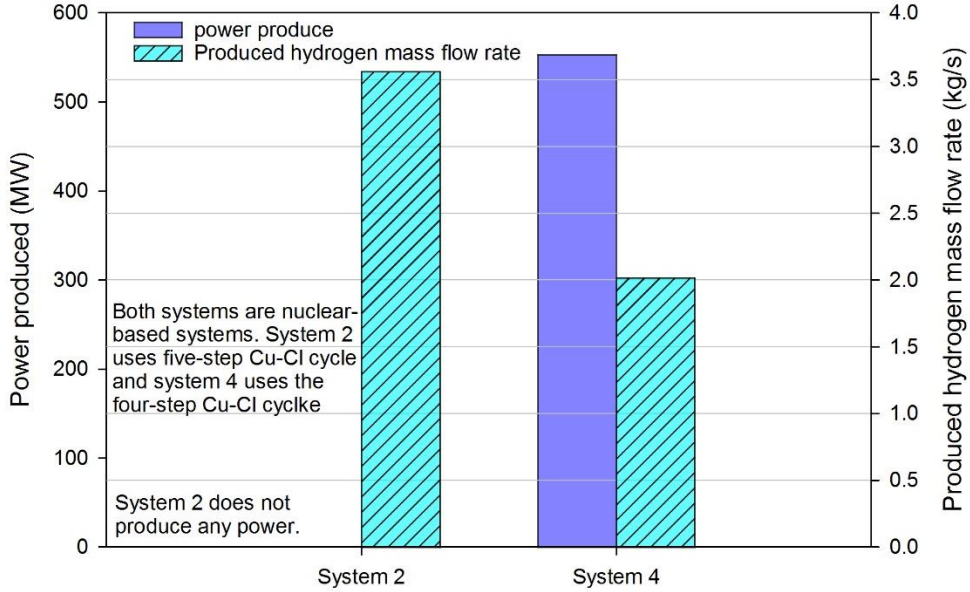

Figure 5.43 The power and hydrogen production rates of the two nuclear-based systems.

The four systems that are proposed produce both hydrogen and power. Figures 5.44-5.46 show the effect of varying the amount of power produced by the system on the hydrogen production rate, energy efficiency, exergy efficiency and the exergy destruction

rate, except for System 1 since the power produced by System 1 depends on the main system parameters and to change it some of the main parameters have to be changed. Resulting in a new system conceptual design. As shown in Figures 5.44 to 5.46 as the power production of the system increases the energy and exergy efficiencies decreases except for System 4. System 4 has the best thermal energy management system compared to the other three proposed systems since it recovers thermal energy from the Cu-Cl cycle that systems 2 and 3 wastes. Also the power production cycle has an energy efficiency close to that of the Cu-Cl cycle and since the hydrogen produced by the Cu-Cl cycle needs to be compressed, then for the case of System 4 as the power production rate increases the energy and exergy efficiencies increase. Shown in Figure 5.46 as the power produced by the integrated system increases the energy and the exergy efficiencies increases. However, the hydrogen production rate decreases, which is due to the conservation of energy. The exergy destruction rate of the integrated system decreases with more power because less hydrogen is produced which translate to less power goes to the compression system which will results in decrease in the overall energy and exergy efficiencies.

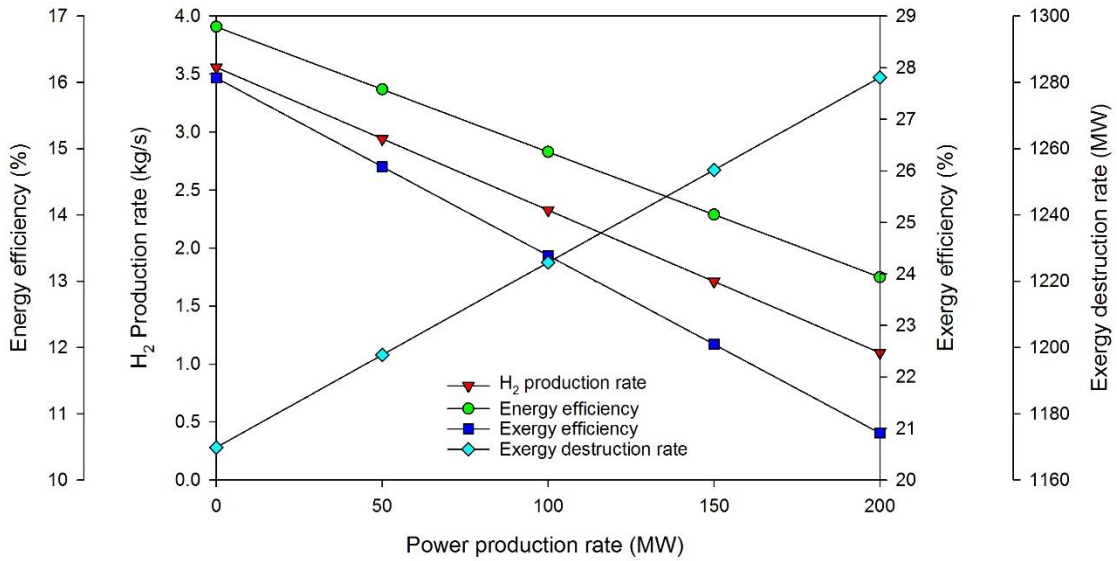

Figure 5.44 The effect of varying the amount of power produced by System 2 (nuclear-based) on the energy efficiency, hydrogen production rate, exergy efficiency and the exergy destruction rate.

Figure 5.47 shows the change in the exergy efficiency of each of the proposed integrated systems with the variation of the ambient temperature. As the ambient temperature increases the exergy efficiency increase for all of the four systems.

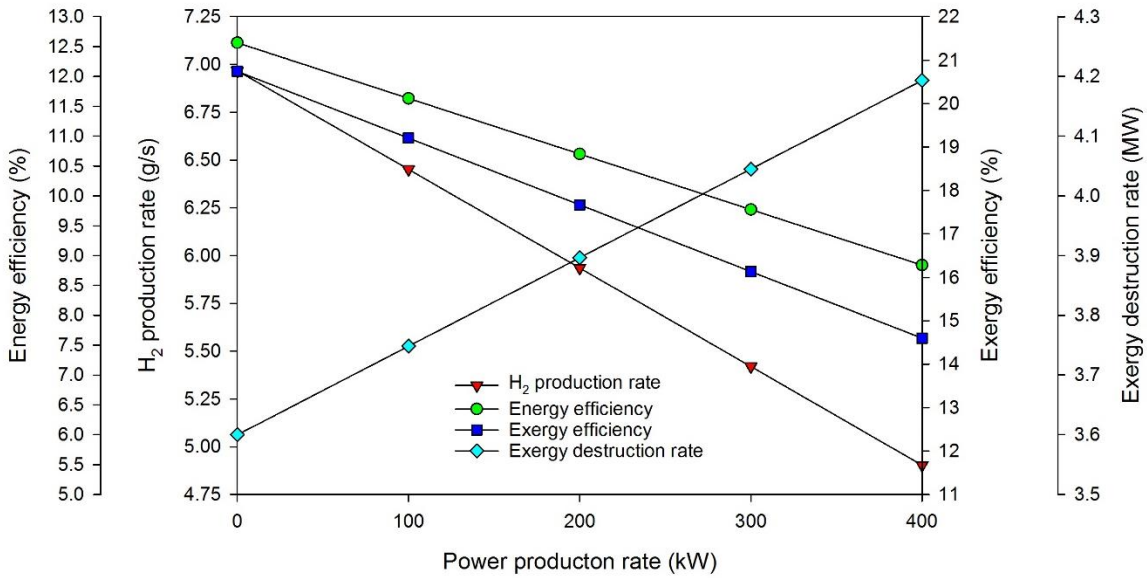

Figure 5.45 The effect of varying the amount of power produced by System 3 (solar-based) on the energy efficiency, hydrogen production rate, exergy efficiency and the exergy destruction rate.

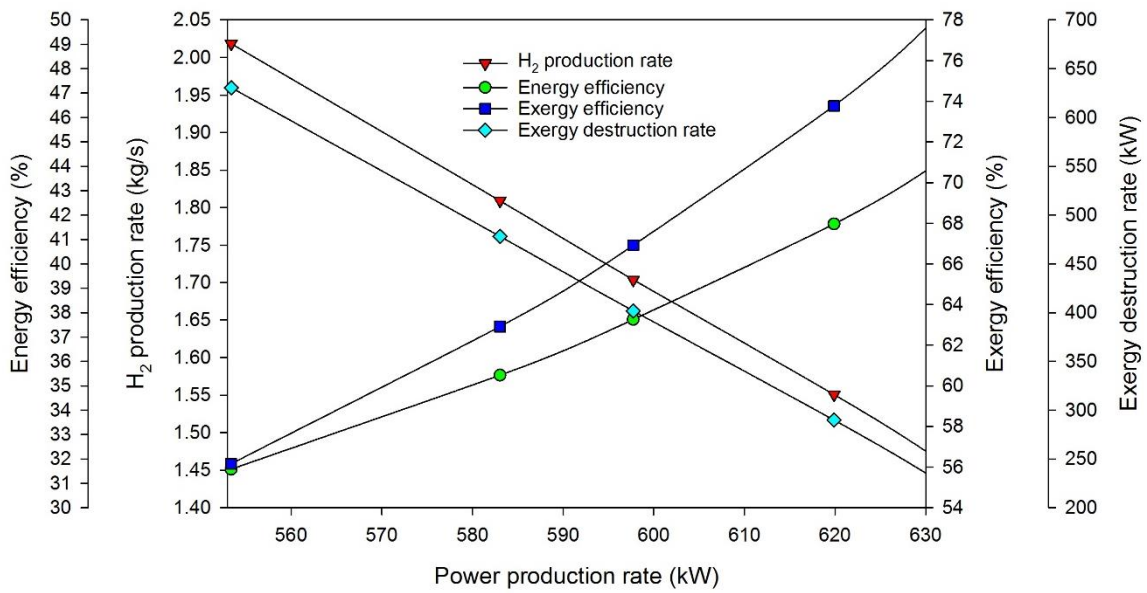

Figure 5.46 The effect of varying the amount of power produced by System 4 (nuclear-based) on the energy efficiency, hydrogen production rate, exergy efficiency and the exergy destruction rate.

The increase in the exergy efficiency with the increase of the ambient temperature is because as the ambient temperature increases the quality (the exergy content) of the dumped streams decreases resulting in more utilization of the capabilities of the systems. The exergy destructions per each kg of hydrogen produced by each of the systems are

shown in Figure 5.48. The increase in the exergy efficiency results in decrease in the exergy destruction.

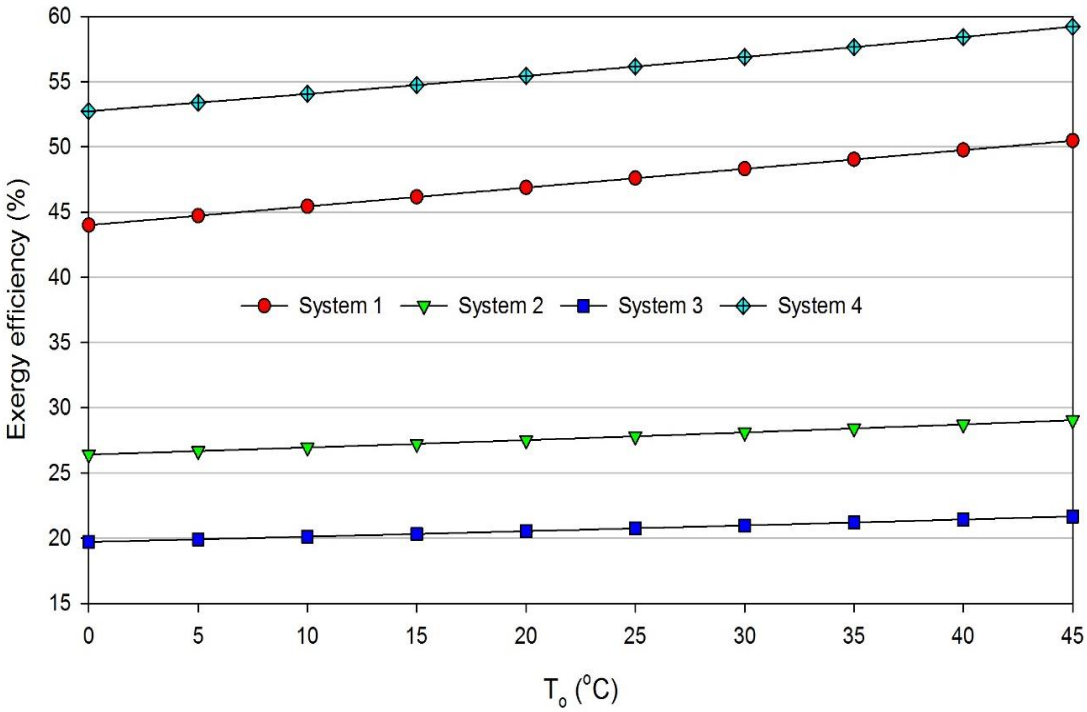

Figure 5.47 The variation of the exergy efficiency of the four systems with the variation of ambient temperature.

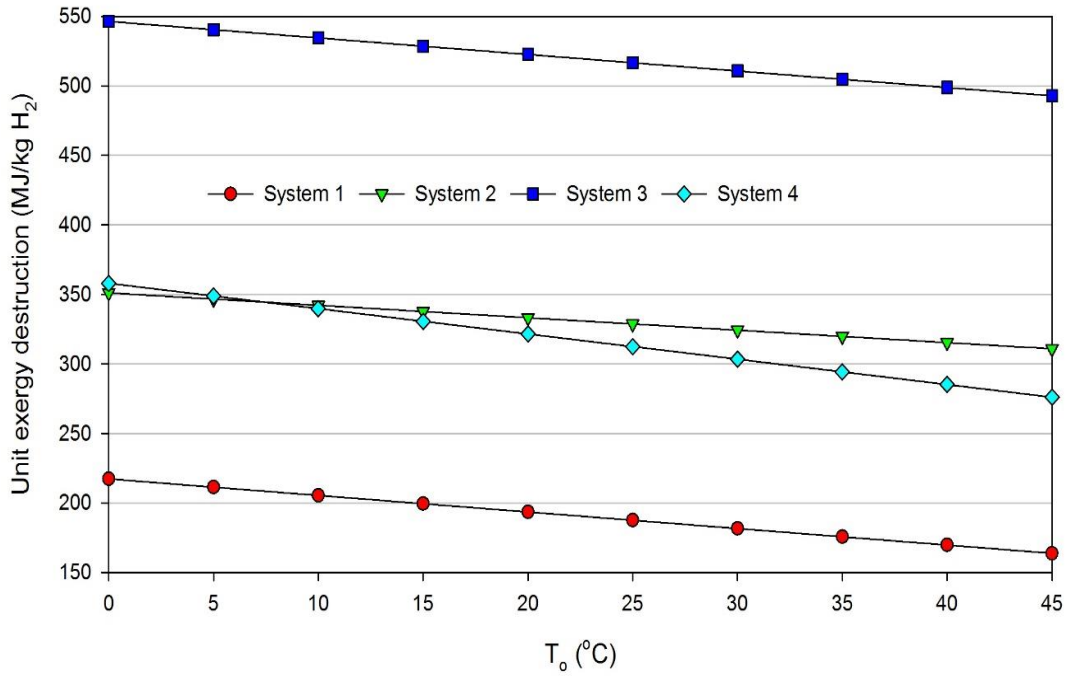

Figure 5.48 The variation of the exergy destruction per each kg produced for each of the four systems with the variation of ambient temperature.

5.5.1 Simplified Greenization Factor

Another comparison between the four systems is done based on the greenization factor, which present the factor of how much CO_2 emissions are reduced based on a reference system. Note that the greenization factor (GF) [88] calculated in this comparison is based on the operating CO_2 emitted during the operation only not considering the maintenance, manufacturing, installation and transportation. The factors not considered in the greenization analysis in this section can be the subject of further analysis of future work through life cycle assessment.

$$\mathrm{GF} = \frac{\dot{m}_{CO_2,ref} - \dot{m}_{CO_2,Sys_i}}{\dot{m}_{CO_2,ref}} \tag{5.1}$$

The results of the greenization factor analysis are presented in Table 5.5.

Table 5.5: The greenization factor of the four systems considered in this thesis. (the reference mass flow rate produced by the system per each kg of hydrogen produced per second is that produced by System 1).

System	Greenization factor
System 1	0
System 2	1
System 3	1
System 4	1

Presented by Table 5.5 systems 3,4 and 5 has a GF of 1 which is very high, and the reason for that is not considering the other factors mentioned earlier in this subsection. It is recommended to perform more detailed GF calculations by considering the other factors.

Chapter 6: Conclusions and Recommendations

In this chapter the main findings of the analysis of the developed systems are presented, followed by qualitative conclusions derived from the main findings. At the end of this chapter a group of recommendations are suggested to continue the research further.

6.1 Conclusions

Current power production plants are modified and integrated with other systems to produce hydrogen, to show the real potential of these plants to operate in a more environmentally benign manner. Systems such as these provide a way to adapt to a cleaner global energy infrastructure, while still recognizing the need to meet energy demands feasibly. This research developed and assessed the performance of four proposed hydrogen production plants from various sources of energy, all of which utilizes the Cu-Cl cycle. All of the four proposed systems were simulated using Aspen Plus process modeling software and EES. The performance assessment of the proposed systems was based on the energy and exergy efficiencies. The results show that the integration of nuclear reactor SCWR with the four step copper and chlorine cycle is a promising integration in terms of energy and exergy efficiencies. Regarding the coal gasification based system, it is suggested that a new air separation technology to be used in the place of the cryogenic air separation unit. The analysis shows that the Cu-Cl cycle is a flexible system that can be connected to different steam producing systems. Hybrid thermochemical decomposition of the water is a promising technology that can be integrated with different sources of energies varying from fossil fuels to the advanced fourth generation nuclear reactors.

An important factor that can affect the selection of the system is the availability of the main energy source. The technologies for harvesting the energy from the nuclear material is not available for all countries, which in turn can be a determining factor in the selection of the hydrogen and power production plant.

The main findings of the thesis research are presented as follows:

- The overall energy and exergy efficiencies of System 1 are 51.3% and 47.6%, respectively.

- System 1 has the capacity to produce 1 kg/s of compressed hydrogen at 700 bar and 4.64 MW of work rate per 8.95 kg/s of Illinois No.6 coal.
- The energy efficiency of System 2 is 16.8% (while the steam circuit is considered).
- The exergy efficiency of System 2 is 27.8% (while the steam circuit is considered).
- System 2 has a hydrogen production rate of 3.56 kg/s.
- The energy and exergy efficiencies of the hydrogen compression system in System 2 are 14.7% and 36.1%, respectively.
- The energy and exergy efficiencies of the supporting Rankine cycle in System 2 are 39.7% and 40.4%, respectively.
- The overall energy and exergy efficiencies of System 3 are 12.6% and 20.7%, respectively.
- System 3 was able to produce 4.97 g/s of compressed hydrogen at 700 bar and 78.0 kW of work rate at a solar intensity of 800 W/m^2.
- The energy and the exergy efficiencies of System 4 are 31.6% and 56.2%, respectively.
- System 4 was able to produce 2.02 kg/s of highly compressed hydrogen at 700 bar, and 553 MW of power.
- The subsystem that destroys the most exergy in System 4 is the power supporting Rankine cycle of 463 kW/mol H_2.

6.2 Recommendations

Hydrogen production plants (four design concepts) were proposed in this thesis. The four proposed hydrogen production plants were thermodynamically designed, modeled and analyzed. These four systems were able to prove that a hybrid thermochemical water decomposition cycle that is based on a copper chlorine cycle is a promising candidate for replacing the usual Rankine cycle. A group of recommendations are presented for further studies and experimental investigation. These recommendations are as follows:

- Systems that integrate a hybrid thermochemical water decomposition cycle utilizing the chemical couple copper and chlorine may consider the method of delivering the heat or recovering the heat to and from the cycle in their energy and exergy analysis.

- In all four systems the power supporting system have the largest share in the system overall exergy destruction. It is recommended that future work should test whether sending all the thermal energy from the solar system to the Cu-Cl cycle and then producing electricity by sending the required fraction of the hydrogen produced to a fuel cell, compared to the current system, has higher energy efficiency.
- Future work in thermal systems integration can include the hybrid thermochemical water decomposition cycle that is based on the Cu-Cl compounds and utilize the wasted heat by upgrading it with the a heat pump.
- Further studies on replacing the power supporting Rankine cycle with a more efficient system should be investigated. A good replacement for the power supporting Rankine cycle is a solid oxide fuel cell, where most of the thermal power received from the nuclear reactor goes to the hybrid thermochemical and electrical water decomposition reactor while part of the produced hydrogen goes to the solid oxide fuel cell that is also heated by the nuclear thermal energy.
- Further studies should conduct more than one energy source integrated with the Cu-Cl cycle and other supporting systems.
- Using nuclear-based power and hydorgen produciotn systems will save the enviroment large mass of emitted CO_2. Further studies can be conducted for different schemes to get the best possible results for the nuclear-based system and report how much CO_2 will be saved by their schemes.
- The sustainability of the proposed systems should be the subject of further research to provide another performance measure for the systems other than energy and exergy efficiencies that were considered in this thesis.
- Economic analysis of the proposed system should be the subject of further research providing another valuable assessing factor.
- Further studies should consider replacing the subsystems with other technologies that can provide the same function, and check the effect of such activity on the overall energy and exergy efficiencies of the system.

References

[1] Dincer I, Rosen MA. Thermal energy storage systems and applications. Wiley; 2003.

[2] Muradov NZ, Veziroglu TN. “Green” path from fossil-based to hydrogen economy: An overview of carbon-neutral technologies. International Journal of Hydrogen Energy 2008;33:6804–6839..

[3] Miller BG. Coal Energy Systems. Elsevier; 2005.

[4] Han W, Hongguang J, Jianfeng S, Rumou L, Zhifeng W. Design of the First Chinese 1 MW Solar-Power Tower Demonstration Plant. International Journal of Green Energy 2009;6:414–425.

[5] Maurer C, Cappel C, Kuhn TE. Methodology and First Results of an R&D Road Map for Facade-integrated Solar Thermal Systems. Energy Procedia 2015;70:704–708.

[6] Giovanardi A, Passera A, Zottele F, Lollini R. Integrated solar thermal facade system for building retrofit. Solar Energy 2015;122:1100–16.

[7] Ha SH, Yu HW, Jang NS, Kim JH, Kim SH, Kim JM. Compact and high-power dye-sensitized solar system integrated with low-cost solar-concentrating polymer lens. Solar Energy Materials and Solar Cells 2016;155:362–7.

[8] Sprenger W, Wilson HR, Kuhn TE. Electricity yield simulation for the building-integrated photovoltaic system installed in the main building roof of the Fraunhofer Institute for Solar Energy Systems ISE. Solar Energy 2016;135:633–643.

[9] Boggs BK, Botte GG. On-board hydrogen storage and production: An application of ammonia electrolysis. Journal of Power Sources 2009;192:573–581.

[10] Aghahosseini S, Dincer I, Naterer GF. Integrated gasification and Cu-Cl cycle for trigeneration of hydrogen, steam and electricity. International Journal of Hydrogen Energy 2011;36:2845–54.

[11] Dincer I, Balta MT. Potential thermochemical and hybrid cycles for nuclear-based hydrogen production. International Journal of Energy Research 2011;35:123–137.

[12] Wang Z, Naterer GF, Gabriel K. Multiphase reactor scale-up for Cu-Cl thermochemical hydrogen production. International Journal of Hydrogen Energy 2008;33:6934–46.

[13] Naterer GF, Gabriel K, Wang ZL, Daggupati VN, Gravelsins R. Thermochemical hydrogen production with a copper-chlorine cycle. I: oxygen release from copper oxychloride decomposition. International Journal of Hydrogen Energy 2008;33:5439–50.

[14] Naterer GF, Dincer I, Zamfirescu C. Hydrogen Production from Nuclear Energy. Springer; 2013.

[15] Naterer GF, Dincer I, Zamfirescu C. Thermochemical Water-Splitting Cycles. Hydrogen Production from Nuclear Energy, Springer; 2013, p. 153–272.

[16] Naterer G, Suppiah S, Lewis M, Gabriel K, Dincer I, Rosen MA, Fowler M, Rizvi G, Easton EB, Ikeda BM, Kaye MH, Lu L, Pioro I, Spekkens P, Tremaine P, Mostaghimi J, Avsec J, Jiang J. Recent Canadian advances in nuclear-based hydrogen production and the thermochemical Cu-Cl cycle. International Journal of Hydrogen Energy 2009;34:2901–2917.

[17] Zamfirescu C, Dincer I, Naterer GF. Thermophysical properties of copper compounds in copper-chlorine thermochemical water splitting cycles. International Journal of Hydrogen Energy 2010;35:4839–4852.

[18] Dincer I, Naterer GF. Overview of hydrogen production research in the Clean Energy Research Laboratory (CERL) at UOIT. International Journal of Hydrogen Energy 2014;39:20592–20613.

[19] Pope K, Wang Z, Naterer GF. Process integration of material flows of copper chlorides in the thermochemical Cu–Cl cycle. Chemical Engineering Research and Design 2016;109:273–281.

[20] Orhan MF, Dincer I, Rosen MA. Efficiency analysis of a hybrid copper-chlorine (Cu-Cl) cycle for nuclear-based hydrogen production. Chemical Engineering Journal 2009;155:132–137.

[21] Ozbilen A, Dincer I, Rosen MA. Development of a four-step Cu–Cl cycle for hydrogen production – Part II: Multi-objective optimization. International Journal of Hydrogen Energy 2016;41:7826–7834.

[22] Orhan MF, Dincer I, Rosen MA. Simulation and exergy analysis of a copper–chlorine thermochemical water decomposition cycle for hydrogen production. Progress in Exergy, Energy, and the Environment 2014:121–132.

[23] Fan J, Zhu L. Performance analysis of a feasible technology for power and high-purity hydrogen production driven by methane fuel. Applied Thermal Engineering 2015;75:103–114.

[24] Ongena J, Van Oost G. Energy for future centuries-Prospects for fusion power as a future energy source. Fusion Sci Technol 2008;53:3–15.

[25] Ponomarev-Stepnoi NN. Nuclear-Hydrogen Power. Atomic Energy 2004;96:375–385.

[26] Honda Worldwide, Products and Technology, Home Energy Station. http://world.honda.com/FuelCell/HomeEnergyStation/HomeEnergyStation2004/ (accessed September 5, 2016).

[27] Jordal K., Anantharaman R., Peters T. A., Berstad D., Morud J., Neksa P., and Bredesen R., High-purity H_2 production with CO_2 capture based on coal gasification. Energy 2015;88:9–17.

[28] Giuffrida A, Romano MC, Lozza G. Thermodynamic analysis of air-blown

gasification for IGCC applications. Applied Energy 2011;88:3949–3958.

[29] Gnanapragasam N V., Reddy B V., Rosen MA. Hydrogen production from coal gasification for effective downstream CO2 capture. International Journal of Hydrogen Energy 2010;35:4933–4943.

[30] Seyitoglu SS, Dincer I, Kilicarslan A. Assessment of an IGCC based trigeneration system for power, hydrogen and synthesis fuel production. International Journal of Hydrogen Energy 2015;41:1–8.

[31] Ozturk M, Dincer I. Thermodynamic assessment of an integrated solar power tower and coal gasification system for multi-generation purposes. Energy Conversion and Management 2013;76:1061–1072.

[32] Zhu L, Zhang Z, Fan J, Jiang P. Polygeneration of hydrogen and power based on coal gasification integrated with a dual chemical looping process: Thermodynamic investigation. Computers & Chemical Engineering 2016;84:302–312.

[33] Liszka M, Malik T, Manfrida G. Energy and exergy analysis of hydrogen-oriented coal gasification with CO_2 capture. Energy 2012;45:142–150.

[34] Cohce MK, Dincer I, Rosen MA. Thermodynamic analysis of hydrogen production from biomass gasification. International Journal of Hydrogen Energy 2010;35:4970–4980.

[35] Bicer Y, Dincer I. Development of a multigeneration system with underground coal gasification integrated to bitumen extraction applications for oil sands. Energy Conversion and Management 2015;106:235–248.

[36] Bicer Y, Dincer I. Energy and exergy analyses of an integrated underground coal gasification with SOFC fuel cell system for multigeneration including hydrogen production. International Journal of Hydrogen Energy 2015;40:13323–37. doi:10.1016/j.ijhydene.2015.08.023.

[37] Ratlamwala TAH, Dincer I. Energy and exergy analyses of a Cu–Cl cycle based integrated system for hydrogen production. Chemical Engineering Science 2012;84:564–573.

[38] Gokon N, Murayama H, Nagasaki A, Kodama T. Thermochemical two-step water splitting cycles by monoclinic ZrO_2-supported $NiFe_2O_4$ and Fe_3O_4 powders and ceramic foam devices. Solar Energy 2009;83:527–537.

[39] Ozbilen A, Dincer I, Rosen MA. Development of a four-step Cu–Cl cycle for hydrogen production – Part I: Exergoeconomic and exergoenvironmental analyses. International Journal of Hydrogen Energy 2016;41:7814–7825.

[40] Orhan MF, Dincer I, Rosen MA. Efficiency comparison of various design schemes for copper-chlorine (Cu-Cl) hydrogen production processes using Aspen Plus software. Energy Conversion and Management 2012;63:70–86.

[41] Ratlamwala TAH, Dincer I. Comparative energy and exergy analyses of two solar-based integrated hydrogen production systems. International Journal of Hydrogen

Energy 2015;40:7568–78.

[42] Toyota Canada: Toyota to Increase "Mirai" Production 2014. http://www.toyota.ca/toyota/en/company-info/news/post/toyota-to-increase-mirai-production (accessed September 13, 2016).

[43] Ratlamwala TAH, Dincer I. Performance assessment of solar-based integrated Cu-Cl systems for hydrogen production. Solar Energy 2013;95:345–356.

[44] Ratlamwala TAH, Dincer I. Experimental study of a hybrid photocatalytic hydrogen production reactor for Cu-Cl cycle. International Journal of Hydrogen Energy 2014;39:20744–20753.

[45] Duffey RB, and Pioro IL. Supercritical Water-Cooled Nuclear Reactors: Review and Status. Nuclear Energy Materials and Reactors. In: Nuclear Materials and Reactors from Encyclopedia of Life Support Systems (EOLSS), developed under the Auspices of the UNESCO, EOLSS Publishers, Oxford, 2005.

[46] Orhan MF. Conceptual design, analysis and optimization of nuclear-based hydrogen production via copper-chlorine thermochemical cycles. Doctoral dissertation, Faculty of Engineering and Applied Science, Mechanical Engineering Program. University of Ontario Institute of Technology, Oshawa, Canada, April 2011.

[47] Esmaili P, Dincer I, Naterer GF. Development and analysis of an integrated photovoltaic system for hydrogen and methanol production. International Journal of Hydrogen Energy 2014;40:11140–11153.

[48] Dinçer I, Zamfirescu C. Sustainable hydrogen production. Elsevier; 2016.

[49] Naterer GF, Dincer I, Zamfirescu C. Hydrogen as a Clean Energy Carrier. Hydrogen Production from Nuclear Energy, Springer; 2013, p. 1–20.

[50] Naterer GF, Dincer I, Zamfirescu C. Water Electrolysis. Hydrogen Production from Nuclear Energy,Springer; 2013, p. 99–152.

[51] Ozcan H, Dincer I. Modeling of a new four-step magnesium-chlorine cycle with dry HCl capture for more efficient hydrogen production. International Journal of Hydrogen Energy 2016;41:7792–7801.

[52] Ozcan H, Dincer I. Performance investigation of magnesiumechloride hybrid thermochemical cycle for hydrogen production. International Journal of Hydrogen Energy 2014;39:76–85.

[53] Ozcan H, Dincer I. Thermodynamic modeling of a nuclear energy based integrated system for hydrogen production and liquefaction. Computers and Chemical Engineering 2016;90:234–46.

[54] Ozcan H, Dincer I. Exergoeconomic optimization of a new four-step magnesium-chlorine cycle. International Journal of Hydrogen Energy 2016. doi:10.1016/j.ijhydene.2016.03.098.

[55] Orhan MF, Dincer I, Rosen MA. Energy and exergy assessments of the hydrogen

production step of a copper–chlorine thermochemical water splitting cycle driven by nuclear-based heat. International Journal of Hydrogen Energy 2008;33:6456–6466.

[56] Orhan MF, Dincer I, Rosen MA. Exergoeconomic analysis of a thermochemical copper–chlorine cycle for hydrogen production using specific exergy cost (SPECO) method. Thermochimica Acta 2010;497:60–66.

[57] Orhan MF, Dincer I, Rosen MA. Design and simulation of a UOIT copper-chlorine cycle for hydrogen production. International Journal of Energy Research 2013;37:1160–1174.

[58] Ozbilen A, Dincer I, Rosen MA. Development of new heat exchanger network designs for a four-step CueCl cycle for hydrogen production 2014.

[59] Ferrandon MS, Lewis M, Tatterson DF, Nankani RV, Kumar M, Wedgewood L, Nitsche LC. The hybrid Cu–Cl thermochemical cycle. I. Conceptual process design and H2A cost analysis. II. Limiting the formation of CuCl during hydrolysis. In: NHA Annual Hydrogen Conference 2008: p. 1–20.

[60] Wu W, and Felicia W. Heat integration of a hydrogen production system with simplistic copper-chlorine (Cu-Cl) thermochemical cycle. In: 5th International Symposium on Advanced Control of Industrial Processes 2014:143-146.

[61] Ferrandon MS, Lewis MA, Alvarez F, Shafirovich E. Hydrolysis of $CuCl_2$ in the Cu-Cl thermochemical cycle for hydrogen production: Experimental studies using a spray reactor with an ultrasonic atomizer. International Journal of Hydrogen Energy 2010;35:1895–904.

[62] Naterer GF, Suppiah S, Stolberg L, Lewis M, Wang Z, Dincer I, Rosen MA, Gabriel K, Secnik E, Easton EB, Pioro I, Lvov S, Jiang J, Mostaghimi J, Ikeda BM, Rizvi G, Lu L, Odukoya A, Spekkens P, Fowler M, Avsec J. Progress of international hydrogen production network for the thermochemical Cu-Cl cycle. International Journal of Hydrogen Energy 2013;38:740–759.

[63] Orhan MF, Dincer I, Rosen MA. The oxygen production step of a copper–chlorine thermochemical water decomposition cycle for hydrogen production: Energy and exergy analyses. Chemical Engineering Science 2009;64:860–9.

[64] Dincer I, Ratlamwala TAH. Development of novel renewable energy based hydrogen production systems: A comparative study. Energy Conversion and Management 2013;72:77–87.

[65] Orhan MF, Dincer I, Rosen MA, Kanoglu M. Integrated hydrogen production options based on renewable and nuclear energy sources. Renewable and Sustainable Energy Reviews 2012;16:6059–82..

[66] The Monthly Energy Review. U.S. Energy Information Administration. April 2016. DOE/EIA-0035(2016/4).

[67] Dincer I, and Rosen MA. Exergy: Energy, Environment and Sustainable Development, 2nd edition. Elsevier; 2012.

[68] Wen CY, Chaung TZ. Entrainment Coal Gasification Modeling. Industrial Engineering Chemistry Process Design and Development 1979;18:684–695.

[69] Augustine AS, Ma YH, Kazantzis NK. High pressure palladium membrane reactor for the high temperature water-gas shift reaction. International Journal of Hydrogen Energy 2011;36:5350–60.

[70] Parry T. Thermodynamics and Magnetism of Cu_2OCl_2. Masters dissertation, Department of Chemistry and Biochemistry. Brigham Young University, Provo, Utah, December 2008.

[71] Chase Jr MW. NIST-JANAF Thermochemical Tables. In: Journal of Physics and Chemistry Reference Data, 4th ed., Monograph 9; 1998.

[72] Knacke O, Kubaschewski O, Hesselmann K. Thermochemical properties of inorganic substances. Springer; 1991.

[73] Lide DR. CRC handbook of chemistry and physics: a ready-reference book of chemical and physical data. CRC Press; 2008.

[74] Perry RH, Green DW, Maloney JO. Perry's Chemical engineers' handbook. McGraw-Hill; 1984.

[75] Bushby SJ, Dimmick GR, Duffey RB, Spinks NJ, Burrill KA, and Chan PSW. Conceptual designs for advanced, high-temperature CANDU reactors. In: the 1st International Symposium on Supercritical Water-Cooled Reactor Design and Technology (SCR-2000) 2000:29-36.

[76] Nguyen-Schäfer H. Rotordynamics of Automotive Turbochargers. Springer; 2012.

[77] Greenway CSP Solar Tower n.d. http://www.greenwaycsp.com/en/field-applications/mersin-5-mwth-solar-tower-plant.aspx (accessed September 1, 2016).

[78] Xu C, Wang Z, Li X, Sun F. Energy and exergy analysis of solar power tower plants. Applied Thermal Engineering 2011;31:3904–3913.

[79] US DOE. Coal conversion systems: technical data book. Springfield, VA: NTIS 1978.

[80] Naterer GF, Dincer I, Zamfirescu C. Nuclear Energy and Its Role in Hydrogen Production. In: Hydrogen Production from Nuclear Energy. Springer; 2013, p. 21–64.

[81] Campbell JM. Gas Conditioning and Processing: The equipment modules. Campbell Petroleum Series; 1984.

[82] Li X, Kong W, Wang Z, Chang C, Bai F. Thermal model and thermodynamic performance of molten salt cavity receiver. Renewable Energy 2010;35:981–988.

[83] Yang W-C. Hydrogen-Fueled Power Systems. In: The Gas Turbine Handbook 2006;15261: p. 107–115.

[84] Demir ME, Dincer I. Development of an integrated hybrid solar thermal power system with thermoelectric generator for desalination and power production. Desalination 2017;404:59-71.

[85] Islam S, Dincer I, Yilbas BS. System development for solar energy-based hydrogen production and on-site combustion in HCCI engine for power generation. Solar Energy 2016;136:65–77.

[86] Yuksel YE, Ozturk M, Dincer I. Thermodynamic performance assessment of a novel environmentally-benign solar energy based integrated system. Energy Conversion and Management 2016;119:109–120.

[87] Almahdi M, Dincer I, Rosen MA. A new solar based multigeneration system with hot and cold thermal storages and hydrogen production. Renewable Energy 2016;91:302–314.

[88] Dincer I, Hogerwaard J, Zamfrescu C. Clean Rail Transportation Options 2016, Springer.